Journal of Biology and Earth Sciences

Volume 2 Number 1 January-June 2012

ISSN: 2084-3577

http://www.journals.tmkarpinski.com/index.php/jbes http://jbes.strefa.pl
jbes@interia.eu

Journal of Biology and Earth Sciences

Photo on the cover: Pinus silvestris in the Pieniny Mountains, Poland. Author: Tomasz M. Karpiński

Publisher and Editor's office:
Tomasz M. Karpiński, ul. Szkółkarska 88B, 62-002 Suchy Las, Poland, e-mail: jbes@interia.eu

Journal of Biology and Earth Sciences is abstracting and/or indexing in:

- AGRO
- ARIANTA
- e-journals.org
- Elektronische Zeitschriftenbibliothek
- Geo-Leo
- Google Scholar
- Index Copernicus
- New Jour
- OARE
- Public Knowledge Project
- WorldCat

Aims and Scope

The aim of the Journal of Biology and Earth Sciences is to provide the platform for exchange of scientific progress in the field of Biology, Medicine and Earth Sciences, and to do so at the highest possible level. The Journal also aims to facilitate the application of new scientific knowledge to the daily practice of the concerned disciplines and addresses both researchers and academics. For the best quality, Editor-in-Chief is supported in work by Co-Editors.

The Journal publishes original contributions, case reports and review articles in the fields of biology, medicine and earth sciences.
Its scope encompasses:
1. in field of biology: botany, ecology, zoology, microbiology, molecular biology, cellular biology, genetics, taxonomy and allied,
2. in field of medicine: all medical aspects of human biology,
3. in field of earth sciences: the geology, mine geology, industrial geology, instrumental and experimental geology, mineralogy, petrography, paleontology, geography, geophysics, soil sciences and allied.

Editorial Policy

The Journal of Biology and Earth Sciences is a peer-reviewed, open-access, article-based, international, scientific Journal, that publishes full-length articles on biological, medical and earth sciences. Journal accepts original research articles, case reports and review articles.
All manuscripts received by the Editor are considered as confidential documents. The manuscript is examined for the conformity to the Instructions for Authors by the Editor. Failure to meet the Instructions results in return of the manuscript for correction before evaluation. A notification of receiving the manuscript is sent by e-mail to the corresponding author within 5 working days.
Articles submitted to the Journal of Biology and Earth Sciences will be reviewed by the Editor(s) according to the highest academic standards. The review process is handled by 1-2 experts in the field. The review process lasts approximately 4-8 weeks.
ITEMS EVALUATED

Invited referees, in confidence, evaluate the manuscript according to the following aspects: Present-day interest, Originality, Adequacy of methodology, Theoretical background, Essential level, Results and interpretation, Importance in its field, Conclusions, Language correctness.
All the above items can be evaluated as Excellent, Good, Fair or Poor. The manuscript can be evaluated as:
- acceptable in its present form
- acceptable after minor revision (no further review required)
- reconsidered after major revision
- not acceptable for publication.

When the review process is finished, a decision e-mail will be sent to the corresponding author, including the comments of the referee(s). Any corrections suggested by the reviewers, should be made within the period of time indicated in the e-mail. If the paper is accepted after major revisions, it will be submitted again for peer review to the same evaluator(s). After a second review of the corrected manuscript, a final decision e-mail concerning publication is sent to the authors. The final decision about accepting the manuscript for publication will be also available online at www.jbes.strefa.pl in the 'Next Issue' section. A proof is provided to the corresponding author before the article is published. The checked proof should be returned to the Editorial Office by e-mail within 5 working days.

The Journal is issued at least twice a year in electronic version. Each article is published online in PDF format at http://jbes.strefa.pl as soon as it is ready for publication. Public access to articles in the Journal of Biology and Earth Sciences free of charge.

Instructions for authors

1. GENERAL
The publication in the Journal of Biology and Earth Sciences is free of charge. The Journal employs on-line plagiarism detection system.

2. ETHICAL GUIDELINES
2.1. Authorship and Acknowledgements
Authors submitting a paper do so on the understanding that the manuscript have been read and approved by all authors and that all authors agree to the submission of the manuscript to the Journal.
2.2. Ethical Approvals
All experimental studies using human or animal subjects should include an explicit statement in the Material and Methods section identifying the review and ethics committee approval for each study.
2.3. Conflict of Interest and Sources of Funding
Authors are requested to provide a statement concerning any commercial associations or patent licenses that might result in a conflict of interest with the work presented in the submitted paper.
2.4. Permissions
Materials copied from other sources must be accompanied by a written statement from both the author and publisher giving permission to Journal of Biology and Earth Sciences for reproduction. It is the author's responsibility to ensure that such permissions are obtained.
2.5. Copyright Assignment
Authors submitting a paper do so on the understanding that the work and its essential substance have not been published before and is not being considered for publication elsewhere. The articles published in this journal are open-access articles distributed under the terms of the Creative Commons Attribution License, which permits non-commercial use, distribution, and reproduction in any medium, provided the original work is properly cited.

3. MANUSCRIPT SUBMISSION PROCEDURE
3.1. Manuscript Files Accepted
The final version of the manuscript, figures and tables should be submitted by e-mail: jbes@interia.eu.
In text of e-mail **authors can propose 1 or 2 reviewer(s)** giving name(s), affiliation(s) and e-mail(s).
Main text and tables must be in Microsoft Word (.doc) format (not write-protected). **Photographs** must be in JPG or TIFF format, preferred resolution >300 dpi. **Drawings and graphs** must be in JPG or EPS format, preferred resolution >300 dpi.
The manuscript must be accompanied by: a written Licence Form, and in case of experimental studies a statement that the protocol of study and informed consent were in compliance with the Helsinki Convention and were approved by local Ethics Committee. Upon acceptance of the manuscript, the author(s) will be asked to send Licence Form to the publisher.
3.2. Blinded Review
All submitted manuscripts will be reviewed by one or two experts in the field. Papers that do not conform to the general aims and scope of the journal will, however, be returned immediately without review. Journal of Biology and Earth Sciences uses single blinded review. The names of the reviewers will not be disclosed to the author submitting a paper.
3.3. E-mail Confirmation of Submission
In course of 5 working days after submission you will receive an e-mail to confirm receipt of your manuscript. If you do not receive the confirmation e-mail, please check your e-mail address carefully in the system. The error may be caused by some sort of spam filtering on your e-mail server.
3.4. Manuscript Status
The Journal will inform you by e-mail once a decision has been made.
3.5. Submission of Revised Manuscripts
To submit a revised manuscript, send it by e-mail: jbes@interia.eu

4. MANUSCRIPT TYPES ACCEPTED
Journal of Biology and Earth Sciences publishes original research articles, case reports and reviews. Articles will be published under the heading of Biology, Medicine or Earth Sciences.
Original Research Articles must describe significant and original experimental observations and provide sufficient detail so that the observations can be critically evaluated and, if necessary, repeated.
Case Reports must describe an individual phenomenon, uncommon case or a new or improved method. Reviews are selected for their broad general interest; should take a broad view of the field.

5. MANUSCRIPT FORMAT AND STRUCTURE
5.1. Language
The language of publications is English and Polish. In the case of publications in Polish are required in addition in English: title, run title, abstract, keywords and descriptions of tables and figures.
5.2. Structure
All articles should include Title Page, Abstract, and References and in addition sections on Source of Funding and Conflict of Interests. Figures, Figure Legends and Tables should be included where appropriate.
Title Page: The title must contain no more than 100 characters including spaces. The title page should include a running title of no more than 40 characters; 5-10 key words, complete names of institutions for each author, and the name, address, telephone number, fax number and e-mail address for the corresponding author.
Conflict of Interest and Source of Funding: Authors are requested to provide a statement concerning any commercial associations or patent licenses that might result in a conflict of interest with the work presented in the submitted paper. Author's conflict of interest (or the absence of conflicts of interest) and the sources of funding for the research will be published under a heading "Conflict of Interest and Source of Funding Statement".
Abstract: is limited to 250 words in length and should not contain abbreviations or references. The abstract should be structured.
Acknowledgements: Under acknowledgements please specify contributors to the article other than the authors accredited.
5.3. Original Research Articles
Main Text should be organized with Introduction, Materials and Methods, Results and Discussion. The background and hypotheses underlying the study, as well as its main conclusions, should be clearly explained. The figures are limited to 8 items.
5.4. Case Report Articles
These should be divided into the following sections: Title page, Abstract, Introduction, Case presentation, Discussion and Conclusions. The word limit is 3000 words, and up to 6 figures may be included.
5.5. Review Articles
Reviews should take a broad view of the field rather than merely summarizing the authors´ own previous work. The use of state-of-the-art evidence-based systematic approaches is expected. Main Text should be organized with Introduction, Review and Conclusions. The figures are limited to 8 items.
5.6. References
Citations in the text should be marked by Arab numbers in square brackets.
a) The arrangement of the references should be in consecutive order (as they are cited in the text).
b) The first six authors should be presented; if are more than six, please use a phrase: et al.
c) The order of the items in each reference should be:
- for journal references: Name(s) of author(s). Title of paper. Abbreviation of journal title. Year, volume number, (issue number): first and last page numbers.
- for book references: Name(s) of author(s). Year. Chapter title. Title of book in italics. Edition, volume: page number(s). Town of publication, publisher.
5.7. Tables and Figures
Tables: should be with no vertical rulings, with a single bold ruling beneath the column titles. Units of measurements must be included in the column title. Max. format A4.
Figures: All figures should be planned to fit within either 1 column width (8.2 cm) or 2 column widths (17.0 cm). Lettering on figures should be in a clear typeface; the same typeface should be used for all figures.
Units should have a single space between the number and the unit, and follow SI nomenclature or the nomenclature common to a particular field (defined in the legend). Do not use pixel-oriented programmes.
Permissions: If all or parts of previously published illustrations are used, permission must be obtained from the copyright holder concerned. It is the author's responsibility to obtain these in writing and provide copies to the Publishers.

6. AFTER ACCEPTANCE
Upon acceptance of a paper for publication, the manuscript will be forwarded to the production of the journal.
6.1 Proof Corrections
The corresponding author will receive an email with the proof PDF file. Corrected proof must be scanned and returned to the Editor within seven working days. Excessive changes made by the author in the proof, excluding typesetting errors, will be charged separately. Please note that the author is responsible for all statements made in his work, including changes made by the copy editor.

Journal of Biology and Earth Sciences

BIOLOGY ORIGINAL ARTICLE

Effect of boron on growth criteria of some wheat cultivars

Ashraf Metwally[1], Rasha El-Shazoly[2] and Afaf M. Hamada[1]

[1]Botany Department, Faculty of Science, Assiut University, Assiut, 71516 Egypt
[2]Science & Mathematics Department, Faculty of Education, Assiut University, New Valley, Egypt

ABSTRACT

Introduction: Toxic soil concentrations of the essential micronutrient boron (B) represent major limitations to crop production worldwide. Plants have a range of defense systems that might be involved in their affinity to resist and tolerate nutrients stress.

Materials and methods: The experiments were carried out to study the differential responses in five wheat cultivars to boron toxicity.

Results: The fresh and dry matter yield of the test wheat cultivars showed marked decrease as the concentration of boron was increased. Elevated concentration of boron had a notable inhibitory effect on the biosynthesis of pigments fractions in the test wheat cultivars as severely as dry matter gain. The adverse concentration effects of boron on some metabolic responses were clearly displayed by shoot and root systems, exhibited in the elevated rates of proline, hydrogen peroxide and malondialdehyde formation. Potassium leakage was severely affected by boron-stress in some cultivars at all tested concentrations, while in some others a moderate damage was manifested only at the higher boron concentrations.

Conclusions: Sakha 93 out of all the different cultivars investigated was found to display the lowest sensitivity to boron-stress, while Gemmeza 9 was the most sensitive one.

Key words: boron, hydrogen peroxide, pigments, potassium leakage, proline, wheat cultivars.

J Biol Earth Sci 2012; 2(1): B1-B9

Corresponding author:
Prof. Afaf M. Hamada
The Department of Botany, Stockholm University
SE-106 91 Stockholm, Sweden
Fax: +46 (0)8- 165525, Tel.: +46 (0)8- 163759
e-mail: afafhamada@yahoo.com

Original Submission: 27 January 2012; Revised Submission: 30 January 2012; Accepted: 01 February 2012

ISSN: 2084-3577
http://www.journals.tmkarpinski.com/index.php/jbes or http://jbes.strefa.pl
e-mail: jbes@interia.eu

INTRODUCTION

Boron (B) toxicity is an important nutritional disorder that can limit plant growth and productivity in arid and semi-arid environments throughout the world. Although B is an essential micronutrient, an excess causes negative physiological effects [1, 2]. Toxic levels of B also cause oxidative stress [3].

As a widespread problem in dry areas where high B levels have their origin from the soil, treating soil to remove or reduce the effect of B is not economically feasible. Selecting or breeding crop cultivars with high tolerance or resistance to B toxicity is the only effective approach to increase yields on high-B soils. Boron tolerance has been identified in many genotypes, and can be transferred by conventional breeding or molecular means to other cultivars, yet significant improvement in yields on boron-toxic soils have yet to be realized [4]. Although, B toxicity has been reported to be a potential nutritional problem in Egyptian soils [5].

The current work was carried out to study the differential response of different wheat cultivars to B toxicity in greenhouse conditions, to keep up with the advances that are possible for selecting some cultivars having certain mechanisms controlling to some extent the possible mode of resistance to B toxicity. Thus, in this investigation it seemed necessary to study further, in long duration experiments, some metabolic changes that may be associated with distorted growth of B-treated Egyptian (*Triticum aestivum* L.) wheat cultivars. Particular attention was focused to investigate the effect of B toxicity in long duration experiment, on growth, photosynthetically active pigments, K^+ leakage, membrane damage, proline and H_2O_2 accumulation in two selected wheat cultivars.

MATERIALS AND METHODS

A greenhouse experiments was carried out in order to study the effect of various levels of boron (B) on growth and some relevant metabolic activities in five wheat cultivars commonly used in Egypt: Gemmeza 7, Gemmeza 9, Giza 168, Sakha 93 and Seds 1. The grains were kindly supplied by the Agricultural Research Center, Giza, Egypt.

Culture technique

Well-selected grains were sterilized and grown in sand culture in 10 cm. diameter plastic pots lined with polyethylene bags. Each pot represents as experimental unit with 15 grains grown in 0.7 kg air-dried and cleaned quartz sand which was kept at approximately 100% of the field capacity by watering with B-free distilled water and left for germination. After 10 days only 5 seedlings were selected on the basis of vigor and uniformity, the undesired seedlings were removed. The nutrient solution was that adopted by Nable [6] consisting of (μM): KNO_3, 5000; $Ca(NO_3)_2$, 2500; $MgSO_4$, 1000; $NH_4H_2PO_4$, 500; Fe-EDTA, 100; NaCl, 10; $ZnSO_4$, 2.5; $CuSO_4$, 0.5; $MnSO_4$, 1; $CoSO_4$, 0.2; Na_2MoO_4, 0.91; $B(OH)_3$, 15; pH, 5.5-6.0. The nutrient solution was added every 2 days. Boron was applied to the soil from H_3BO_3 and applied to the soil at 10 days old seedlings. The plants were grown in a naturally light greenhouse at Botany Department, Faculty of Science, Assiut University.

Experimental design

The experiments were carried out using five wheat cultivars in order to detect the low B-sensitive cultivar versus the high sensitive one. The seedlings were grown in final B concentration of: 0.5, 1, 2, 3, 6 mg kg^{-1} soil for ten days. The tolerance parameters in this experiment were: fresh biomass, dry biomass accumulation, chlorophylls a and b and carotenoids, lipid peroxidation, H_2O_2, proline, and K^+ leakage.

Harvesting and plant growth yield

At the end of the experimental period, plants were fractionated into roots and shoots. The shoots and roots were quickly weighed separately for fresh weight (FW) determination. Freshly harvested roots and shoots were oven-dried at 70ºC for 48 hours in order to determine the dry weight (DW) and to follow some analysis.

Determination of photosynthetic pigments

The photosynthetic pigments, via, chlorophyll a, chlorophyll b and carotenoids, were extracted from fresh leaves samples and absorbance readings determined with a spectrophotometer (Unico UV-2100 spectrophotometer). Chlorophylls and carotenoids concentrations were calculated using equations as cited by Lichtenthaler [7]. The pigment fractions were calculated as mg g^{-1} FW.

Determination of H_2O_2

The H_2O_2 content of the shoots and roots samples were colorimetrically measured as described by Mukherjee & Choudhuri [8]. The concentration of H_2O_2 was calculated from a standard curve and expressed as mmol g^{-1} FW.

Determination of potassium leakage

Potassium leakage was determined according to the flame photometric (using Carl Zeiss flame photometer) method of Williams & Twine [9].

Determination of membrane damage

Lipid peroxidation was determined by measuring the amount of malondialdehyde (MDA) produced by the thiobarbituric acid (TBA) reaction as described by Heath & Packer [10]. The MDA concentration was determined by its molar extinction coefficient (155 mM^{-1} cm^{-1}) and the results expressed as µmol MDA g^{-1} FW.

Determination of proline

Free proline was extracted from fresh leaves and root samples and estimated by ninhydrin reagent [11]. Proline concentration was determined using calibration curve and expressed as µg proline g^{-1} FW.

RESULTS

Fresh and dry matter yield

Most of the test cultivars exhibited a gradual reduction in fresh and dry matter yield of shoots and roots, by increasing B concentration in the sand culture media, while the fresh matter of Sakha 93 was enhanced (Fig. 1). The adverse concentration effects of B toxicity stress on growth criteria were clearly demonstrated by wheat cultivars treated with the highest B level.

Table. 1. Effect of different concentrations of B (mg Kg^{-1} soil) on Chl.a, Chl.b, and carotenoids content of 20-day-old wheat cultivars treated with B for 10 days. The data are given as average of six replicates ± standard error. Different letters (a, b, c and d) in each row (for Chl. a; Chl. b or Carot. of each genotype) represent significance at p=0.05 level based on Duncan's multiple range tests.

Genotype	Pigments (mg g^{-1} FW)	B (mg Kg^{-1} soil)					
		0	0.5	1	2	3	6
G7	Chl. a	1.148^{d} ± 0.00	1.064^{dc} ± 0.01	1.032^{c} ± 0.03	0.942^{b} ± 0.05	0.929^{b} ± 0.01	0.809^{a} ± 0.01
	Chl. b	0.226^{c} ± 0.00	0.209^{cb} ± 0.00	0.1916^{ba} ± 0.01	0.1818^{ba} ± 0.00	0.191^{a} ± 0.00	0.1812^{a} ± 0.01
	Carot.	0.378^{c} ± 0.00	0.368^{cb} ± 0.00	0.366^{cb} ± 0.01	0.344^{ba} ± 0.01	0.324^{a} ± 0.01	0.324^{a} ± 0.00
G9	Chl. a	1.23^{d} ± 0.04	1.06^{c} ± 0.02	0.977^{c} ± 0.02	1.074^{c} ± 0.03	0.726^{b} ± 0.03	0.239^{a} ± 0.01
	Chl. b	0.282^{c} ± 0.02	0.251^{c} ± 0.00	0.199^{b} ± 0.01	0.195^{b} ± 0.00	0.187^{b} ± 0.00	0.123^{a} ± 0.01
	Carot.	0.418^{c} ± 0.01	0.422^{c} ± 0.01	0.392^{bc} ± 0.01	0.392^{bc} ± 0.02	0.365^{b} ± 0.03	0.267^{a} ± 0.01
G168	Chl. a	1.35^{d} ± 0.01	1.28^{c} ± 0.01	1.26^{c} ± 0.00	1.25^{c} ± 0.01	1.17^{b} ± 0.03	0.82^{a} ± 0.01
	Chl. b	0.377^{d} ± 0.01	0.363^{c} ± 0.00	0.355^{c} ± 0.00	0.353^{c} ± 0.00	0.329^{b} ± 0.01	0.175^{a} ± 0.00
	Carot.	0.46^{cb} ± 0.00	0.441^{b} ± 0.01	0.468^{c} ± 0.00	0.463^{c} ± 0.00	0.452^{bc} ± 0.01	0.323^{a} ± 0.00
S1	Chl. a	1.21^{c} ± 0.06	1.09^{b} ± 0.01	1.05^{b} ± 0.00	1.05^{b} ± 0.01	1.04^{b} ± 0.01	0.79^{a} ± 0.03
	Chl. b	0.209^{c} ± 0.01	0.19^{bc} ± 0.00	0.189^{bc} ± 0.01	0.188^{b} ± 0.00	0.183^{b} ± 0.01	0.148^{a} ± 0.01
	Carot.	0.408^{c} ± 0.01	0.38^{bc} ± 0.01	0.38^{bc} ± 0.00	0.386^{bc} ± 0.00	0.36^{b} ± 0.00	0.282^{a} ± 0.00
S93	Chl. a	1.32^{b} ± 0.08	1.3^{b} ± 0.03	1.26^{ab} ± 0.05	1.29^{ab} ± 0.03	1.17^{ab} ± 0.04	1.13^{a} ± 0.01
	Chl. b	0.34^{a} ± 0.01	0.34^{a} ± 0.01	0.34^{a} ± 0.02	0.31^{a} ± 0.00	0.31^{a} ± 0.01	0.30^{a} ± 0.01
	Carot.	0.425^{ab} ± 0.01	0.437^{b} ± 0.00	0.439^{b} ± 0.01	0.439^{b} ± 0.01	0.417^{ab} ± 0.01	0.40^{a} ± 0.01

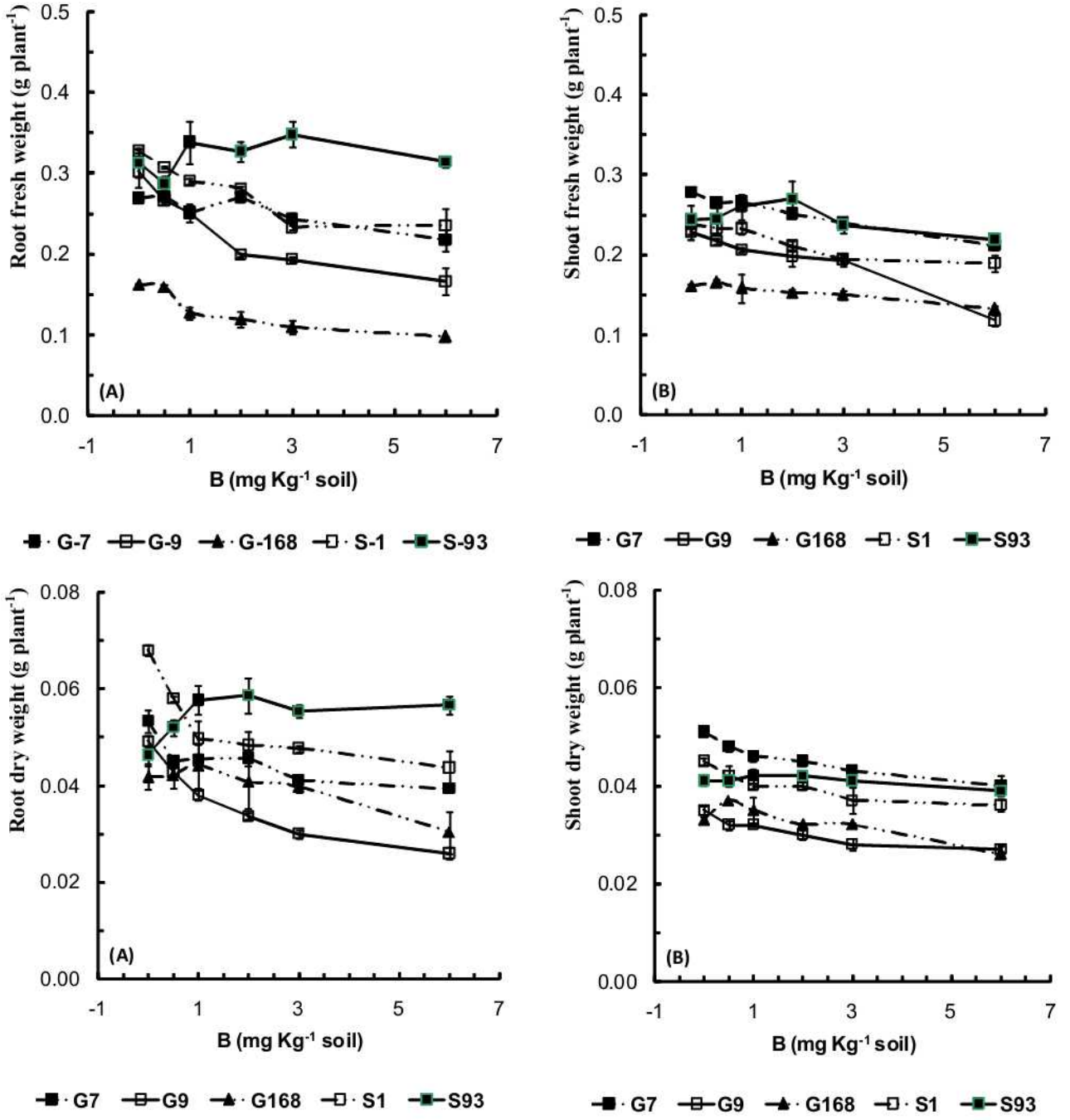

Fig. 1. Effect of different concentrations of B (mg Kg^{-1} soil) on fresh (upper fig.) and dry (lower fig.) weight of shoots and roots of 20-day-old wheat cultivars treated with B for 10 days. [The data are given as average of six replicates ± standard error].

Photosynthetic pigments

The increase in B level in the culture medium was generally associated with a gradual fall in pigments biosynthesis (chl. a, chl. b and carotenoids) in all wheat cultivars leaves (Table 1). Moreover, photosynthetic pigments concentration was highly inhibited at 6 mg B in Gemmeza 9 as compared to Sakha 93.

Membrane integrity

The oxidative damage caused by B toxicity was studied by detecting malondialdehyde (MDA) concentration in shoots and roots indicating lipid peroxidation degree, H_2O_2 concentration and potassium leakage.

The data herein obtained clearly demonstrate that H_2O_2 concentration in shoots of the various wheat cultivars was stimulated by the most B levels, while it fluctuated in roots of the test cultivars (Fig. 2).

Potassium efflux of the wheat cultivars leaves increased in response to increase B supply in the culture medium (Fig. 3).

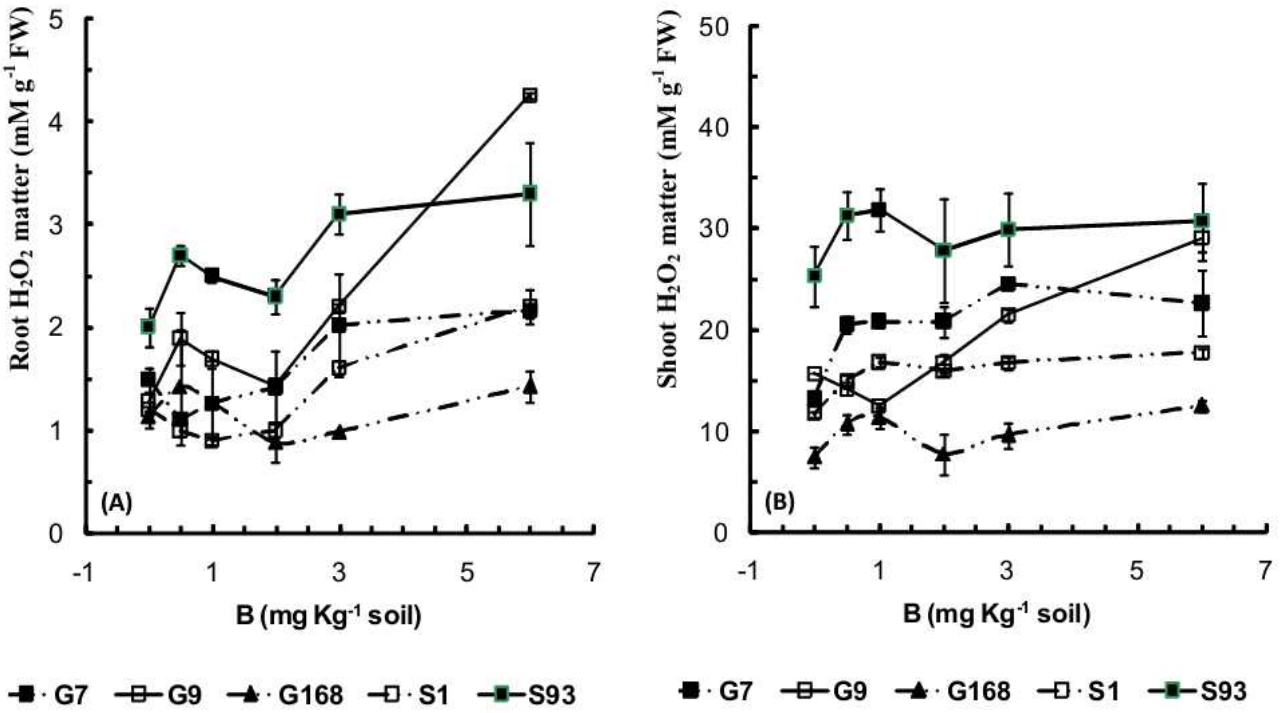

Fig. 2. Effect of different concentrations of B (mg Kg^{-1} soil) on H_2O_2 concentrations of shoots and roots of 20-day-old wheat cultivars treated with B for 10 days. [The data are given as average of six replicates ± standard error].

The increase in B level was associated with significant increase in the concentration of MDA in roots of the different parts of the test cultivars (Fig. 4).

Proline accumulation

The data in Fig. 5 revealed that the increase in B level in the culture medium had a significant stimulatory effect on the accumulation of proline in the shoots of the test wheat cultivars. On other hand, proline accumulation in roots showed differences between the test cultivars and the B levels.

DISCUSSION

Boron deficiency and toxicity severely limit crop production worldwide [12, 13]. Toxicity is more difficult to manage agronomically and is best dealt with by using boron-tolerant varieties. Genetic variation for B-toxicity tolerance is known for a number of crop plant species.

Fresh and dry matter yield

In this study, fresh and dry matter yield of shoots and roots varied among the test cultivars. High concentration of B strongly inhibited dry matter gain in shoots and roots of the test plants. High B treatment enhanced the growth rate of the tolerant Sakha 93 and reduced that of susceptible

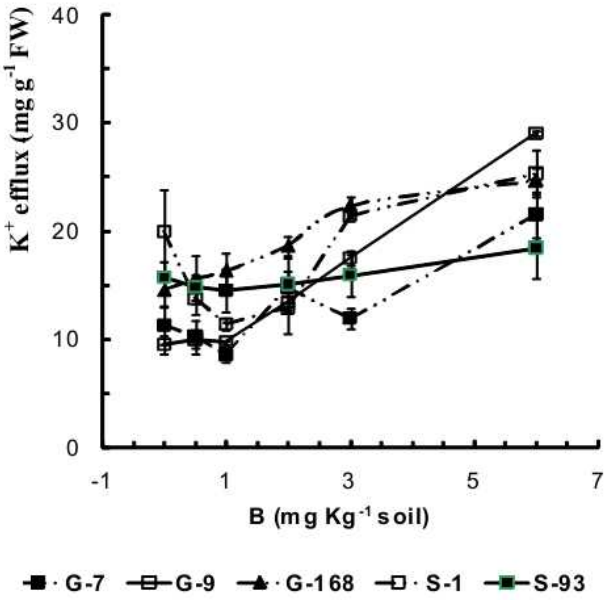

Fig. 3. Effect of different concentrations of B (mg Kg^{-1} soil) on K^+ leakage of shoots of 20-day-old wheat cultivars treated with B for 10 days. [The data are given as average of six replicates ± standard error].

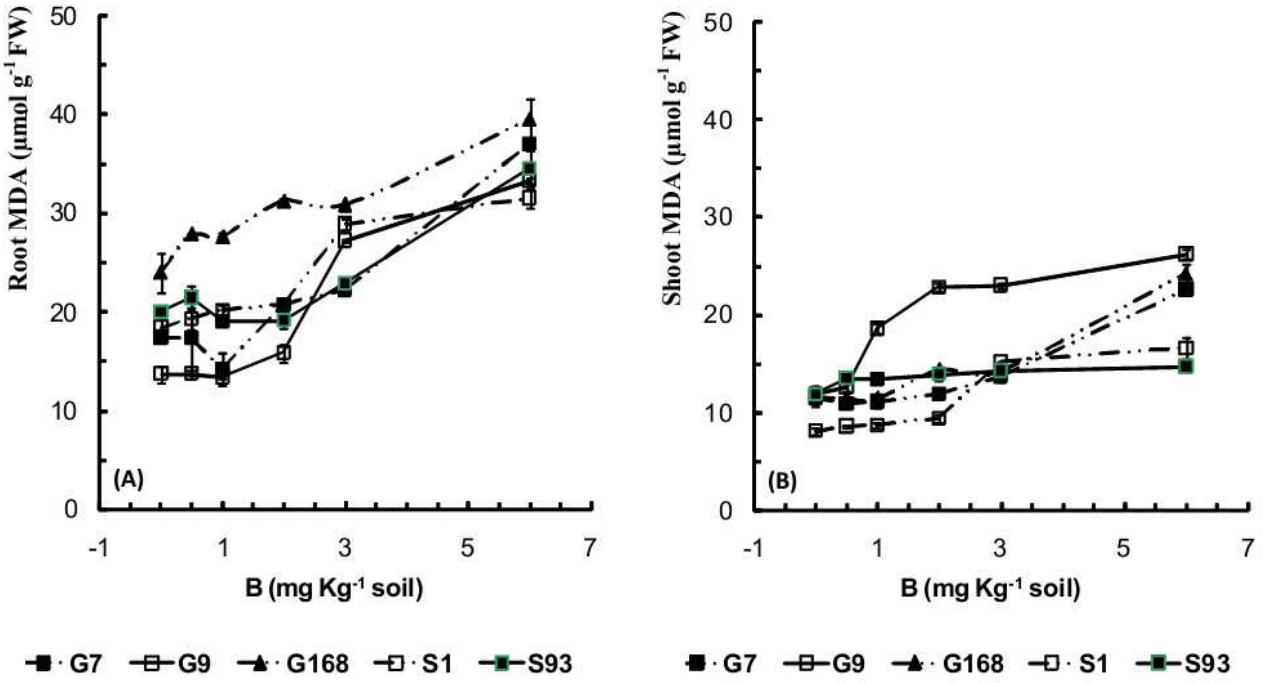

Fig. 4. Effect of different concentrations of B (mg Kg^{-1} soil) on MDA (malondialdehyde) production in shoots and roots of 20-day-old wheat cultivars treated with B for 10 days. [The data are given as average of six replicates ± standard error].

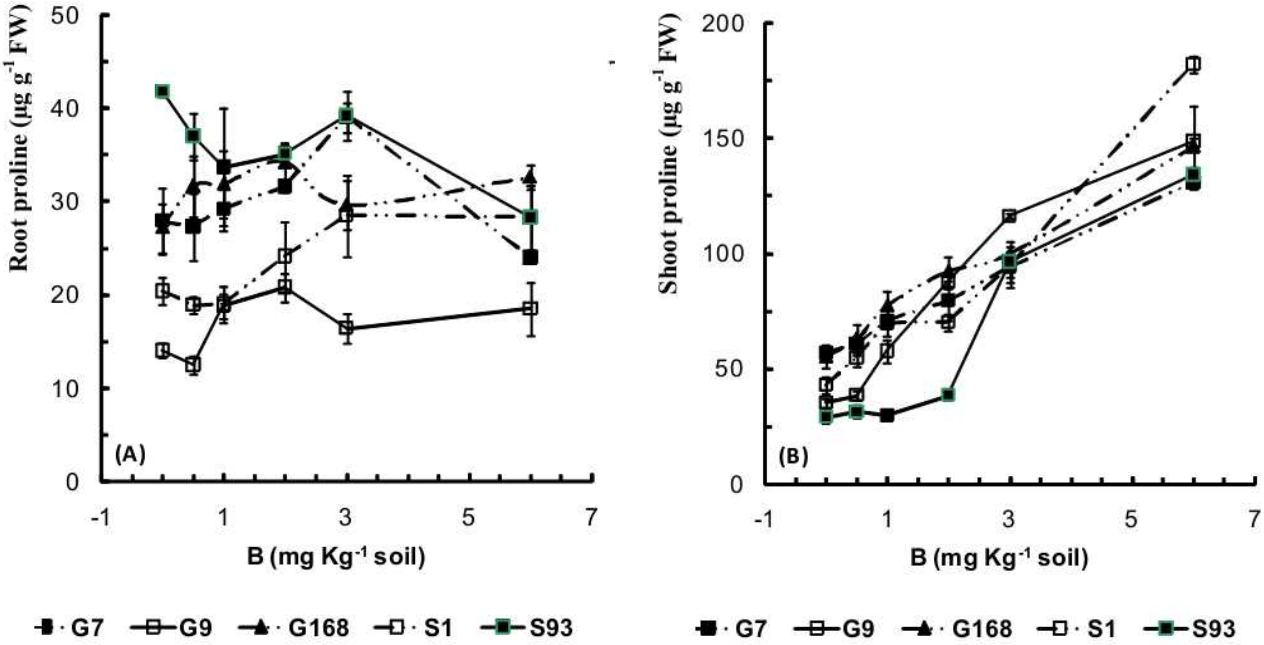

Fig. 5. Effect of different concentrations of B (mg Kg^{-1} soil) on proline concentration in shoots and roots of 20-day-old wheat cultivars treated with B for 10 days. [The data are given as average of six replicates ± standard error].

Gemmeza 9. The effectiveness of the different B levels varied in the different test cultivars, two cultivars (Sakha 93 and Giza 168) were relatively more tolerant to B stress, compared with Gemmeza 7 and Gemmeza 9 which were B-sensitive. So, the adverse concentration effects of B stress on wheat growth appeared to be cultivar dependent. In this context, McDonald et al. [14] found that there was no significant effect on dry matter production and no consistent effect on grain yield in barley lines. Small yield increases in lines selected for improved B tolerance have been reported previously, but with little explanation of the causes [15]. The work of Riley [16, 17] has demonstrated that B could accumulate to high concentrations (50-70 mg kg^{-1}) in barley before there was a significant reduction in growth and the expression of symptoms could be quite severe before growth was reduced. This agrees with McDonald et al. [14], who observed that with barley line VB9104, where the negative correlation between yield and shoot B concentration only occurred when shoot B concentrations exceeded 80 mg kg^{-1}. Also, Ardic et al. [18] concluded that the inhibition in root elongation of chickpea Küsmen may be correlated with a decrease in either cell numbers or cell width [19]. Moreover, improved growth of chickpea Gökce in the presence of excess B might be related to the ability of this cultivar to reduce the intracellular concentration of B by active efflux of B from the roots, as also reported by others [20, 21].

Photosynthetic pigments

The response of the test cultivars depends on the level of the applied B in the culture medium. The increase in B-level was generally associated with a gradual fall in pigments biosynthesis. The adverse effects of B-stress on Gemmeza 9 were more pronounced at the highest B levels, a response which reflects its sensitivity due to inhibited pigments biosynthesis, degradation of the synthesized pigments and/or damage of the photosynthetic apparatus. The reduction of the leaf area was attributed to decrease in the chlorophyll concentration and CO_2 fixation [22]. In B-immobile species B tends to accumulate at the tips and the edges of the leaves [23]. Although loss of chlorophyll is one of the early symptoms of the B toxicity the underlying reason behind the chlorophyll loss due to high B concentration is yet to be clarified. If the decrease in the metal ions observed in leaves sprayed with B is valid for Mg^{2+} ions the loss of chlorophyll can be related to the lack of Mg^{2+} ions [24, 25]. In studies of kiwifruit leaf anatomy, B toxicity induced a decrease of the volume of mesophyll cells, and an increase of the volume of intercellular spaces and cell damage [26]. According to Pereira et al. [27] one of the probable reasons for the reduction of photosynthesis is the structural damage of thylakoids, which affects the photosynthetic transport of electrons.

The increase in B concentration in the culture medium was found to induce inhibitory effects on carotenoids content in the sensitive cultivars compared with the tolerant one. This might be responsible, at least in part, for protection against oxidative damage. Carotenoids are able to accept excitation energy from triplet chlorophyll and thereby help prevent singlet oxygen formation [28].

Membrane integrity

Under stress conditions, including excess [29] or deficiency [30] of nutrient elements, accumulation of reactive oxygen species (ROS) are commonly generated [31]. Karabal et al. [32] observed in barley cultivars that B toxicity induced oxidative and membrane damage in leaves. Also, in apple (*Malus domestica*) and grapevine (*Vitis vinifera*), it has been reported that B toxicity induces oxidative damage by lipid peroxidation and hydrogen peroxide accumulation [33, 34]. Gunes et al. [33] concluded that the consequent decrease in CO_2 concentration in leaf mesophyll tissue, results in an accumulation of NADPH. Under such conditions where NADPH is limiting, oxygen acts as an alternate acceptor of electrons, resulting in the formation of superoxide radicals [35]. In this investigation, the B-toxicity treatments diminished growth and boosted the amount of H_2O_2 and malondialdehyde in the root and shoot tissues of the test cultivars. These trends were more pronounced in Gemmeza 9 (the B-sensitive cultivar) than in Sakha 93 (the B-tolerant cultivar).

This is in accordance with Nable et al. [36] who concluded that relative tolerance of genotype of a give species to B is associated with differences in their abilities to passively transport B, probably caused by differences in membrane composition, affecting transmembrane movement of B. By using artificial membranes and *Arabidopsis* mutants that differ in sterol and fatty acid compositions, Dordas & Brown [37] demonstrated that, lipid composition of the plasma membrane can affect the total B uptake.

Potassium leakage is usually used as a criterion for the stability and integrity of membranes. In this investigation, K^+ efflux of the test cultivars leaves

increased in response to increase B supply in the culture medium. Such leakage of ionic solutes and K^+ efflux [38] as well as leakage of cellular metabolites [39] are frequently used to assess membrane integrity. According to Sairam et al. [35] and Sairam & Saxena [40] plant species respond differently to oxidative injury as a result of variation in their antioxidant system under stress conditions.

Proline accumulation

The stimulated proline accumulation in the test wheat cultivars under the influence of high levels of the applied B is in agreement with the result obtained by Gunes et al. [41]. According to Alia-Saradhi [42] heavy metals lead to proline accumulation, if toxicity of B is considered to be an oxidative stress like salinity or heavy metal as suggested by Molassiotis et al. [34], our results are consistent with the previous reports. Proline increases the stress tolerance of the plants through such functions as osmoregulation, the protection of enzymes against denaturation, and the stabilization of protein synthesis [43]. Increased proline levels are another common response of plants upon osmotic stress [32]. Proline protects enzymes and membranes against oxidative stress [44]. An increased proline level together with enhanced H_2O_2 contents is a common response of plant cells to osmotic stress treatments. The data herein obtained clearly demonstrate that under B toxicity significant changes were encountered in proline and H_2O_2 contents.

CONCLUSION

In the light of these results Sakha 93 can be assumed to have a certain affinity to tolerate high B-stress conditions. Thus, it was selected as the most B-tolerant, out of five, test cultivars and Gemmeza 9 as the most B-sensitive one. Sakha 93 was the lowest sensitive cultivar, in which the root system fresh weight exhibited no inhibition. In contrast, Gemmeza 9 revealed the highest degree of sensitivity where the reduction in its root system fresh weight reached 43%.

EXPLANATION:
This article is a part of Rasha El-Shazoly M.Sc. thesis.

REFERENCES

1. Nable RO, Cartwright B, Lance RC. 1990. Genotypic differences in boron accumulation in barley: relative susceptibilities to boron deficiency and toxicity. In: Genetic Aspects of Plant Mineral Nutrition (Eds. N. El. Bassam, M. Damborth & B. Laoghman): pp. 243-251. Kluwer Academic Publishers, Dordrecht, Boston.
2. Keles Y, Öncel I, Yenice N. Relationship between boron content and antioxidant compounds in *Citrus* leaves taken from field with different water source. Plant Soil 2004; 265: 345–353.
3. del Rio LA, Corpas FJ, Sandalio LM, Palma JM, Barroso JB. Plant peroxisomes, reactive oxygen metabolism and nitric oxide. IUBMB Life 2003; 55: 71-81.
4. Reid R. Can we really increase yields by making crop plants tolerant to boron toxicity? Plant Sci 2010; 178: 9–11.
5. Hassan FA. 1984. Factors affecting boron status under saline and calcareous soil conditions. Ph.D. Thesis, Zagazig University, Egypt.
6. Nable RO. Resistance to boron toxicity amongst several barley and wheat cultivars: a preliminary examination of the resistance mechanism. Plant Soil 1988; 112: 45–57.
7. Lichtenthaler HK. 1987. Chlorophylls and Carotenoids: Pigments of Photosynthetic Biomembranes. In: Methods in Enzymology Vol. 148: pp. 350-183. Academic press, Orlando, Fl., USA.
8. Mukherjee SP, Choudhuri MA. Implications of water stress-induced changes in the levels of endogenous ascorbic acid and hydrogen peroxide in *Vigna* seedlings. Physiol Plantarum 1983; 58: 166-170.
9. Williams CH, Twine JR. 1960. Flame Photometric method for sodium, potassium and calcium. In: Peach K, Tracey MV (ed.); Modern Methods of Plant Analysis. Vol. 5: pp. 3-5. Springer Verlag, Berlin.
10. Heath RL, Packer L. Photoperoxidation in isolated chloroplasts. I. Kinetics and stochiometry of fatty acid peroxidation. Arch Biochem Biophys 1968; 125: 189-198.
11. Bates LS, Waldren RP, Teare ID. Rapid determination of free proline for water-stress studies. Plant Soil 1973; 39: 205-207.
12. Nable RO, Paull JG. Mechanism and genetics of tolerance to boron toxicity in plants. Curr Topics Plant Biochem Physiol 1991; 10: 257-273.
13. Gupta UC. 1993. Factors affecting boron uptake by plants. In: Boron and its role in crop production (Gupta, UC, Eds), Boca Raton: CRC Press Inc.: pp. 87-104.
14. McDonald GK, Eglinton JK, Barr AR. Assessment of the agronomic value of QTL on chromosomes 2H and 4H linked to tolerance to boron toxicity in barley (*Hordeum vulgare* L.). Plant Soil 2010; 326: 275–290.

15. Emebiri L, Michael P, Moody D. Enhanced tolerance to boron toxicity in two-rowed barley by marker-assisted introgression of favourable alleles derived from Sahara 3771. Plant Soil 2009; 314: 77-85.
16. Riley MM. Boron toxicity in barley. J Plant Nutr 1987; 10: 2109–2115.
17. Riley MM, Robson AD. Patterns of supply affects boron toxicity in barley. J Plant Nutr 1994; 17: 1721–1738.
18. Ardic M, Sekmen AH, Turkan I, Tokur S, Ozdemir F. The effects of boron toxicity on root antioxidant systems of two chickpea (*Cicer arietinum* L.) cultivars. Plant Soil 2009; 314: 99-108.
19. Choi EY, Kolesik P, McNeill A, Collins H, Zhang Q, Huynh BL, Graham R, Stangoulis J. The mechanism of boron tolerance for maintenance of root growth in barley (*Hordeum vulgare* L.). Plant Cell Environ 2007; 30: 984-993.
20. Reid RJ, Hayes JE, Post A, Stangoulis JCR, Graham RD. A critical analysis of the causes of boron toxicity in plants. Plant Cell Environ 2004; 25: 1405–1414.
21. Sutton T, Baumann U, Hayes J, Collins NC, Shi Bu-Jun, Schnurbusch T, Hay A, Mayo G, Pallotta MA, Tester M, Langridge P. Boron-toxicity tolerance in barley arising from efflux transporter amplification. Science 2007; 318: 1446–1449.
22. Lovatt CJ, Bates LM. Early effects of excess boron on photosynthesis and growth of *Curcubita pepo*. J Exp Bot 1984; 35: 297-305.
23. Brown PH, Shelp BJ. Boron mobility in plants. Plant Soil 1997; 193: 85-101.
24. Power PP, Woods WG. The chemistry of boron and its speciation in plants. Plant Soil 1997; 193: 1-13.
25. Reinbott TM, Blevins DG, Schon MK. Content of boron and other elements in main stem and branch leaves and seed of soybean. J Plant Nutr 1997; 20: 831-843.
26. Sotiropoulos TE, Therios IN, Dimassi KN, Bosabalidis A, Kofidis G. Nutritional status, growth, CO_2 assimilation, and leaf anatomical responses in two kiwifruit species under boron toxicity. J Plant Nutr 2002; 25: 1249-1261.
27. Pereira WE, de Siqueira DL, Martínez CA, Puiatti M. Gas exchange and chlorophyll fluorescence in four citrus rootstocks under aluminum stress. J Plant Physiol 2000; 157: 513-520.
28. Asada K 1996. Radical production and scavenging in the chloroplasts. In: Photosynthesis and the environment. NR Baker, Eds. Kluwer, Dordrecht, Netherlands: pp. 123-150.
29. Romero-Puertas MC, Palma JM, Gomez M, del Rio LA, Sandalio LM. Cadmium causes the oxidative modification of proteins in pea plants. Plant Cell Environ 2002; 25: 677–686.
30. Molassiotis A, Tanou G, Diamantidis G, Patakas A, Therios I. Effects of 4-month Fe deficiency exposure on Fe reduction mechanism, photosynthetic gas exchange, chlorophyll fluorescence and antioxidant defense in two peach rootstocks differing in Fe deficiency tolerance. J Plant Physiol 2006; 163: 176-185.
31. Mittler R. Oxidative stress, antioxidants and stress tolerance. Trends Plant Sci 2002; 7: 405–410.
32. Karabal E, Yücel M, Öktem HA. Antioxidant responses of tolerant and sensitive barley cultivars to boron toxicity. Plant Sci 2003; 164: 925–933.
33. Gunes A, Soylemezoglu G, Inal A, Bagci EG, Coban S, Sahin O. Antioxidant and stomatal responses of grapevine (*Vitis vinifera* L.) to boron toxicity. Sci Horticulturae 2006; 110: 279–284.
34. Molassiotis A, Sotiropoulos T, Tanou G, Diamantidis G, Therios I. Boron-induced oxidative damage and antioxidant and nucleolytic responses in shoot tips culture of the apple rootstock EM9 (*Malus domestica* Borkh). Environ Exp Bot 2006; 56: 54–62.
35. Sairam RK, Deshmukh PS, Saxena DC. Role of antioxidant systems in wheat genotypes tolerance to water stress. Biol Plantarum 1998; 41: 387–394.
36. Nable RO, Banuelos GS, Paull JG. Boron toxicity. Plant Soil 1997; 198: 181-198.
37. Dordas C, Brown PH. Permeability of boric acid across lipid bilayers and factors affecting it. J Membr Biol 2000; 175: 95-105.
38. Palta JP, Levitt J, Stadelmann EJ. Freezing injury in onion bulb cells. I. Evaluation of the conductivity method and analysis of ion and sugar efflux from injured cells. Plant Physiol 1977; 60: 393-397.
39. Navari-Izzo F, Quartacci MF, Melfi D, Izzo R. Lipid composition of plasma membranes isolated from sunflower seedlings grown under water-stress. Physiol Plantarum 1993; 87: 508-514.
40. Sairam RK, Saxena DC. Effect of elevated temperature on oxidative stress and antioxidant activity in wheat genotypes. Possible mechanism of heat stress tolerance. Biol Plantarum 2000; 43: 245-251.
41. Gunes A, Inal A, Bagci EG, Coban S, Sahin O. Silicon increases boron tolerance and reduces oxidative damage of wheat grown in soil with excess boron. Biol Plantarum 2007; 51: 571–574.
42. Alia-Saradhi PP. Proline accumulation under heavy metal stress. J Plant Physiol 1991; 138: 554-558.
43. Kuznetsov VV, Shevyakova NI. Stress responses of tobacco cells to high temperature and salinity. Proline accumulation and phosphorilation of polypeptides. Physiol Plantarum 1997; 100: 320-326.
44. Agarwal S, Pandey V. Antioxidant enzyme responses to NaCl stress in *Cassia angustifolia*. Biol Plantarum 2004; 48: 555–560.

Journal of Biology and Earth Sciences

BIOLOGY ORIGINAL ARTICLE

Anti-inflammatory, antipyretic and antioxidant activities of the earthworms extract

Hossam M. Omar[1], Zedan Z. Ibraheim[2], Nasser A. El-Shimy[1], Rouwaida S. Ali[1]

[1]Department of Zoology, Faculty of Science, Assiut University, Egypt

[2]Department of Pharmacognosy, Faculty of Pharmacy, Assiut University, Egypt

ABSTRACT

Introduction: Earthworms are the major biomass in soil. They have been widely used in traditional Chinese medicine for a long time. However, in the past few decades with the development of biochemical technologies the research on the pharmaceutical effects of earthworms has been commencement.

Aims: Experiments were conducted to recognize the therapeutic properties such as anti-inflammatory, antipyretic and antioxidant activities of biologically active extract isolated from two species of earthworm (*Pheretima hawayana* Rosa and *Allolobophora caliginosa* Savigny).

Materials and methods: Inflammation in the hind paw of albino rat (*Rattus rattus*) was induced by histamine, pyrexia was induced by *Escherichia coli* in rats and liver damage was induced by injection of rats with CCl_4. Anti-inflammatory drug - indomethacin, anti-pyretic drug - paracetamol and antioxidant drug - silymarin plus were used as standard drugs for comparison.

Results: Administration of earthworms extract (100 mg/kg) and indomethacin (10 mg/kg), paracetamol (150 mg/kg), silymarin plus (150 mg/kg) as standard drugs reduced and restored to normal the changes that induced by histamine, *Escherichia coli* and CCl_4 in rats.

Conclusions: The present study conclude that both extracts of earthworms gave result as anti-inflammatory and anti-pyretic similar to the standard drugs. The extract of the two species showed various responds as antioxidants against CCl_4 induced hepatotoxicity.

Key words: earthworm extract, anti-pyretic, anti-inflammation, antioxidant, histamine, indomethacin, paracetamol, CCl_4.

J Biol Earth Sci 2012; 2(1): B10-B17

Corresponding author:
Prof. Hossam M. Omar
Department of Zoology, Faculty of Science,
Assiut University, Assiut, 71516, Egypt
e-mail: hossameldin.mo@gmail.com

Original Submission: 27 January 2012; Revised Submission: 06 February 2012; Accepted: 07 February 2012

ISSN: 2084-3577
http://www.journals.tmkarpinski.com/index.php/jbes or http://jbes.strefa.pl
e-mail: jbes@interia.eu

INTRODUCTION

Earthworms are soil macroinvertebrates oligochaete animals that ply an important role in the sustainability of soil fertility and productivity. Earthworms are the major biomass in soil. The conditions of the environment and nature of food affect on the chemical composition of earthworms [1]. They have been widely used in traditional Chinese medicine for thousands of years. However, in the past few decades, with the development of biochemical technologies, the research on the pharmaceutical effects of earthworms has been initiated [2]. Earthworm protein and its coelomic fluid were reported to exhibit cytolytic, proteolytic, haemolytic, mitogenic, tumorstatic, antibacterial and anti-inflammatory activities [3].

Recently Prakash et al. [4] and Balamurugan et al. [5] have reported that the presence of anti-ulceral and anti-oxidative properties of earthworm paste of *Lampito mauritii*. However there are no scientific data available to prove the argue of the traditional medicine practitioners about the medicinal effectiveness of earthworms [6].

In order to analyze some of the ethnomedical uses of earthworm, the current experiments were undertaken to study the anti-pyretic, anti-inflammatory and antioxidant activity of the whole tissue extract from two earthworm species, *Allolobophora caliginosa* Savigny and *Pheretima hawayana* Rosa - invertebrate oligochaete annelids compared to standard drugs paracetamol, indomethacin and silymarin plus as standard antipyretic, anti-inflamatory and antioxidant drug respectively.

MATERIALS AND METHODS

Preparation of earthworm extract from *Pheretima hawayana* Rosa (EA) and *Allolobophora caliginosa* Savigny (EP)

Earthworms, *Pheretima hawayana* Rosa and *Allolobophora caliginosa* Savigny were collected during the period of January to April 2009 by hand-sorting from soil in Abu-Korkas El Minia Governorate, Egypt. 1000 sexually mature worms were kept in 0.65% NaCl at room temperature for 1–2 h with a few changes of solution until their digestive systems became clean. Earthworms were then removed from the solution and cutted with scissors. Three grams of earthworm tissue were homogenized in 40 ml of chloroform/methanol (v/v) solution and left overnight at 40°C. The following day, 16 ml of distilled water was added to the homogenate, mixed and centrifuged at 5000 rpm for 10 min. Three clearly visible layers were obtained. The upper water/methanol layer was pipette out and evaporated on a rotavapor until no methanol was left. An opalescent fluid with pH 7 was obtained, the two extracts of EA and EP, were then freeze-dried and kept at 4°C until use [6].

Selection of experimental animals

Healthy and pure strain male albino rats (*Rattus rattus*), weighing 100–120 g was procured from the Department of Animal Production, Faculty of Agriculture, El-Minia University, El-minia, Egypt. They were housed in the animal house of Zoology Department, Faculty of Science, Assuit University in metal cages in groups of sex per cage and were kept in a room temperature with normal light/dark cycle. They were allowed to acclimatize for one week before the experiments and fed a standard diet and given water *ad libitum*.

All experimental protocols held on animals were done according to regulations set by the Institutional Animal Care and approved by Assiut University.

Methods of anti-inflammatory activity

Inflammation in the hind paw of rats was induced as described by Winter et al. [7]. Male rats were divided into 4 groups comprising 6 rats in each. Of these 4, the control group received only distilled water 2ml/kg, the second group received a standard drug indomethacin (10 mg/kg) and the other two experimental groups received earthworm extract (EE, 100 mg/kg). The indomethacin and EE were administered orally 1 h prior to the sub plantar injection of freshly prepared histamine (1 mg/kg). One hour after drug administration the paw oedema volume was measured by using a thread to determine the diameter of oedema formation size at 1, 2 and 3 h.

Anti-pyretic activity

The anti-pyretic activity of EA and EP were evaluated using *Escherichia coli*-induced pyrexia in rats [8]. Fever was induced by injection of 5 ml/kg (s.c.) of 15% aqueous suspension of *Escherichia coli* (10^8 CFU/ml) in normal saline below the nape of the neck and rectal temperature was recorded by a clinical thermometer at 1, 2 and 3 hour after

Escherichia coli injection. Prior to experiments, rats were maintained in separate cages for 3 days and with those rats approximately constant rectal temperature were selected for the study. Paracetamol (150 mg/kg, p.o.) was used as standard drug for comparing the anti-pyretic action of EE. *Escherichia coli* was prepared in the Bacterial Research Laboratory, Department of Botany, Assiut University.

Antioxidants activity

Thirty rats were divided into 5 groups comprising 6 rats in each. Of these 5, the control group received only vehicle, the second group received CCl_4 (2 ml/kg) once a day for 7 days and the other three experimental groups received CCl_4 (2 ml/kg) followed by silymarin plus (150 mg/kg) and EA and EP (100 mg/kg) once a day orally for 7 days respectively. After 24 hours from the last injection rats were dissected for collection of liver and blood. Plasma was separated by centrifugation of blood at 2500 rpm for 15 min and stored at -20°C. 10% w/v homogenate of liver was prepared in 0.1 M phosphate buffer (pH 7.4) using homogenizer (IKA Yellow line DI 18 Disperser, Germany) and stored at -20°C for biochemical analysis.

Plasma glucose level was determined by glucose oxidase colorimetric method according the method of Trinder [9]. Alanine aminotransaminase (ALT) and aspartate amino-transferase (AST) were assayed by colorimetric method according to Young [10]. Lipid peroxidation as TBARS was determined according to the method of Ohkawa et al. [11]. Glutathione (GSH) was determined using the method of Beutler et al. [12]. Superoxide dismutase (SOD) activity was determined according to its ability to inhibit the autoxidation of epinephrine in alkaline medium according to the method of Misra and Fridovich [13]. Catalase (CAT) activity was determined basing on its ability to decompose hydrogen peroxide according to the method of Luck [14]. Total protein concentration in liver homogenates was determined by the method of Lowry et al. [15].

Statistical analysis

Data were statistically evaluated using one-way analysis of variance (ANOVA) (Prism program for Windows, version 3, Graph Pad Software, Inc, San Diago CA, USA). The values were considered significant when $P<0.05$.

RESULTS

Anti-inflammatory status

Results in figure (Fig. 1) revealed that histamine induced acute phase rat hind paw oedema. The oedema volume was reduced significantly ($P<0.01$) by the administration of indomethacin (10 mg/kg), or each of earthworm extract EA and EP (100 mg/kg) after 1, 2 and 3 h of histamine administration.

Anti-pyretic activity

Injection of *Escherichia coli* suspension markedly elevated the rectal temperature after 1h of administration to rats. Treatments with each earthworm extract (EA and EP) at the doses 100 mg/kg decreased the rectal temperature compared to the standard antipyretic drug paracetamol (150 mg/kg). The result obtained from both paracetamol and earthworm extract EA and EP treated rats were compared with the control group and a significant reduction ($P<0.05$) in the fever that induced by *Escherichia coli* was observed after 4 four (Fig. 2).

Antioxidant activity

The level of glucose and transaminase activities (ALT and AST) in plasma of rats treated with CCl_4 was significantly increased compared to that of normal control. Treatment of CCl_4-treated rats with silymarin plus or EA and EP extracts restored the increase to about the normal control (Fig. 3).

Oxidative parameters in the table indicate that lipid peroxidation as TBARS (nmol/mg protein) was increased ($P<0.001$) in hepatic tissue of rats treated with CCl_4 compared to that of control group, however, restored to its normal control with co-treatment of rats with silymarin plus or EA and EP. The level of GSH and SOD and CAT activities were decreased in the hepatic tissue of rats treated with CCl_4 compared to control group. Silymarin plus and each of the earthworms extract treatment caused an increase in GSH level and the activities of SOD and CAT in the hepatic tissue compared to that of CCl_4-treated rats (Table 1).

DISCUSSION

Histamine is an important mediator of inflammation and it is a potent vasodilator that increases vascular permeability [16]. The present study reveal that histamine-induced paw oedema in rats was reduced by earthworm extract similar to

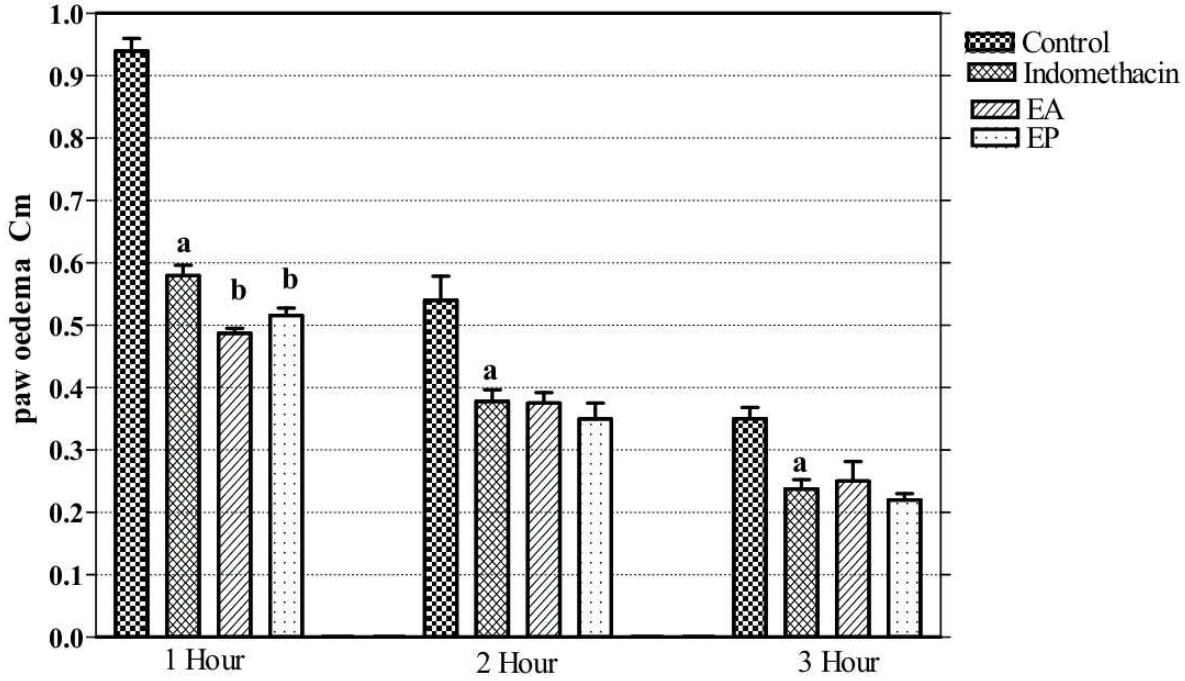

Fig. 1. Effect of treatment with *Allolobophora caliginosa* Savigny (EA and *Pheretima hawayana* Rosa (EP) extracts on histamine induced rat paw oedema volume compared to indomethacin.

• Data are the mean ± SE, where n=6.

• Columns with different letters are significantly different at probability at P<0.01. **a**: Means there is significant difference between the group of control and indomethacin and **b**: Means there is significant difference between the group of indomethacin and earthworm extract treated groups.

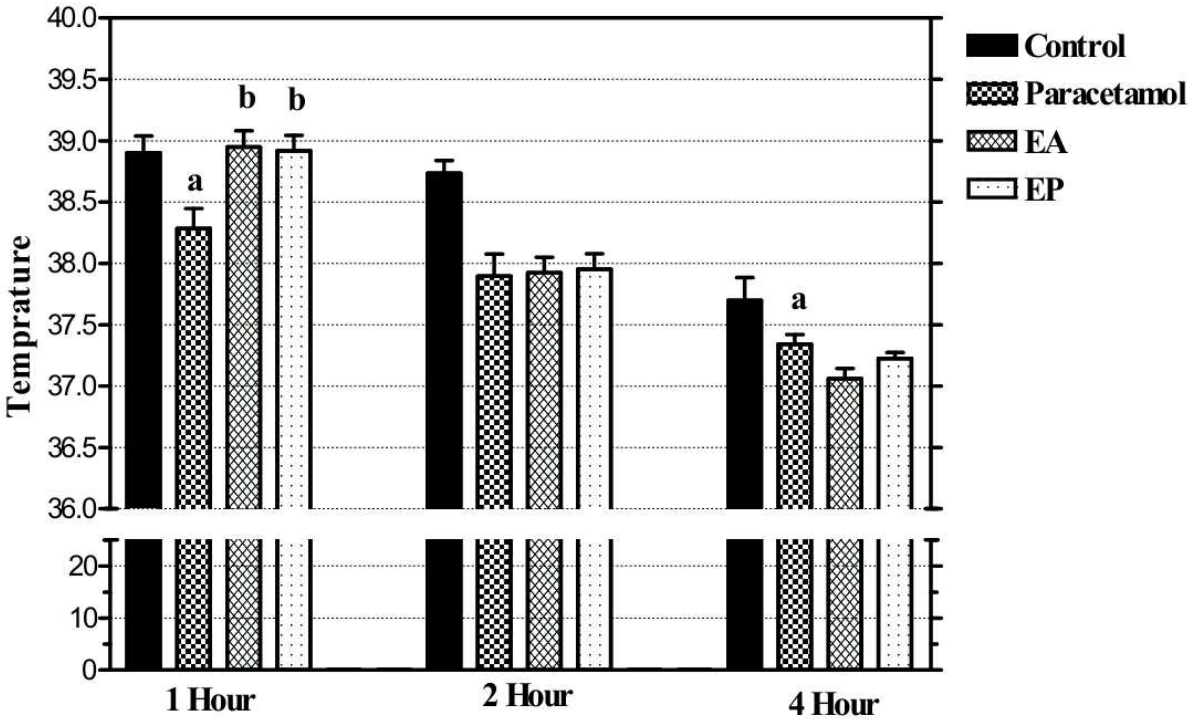

Fig. 2. Effect of treatment with *Allolobophora caliginosa* Savigny (EA) and *Pheretima hawayana* Rosa (EP) extracts compared to paracetamol on rectal temperature of rats induced by *Escherichia coli*.

• Data are Means ± SE, where n=6.

• Columns with different letters are significantly different at probability at P<0.05. **a**: Means there is significant difference between the group of control and paracetamol and **b**: Means there is significant difference between the group of paracetamol and earthworm extract treated groups.

indomethacin. This result indicates that EE has anti-transductive and anti-proliferative activities and the antihistaminic activity of the extract may be related to the inhibition of inflammation mediator [6]. Yegnanarayan et al. [17] found that the maximum anti-inflammatory activity at a dose 160 mg/kg of total earthworm extract extracted from petroleum ether than from other solvents like benzene, chloroform and ether. Also, Ismail et al. [18] established that, the petroleum ether fraction of total earthworm paste, has better anti-inflammatory activity in albino rat and they found that 160 mg/kg total earthworm paste functions similarly to that of aspirin in carrageenin-induced oedema.

The present study revealed that the earthworm extract significantly decreased *Escherichia coli* -induced fever. Fever is the body's natural defense because it creates an environment, which is not suitable for infectious agents and damaged tissue [19]. Suppression in elevating body temperature might be due to anti-inflammatory effects of the earthworm extract [6].

The present study, increased AST, ALT activities and glucose level in the rats treated with CCl_4 are due to extensive liver damage and alteration in the permeability of the hepatic cell membrane leading

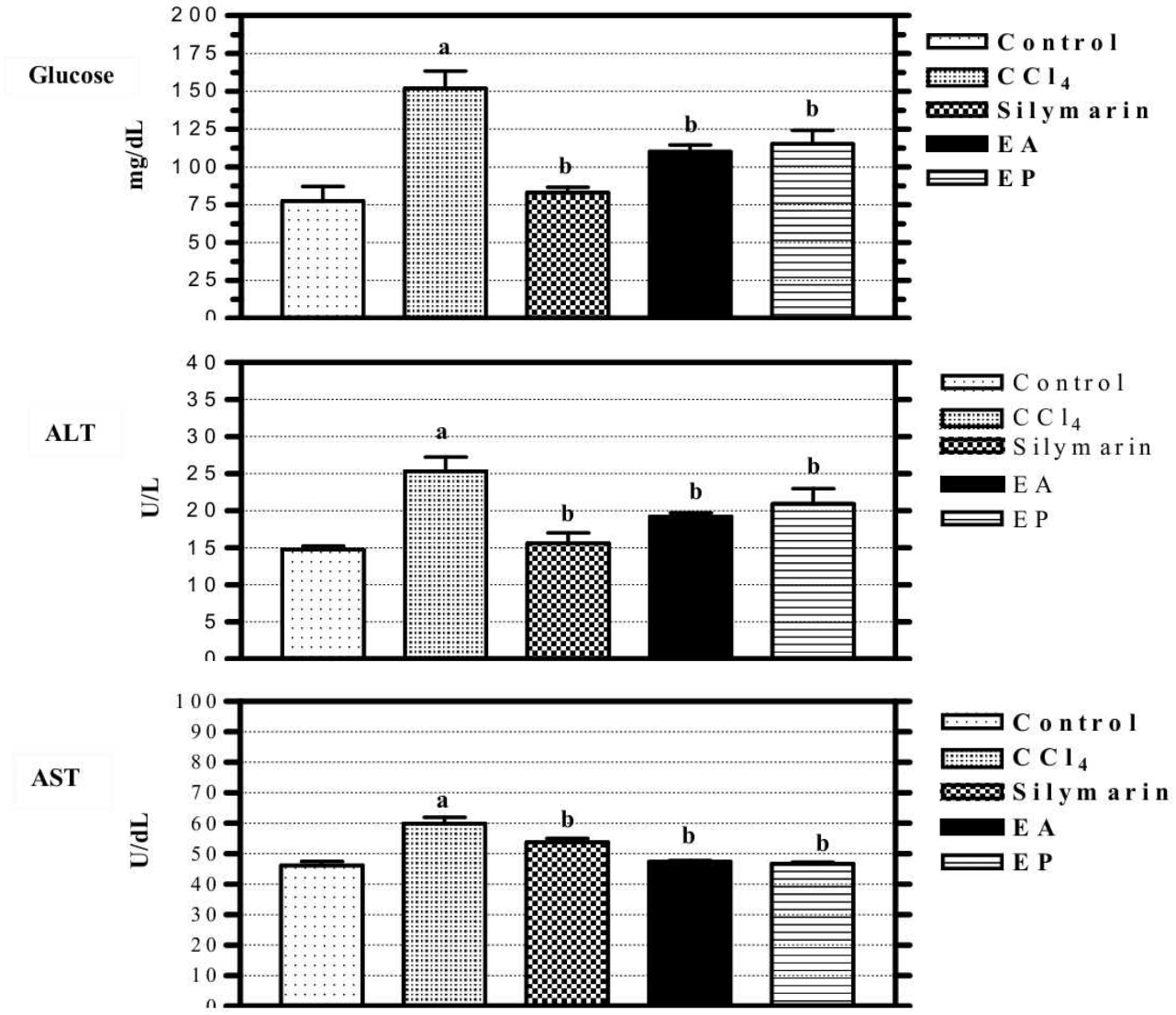

Fig. 3. Effect of treatment with *Allolobophora caliginosa* Savigny (EA) and *Pheretima hawayana* Rosa (EP) extracts compared to paracetamol compared to silymarin plus on plasma glucose, ALT, AST and albumin of the normal and CCl_4-treated rats.

• Data show are mean ± SE, where n=6.

• Columns with different letters are significantly different. **a**: Means there is significant difference between the group of control and CCl_4 and **b**: Means there is significant difference between the group of CCl_4 and silymarin plus and earthworm extract treated groups.

Table 1. Effect of treatment with each of *Allolobophora caliginosa* Savigny (EA) and *Pheretima hawayana* Rosa (EP) extracts compared to silymarin plus on oxidative stress parameters in the liver tissue of male albino rat treated with CCl_4.

- Values represent Means ± SE, where n=6; * P<0.05, ** P<0.01, *** P<0.001.
- a= Means there is significant difference between the group of control and CCl_4 treated group.
- b= Means there is significant difference between the group of CCl_4 and silymarin plus and earthworm extract treated groups

Groups / Parameters	Control	CCl_4	Silymarin plus	EA	EP
TBARs (nmol/mg proteins)	3.80±0.04	$7.24\pm0.24^{a***}$	$5.06\pm0.22^{b***}$	$4.63\pm0.54^{b***}$	$4.48\pm0.28^{b***}$
GSH (µmol/mg proteins)	7.05±0.24	$2.82\pm0.28^{a***}$	$5.15\pm0.25^{b**}$	4.35±0.07	4.45±0.10
SOD (U/min/mg proteins)	9.38±0.22	$5.27\pm0.24^{a***}$	$7.54\pm0.58^{b***}$	$8.12\pm0.58^{b***}$	$8.31\pm0.43^{b***}$
CAT (U/min/mg proteins)	1.65±0.12	$0.55\pm0.08^{a***}$	$2.22\pm0.49^{b***}$	$4.65\pm0.14^{b***}$	$3.60\pm0.095^{b***}$

to release of the enzymes into circulation [20-22]. Treatments with earthworm extract as well as silymarin plus decreased the activity of AST, ALT and glucose level, indicating that earthworm extract may protect and accelerate the hepatocytes regeneration. Similarly, Balamurugan et al. [23] found that serum ALT and AST levels increased markedly after the paracetamol administration and returned to its normal levels by treatment with earthworm extract. In addition, CCl_4 induced liver damage in rats was protected by *Phellinus merrillii* and *Coccinia grandis* extract [24, 25].

In the current study, the increase in the level of TBARS due to administration of CCl_4 indicates enhanced lipid peroxidation leading to tissue damage and failure of antioxidant defense mechanisms in preventing the formation of excessive free radicals [26]. Lipid peroxidation has been postulated as the destructive process in liver injury due to CCl_4 administration [27]. The hepatotoxic effects of CCl_4 are largely due to its active metabolite, trichloromethyl radical [28]. These activated radicals bind covalently to the macromolecules and induce peroxidative degradation of membrane lipids of endoplasmic reticulum rich in polyunsaturated fatty acids. This leads to the formation of lipid peroxides and degradation of biomembranes [29]. Treatment of rats that exposed to CCl_4 with earthworms extract significantly reduced the level of TBARS simialar to the silymarin plus, indicating its potential role to protect the hepatocytes. Similarily, extracts of stem and leaf of *Acathus montanus* and *Cassia tora* leaf pre-treatment protected against CCl_4 induced liver damage in rats as evidenced by marked decrease in lipid peroxidation [30, 31].

In the current study, it was observed that administration of earthworm extract caused a significant increase in activities of antioxidant enzymes SOD and CAT which diminished by CCl_4 treatment. Earthworm extract suppress the formation of reactive oxygen species and protect the antioxidant machinery like silymarin plus. Similarly, Balamurugan et al. [23] observed that administration of earthworm extract caused a significant increase in the hepatic activities of SOD and CAT in the paracetamol treated rats. CAT decomposes hydrogen peroxide and protects the tissues from highly reactive hydroxyl radicals. Therefore reduction in the activity of CAT may result in a number of deleterious effects due to the assimilation of superoxide radical and hydrogen peroxide. However, SOD scavenges the superoxide anion to form H_2O_2 and is a sensitive index for hepatocellular damage [32]. Moreover, methanolic extract of *Thespesia populnea* bark administered in the rats with CCl_4 caused increased in the activities of SOD and CAT [33].

In the present study, GSH content was significantly enhanced after earthworm extract treatment, confirming its capacity of scavenging free radicals. The same results was obtained by Balamurugan et al., [23] but with using paracetamol induced hepatotoxic effect instead of CCl_4. GSH removes free radical species such as H_2O_2, superoxide radicals and maintains membrane

protein thiols [34]. GSH was decreased while lipid peroxides was increased in hepatic tissue of male albino rats treated with CCl_4 [26, 35]. Moreover, the other cellular mechanism to prevent the oxidative stress damage by EE is the modulation of the genes of antioxidant enzymes, such as SOD and CAT [36, 37]. In conclusion the whole body extract of earthworms has anti-pyretic, anti-inflmmatory and antioxidant activity and the mode of action was various according to the species of earthworms.

ACKNOWLEDGEMENT

We thank Dr. Mohamed Hemida Abd Alla Prof. of Bacteriology, Botany Department, Assiut University for your help in the preparation of *Escherichia coli*.

TRANSPARENCY DECLARATION

The authors declare no conflicts of interest.

REFERENCES

1. Spoehr AH, Milner WH. The chemical composition of *Chlorella*; effect of environmental conditions. Plant Physiol 1949; 24 (1): 120–149.
2. Chen H, Takahashi S, Imamura M, Okutani E, Zhang ZG, Chayama K, Chen BA. Earthworm fibrinolytic enzyme: anti-tumor activity on human hepatoma cells in vitro and in vivo. Chin Med J 2007; 120 (20): 898-904.
3. Cooper EL. CAM, eCAM, Bioprospecting: The 21st century pyramid. Evidence-based Compl Alternative Med 2005; 2 (2): 125-127.
4. Prakash J, Gupta KS, Kochupillai V. Chemo preventive activity of *Withania somnifera* in experimentally induced fibro sarcoma tumors in Swiss albino rats. Phytother Res 2001; 15 (3): 240-244.
5. Balamurugan M, Parthasarathi K, Cooper EL, Ranganathan LS. Earthworm paste (*Lampito mauritii*, Kinberg) alters inflammatory, oxidative, haematological and serum biochemical indices of inflamed rat. European. Rev Med Pharmacol Sci 2007; 11: 77–90.
6. Balamurugan M, Parthasarathi K, Ranganathan LS, Cooper EL. Anti-inflammatory and anti-pyretic activities of earthworm extract — *Lampito mauritii* (Kinberg). J Ethnopharmacol 2009; 121 (2): 330-332.
7. Winter C, Risely E, Nuss G. Carrageenin induced oedema in hind paw of the rats as an assay for antiinflammatory drugs. Proc Soc Exp Biol Med 1962; 111: 544–547.
8. Al-Ghamdi M. The anti-inflammatory, analgesic and antipyretic activity of *Nigella sativa*. J Ethanopharmacol 2001; 76: 45–48.
9. Trinder P. Quantitative determination of glucose using the GOP-PAP method. Clin Biochem 1969; 6: 24-27.
10. Young DS. 1990. Effects of drugs on clinical laboratory tests. 3rd ed. Washington, DC. AACC Press.
11. Ohkawa H, Ohishi N, Yagi K. Assay for lipid peroxides in animal tissue by thiobarbaturic acid reaction. Analyt Biochem 1979; 95 (2): 351-358.
12. Beutler E, Duron O, Kelly BM. Improved method for the determination of blood glutathione. J Lab Clin Med 1963; 61: 882-888.
13. Misra HP, Fridovich I. The role of superoxide anion in the autoxidation of epinephrine and a simple assay for superoxide dismutase. J Biol Chem 1972; 247 (10): 3170-3175.
14. Luck H. 1963. Catalase. In: Methods of enzymatic analysis. Bergmeyer HU, editor. New York: Verlag Chemical and Academic Press, pp: 885-888.
15. Lowry OH, Rosebrough NJ, Farr AL, Randall RJ. Protein measurement with the Folin phenol reagent. J Biol Chem 1951; 41: 1863-1870.
16. Linardi A, Costa SKP, Da Silva GR, Antunes E. Involvement of kinins, mast cells and sensory neurons in the plasma exudation and paw edema induced by staphylococcal enterotoxin-B in the mouse. Eur J Pharmacol 2002; 399: 235–242.
17. Yegnanarayan R, Ismail S, Shortri D. Anti-inflammatory activity of two earthworm potions in Carrageenan pedal oedema test in rats. Indian J Physiol Pharmacol 1988; 32: 72–74.
18. Ismail SA, Pulandiran K, Yegnanarayan R. Anti-inflammatory activity of earthworm extracts. Soil Biol Biochem 1992; 24 (12): 1253-1254.
19. Zeil R, Krupp P. 1974. Temperature regulation and drug action. In: Schorbaum, E., Lomax, P., Jacob, J. (Eds.), 2nd International Symposium on The Pharmacology of Thermoregulation. Paris. S. Karger AG Publisher, Basel: pp. 233–241.
20. Park EJ, Jeon CH, Ko G, Kim J, Sohn DH. Protective effect of curcumin in rat liver injury induced by carbon tetrachloride. J Pharm Pharmacol 2000; 52 (4): 437–440.
21. Yokogawa K, Watanabe M, Takeshita H, Nomura M, Mano Y, Miyamoto K. Serum aminotransferase activity as a predictor of clearance of drugs metabolized by CYP isoforms in rats with acute hepatic failure induced by carbon tetrachloride. Int J Pharmaceut 2004; 269 (2): 479–489.
22. Minami K, Saito T, Narahara M, Tomita H, Kato H, Sugiyama H, Katoh M, Miki N, Yokoi T. Relationship between hepatic gene expression profiles and hepatotoxicity in five typical hepatotoxicant administered rats. J Toxicol Sci 2005; 87 (1):

296–305.

23. Balamurugan M, Parthasarathi K, Ranganathan LS, Cooper EL. Hypothetical mode of action of earthworm extract with hepatoprotective and antioxidant properties. J Zhejiang Univ Sci 2008; 9 (2): 141–147.
24. Chang HY, Peng WH, Sheu MJ, Huang GJ, Tseng MC, Lai MT, Ho YL, Chang YS. Hepatoprotective and antioxidant effects of ethanol extract from *Phellinus merrillii* on carbon tetrachloride-induced liver damage. Am J Chin Med 2007; 35 (5): 793–804.
25. Kumar PV, Sivaraj A, Elumalai EK, Kumar BS. Carbon tetrachloride-induced hepatotoxicity in rats-protective role of aqueous leaf extracts of *Coccinia grandis*. Intl J Pharm Tech Res 2009; 1 (4): 1612-1615.
26. Gupta K, Chitme H, Dass SK, Misra N. Antioxidant activity of *Chamomile recutita capitula* methanolic extracts against CCl_4-induced liver injury in rats. J Pharmacol Toxicol 2006; 1: 101-107.
27. Vajdovich P, Szilagyi A, Gall T. Evaluating of blood lipid peroxidation parameters in carbon tetrachloride (CCl_4) toxicity in sheep. Acta Vet Hung 1995; 43 (3): 423–429.
28. Johnson D, Kroening C. Mechanism of early carbon tetra chloride toxicity in cultured rat hepatocytes. Pharmacol Toxicol 1998; 83 (6): 231–239.
29. Kaplowitz N, Aw TY, Simon FR, Stolz A. Drug induced hepatotoxicity. Ann Intern Med 1986; 104 (6): 826–839.
30. Patrick-Iwuanyanwu KC, Wegwu MO. Prevention of carbon tetrachloride (CCl_4)-induced liver damage in rats by *Acanthus montanus*. Asian J Biochem 2008; 3: 213-220.
31. Rajan VA, Shanmugavalli N, Sunitha GC, Mashankar V. Epatoprotective effects of *Cassia tora* on CCl_4 induced liver damage in albino rats. Indian J Sci Technol 2009; 2 (3): 41-44.
32. Curtis J, Mortiz M, Snodgrass PJ. Serum enzymes derived from liver cell fraction and response to carbon tetrachloride intoxication in rats. Gastroenterol 1972; 62 (1): 84–92.
33. Ilavarasan R, Vasudevan M, Anbazhagan S, Venkataraman S, Sridher S. Hapatoprotective activity of *Thespesia populnea* bark extracts against carbon tetrachloride-induced liver injury in rats. Nat Prod Sci 2003; 9 (2): 83–86.
34. Prakash M, Balamurugan M, Parthasarathi K, Gunasekaran G, Cooper EL, Ranganathan LS. Anti-ulceral and anti-oxidative properties of “earthworm paste” of *Lampito mauritii* (Kinberg) on *Rattus norvegicus*. Eur Rev Med Pharmacol Sci 2007; 11: 9-15.
35. Venukumar M, Latha MS. Antioxidant activity of *Curculigo orchioides* in carbon tetrachloride-induced hepatopathy in rats. Indian J Clin Biochem 2002; 17 (2): 80-87.
36. Shull S, Heintz HN, Periasamy M, Manohor M, Jansseny YM, Marsh JP, Mossman TB. Differential regulation of antioxidant enzymes in response to oxidants. J Biol Chem 1991; 266 (36): 24398-24403.
37. Crawford D. 1999. Regulation of mammalian gene expression by reactive oxygen spicies. In: Gilbert D, Cotton C. (Eds.). Reactive oxygen species in biological system. Plenum, New York, pp. 155-171.

Journal of Biology and Earth Sciences

BIOLOGY ORIGINAL ARTICLE

Evaluation of some bean lines tolerance to alkaline soil

Abeer A. Radi[1], Dalia A. Abdel-Wahab[2], Afaf M. Hamada[1]

[1]Botany Department, Faculty of Science, Assiut University, Assiut, 71516 Egypt

[2]Science & Mathematics Department, Faculty of Education, Assiut University, New Valley, Egypt

ABSTRACT

Introduction: In less arid climates, salts are less concentrated and sodium dominates in carbonate and bicarbonate forms, which enhance the formation of alkaline soils. The development and identification of salt-tolerant crop cultivars or lines would complement salt management programs to improve the productivity and yields of salt stressed plants.

Materials and methods: This work was to study the evaluation of alkalinity tolerance of some bean lines grown under different levels of sodium carbonate (Na_2CO_3) to select the most alkalinity tolerant lines versus the most-sensitive ones out of 6 lines of the test plants.

Results: The symptoms induced by alkalinity included reduction in root, shoot growth, and leaf area which were more severe in some bean lines. Potassium leakage was severely affected by alkalinity in some lines at all tested levels, while in some others a moderate damage was manifested only at the higher levels. The increase in Na_2CO_3 level was associated with a gradual fall in chlorophyll a and b biosynthesis of all the test bean lines. However, alkalinity at low and moderate levels had a favourable effect on the biosynthesis of carotenoids in all the test bean lines. The increase in Na_2CO_3 supply had a considerable stimulatory effect on sodium accumulation, while potassium accumulation fluctuated in organs of bean lines.

Conclusion: Assiut 1104 out of all the different lines investigated was found to display the lowest sensitivity to alkalinity stress, while Assiut 12/104 was the most sensitive one.

Key words: alkalinity, bean, leaf area, photosynthetic pigments, potassium, sodium.

J Biol Earth Sci 2012; 2(1): B18-B27

Corresponding author:
Prof. Afaf M. Hamada
The Department of Botany, Stockholm University
SE-106 91 Stockholm, Sweden
Fax: +46 (0)8- 165525, Tel.: +46 (0)8- 163759
e-mail: afafhamada@yahoo.com

Original Submission: 27 January 2012; Revised Submission: 06 February 2012; Accepted: 07 February 2012

ISSN: 2084-3577
http://www.journals.tmkarpinski.com/index.php/jbes or http://jbes.strefa.pl
e-mail: jbes@interia.eu

INTRODUCTION

Salinity stress is a widespread environmental problem. Although considerable effort has been devoted to solve this problem, two very important aspects have been neglected, i.e. salt-alkali stress and complex salt stress. Most of salinity and all of the sodicity develop naturally. However, a significant proportion of recently cultivated agricultural land has become saline because of land clearing or irrigation. Among these, saline and alkaline soils are the major constraints limiting economic yields of crop plants.

The problem of soil alkalinization due to $NaHCO_3$ and Na_2CO_3 may be more severe than the problem of soil salinization caused by the neutral salts, such as sodium chloride (NaCl) and sodium sulphate (Na_2SO_4), as the alkaline salts are more destructive to plants than neutral salts [1-3]. Some reports clearly demonstrated that alkali stress was more severe than salt stress [4, 5]. Generally, salt stress involves osmotic effects and specific ion effects [6], the former mainly dependent on salt concentration. For alkali stress, in addition to these two types of effects, there is another important factor, high pH. Because soil salinization and alkalinization frequently co-occur, the conditions in the naturally salinized and alkalinized soil are very complex. Salt stress changes the morphological, physiological and biochemical responses of plants [7, 8]. High salinity disturbs intracellular ion homeostasis, leading to membrane damage, metabolic inactivation and secondary effects that ultimately result in cell death [9, 10].

Soil salinization is an irreversible occurrence [11], which necessitates the creation of new salt-resistant and economic crop plants. To create such genotypes, we have to comprehend the biochemical mechanisms forming the basis of salt resistance. Morphophysiological traits for breeding of salt tolerance are extensively reviewed elsewhere [12]. They are based on the understanding that the mechanisms of salinity tolerance fall into any of the following categories: tolerance to osmotic stress; Na^+ exclusion from leaves; or tolerance of tissue to accumulated Na^+ [12].

Vicia faba beans are considered the main legume of Middle Eastern countries [13]. Also, Cordovilla et al. [14] reported that faba bean is often grown on saline soils in the Middle East and Mediterranean regions. The importance of beans in Egypt is as an essential and relatively inexpensive dietary source of protein for both humans and animals. In Egypt, faba bean represents about 2 percent of the value of field crops, occupying about 123 480 hectares (ha) out of the total 6.5 million ha of cropped area [15].

Therefore, increasing salinity and alkaline tolerance for bean genotypes is one of the cheap methods to spread growing bean in salinized and alkalinized areas. Thus, the aim of this work was to investigate and compare the effect of alkalinity on growth criteria, membrane damage, photosynthetic pigments and ions accumulation of six bean lines grown under controlled conditions, in order to assess Na_2CO_3 alkalinity tolerance, to order lines with respect to their response to the alkaline stress.

MATERIALS AND METHODS

Plant material

All the studies were carried out at seedling stage in six faba bean (*Vicia faba* L.) lines: Assiut 1104, Assiut 12/104, Assiut 6/84, Assiut 115, Assiut 295 and Assiut 1/67, were kindly provided by Agronomy Department, Faculty of Agriculture, Assiut University. Different alkalinity stress treatments were imposed to these seedlings. The whole experiment was replicated twice.

Culture technique and experimental design

Well-selected bean seeds were surface-sterilized in 20% (v/v) commercial bleach for 20 min, rinsed thoroughly in distilled water and soaked in distilled water for 12 h, then sown in 10 cm diameter plastic pots lined with polyethylene bags, each contains 4 seeds in one kg of soil composed of mixed sieved air-dried clay and sand (2:1 by volume) and kept at approximately 100% of the field capacity. In this work a completely randomized design was adopted with six replicates.

The experiment was carried out using six test lines in order to determine the lowest alkalinity-sensitive line versus the highest sensitive one. Each bean line was grown in culture media supplied with: 0, 10, 20, 40, 60, 80 and 100 mM Na_2CO_3 (pH ranging from 8.24-10) and re-watered with the previous levels of Na_2CO_3. The test plants were left to grow under the previously mentioned conditions till the end of experimental period which extended to 35 days.

Determination of fresh, dry weight and leaf area

Fresh weight was determined directly after harvest of plants. The dry weight was obtained after drying the plant tissues for 48 h at 72ºC. Leaf area was measured using the disk method [16].

Potassium leakage

Cell membrane stability was carried out as given by Premachandra et al. [17]. Potassium leakage was determined by flame photometer according to the method described by Williams and Twine [18].

Determination of photosynthetic pigments

The fractions of pigments (chlorophyll a, chlorophyll b and carotenoids) were estimated using the spectrophotometric method recommended by Lishtenthaler [19].

Sodium and potassium concentration

Sodium and potassium were determined by flame photometer method [18].

Statistical analysis

Data were subjected to statistical analysis using statistical programme package SPSS (version 16). The one-way analysis of variance (ANOVA) followed by Duncan multiple range test were employed and the differences between individual means were deemed to be significant at $p<0.05$.

RESULTS

Shoot and root growth

Plant growth is considered as an indicator for the response of different plant systems to alkalinity stress. The symptoms induced by alkalinity included reduction in root, shoot growth, and leaf area which were more severe in some lines (Figs. 1 and 2). The fresh and dry matter yield of root and shoot showed marked decreases as the level of Na_2CO_3 was increased. The adverse effect of alkalinity stress was clearly demonstrated by bean lines treated with 60 and 80 mM Na_2CO_3. On the other hand, it was noticed that the successive increases in alkalinity level did not attenuate the fresh and dry matter gain in bean line Assiut 1104 as severely as in case of line Assiut 12/104. Moreover, injurious effects followed by the death of the test plants at the end of the experimental period were exhibited by all bean lines at 100 mM Na_2CO_3.

Leaf area

The data herein obtained clearly demonstrate that the leaf area was substantially affected by the different alkalinity levels (Fig. 2). The increase in alkalinity in the culture medium was generally associated with a gradual fall in leaf area in almost all the tested bean lines. The presence of Na_2CO_3, in the culture medium at a concentration of 80 mM greatly, reduced leaf area of line Assiut 12/104 than the other ones. However, the leaf area in Assiut 1104 was nearly as twice as that of the most sensitive line Assiut 12/104.

Membrane damage and potassium leakage

The cellular membrane dysfunction due to stress is well expressed in increased permeability and leakage of ions. Potassium leakage is usually used as a criterion for the stability and integrity of membranes. In the present work, K^+ efflux from the leaves of bean lines increased in response to increasing levels of Na_2CO_3 in the culture medium (Fig. 3). The adverse effects of alkalinity treatments on K^+ leakage were more pronounced in line Assiut 12/104 than other ones. The percentage of K^+ leakage from this bean line at 80 mM was almost two-fold that observed in case of Assuit 1104 line.

Photosynthetic pigments

The effect of Na_2CO_3 supply on photosynthetic pigments (chlorophyll a, chlorophyll b, chlorophylls a+b and carotenoids) biosynthesis in leaves of six bean lines was examined in the present study. Results presented in Fig. 4 indicate that the increase in Na_2CO_3 level in the culture medium was generally associated with a significant or non-significant gradual fall in chlorophyll a and b biosynthesis in leaves of all the test bean lines. However, it could be noticed that the successive increases in the alkalinity level did not reduce chlorophyll a biosynthesis as severely as chlorophyll b. On the other hand, alkalinity up to 60 mM had a favourable effect on the biosynthesis of carotenoids in all the test bean lines.

Sodium and potassium concentration

Considerable differences in Na^+ and K^+ concentration in the test bean lines were induced by the various levels of alkalinity (Figs. 5 and 6).

a. Sodium concentration

The effectiveness of the different Na_2CO_3 levels on Na^+ accumulation varied in the different organs

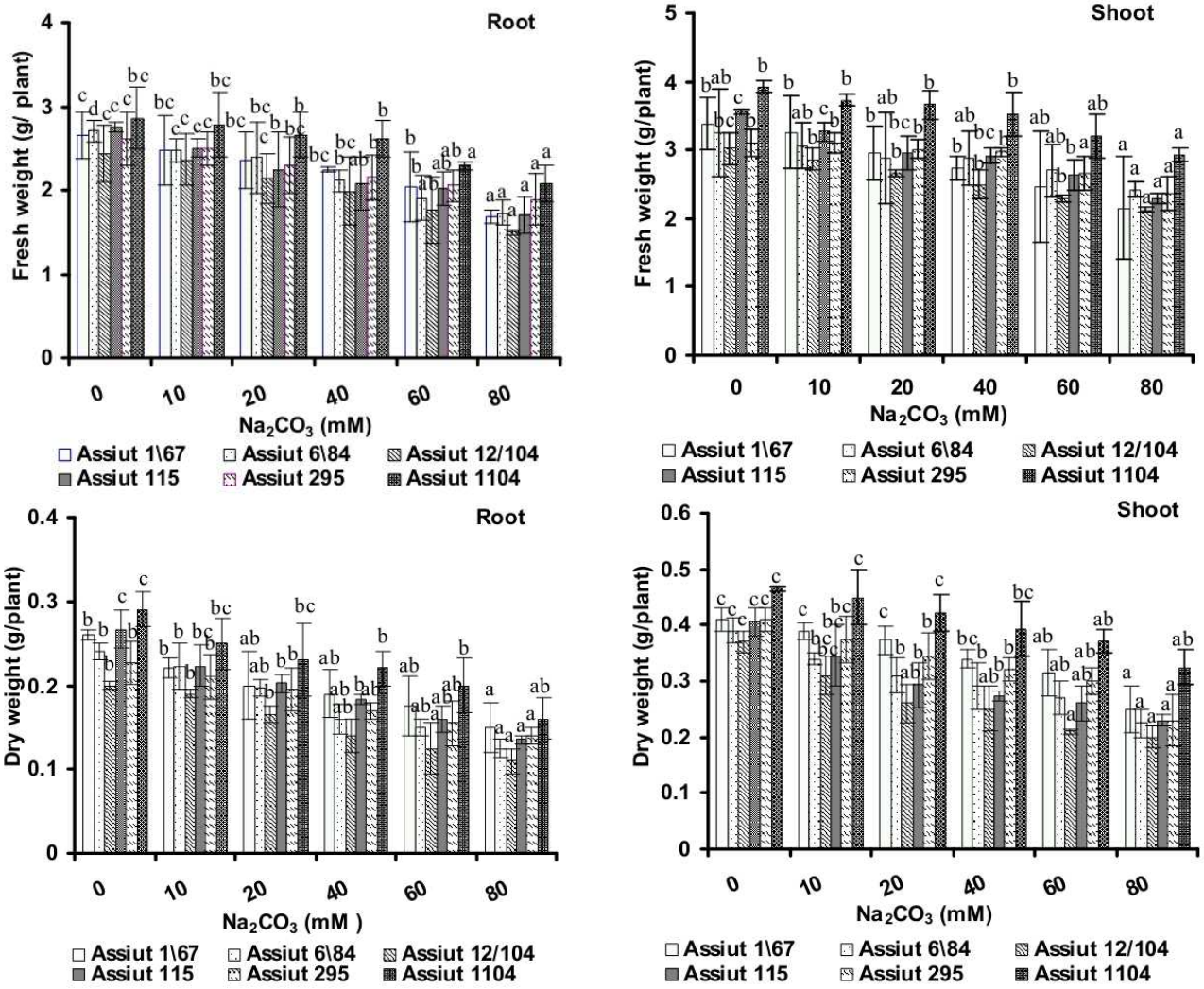

Fig. 1. Effect of different concentrations of Na_2CO_3 on fresh and dry weight of roots and shoots of 35-day-old bean lines. The data are given as averages of six replicates from two independent experiments ± standard division. Bars carrying different letters within each cultivar are significantly different at P<0.05.

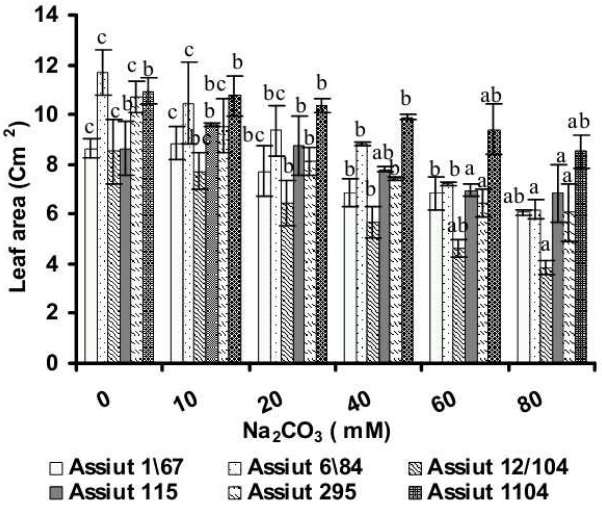

Fig. 2. Effect of different concentrations of Na_2CO_3 on leaf area of 35-day-old bean lines. The data are given as averages of six replicates from two independent experiments ± standard division. Bars carrying different letters within each cultivar are significantly different at P<0.05.

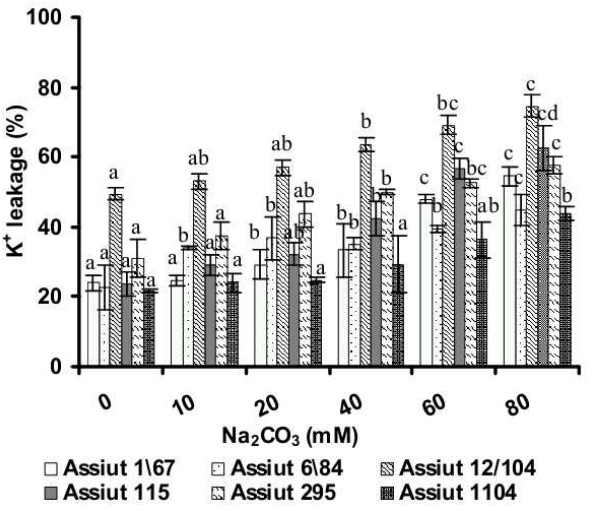

Fig. 3. Effect of different concentrations of Na_2CO_3 on % of K^+ leakage from leaves of 35-day-old bean lines. The data are given as averages of six replicates from two independent experiments ± standard division. Bars carrying different letters within each cultivar are significantly different at P<0.05.

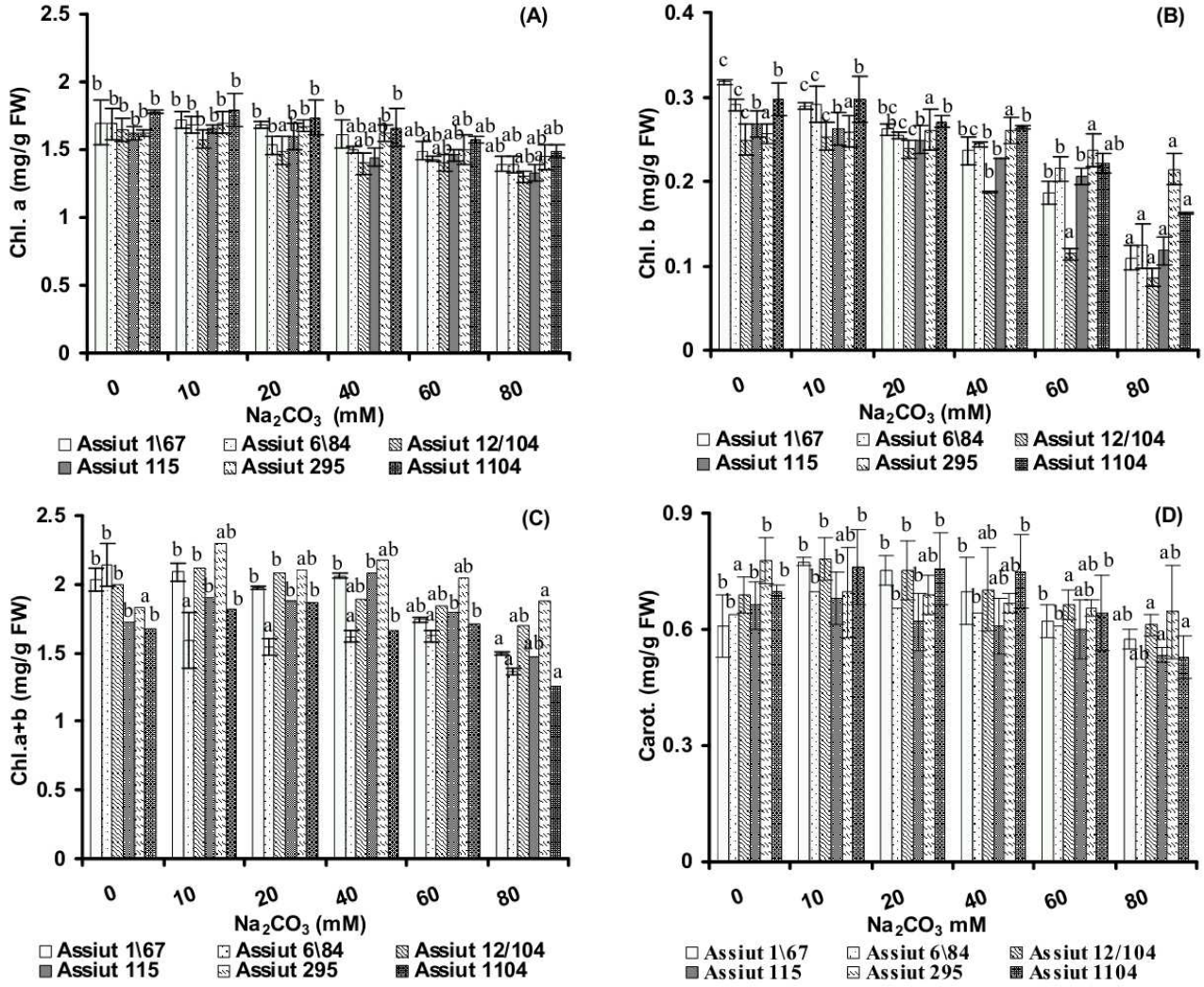

Fig. 4. Effect of different concentrations of Na_2CO_3 on photosynthetic pigments of 35-day-old bean lines (A) chlorophyll a (chl. a), (B) chlorophyll b (chl. b), (C) chlorophyll a+b (chl. a+b) and (D) carotenoids (carot.). The data are given as averages of six replicates from two independent experiments ± standard division. Bars carrying different letters within each cultivar are significantly different at $P<0.05$.

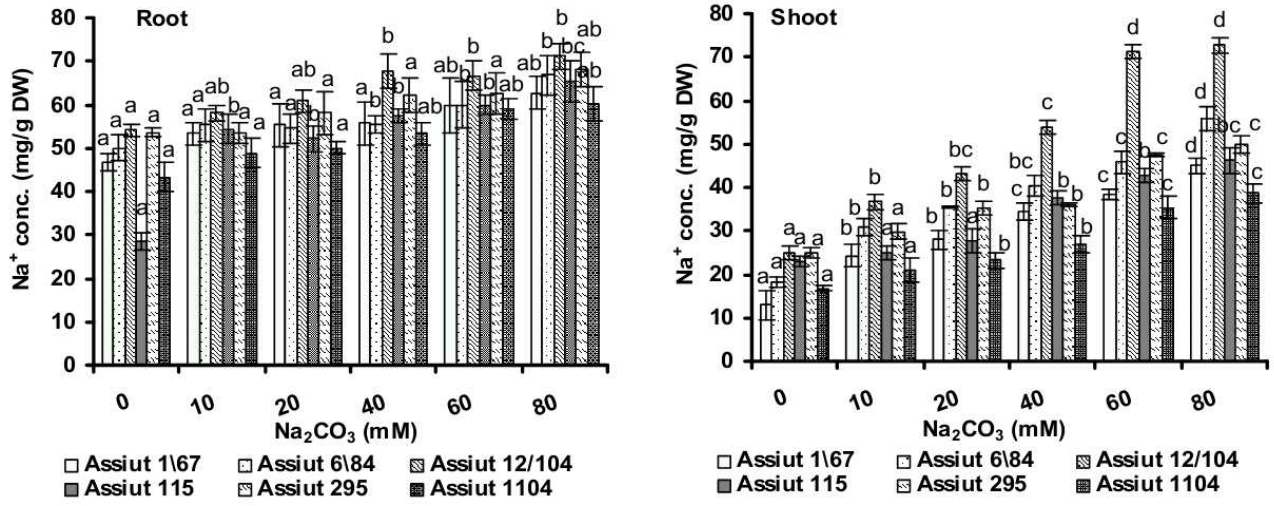

Fig. 5. Effect of different concentrations of Na_2CO_3 on sodium concentration of roots and shoots of 35-day-old bean lines. The data are given as averages of six replicates from two independent experiments ± standard division. Values followed by the different letters within each column are significantly different at $P<0.05$.

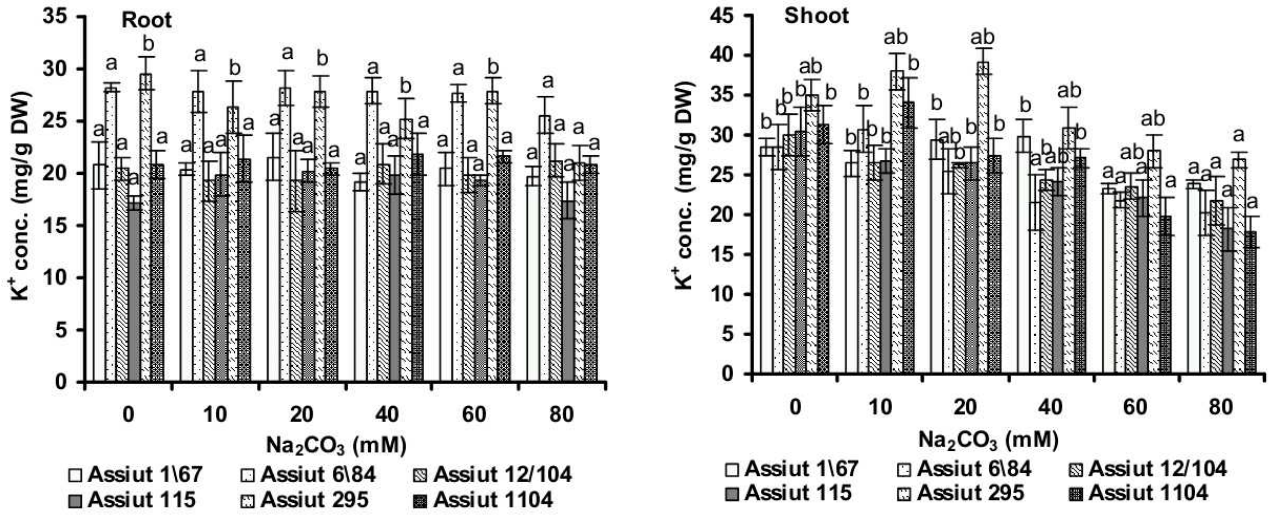

Fig. 6. Effect of different concentrations of Na_2CO_3 on potassium concentration of roots and shoots of 35-day-old bean lines. The data are given as averages of six replicates from two independent experiments ± standard division. Values followed by the different letters within each column are significantly different at P<0.05.

of the test plants. It is clear that when Na_2CO_3 was provided in high concentrations (60 and 80 mM) more Na^+ was accumulated in shoots of bean lines than when supplied in relatively lower level (10 mM) in the culture medium. On the other hand, all the investigated levels of Na_2CO_3 induced a significant or non-significant stimulatory effect on the accumulation of Na^+ in most bean lines roots. It is worth mentioning that Assiut 12/104 line, which is the most sensitive one, accumulated the highest Na^+ concentration in roots and shoots.

b. Potassium concentration

The results given in Fig. 6 demonstrate that the K^+ concentration in roots and shoots of the experimental lines was markedly affected by Na_2CO_3 level in the culture media. Potassium concentration declined considerably in the shoots at the highest level of the applied salt (80 mM), while it slightly affected in roots of the treated plants.

DISCUSSION

The growth reflects many vital plant activities during vegetative growth and so is a good index for measuring plant responses to various stresses. The results of this study indicate that the different concentrations of Na_2CO_3 result in remarkable differences between the studied six broad bean lines in their tolerance to alkalinity stress. The data indicated the adverse effect of alkalinity stress was clearly demonstrated by some bean lines treated with 60 and 80 mM Na_2CO_3. The deleterious effects of Na_2CO_3 on growth of broad bean lines and development obtained from results of the present study of fresh and dry matter of root and shoot indicated that the high pH and ion imbalance around the rhizosphere caused by alkaline salt [20-23]. The growth inhibitory effects of salinity can also be affected by variation in the activity of calcium or potassium ions in the saline root medium [24]. Moreover, growth reduction can be ascribed to a reduced cell-extension growth because of lower plastic cell-wall extensibility [25]. Decreased cell-wall extensibility is partially explained by limited apoplastic acidification in sensitive maize species caused by osmotic stress [26, 27].

The data herein obtained demonstrated that increase in alkalinity in the culture medium at 80 mM level greatly reduced leaf area of line Assiut 12/104 than the other ones. A reduction in leaf area with excess alkalinity has been reported for several greenhouse crops (chrysanthemum, mini-rose, vinca, and hibiscus) irrigated with alkaline water [28]. Mohamedin et al. [29] reported that leaf area index of sunflower plants grown on saline, saline alkali and alkaline soils significantly decreased as compared with those obtained from plants grown on non saline soil. This means that the growth of sunflower seedlings was inhibited by salinity and alkalinity. Both stresses together tended to be more serious in plants grown on alkaline soil relative to those grown on saline and saline alkali soils [29]. This means that the deleterious effects on growth by salinity were more pronounced with increasing alkalinity. Confirming the results obtained here Sanchez Blanco et al. [30], Serpil et al. [31] and Shi

and Sheng [32] reported that the effect of salinity and alkalinity on leaf area were significant. These authors concluded that the effects of salinity and alkalinity on electrolyte leakage rate were insignificant and the effect of alkalinity was greater than that of salinity. They added that stressed plants had a significantly lower leaf area than the control ones and the most important effect of stress was the reduction of leaf area and decreased growth rate. Also, Heuer [33] concluded that differences in biomass allocation may play a significant role under field conditions as maintenance of leaf area is crucial for allowing good crop yield in salt-treated plants.

The permeability of plasma membrane is a clear index that reflects the degree of stress-induced injury to plants [34, 35]. The permeability of the cell membrane of *Aneurolepidium chinense* seedlings was not only increased with rising salinity but also with rising alkalinity, thus the stress caused injury on plasma membrane [36]. In this study, high alkalinity (60, 80 mM Na_2CO_3) treatments induced significant increases in electrolyte leakage in the stressed plants compared with those in the control ones. Similar results were obtained by Lutts et al. [37] and Kaya et al. [38] who reported that high salt concentration increased the membrane permeability of sensitive rice varieties and strawberry plants, respectively. In the present investigation, K^+ efflux of the bean lines leaves increased in response to increasing levels of Na_2CO_3 in the culture medium. In this connection, Tuna et al. [39, 40] reported that electrolyte leakage increased in the leaves of maize plants grown under salt stress.

Chlorophylls and carotenoids are the main photosynthetic pigments of higher plants. In the current study, the increase in Na_2CO_3 level in the culture medium was associated with a gradual fall in chlorophyll a and b biosynthesis in leaves of all bean lines. However, alkalinity up to 60 mM had a favorable effect on the biosynthesis of carotenoids in all the tested bean lines. Such findings agree with Shi and Zhao [41] who reported that alkalinity stress might be caused Mg^{2+} precipitation and led to inhibition of chlorophyll synthesis. Alternatively, alkalinity stress might enhance the activity of the chlorophyll degrading enzyme chlorophyllase [42]. Alkalinity stress interferes with selective absorption for K^+-Na^+ in roots and results in high intracellular content of Na^+ to the disturbed sub-cellular partition of Na^+, which would cause the high Na^+ in cytoplasm and the destruction of structure and function of chloroplasts [3]. Also, Elstner [43] reported that the disturbance of the balance of certain ions (e.g. Na^+) under saline and alkaline conditions could inhibit proteinase activity and alter the chlorophyll concentration in leaves, leading to reduced photosynthesis in the plants. Iron deficiency may be another possible reason for the reduction of Chl concentration. Iron is essential for the proper functioning of multiple metabolic and enzymatic processes such as electron transport, nitrogen fixation, Chl biosynthesis and photosynthesis [44, 45] during plant growth and development. Though there was sufficient iron in the treatment solutions, the high pH can cause chemical reactions that make iron insoluble into solid forms and unavailable to plant roots. The reduction in Chl concentration during the growing season can reduce plant growth, vigor, and tolerance to stress conditions [46].

Sodium and potassium are important components of salt stress [47]. Usually, Na^+ increases and K^+ decreases in salt stressed plants [48]. It is accepted that competition exists between Na^+ and K^+ leading to a reduced level of internal K^+ at high external NaCl concentration [49, 50]. This can result in high Na:K ratios that reduce plant growth and eventually become toxic [51, 52]. This phenomenon could be attributed to cation imbalance in plasma membrane which is destroyed more severely by alkaline stress. In this investigation, variations in the accumulation of Na^+ and K^+ were induced by the different concentrations of Na_2CO_3 (10-80 mM). Application of this salt in soil caused Na^+ accumulation in the test bean plants, and the highest Na^+ content in shoots and roots was consistently found in plants subjected to the highest salt level. It was found that the bean line Assuit 12/104 accumulated more Na^+ in its shoots and roots compared with Assuit 1104. Legumes in general respond to salinity by excluding Na^+ ions from their leaves. In fact, salt tolerance of glycophytes is believed to be related to their ability to avoid accumulating excess monovalent cations in their leaves [53, 54]. In this context, Schachtman and Munns [55] reported that salt tolerant *Triticum* species had lower rate of Na^+ accumulation than the salt-sensitive ones. Na^+ concentration in shoots increased as the amount of salt provided in the growing medium increased [56]. Differences in Na^+ accumulation may also be involved in genotypic performance under saline conditions [57], which suggests that toxic ions may accumulate more in

the susceptible genotypes due to higher transpiration.

The data obtained in this study demonstrate that Assiut 1104 out of all the test lines was found to display the lowest sensitivity to alkalinity stress, while Assiut 12/104 was the most sensitive line. Na^+ exclusion and a subsequent high K^+/Na^+, usually from leaves and shoots, have been proposed as screening traits for tolerance to moderate salinity [58, 59]. It is widely accepted that competition exists between Na^+ and K^+ leading to a reduced level of internal K^+ at high external salinity concentration [60, 61]. This competition could be at uptake level or transport level or both. In maize, salinity decreased growth due to K^+ deficiency induced by excessive Na^+ which caused reduction in uptake and translocation of K^+ to shoots [60]. Also, Hafsi et al. [62] observed that salinity decreased K^+ concentration in all organs, except for roots of *Hordeum maritimum* plants. Tuna et al. [40] reported that K^+ concentration in leaf and root tissues was much lower in salinity stressed maize plants compared to unstressed ones. This trend could be explained by: (1) a reduction in the performance of the absorption system, and consequently a limitation of K^+ absorption [63], and/or (2) a competition for the uptake of K^+ and Na^+ ions [64].

In the light of the precedent experiment, Assiut 1104 out of all the test lines was found to display the lowest sensitivity to alkalinity stress, while Assiut 12/104 was the most sensitive line. No consistent line differences in growth criteria were found in the remaining four lines. This genotypic ranking agrees with Yousfi et al. [56, 59], who suggested that genetic variability for salinity tolerance in durum wheat is maintained through the entire crop cycle. Therefore, genotypic evaluation during the first part of the crop cycle (perhaps even at the seedling stage) may be a valid option to select for salt tolerance in durum wheat.

TRANSPARENCY DECLARATION

The authors declare no conflicts of interest.

REFERENCES

1. Shi DC, Yin LJ. Difference between salt (NaCl) and alkaline (Na_2CO_3) stresses on *Puccinellia tenuiflora* (Griseb.) Scribn. et Merr. plants. Acta Bot Sin 1993; 35: 144–149.
2. Yang CW, Chong JN, Kim CM, Li CY, Shi DC, Wang DL. Osmotic adjustment and ion balance traits of an alkali resistant halophyte *Kochia sieversiana* during adaptation to salt and alkali conditions. Plant Soil 2007; 294: 263–276.
3. Yang CW, Wang P, Li CY, Shi DC, Wang DL. Comparison of effects of salt and alkali stresses on the growth and photosynthesis of wheat. Photosynthetica 2008; 46: 107-114.
4. Campbell SA, Nishio JN. Iron deficiency studies of sugar beet using an improved sodium bicarbonate-buffered hydroponics growth system. J Plant Nutr 2000; 23: 741–757.
5. Hartung W, Leport L, Ratcliffe RG, Sauter A, Duda R, Turner NC. Abscisic acid concentration, root pH and anatomy do not explain growth differences of chickpea (*Cicer arietinum* L.) and lupin (*Lupinus angustifolius* L.) on acid and alkaline soils. Plant Soil 2002; 240: 191-199.
6. Munns R. Comparative physiology of salt and water stress. Plant Cell Environ 2002; 25: 239-250.
7. Amirjani MR. Effects of salinity stress on growth, mineral composition, proline content, antioxidant enzymes of soybean. Am J Physiol 2010; 5: 350-360.
8. Siringam K, Juntawong N, Cha-um S, Kirdmanee C. Salt stress induced ion accumulation, ion homeostasis, membrane injury and sugar contents in salt-sensitive rice (*Oryza sativa* L. spp. indica) roots under isoosmotic conditions. Afr J Biotechnol 2011; 10: 1340-1346.
9. Flowers TJ. Improving crop salt tolerance. J Exp Bot 2004; 55: 307–319.
10. Anil VS, Krishnamurthy H, Mathew MK. Limiting cytosolic Na^+ confers salt tolerance to rice cells in culture: a two-photon on microscopy study of SBFI-loaded cells. Physiol Plantarum 2007; 129: 607–621.
11. Rozema J, Flowers T. Crops for a salinized world. Science 2008; 322: 1478–1480.
12. Munns R, Tester M. Mechanisms of salinity tolerance. Annu Rev Plant Biol 2008; 59: 651–681.
13. Shetty P, Atallah MT, Shetty K. Stimulation of total phenolics, L-DOPA and antioxidant activity through proline linked pentose phosphate pathway in response to proline and its analogue in germinating faba bean (*Vicia faba* L.). Process Biochem 2003; 38: 1707-1717.
14. Cordovilla MP, Ligero F, Lluch C. Effects of NaCl on growth and nitrogen fixation and assimilation of inoculated and KNO_3 fertilized *Vicia faba* L. and *Pisum sativum* L. plants. Plant Sci 1999; 140:

127–136.

15. FAO. 2005. Global network on integrated soil management for sustainable use of salt-affected soils. FAO land and plant nutrition management service, Rome, Italy: FAO Land and Plant Nutrition Management Service. Available in: http://www.fao.org/ag/agl/agll/spush.
16. Watson DJ, Watson MA. Studies in potatoes agronomy. Effect of variety, seed size and spacing on growth, development and yield. J Agricult Sci 1953; 66: 241–249.
17. Premachandra GS, Saneoka AH, Fujta K, Ogata S. Leaf water relations, osmotic adjustment, cell membrane stability, epicuticular wax load and growth as affected by increasing water deficits in sorghum. J Exp Bot 1992; 43: 1569-1576.
18. Williams V, Twine S. 1960. Flame photometric method for sodium, potassium and calcium. In: Modern Methods of Plant Analysis by Peach K. and Tracey MV. Springer-Verlag Berlin, 56: 6-12.
19. Lishtenthaler HK. 1987. Chlorophylls and carotenoids: Pigments of photosynthetic biomembranes. In: Methods in Enzymology Vol. 148: pp. 183-350. Academic Press, Orlando, Fl., USA.
20. Shi DC, Sheng YM, Zhao KF. Stress effects of mixed salts with various salinities on the seedlings of *Aneurolepidium chinense*. Acta Bot Sin 1998; 40: 1136–1142.
21. Valdez-Aguilar LA, Reed DW. Comparison of growth and alkalinity-induced responses in two cultivars of hibiscus (*Hibiscus rosa-sinensis* L.). HortScience 2006; 41: 1704–1708.
22. Valdez-Aguilar LA, Reed DW. Response of selected greenhouse ornamental plants to alkalinity in irrigation water. J Plant Nutr 2007; 30: 441–452.
23. Valdez-Aguilar LA, Reed DW. Influence of potassium substitution by rubidium and sodium on growth, ion accumulation, and ion partitioning in bean under high alkalinity. J Plant Nutr 2008; 31: 867–883.
24. Wu SJ, Ding L, Zhu JK. SOSl, a genetic locus essential for salt tolerance and potassium acquisition. Plant Cell 1996; 8: 617-627.
25. Van Volkenburgh E, Boyer JS. Inhibitory effects of water deficit on maize leaf elongation. Plant Physiol 1985; 77: 190–194.
26. Pitann B, Schubert S, Mühling KH. Decline in leaf growth under salt stress is due to an inhibition of H^+ pumping activity and increase in apoplastic pH of maize leaves. J Plant Nutr Soil Sci 2009; 172: 535–543.
27. Zörb C, Noll A, Karl S, Leib K, Yan F, Schubert S. Molecular characterization of Na^+/H^+ antiporters (ZmNHX) of maize (*Zea mays* L.) and their expression under salt stress. J Plant Physiol 2005; 162: 55–66.
28. Valdez-Aguilar LA. 2004. Effect of alkalinity in irrigation water on selected greenhouse crops. PhD thesis in Horticulture, Texas A&M University, 500014: pp. 489.
29. Mohamedin AAM, Abd El-Kader AA, Badran NM. Response of sunflower (*Helianthus annuus* L.) to plants salts stress under different water table depths. J Appl Sci 2006; 2: 1175-1184.
30. Sanchez Blanco MJ, Rodriguez P, Morales MA, Ortuco MF, Torrecillas A. Comparative growth and water relation of *Cistus albidus* and *Cistus monspelensis* plants during water deficit conditions and recovery. Plant Sci 2002; 162: 107-113.
31. Serpil Ü, Yűksel K, Elif Ü. Proline and ABA levels in two sunflower genotypes subjected to water stress. Bulg J Plant Physiol 2004; 30: 34-47.
32. Shi D, Sheng Y. Effect of various salt-alkaline mixed stress conditions on sunflower seedlings and analysis of their stress factors. Environ Exp Bot 2005; 54: 8-21.
33. Heuer B. 2006. Photosynthetic carbon metabolism of crops under salt stress. In: M. Pessarakli, ed. Handbook of Photosynthesis: pp. 779–792. Taylor & Francis Group, Boca Raton, Florida.
34. Hong L, Lin W. Effects of salt stress on root plasma membrane characteristics of salt-tolerant and salt-sensitive buffalo grass clones. Environ Exp Bot 1996; 36: 239–247.
35. Surjus A, Durand M. Lipid changes in soybean root membranes in response to salt treatment. J Exp Bot 1996; 47: 17–23.
36. Shi D, Wang D. Effects of various salt-alkali mixed stresses on *Aneurolepidium chinense* (Trin.) Kitag. Plant Soil 2005; 271: 15-26.
37. Lutts S, Kinet JM, Bouharmont J. Effects of salt stress on growth, mineral nutrition and proline accumulation in relation to osmotic adjustment in rice (*Oryza sativa* L.) cultivars differing in salinity tolerance. Plant Growth Regul 1996; 19: 207–218.
38. Kaya C, Ak BE, Higgs D, Murillo-Amador B. Influence of foliar applied calcium nitrate on strawberry plants grown under salt stress conditions. Austr J Exp Agric 2002; 42: 631–636.
39. Tuna AL, Kaya C, Dikilitas M, Yokas I, Burun B, Altunlu H. Comparative effects of various salicylic acid derivatives on key growth parameters and some enzyme activities in salinity stressed maize (*Zea mays* L.) plants. Pakistan J Bot 2007; 39: 787-798.
40. Tuna AL, Kaya C, Dikilitas M, Higgs D. The combined effects of gibberellic acid and salinity on some antioxidant enzyme activities, plant growth parameters and nutritional status in maize plants. Environ Exp Bot 2008; 62: 1-9.
41. Shi DC, Zhao KF. Effects of NaCl and Na_2CO_3 on growth of *Puccinellia tenuiflora* and on present state of mineral elements in nutrient solution. Acta Pratacult Sin 1997; 6: 51-61.

42. Reddy MP, Vora AB. Changes in pigment composition, Hill reaction activity and saccharides metabolism in bajra (*Pennisetum typhoides* S & H) leaves under NaCl salinity. Photosynthetica 1986; 20: 50-55.
43. Elstner EF. Oxygen activation and oxygen toxicity. Annu Rev Plant Physiol Plant Mol Biol 1982; 33: 73-96.
44. Briat JF. 2007. Iron dynamics in plants. In: Delseny, M. (Ed.): Incorporating Advances in Plant Pathology. Advances in Botanical Research, Vol. 46: pp. 138-169. Academic Press, London.
45. Jeong J, Guerinot ML. Homing in on iron homeostasis in plants. Trends Plant Sci 2009; 14: 280-285.
46. Yang JY, Zheng W, Tian Y, Wu Y, Zhou DW. Effects of various mixed salt-alkaline stresses on growth, photosynthesis, and photosynthetic pigment concentrations of *Medicago ruthenica* seedlings. Photosynthetica 2011; 49: 275-284.
47. Cheeseman JM. Mechanisms of salinity tolerance in plants. Plant Physiol 1988; 87: 547-550.
48. de-Lacerda CF, Cambraia J, Oliva MA, Ruiz HA, Prisco JT. Solute accumulation and distribution during shoot and leaf development in two sorghum genotypes under salt stress. Environ Exp Bot 2003; 49: 107–120.
49. Asch F, Dingkuhn M, Wittstock C, Döerffling K. Sodium and potassium uptake of rice panicles as affected by salinity and season in relation to yield and yield components. Plant Soil 1999; 207: 133–145.
50. Rus A, Lee B, Muñoz-Mayer A, Sharkhuu A, Miura K, Zhu JK, Bressan RA, Masegawa PM. AtHKT1 facilitates Na^+ homeostasis and K^+ nutrition in plants. Plant Physiol 2004; 136: 2500–2511.
51. Cuin TA, Miller AJ, Laurie SA, Leigh RA. Potassium activities in cell compartments of salt-grown barley leaves. J Exp Bot 2003; 54: 657-661.
52. Schachtman D, Lio W. Molecular pieces to the puzzle of the interaction between potassium and sodium uptake in plants. Trends Plant Sci 1999; 4: 281–287.
53. Läuchli A. 1984. Salt exclusions: An adaptation of legumes for crops and pastures under saline conditions. In: Staples, R.C. and Toenniessen, G.H. (Eds.): Salinity Tolerance in Plants: Strategies for Crop Improvement: pp. 171–189. John Wiley and Sons, New York.
54. Lauter DJ, Meiri A, Shuali M. Isoosmotic regulation of cotton and peanut at saline concentrations of K and Na. Plant Physiol 1988; 87: 911–916.
55. Schachtman DP, Munns R. Sodium accumulation in leaves for *Triticum* species that differ in salt tolerance. Austr J Plant Physiol 1992; 19: 331–340.
56. Yousfi S, Serret MD, Voltas J, Araus JL. Effect of salinity and water stress during the reproductive stage on growth, ion concentrations, $\Delta^{13}C$, and $\delta^{15}N$ of durum wheat and related amphiploids. J Exp Bot 2010; 61: 3529–3542.
57. Zheng Y, Jia A, Ning T, Xu J, Li ZI, Jiang G. Potassium nitrate application alleviates sodium chloride stress in winter wheat cultivars differing in salt tolerance. J Plant Physiol 2008; 14: 1455-1465.
58. Dvorak J, Noaman M, Goyal S, Gorham J. Enhancement of salt-tolerance of *Triticum turgidum* L. by the Knal locus transferred from the *Triticum aestivum* L. Theor Appl Genet 1994; 87: 872–877.
59. Yousfi S, Serret MD, Araus JL. Shoot $\delta^{15}N$ gives a better indication than ion concentration or $\Delta^{13}C$ of genotypic differences in the response of durum wheat to salinity. Funct Plant Biol 2009; 36: 144–155.
60. Botella MA, Martinez V, Pardines J, Cerda A. Salinity induced potassium deficiency in maize plants. J Plant Physiol 1997; 150: 200–205.
61. Gorham J, Wyn Jones RG, Bristol A. Partial characterization of the trait for enhanced K^+-Na^+ discrimination in the D genome of wheat. Planta 1990; 180: 590-597.
62. Hafsi C, Lakdhar A, Rabhi M, Debez A, Abdelly C, Ouerghi Z. Interactive effects of salinity and potassium availability on growth, water status, and ionic composition of *Hordeum maritimum*. J Plant Nutr Soil Sci 2007; 170: 469–473.
63. Soltani A, Hajji M, Grignon C. Factors which limit the mineral nutrition of barley in the presence of NaCl. Agronomie 1990; 10: 857–866.
64. Parida AK, Das AB. Salt tolerance and salinity effects on plants. Ecotoxicol Environ Saf 2005; 60: 324–349.

Journal of Biology and Earth Sciences

BIOLOGY ORIGINAL ARTICLE

Hepatoprotective effects of vitamin C, DPPD, and L-cysteine against cisplatin-induced oxidative stress in male rats

Hossam M. Omar[1], Emad A. Ahmed[1], Sarry Abdel-Ghafar[2], Sohair Mohammed[1], Ahmed Y. Nasser[3]

[1]Department of Zoology, Faculty of Science, Assiut University, Egypt

[2]Department of Pathology, Faculty of Veterinary Medicine, Assiut University, Egypt

[3]Department of Medical Biochemistry, Faculty of Medicine, Assiut University, Egypt

ABSTRACT

Cisplatin (CP) is considered as a major antineoplastic drug against a broad spectrum of malignancies. CP acts on cancer cells by releasing free radicals which at the same time damage liver and kidney cells. The tissue specific toxicity of cisplatin to the kidneys is well documented. However, at higher doses less common toxic effects such as hepatotoxicity may arise. Strategies to protect tissues against CP toxicity are of clinical interest. In this study, we aimed to investigate the hepatotoxicity of CP which it may be mediated by oxidative stress and to establish whether some antioxidants, namely vitamin C, N,N-diphenyl-p-phenylenediamine (DPPD) and L-cysteine, may provide protection against CP hepatotoxicity. Forty adult male albino rats (120-150 g) were divided into 5 groups (8 rats each). CP was injected once a week (2 mg/kg) for four weeks. The antioxidants DPPD (125 mg/kg b.w.), vitamin C (100 mg/kg) and L-cysteine (100 mg/kg) were also injected once a week 24 hour prior to CP injection. The control group was injected with saline. All doses were injected intraperitoneally. Rats of different groups were killed by cervical dislocation, 24 hours after the last injection and blood was collected into a sterilized tube containing EDTA to separate plasma. The livers was taken for histological and biochemical examinations. CP-induced oxidative stress was indicated by increased level of LPO and superoxide anion in hepatic tissue and plasma. Also, CP induced decline of antioxidant enzymes such as SOD, CAT, GST and GGT and a decreased level of GSH, Vit. C and Vit. E in hepatic tissue and plasma. Treatment with Vit. C, DPPD and L-cysteine in combination with CP restored LPO and superoxide anion, the activities of SOD, GST, CAT and GGT and the content of GSH, Vit. C and Vit. E to about normal control levels. In conclusion treatment with Vit. C, DPPD or L-cysteine in combination with CP may be effective to protect from oxidative hepatic injury that induced by CP treatment.

Key words: cisplatin, hepatotoxicity, DPPD, vitamin C, L-cysteine, oxidative stress, rats, chemotherapy.

J Biol Earth Sci 2012; 2(1): B28-B36

Corresponding author:
Prof. Hossam M. Omar
Department of Zoology, Faculty of Science,
Assiut University, Assiut, 71516, Egypt
e-mail: hossameldin.mo@gmail.com

Original Submission: 27 February 2012; Revised Submission: 16 March 2012; Accepted: 18 March 2012

ISSN: 2084-3577
http://www.journals.tmkarpinski.com/index.php/jbes or http://jbes.strefa.pl
e-mail: jbes@interia.eu

INTRODUCTION

Cisplatin (CP) is an inorganic platinum compound with a broad spectrum antineoplastic activity against various types of tumors. CP, has been extensively used for chemotherapy of various cancers, including that of the liver [1-3]. However, while CP generates acceptable outcome in chemotherapy of some cancers, it also exhibits severe toxicity and undesirable side effects [4-6] such as myelosuppression, nephrotoxicity, ototoxicity, neurotoxicity and bone marrow suppression [7-8]. The mechanism of hepatotoxicity induced by CP is not well understood at present. It has been found that CP is taken up preferentially and accumulated in human liver cells resulting in an enhanced production of reactive oxygen species (ROS) [9-10]. Although endogenous antioxidant systems including superoxide dismutase (SOD), catalase (CAT) and glutathione peroxidase (GSH-Px), can prevent ROS toxic effects in normal healthy conditions, however, excessive ROS generation caused by cisplatin may overcome the natural antioxidant defences of hepatocyte and lead to the lipid peroxidation and delayed-onset liver injury [11]. Until now a large number of studies have been focused on the ways for prevention of CP side effects via supplementation of preventive agents simultaneously [12-16].

Vit. C is essential nutrient that functions as a nonenzymatic antioxidants to prevent the propagation of free radical reaction in the cytosol. It is remarkably decreases the nephrotoxicity of cisplatin without reducing its antitumor activity [17]. N,N-diphenyl–p-phenylenediamine (DPPD) is a potent antioxidant and can affect the efficiency of the microsomal enzymes system that involved in the metabolism of foreign compounds [18]. DPPD was a more effective inhibitor of lipid peroxidaion, since it is known for its ability to scavenge free radicals powerfully [19]. Sulfur containing amino acids play important roles in maintaining the integrity of cellular systems by influencing the cellular redox state and the capacity to detoxify toxic compounds. Methionine and L-cysteine (Cys) are the two principal sulfur-containing amino acids in mammals [20]. Along with a host of proteins, L-cysteine is a precursor of GSH, which is considered pivotal for the detoxification of cellular oxidative stress [21].

Thus, this study was undertaken to evaluate the side effect of cisplatin on the oxidative stress parameters in the plasma and hepatic tissues and the histological changes of liver of male albino rats. Also, to assess the efficacy of Vit. C, DPPD and L-cysteine as antioxidants in minimizing or reversing these side effects.

MATERIALS AND METHODS

Animals and experimental design

Forty Sprague-Dawley rats of 120-150 g were randomly divided into two main categories. The first contain 8 rat served as controls and injected with vehicles only. The second category was subdivided into four groups.

The first group: G1, was injected intravenously with CP (2 mg/kg body weight) once a week for 4 weeks in a total dose 8 mg/kg body weight [22].

The second group: G2, was injected intravenously with CP (2 mg/kg body weight) once a week for 4 weeks in a total dose 8 mg/kg body weight and Vit. C at a dose of 100 mg/kg body weight, i.p [23] 24 h prior CP injection.

The third group: G3, was injected intravenously with CP (2 mg/kg body weight) once a week for 4 weeks in a total dose 8 mg/kg body weight and DPPD at a dose of 125mg/kg body weight, i.p. [24].

The fourth group: G4, was injected intravenously with CP (2 mg/kg body weight) once a week for 4 weeks in a total dose 8 mg/kg body weight and L-Cys at a dose of 100 mg/kg body weight, i.p. [25]. All animals were injected in similar volume injections.

All experimental protocols held on animals were done according to regulations set by the Institutional Animal Care and approved by Assiut University.

Collection and preparation of samples

Rats of the five groups were killed by cervical dislocation 24 hours after the last injection. Blood was collected into a sterilized tube containing EDTA. Liver was removed and washed in 0.1 M phosphate buffer (pH 7.4) and stored at -20°C for biochemical analysis. 10% w/v homogenate of liver was prepared by homogenization in (0.1 M) phosphate buffer (pH 7.4) using IKA Yellow line DI homogenizer (18 Disperser, Germany). The homogenates were centrifuged at 6000 rpm for 1 h at 4°C and the supernatant cytosols were kept frozen at 200°C for the subsequent biochemical assays.

Biochemical measurements

A total protein was measured by the method of Lowry et al. [26]. Lipid peroxides as thiobarbituric acid reactive substances (TBARs) was determined according to the method of Ohkawa et al. [27]. Glutathione was determined using the method of Beutler et al. [28].

Superoxide anion was measured according the procedure of Prodczasy and Wei [29], which is based on the reduction of iodonitrotetrazolium. Superoxide dismutase activity was determined according to its ability to inhibit the autoxidation of epinephrine at alkaline medium according to Misra and Fridovich [30]. Catalase activity was estimated by procedure of Luck [31], basing on its ability to decompose H_2O_2.

Glutathione S-transferase activity was assayed using 1-chloro-2,4-dinirtobenzene as substrate according to the method of Habig et al. [32]. γ-glutamyl transpeptidase activity was assayed by the method of Meister et al. [33] using γ-glutamyl-p-nitroanilide as a substrate. Vit. E was measured using Emmerie-Engel reaction based on the reduction of ferric to ferrous ions forming a red complex with α,α-dipyridyl according to the method of Roe [34]. Vit. C was measured as described by Jagota and Dani [35].

Histological evolutions

Pieces of liver was quickly removed and fixed in 10% neutral buffered formalin for histological investigations. Then sections (7 µm) of control and treated kidneys were mounted on slides and dried overnight at 37°C. Sections were dewaxed in xylene and hydrated in a graded series of alcohols and stained for hematoxylin and eosin for histological evaluation.

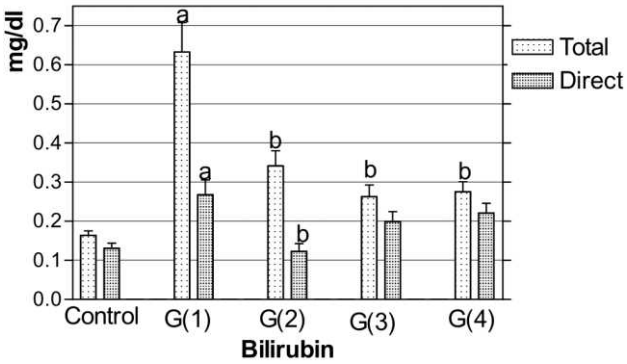

Fig. 1. Effect of treatment with Vit. C, DPPD or L-cysteine on bilirubin level in plasma of male albino rat treated with cisplatin.

Statistical analysis

The results were analyzed by one way analysis of variance (ANOVA) followed by Newman-Keuls Multiple Comparison Test as post-Test by using Prism Program for Windows, version 3.0 (Graph Pad Software, Inc., San Diago CA. USA). The significance difference between groups was accepted at $P<0.05$.

RESULTS

Treatment of rats with CP results in a significant increase in total and direct bilirubin level in plasma compared to the control group. Co-treatment of rats with Vit. C, DPPD and L-cysteine results in a significant decrease in total bilirubin level in plasma, however direct bilirubin decreased only in the rats co treated with Vit. C compared to cisplatin treated

Table 1. Effect of treatment with Vit. C, DPPD and L-cysteine on lipid peroxidation and superoxide anion in liver and plasma of male albino rat treated with cisplatin. Values represent mean ± SE.

Groups	Lipid peroxidation (nmol MDA/mg protein)		Superoxide anion (nmol/mg protein)	
	Plasma	Liver	Plasma	Liver
Control	0.6 ± 0.007	0.21±0.015	9.57±0.33	9.86±0.16
Cisplatin	0.11± 0.013[a]	0.25±0.011[a]	13.52±0.71[a]	13.96±0.95[a]
Cisplatin + Vit. C	0.09±0.016	0.13±0.02[a]	10.35±0.65[b]	9.28±0.87[b]
Cisplatin + DPPD	0.08±0.01	0.16±0.006[b]	8.85±0.41[b]	6.39±0.44[b]
Cisplatin + L-Cysteine	0.08±0.01	0.17±0.007[b]	9.75±0.50[b]	6.43±0.49[b]

a = significance difference between control group and CP treated group.

b = significance difference between CP treated group and Vit. C, DPPD and L-cysteine co-treated group.

Table 2. Effect of treatment with Vit. C, DPPD and L-cysteine on enzymatic and non enzymatic antioxidant in liver and plasma of male albino rat treated with cisplatin.Values represent mean ± SE.

Parameter / Group		Control	Cisplatin	Cisplatin +Vit. C	Cisplatin + DPPD	Cisplatin + Cysteine
GSH (µg/mg protein)	Liver	1.28±0.113	0.84±0.126 [a]	2.07±0.230 [b]	2.23±0.152 [b]	1.08±0.136
	Plasma	2.26±0.129	1.49±0.101 [a]	1.94±0.158 [b]	1.55±0.072	0.82±0.073 [b]
Vitamin E (µg/mg protein)	Liver	4.56±0.161	0.99±0.049 [a]	2.76±0.196 [b]	3.05±0.123 [b]	4.01±0.283 [b]
	Plasma	3.39±0.166	0.87±0.052 [a]	2.10±0.267 [b]	1.81±0.158 [b]	1.54±0.084 [b]
Vitamin C (µg/mg protein)	Liver	0.08±0.004	0.05±0.005 [a]	0.07±0.008	0.07±0.003	0.09±0.011 [b]
	Plasma	0.20±0.011	0.13±0.011 [a]	0.08±0.014 [b]	0.06±0.008 [b]	0.13±0.019
GGT (nmol/min/mg protein)	Liver	0.51±0.094	0.23±0.014 [a]	0.78±0.044 [b]	0.54±0.061 [b]	0.60±0.080 [b]
	Plasma	0.84±0.052	0.51±0.049 [a]	0.50±0.040	0.46±0.050	0.50±0.037
GST (nmol/min/mg protein)	Liver	19.48±1.04	16.05±1.01 [a]	22.05±0.76 [b]	22.83±0.87 [b]	20.82±1.65 [b]
	Plasma	40.81±2.23	23.78±3.29 [a]	24.03±1.73	33.73±2.17 [b]	30.89±1.87
SOD (U/mg protein)	Liver	8.34±0.44	6.63±0.34 [a]	8.56±0.44 [b]	8.86±0.49 [b]	10.03±0.68 [b]
	Plasma	3.90±0.34	2.55±0.15 [a]	3.13±0.26	2.95±0.37	2.81±0.22
CAT (U/mg protein)	Liver	14.90±1.87	9.10±1.21 [a]	12.80±0.51 [b]	13.96±0.64 [b]	13.46±1.03 [b]
	Plasma	0.72±0.04	0.38±0.06 [a]	0.52±0.05	0.82±0.06 [b]	0.72±0.05 [b]

rats (Fig. 1).

Table 1 shows the level of lipid peroxidation and superoxide anion in plasma and hepatic tissue of control and different treated rats. Lipid peroxidation and superoxide anion were significantly increased in plasma and hepatic tissue of CP treated rats compared to control. Vit. C, DPPD and L-cysteine co-treatment caused a significant decrease in plasma and hepatic superoxide anion compared to CP treated group, however lipid peroxidation was significantly decreased in hepatic tissue.

The levels of non enzymatic antioxidants; GSH, Vit. C and E and the activities of enzymatic antioxidants; GGT, GSH, SOD and CAT in plasma and hepatic tissue were significantly lower in CP treated rats than control (Table 2). Co-treatment of rats with antioxidants Vit. C, DPPD and L-cysteine result in a significant increase in almost the previous parameters compared to CP treated rats.

Liver of rat from control group showing normal histological structure (Fig. 2A). In CP treated rats the hepatic parenchyma showed multiple necrotic foci. These foci were infiltrated with mononuclear cells in some cases and the portal area showed hyperplasia of the bile duct with mononuclear cell reaction (Fig. 2B &C). The liver of rats co-treated with Vit. C showed edema in the Disse space with small necrotic foci in some cases (Fig. 2D). The liver of rats co-treated with DPPD was more or less similar to normal (Fig. 2E). In liver of rats co-treated with L-cysteine the hepatocyte showed presence of necrotic foci infiltrated with mononuclear cells and the portal area showed slight cellular infiltration (Fig. 2F).

DISCUSSION

Anticancer drugs are used as a common therapy against different kinds of cancer. Those drugs impact physiological side effects in non-tumor cells mostly by free radical formation and oxidant injury. It is known that CP is significantly taken up in human liver cells, resulting in an enhanced production of ROS and hepatotoxicity [36]. In the present study hepatotoxicity by CP treatment is characterized by a significant increase in total and

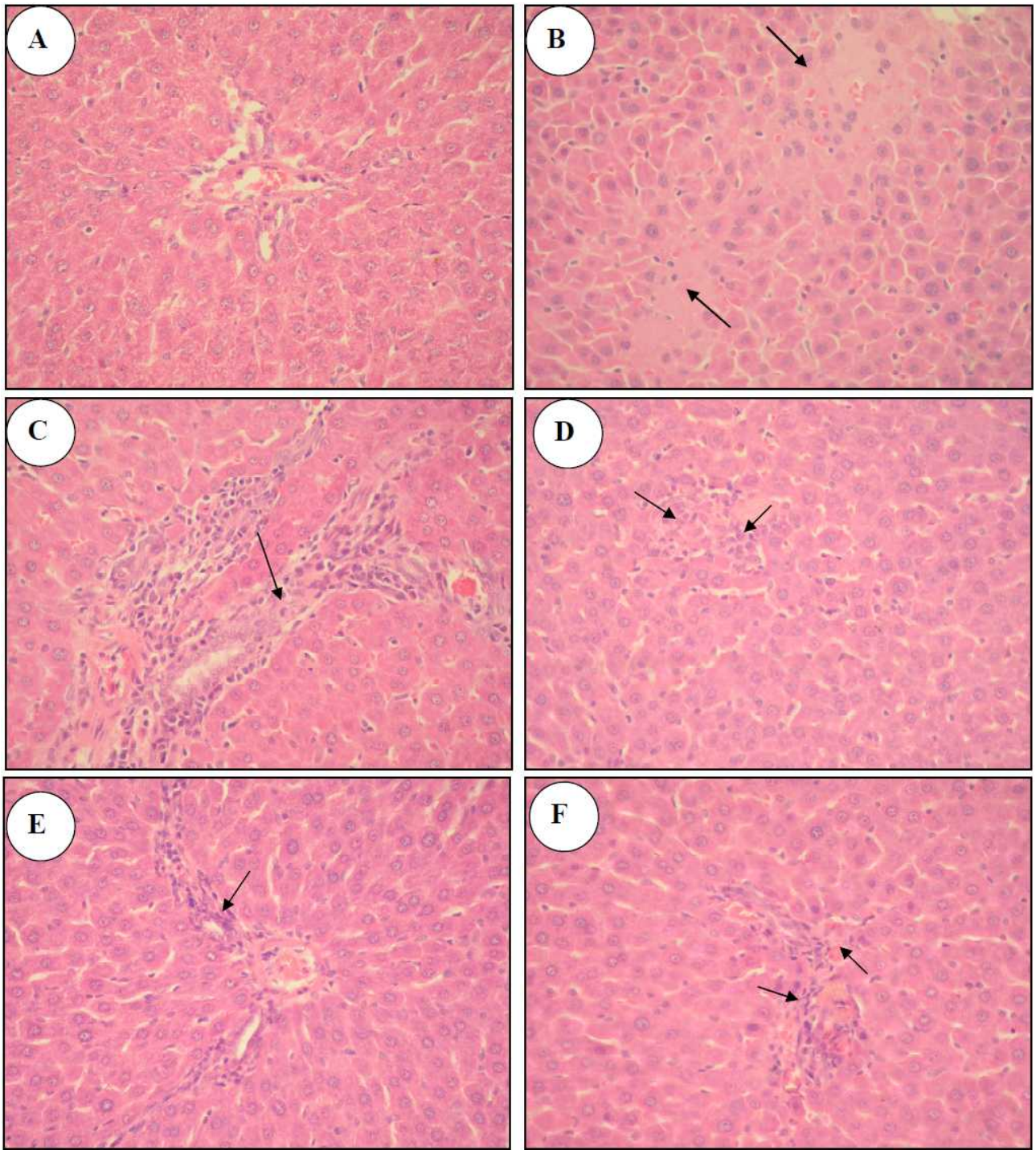

Fig. 2. Histotogical effects of cisplatin in rat liver.

A: normal rat liver.

B, C: Marked histological abnormalities seen in rats treated with cisplatin showing multiple necrotic foci in the hepatic parenchyma and hyperplasia of the bile duct in the portal area.

D: Cisplatin + Vit. C group showing slight necrotic foci in the hepatic parenchyma infiltrated with mononuclear cells.

E: Cisplatin + DPPD group showing mononuclear cell reaction in the portal area.

F: Cisplatin + L-cysteine group showing congestion and mononuclear cell reaction in the portal area but less than liver in cisplatin treated rats.

direct billirubin (Fig. 1). Similarly, Cavelli et al. [37] found that liver toxicity of CP was characterized by mild to moderate elevation of serum transaminases and billirubin. In the present study elevated billirubin by CP was matched with histological changes in the liver tissues (Fig. 2B & C) which showed multiple necrotic foci in the hepatic parenchyma and hyperplasia of the bile duct in the portal area. In this aspect, the most pronounced histopathological abnormalities observed in rat treated with 1mg/kg body weight of CP was present of necrotic tissues [38]. CP is thought to kill cells by forming DNA adducts, causing G2 arrest in the cell cycle, triggering apoptosis [39]. However, 5 days after CP administration at a dose of 7 mg/kg has no changes in the serum activity of ALT and GGT and histopathological observation in the liver tissue of rat [40].

Co-treatment of rats with either Vit. C, DPPD and L-cysteine caused a significant decrease in total and direct or conjugated billirubin with improvement in the histological changes that induced by CP (Fig. 2D, E & F). In consistence, procainamide hydrochloride counteract the hepatoxicity induced by CP in rats as demonstrated by the normalization of transaminases as well as histological analysis of liver tissue [41]. Previous studies documented the importance of oxidative stress in CP-induced toxicity [38, 42-44]. The most abundant ROS generated in living cells are superoxide anions and its derivatives hydroxyl radical which induces lipid peroxidation [45]. In the present study CP treatment caused a significant increase in both thiobarbituric acid substances (TBARs) and superoxide anion (O^{-}_{2}) in plasma and hepatic tissues compared to control rats. Similar results was obtained in plasma and liver of rats treated with CP by Yousef et al. [43]. In this aspect TBARs are produced by LPO a good indicators of oxidative stress [46]. In addition, Chirino, et al. [47] suggested that O^{-}_{2} derived from NADPH oxidase triggers some of the side effects of CP administration. The increase of O^{-}_{2} may be simply consequence of the mitochondrial dysfunction and the decrease in SOD activity [48]. Administration of Vit. C, DPPD, or L-cys 24 h prior CP injection result in a significant decrease in TBARs and O^{-}_{2} in hepatic tissue compared to CP treated group. Similarly, Yousef et al. [43] found that grape seed proantocyandin extract decreased TBARs in plasma and liver of rats treated with CP. Moreover, DPPD and L-cysteine decreased TBARs and O^{-}_{2} in testes of rats treated with CP [44]. However, Vit. C only decreased TBARs and O^{-}_{2} in the spleen of rats treated with CP [49]. CP-induced increases in LPO in hepatic tissue of rats was protected by silymarin and Royal jelly treatment [13, 15]. However, Avci et al. (14) found that LPO that induced in hepatic tissue by CP was not inhibited by tomato. The interpretation for the role of L-cysteine is the presence of a sulfhydryl group which gives it the potential to function as a chelating agent [16, 50].

The result of the present study indicate that CP administration significantly altered the content of GSH, Vit. C and E and the activities of CAT, SOD, GGT and GST activities in plasma and liver tissues (Table 2). The present results support the hypothesis that the mechanism of CP toxicity is related to the antioxidant depletion. A significant decrease in the antioxidants and increase in ROS in different organs was reported [13-15, 43, 51-53]. The depletions of GSH level seems to be a prime factor that permits LPO [54]. However, the decrease in SOD activity could cause the initiation and propagation of LPO in CP treated rats [55]. The decreased SOD activity might be due to the loss of copper and zinc which are essential for the enzyme activity [43]. Moreover, the inhibition of SOD and CAT may be due to the increased generation of superoxide anion which significantly increased in the present results. Furthermore, the high GGT activity in hepatic tissue after CP treatment offers evidence that the enzyme in the hepatocytes hydrolyses the GSH leading depletion of hepatic GSH content [52]. Naqshbandi et al. [53] concluded that CP elicited deleterious hepatotoxic effects by suppressing antioxidant defense mechanism. In contrast Prattibha et al. [52] found a significant increase in GST and GGT activities in hepatic tissue after CP treatment (0.4 mg/kg, i.p. daily for 8 weeks) and suggested that GSH my be utilized in biotransformation reaction for conversion of CP to CP-GSH complex which is then exported out of hepatocytes. Hepatotoxic effects by CP were ameliorated by dietary supplementation with fish oil, silymarin, royal jelly and grape seed proanthocyanidin [13, 15, 43, 53] respectively. Present of the previous compounds with CP normalized the levels of TBARs, GSH and the activities of antioxidants enzymes to the normal levels of control.

Thus the present results suggest that Vit. C,

DPPD, L-cysteine posses significant potential to prevent CP-induced oxidative stress and hepatotoxicity via scavenging free radical and regeneration of antioxidant defense system.

TRANSPARENCY DECLARATION

The authors declare no conflicts of interest.

REFERENCES

1. Yeo W, Mok TS, Zee B, Leung TW, Lai PB, Lau WY et al. A randomized phase III study of doxorubicin versus cisplatin/interferon alpha-2b/doxorubicin/ fluorouracil (PIAF) combination chemotherapy for unresectable hepatocellular carcinoma. J Natl Cancer Inst 2005; 97: 1532-1538.
2. Lin CC, Hsu CH, Huang CY, Cheng AL, Chen J, Vogelzang NJ, Pu YS. Weekly cisplatin plus infusional high-dose 5-fluorouracil and leucovorin (P-HDFL) for metastatic urothelial carcinoma: an effective regimen with low toxicity. Cancer 2006; 106: 1269-1275.
3. Yuan JN, Chao Y, Lee WP, Li CP, Lee RC, Chang FY et al. Chemotherapy with etoposide, doxorubicin, cisplatin, 5-fluorouracil, and leucovorin for patients with advanced hepatocellular carcinoma. Med Oncol 2008; 25: 201-206.
4. Alvarez-Cabellos R, Garcia-Carbonero R, Garcia-Lacalle C, Gomez P, Tercero A, Sanchez D, Paz-Ares L. Fluorouracil-based chemotherapy in patients with gastrointestinal malignancies: influence of nutritional folate status on toxicity. J Chemother 2007; 19: 744-749.
5. Ajani JA. Optimizing docetaxel chemotherapy in patients with cancer of the gastric and gastroesophageal junction: evolution of the docetaxel, cisplatin, and 5-fluorouracil regimen. Cancer 2008; 113: 945-955.
6. Dank M, Zaluski J, Barone C, Valvere V, Yalcin S, Peschel C, et al. Randomized phase III study comparing irinotecan combined with 5-fluorouracil and folinic acid to cisplatin combined with 5-fluorouracil in chemotherapy naive patients with advanced adenocarcinoma of the stomach or esophagogastric junction. Ann Oncol 2008; 19: 1450-1457.
7. Sastry J, Kellie SJ. Severe neurotoxicity, ototoxicity and nephrotoxicity following high-dose cisplatin and amifostine. Pediatr Hematol Oncol 2005; 22: 441–445.
8. Pabla N, Dong Z. Cisplatin nephrotoxicity: mechanisms and renoprotective strategies. Kidney Int 2008; 73: 994–1007.
9. Sadzuka Y, Shoji T, Takino Y. Effect of cisplatin on the activities of enzymes which protect against lipid peroxidation. Biochem Pharmacol 1992; 43: 1873–1875.
10. Siddik ZH. Cisplatin: mode of cytotoxic action and molecular basis of resistance. Oncogene 2003; 22: 7265–7279.
11. Yilmaz HR, Sogut S, Ozyurt B, Ozugurlu F, Sahin S, Isik B. The activities of liver adenosine deaminase, xanthine oxidase, catalase, superoxide dismutase enzymes and the levels of malondialdehyde and nitric oxide after cisplatin toxicity in rats: protective effect of caffeic acid phenethyl ester. Toxicol Health 2005; 21: 67–73.
12. Ali BH, Al-Moundhri MS. Agents ameliorating or augmenting the nephrotoxicity of cisplatin and other platinum compounds: a review of some recent research. Food Chem Toxicol 2006; 44: 1173-1183.
13. Mansour HH, Hafez HF, Fahmy NM. Silymarin modulates cisplatin-induced oxidative stress and hepatotoxicity in rats. J Biochem Mol Biol 2006; 39: 656-661.
14. Avci A, Cetin R, Ergüder IB, Deverim E, Kilicoglu B, Candir, et al. Cisplatin causes oxidation in rat liver tissues: Possible protective effects of andtioxidant food supplementation. Turk J Med Sci 2008; 38: 117-112.
15. Karadeniz A, Simsek N, Karakus E, Yildirin S, Kara A, Can I, et al. Royal jelly modulates oxidative stress and apoptosis in liver and kidneys of rats treated with cisplatin. Oxidative Med Cell Longev 2011; 2011: 1-10.
16. Ibrahim MY, Abdul ABH, Ibrahim TAT, Abdel Wahab SI, Elhassan MM, Mohan S. Attentuation of cisplatin-induced nephrotoxicity in rats using zerumbone. Afr J Biotechnol 2010; 9: 4434-4441.
17. Choung SY, Kong JM. Protective Effects of Vitamin C on Cisplatin Nephrotoxicity. Arch Pharm Res 1994; 17: 11-16.
18. Torrielli MV, Pani F, Gabriel L, Gravela E. 1974. The pathophysiological significance of the hepatic DMES in the liver damage induced by CC14 and white phosphorus. In: Duncan WAM, ed., Experimental Model Systems in Toxicology and Their Significance in Man. Proc. Eur. Soc. for the Study of Drug Toxicity; 15: 294-300.
19. Sugihara K, Nakano S, Koda M, Tanaka K, Fukuishi N, Gemba M. Stimulatory Effect of Cisplatin on Production of Lipid Peroxidation in Renal Tissues. Jpn J Pharmacol 1987; 43: 247-252.
20. Liao Y, Lu X, Lu C, Li G, Jin Y, Tang H. Selection of agents for prevention of cisplatin-induced hepatotoxicity. Pharmacol Res 2008; 57: 125-131.
21. Dröge W. Oxidative stress and ageing: is ageing a cysteine deficiency syndrome? Philos Trans R Soc 2005; 360: 2355–2372.
22. Ravi R. Mechanism of protection by

diethyldithiocarbamate against cisplatin ototoxicity: antioxidant system, Fundamental and applied toxicology. Official J Soc Texaco 1995; 26(2): 293-300.
23. Al-Shamsi M, Amin A, Adeghate E. The Effect of Vitamin C on the Metabolic Parameters of Experimental Diabetes Mellitus. Am J Pharmacol Toxicol 2007; 2: 4-9.
24. Hannemann J, Duwe J, Baumann K. Iron- and ascorbic acid-induced lipid peroxidation in renal microsomes isolated from rats treated with platinum compounds. Cancer Chemother Pharmacol 1991; 28: 427–433.
25. Azarnia M, Shakour A, Rostami P, Sanaie-Mehr A. The protective role of cysteine against follicular atresia induced by lead in mouse. Acta Med Iranica 2004; 42: 83-88.
26. Lowry OH, Rosebrough NJ, Farr AL, Randall RJ. Protein measurement with the Folin phenol reagent. J Biol Chem 1951; 41: 1863-1870.
27. Ohkawa H, Ohishi N, Yagi K. Assay for lipid peroxides in animal tissue by thiobarbaturic acid reaction. Anal Biochem 1979; 95: 351-358.
28. Beutler E, Duron O, Kelly BM. Improved method for the determination of blood glutathione. J Lab Clin Meth 1963; 61: 882-888.
29. Prodezasy JJ, Wei R. Reduction of iodonitrotetrazolium violt by superoxide radicals. Biochem Biophys Res Comm 1988; 150: 1294-1301.
30. Misra HP, Fridovich I. The role of superoxide anion in the autoxidation of epinephrine and a simple assay for superoxide dismutase. J Biol Chem 1972; 247: 3170-3175.
31. Luck H. 1963. Catalase. In: Bergmer H-U, ed. Methods of enzymatic analysis. Academic Press, New York: 885-888.
32. Habig WH, Pabst MJ, Jokoby WB. Glutathion s-transferase. J Biol Chem 1974; 249: 7130-7139.
33. Meister A, Tate SS, Griffith OW. γ-glutamyl transpeptidase. Methods in Enzymology 1981; 77: 237-253.
34. Roe JH. 1961. Standard methods of clinical chemistry. Vol. 3. ed. David Selgson. Acad. Press. New York, p: 35.
35. Jagota SK, Dani HM. A new colorimetric technique for estimation of vitamin C using Folin Phenol reagent. Annal Biochem 1982; 127: 178-182.
36. Yu YN, Chen H, Li Y. Effect of bicyclol on cisplatin-induced hepatotoxicity in the hepatocarcinoma tumour-bearing mice. Basic Clin Pharmacol Tocicol 2009; 104: 300-305.
37. Cavelli F, Tschopp L, Sonntag RW, Zimmermann A. Cisplatin-induced hepatic toxicity. Cancer Treat Rep 1978; 62: 2125-2126.
38. El-Sayyad HI, Ismail MF, Shalaby FM, Abou-ElMagd RF, Gaur RL, Fernando A, et al. Histopathological effects of cisplatin, doxorubicin and 5-flurouracil (5-FU) on the liver of male albino rats. Int J Biol Sci 2009; 5: 466-473.
39. Kishimoto S, Miyazawa K, Terakawa Y, Ashikari H, Ohtani A, Fukushima S, Takeuchi Y. Cytotoxicity of cis-[((iR,2R)-1,2-cyclohexanediamine-N,N-)bis(myristato)]-platinum (II) suspended in lipodol in a newly established cisplatin-resistant rat hepatoma cell line. Jpn J Cancer Res 2000; 91: 1326-1332.
40. Al-Majed AA. Carnitine deficiency provokes cisplatin-induced hepatotoxicity in rats. Basic Clin Pharmacol Toxicol 2007; 100: 145-150.
41. Zicca A, Cafaggi S, Mariggio M, Vannozzi M, Ottone M, Bocchini V, et al. Reduction of cisplatin hepatotoxicity by procainamide hydrochloride in rats. Eur J Pharmacol 2002; 442: 265-272.
42. Yagmarca M, Bas O, Mollaoglu H, Sahin O, Nacar A, Karaman O, Songurb A. Protective effects of erdosteine on doxourubicin-induced hepatotoxicity in rats. Arch Med Res 2007; 38: 380-385.
43. Yousef MI, Saad AA, El-Shennawy LK. Protective effect of grape seed proanthocyanidin extract against oxidative stress induced by cisplatin in rats. Food Chem Toxicol 2009; 47: 1176-1183.
44. Ahmed EA, Omar HM, Abdlelghaffar SK, Ragb SMM, Nassar AY. The antioxidant activity of vitamin C, DPPD, L-cysteine against cisplatin-induced testicular oxidative damage in rats. Food Chem Toxicol 2010; 49: 1115-1121.
45. Mukherjee S, Banerjee SK, Maulik M, Dinda AK, Talwar KK, Maulik SK. Protection against adriamycin-induced cardiotoxicity by garlic: role of endogenous antioxidants and inhibition of TNF-a expression. BMC Pharmacol 2003; 3: 1-9.
46. Karthikeyan K, Sarala BR, Devarj N. Cardioprotective effect of grape seed proanthocyanidins on isoproterenol-induced myocardial injury in rats. Int J Cardiol 2007; 115: 326-333.
47. Chirino YI, Sanchez-Gonzalez DJ, Martinez-Martinez CM, Cruz C, Pedraza-Chaverri J. Protective effects of apocynin against cisplatin-induced oxidative stress and nephrotoxicity. Toxicology, 2008; 245: 18-23.
48. Farfan Labonne BE, Gutierrez M, Gomez-Quiroz LE, Konigsberg Fainstein M, Bucio L, Souza V, et al. Acetaldhyde-induced mitochondrial dysfunction senzsitizes hepatocytes to oxidative damage. Cell Biol Toxicol 2009; 25: 599-609.
49. Omar HM, Ragab SMM, Ahmed EA, Nassar AY. The ameliorating effect of vitamin C and DPPD on the toxicity of cisplatin in rats. 14th Sci. Cong. Fac.Vet. Med. Assiut Univ., Egypt. 2010: 295-312.
50. Moldeus P. L-cysteine. Methods in Enzymology 1994 234: 482-492.
51. Atesahin A, Karahan I, Turk G, Gur S, Yilmaz S, Ceribasi AO. Protective role of lycopene on cisplatin-induced changes in sperm characteristics, testicular

damage and oxidative stress in rats. Reprod Toxicol 2006; 21: 42-47.

52. Pratibha R, Sameer R, Rataboli PV, Bhiwgade DA, Dhume CY. Enzymatic studies of cisplatin induced oxidative stress in hepatic tissue of rats. Eur J Pharmacol 2006; 532: 290-293.
53. Naqshbandi A, Jhan MW, Rizwan S, Yusufi ANK, Khan F. Studies on the protective effect of fish oil against cisplatin induced hepatotoxicity. Biol Med 2011; 3: 86-97.
54. Badary OA, Abdel-Maskoud S, Ahmed WA, Owieda GH. Naringenin attenuates cisplatin nephrotoxicity in rats. Life Sci 2004; 76: 2125-2135.
55. Ajith TA, Usha S, Nivitha V. Ascorbic acid and alpha-tocopherol protect anticancer drug cisplatin induced nephrotoxicity in mice: a comparative study. Int J Clin Chem 2007; 375: 82-86.

Journal of Biology and Earth Sciences

BIOLOGY ORIGINAL ARTICLE

Analysis of FAME for two species of earthworms *Allolobophora caliginosa* Savigny and *Pheretima hawayana* Rosa (*Annelida-Oligochaeta*)

Hossam El-Din M. Omar[1], Zedan Z. Ibraheim[2], Nasser A. El-Shimy[1], Rouwaida S. Ali[1]

[1]*Department of Zoology, Faculty of Science, Assiut University, Egypt*

[2]*Department of Pharmacognosy, Faculty of Pharmacy, Assiut University, Egypt*

ABSTRACT

Analysis of fatty acid (FA) is one of the most commonly used tools for investigating microbial populations in ecological studies. Fatty acids can be extracted and esterified to form fatty acid methyl esters (FAME) when analyzed using gas chromatography–mass spectrometry, the resulting profile contains some microbial biomarkers. The aim of the present study to analysis FAME present in two species of earthworms exhibit the same environment. The thin layer chromatography of earthworm *Allolobophora caliginosa* Savigny showed three major spots corresponding to FAME while that of earthworm *Pheretima hawayana* Rosa showed two major spots. The GC-MS analysis of *Allolobophora caliginosa* Savigny extract showed the presence of at least 23 peaks, only two peaks were identified from their R_t and Ms spectrum, hexadecanoic acid methyl ester and octadecenoic acid methyl ester. While the chromatogram of *Pheretima hawayana* Rosa extract showed at least 20 peaks, five of them were identified; butanedioic acid dimethyl ester, pentadecanoic acid 14-methyl ester, 2-hydroxy-hexadecanoic acid methyl ester, 9-octadecenoic acid methyl ester and octadecanoic acid methyl ester. In conclusion, in spite of the two species of earthworms from the same environment, but their content of FAME was different and that may explain why the biological activity of the whole body extract was different.

Key words: soil, earthworms, FAMEs, gas chromatography, mass spectra.

J Biol Earth Sci 2012; 2(1): B37-B44

Corresponding author:
Prof. Hossam El-Din M. Omar
Department of Zoology, Faculty of Science,
Assiut University, Assiut, 71516, Egypt
e-mail: hossameldin.mo@gmail.com

Original Submission: 25 April 2012; Revised Submission: 20 May 2012; Accepted: 30 May 2012

ISSN: 2084-3577
http://www.journals.tmkarpinski.com/index.php/jbes or http://jbes.strefa.pl
e-mail: jbes@interia.eu

INTRODUCTION

Earthworms are among the most important animals living in soil, both for their role in agriculture and in terrestrial ecology. They also play an important role in the decomposition of organic matter, nutrient mineralization and primary production in terrestrial ecosystem. They help improve soil structure and soil chemical and biological properties [1]. Moreover, soil contains a large diversity of microorganisms which are an unavoidable constituent of earthworms natural diet [2, 3]. Analysis of phospholipid fatty acid composition is one of the most commonly used tools for investigating microbial populations in ecological studies because phospholipids fatty acid are rapidly synthesized during microbial growth and provides an accurate census of the current living community. Fatty acid biomarkers provide a high-resolution method to define feeding strategies of decomposer invertebrates and to determine their diets in situ. Lipid analysis has considerable potential as a new tool in soil food web studies [4]. Twenty-one phospholipid fatty acids (saturated, mono- and polyunsaturated, and branched) ranging from 10 to 18 carbon atoms were identified and quantified by GC-MS in the analyzed samples. Their corresponding retention times, molecular weights and identification are reported by Gómez-Brandón et al. [5].

All cells contain fatty acids (FAs) that can be extracted and esterified to form fatty acid methyl esters (FAMEs). When the FAMEs are analyzed using gas chromatography–mass spectrometry, the resulting profile constitutes a 'fingerprint' of the microorganisms in the sample, since it contains some microbial biomarkers [6]. Moreover, specific FAs permitted to determine the differences between samples and to evaluate the effect of earthworms in the decomposition of organic matter [7]. Based on the mass spectral 41 kinds of double-bond positional isomers of the monounsaturated FAs were identified [8]. Moreover, the analysis of FAs by GC-MS in different species of earthworms were studied [9-12].

In this study, FAME profiles were analyzed by GC-MS to assess the diversity of fatty acids and to compare the FAME contents of two earthworm species from the same localities and to interpret why the whole body extract of the two species have different biological activity.

MATERIALS AND METHODS

Earthworms collection

Two species of earthworms *Pheretima hawayana* Rosa and *Allolobophora caliginosa* Savigny are the mostly abundant earthworm species in Egypt were used in the present experiment. Earthworms were collected during the period of January to April 2009 by hand-sorting from soil in Abu-Korkas El Minia Governorate, Egypt. All experimental protocols held on animals were done according to regulations set by the Institutional Animal Care and approved by Assiut University.

Preparation of the fatty acid according to Johnson and Davenport [13]

The lipids of two gram of earthworm was extract in chloroform–methanol. The extract was refluxed with 0.5 N ethanolic potassium hydroxide for 3 hours on a boiling water bath. The major part of the alcohol present was distilled off and the aqueous lipid was diluted with distilled water then extracted with several portion of ether. The combined ether extract was washed with water until the washing became free from any alkalinity then dehydrated over anhydrous sodium sulphate and distilled off under reduced pressure. The alkaline aqueous solution that remained after removal of unsaponifiable matter was acidified with sulphuric acid (20%) and the liberated fatty acids were extracted with ether (50 ml × 3). The combined ether extract was washed several times with distilled water till the washings were free from any acidity. The ether extract was dried over anhydrous sodium sulphate. The solvent was distilled off under reduced pressure to give a viscous residue of free fatty acids, which have yellowish brown colour. A part of residue was subjected to methylation as describe by Nonaka, et al. [14] by mixing with anhydrous K_2CO_3 (2.09 g) and $(CH_3)_2SO_4$ (5 ml) in dry acetone and refluxed for 4 hr. After filtration, the filtrate was concentrated to remove acetone, diluted with water and extracted with ethyl acetate. The ethyl acetate layer was washed with water, dried over anhydrous sodium sulphate, and then concentrated to yield an oily residue of fatty acid methyl esters kept for further investigation.

Thin layer chromatography of fatty acid methyl esters

This procedure was carried out as described by

Cerbulis and Ard [15]. Silica Gel G plates were reactivated at 100°C for 1 hr. Samples were applied at 2 cm intervals and 2cm from the base alongside with an authentic fatty acid methyl ester were developed in one-dimensional chromatography. The developing solvents were petroleum ether-diethyl ethyl acetate (80: 20: 1 v/v/v). Iodine vapor was used to make the lipids visible (or spraying with 10% methanolic H_2SO_4 and heated in oven at 100°C for 5 min).

GS-MS analysis of FAMEs

The FSMEs were finally analyzed and identified by GC-MS, Agilent (689ON-5975B), column (DB-5. (60M × 250 µm × 0.25 µm), Carrier gas (Helium, 26 CM/sec), Injection (Split, 250°C - split ratio 1: 50, and detector MSD, 280°C transfer line. To identify FAMEs, retention times were compared to those obtained for standard FAMEs. The FAMEs were quantified by comparing the peak areas with those of the internal standard peak (Chemistry Department, Faculty of Science, Assiut, Egypt).

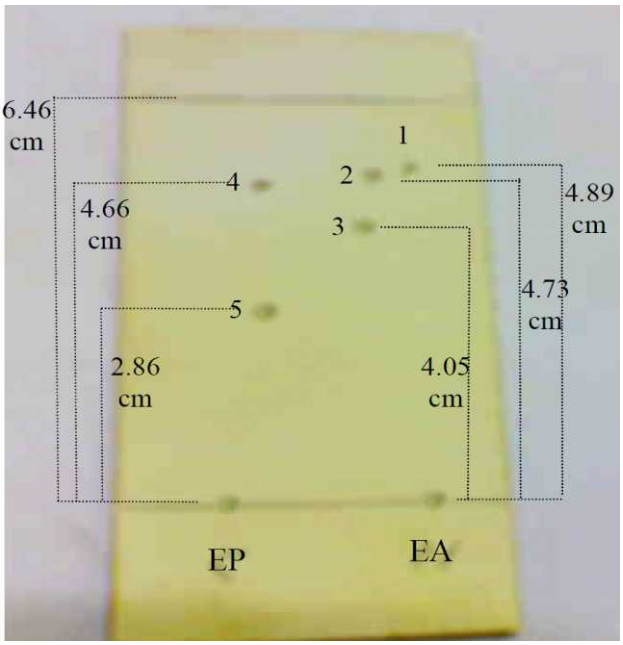

Fig. 1. Thin layer chromatography of the FAME of *Allolobophora caliginosa* Savigny (EA) and *Pheretima hawayana* Rosa (EP).

RESULTS

The thin layer chromatography (Figure 1) of earthworm *Allolobophora caliginosa* Savigny (EA) showed only three major spots corresponding to FAMES while that of earthworm *Pheretima hawayana* Rosa (EP) showed two major spots. This indicate that at least three FAMES are found in earthworm *Allolobophora caliginosa* Savigny while at least two FAMES are found in earthworm *Pheretima hawayana* Rosa.

The GC-MS chromatogram of *Allolobophora caliginosa* Savigny FAME showed the presence of at least 23 peaks, however only two peaks were identified from their R_t and Ms spectrum (Figure 2 & Table 1). While the chromatogram of Pheretima hawayana Rosa FAME showed at least 20 peaks, five of them were identified (Figure 3 & Table 2). The identity of these compounds was done form of their R_t and by comparison of these peaks with the internal standards FAME peaks from gas chromatography database and confirmed by the MS fragmentation pattern. It revealed the presence of methyl esters of hexadecanoic acid methyl ester, octadecenoic acid methyl ester, butanedioic acid dimethy ester, 14-methyl-pentadecanoic acid methyl ester, 2-hydroxy-hexadecanoic acid methyl ester, and 9-octadecenoic acid methyl ester. The identity of these common compounds of triglycerides was made by comparison of these peaks with the standards by gas chromatography and confirmed by the fragmentation pattern with those of standard mass spectra. The data indicated that amongst these FAs no any aromatic ring is present.

Table 1. Identified FAME of earthworm *Allolobophora caliginosa* Savigny.

Systematic Name	Common Name	Mol. formula	Mol. Wt	Carbon N0	Retention Time	Relative of identified
Hexadecanoic acid methyl ester	Methyl Palmitate	$C_{17}H_{34}O_2$	270	17	35.404	71.53
Octadecenoic acid methyl ester	Methyl Stearate	$C_{19}H_{38}O_2$	298	19	38.658	28.47

Table 2. Identified FAME in earthworm *Pheretima hawayana* Rosa.

Systematic Name	Common Name	Mol. Formula	Mol. Wt	Carbon N0	Retention Time	Relative of identified
Butanedioic acid dimethyl ester	Methyl succinate	$C_6H_{10}O_4$	146	6	18.619	8.13
Pentadecanoic acid 14- methyl ester	Isopalmitic	$C_{17}H_{34}O_2$	270	17	35.405	47.91
2-hydroxy - hexadecanoic acid methyl ester	2-hydroxy palmitic acid	$C_{17}H_{34}O_3$	286	17	37.433	9.84
9-Octadecenoic acid methyl ester	Methyl oleate	$C_{19}H_{36}O_2$	296	19	38.357	17.70
Octadecanoic acid methyl ester	Methyl Stearate	$C_{19}H_{38}O_2$	298	19	38.658	16.41

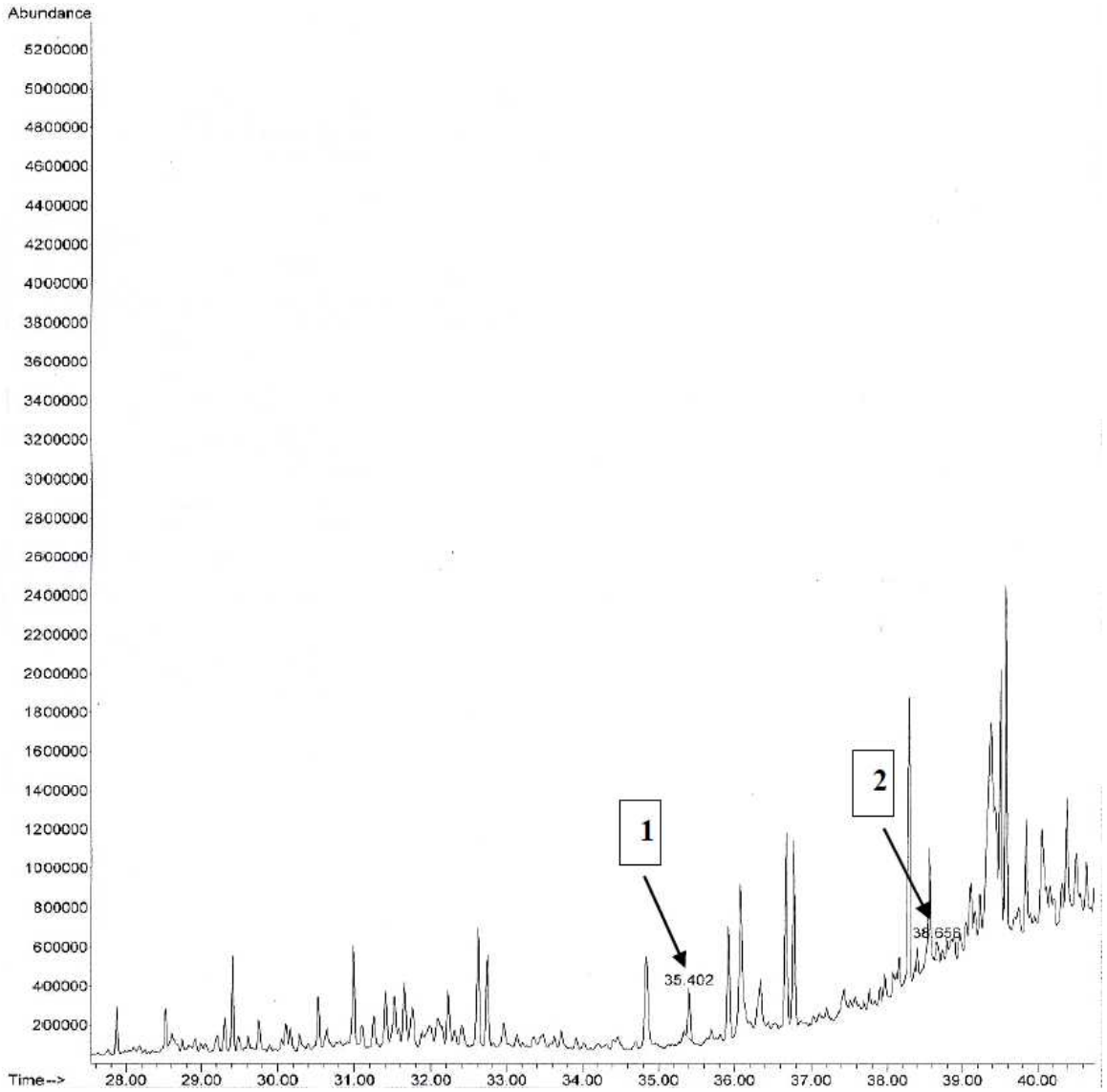

Fig. 2. Showed at least 23 peak were appeared in the capillary gas chromatogram of *Allolobophora caliginosa* Savigny, only two of these were identified as FAME.

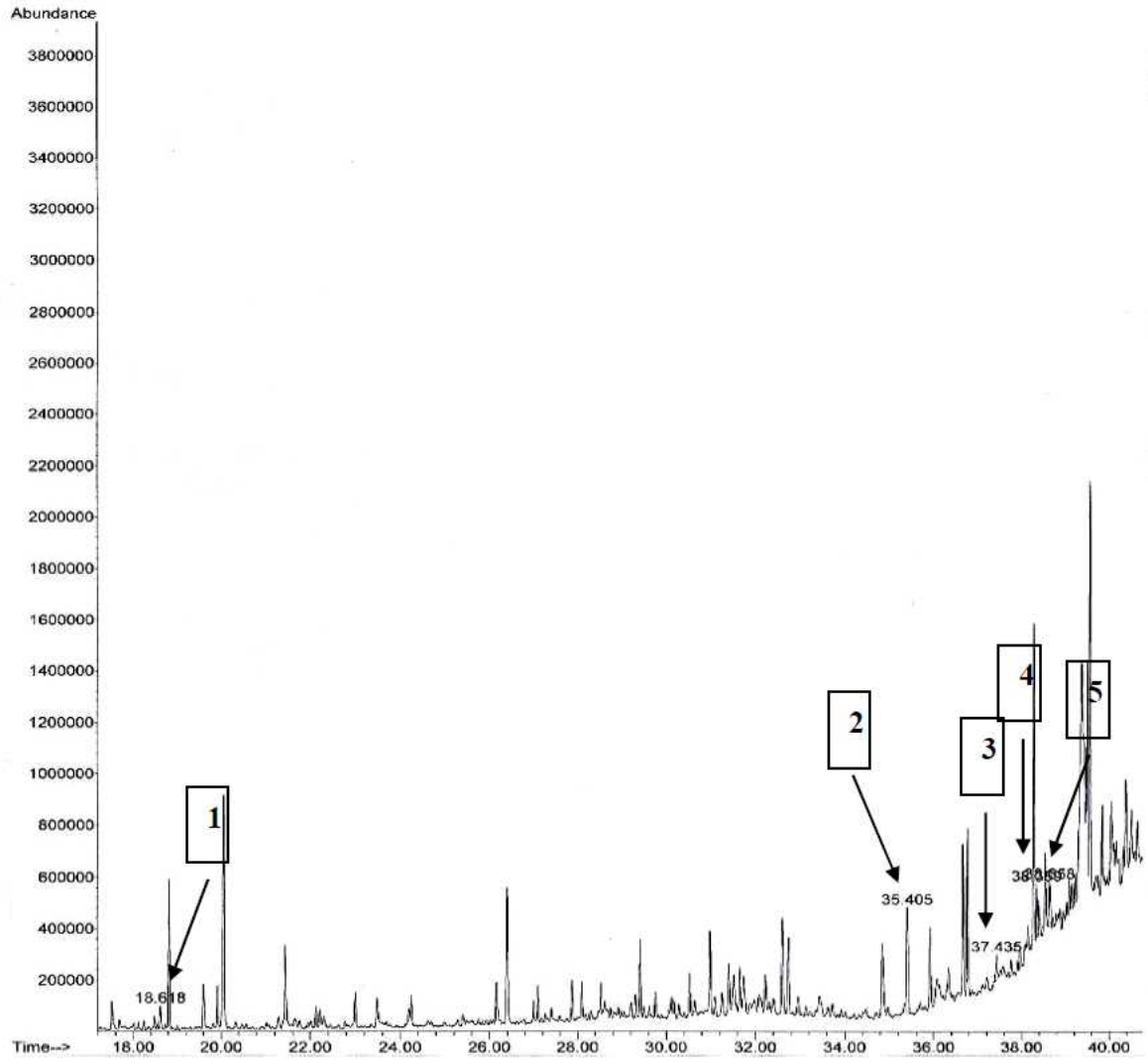

Fig. 3. Showed at least 20 peak were appeared in the capillary gas chromatogram of *Pheretima hawayana* Rosa, only 5 of these were identified as FAME.

In the earthworm *Allolobophora caliginosa* Savigny tow peaks were identified. The peak with R_t (35.404 min. 71%) was identified as hexadecanoic acid methyl ester commonly known as palmitic acid from its Rt and MS fragmentation pattern. The molecular formula was deduced to be $C_{17}H_{34}O_2$ from the molecular ion peak which appeared at m/z 270. The possible fragmentation pattern may be as follow:

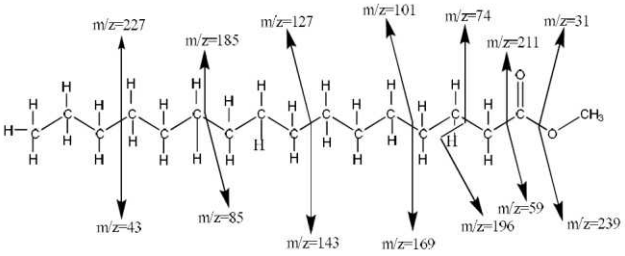

The peak with R_t (38.658 min. 28%) was identified as octadecenoic acid methyl ester commonly known as stearic acid from its R_t and MS fragmentation pattern as follow:

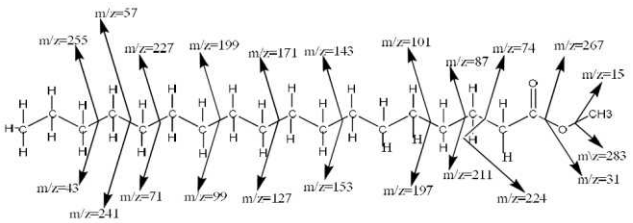

From the methylated fatty acid fraction of the earthworm Pheretima hawayana Rosa five FAMEs peaks were identified. The peak with R_t (18.619 min. 9%) was identified butanedioic acid dimethyl ester (methyl succinate) from its R_t and MS fragmentation pattern.

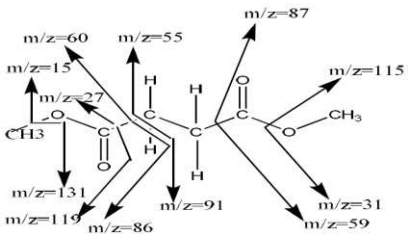

The peak with R_t (35.405 min. 56%) was identified as pentadecanoic acid 14 methyl ester (isopalmitic acid) from its R_t and MS fragmentation pattern.

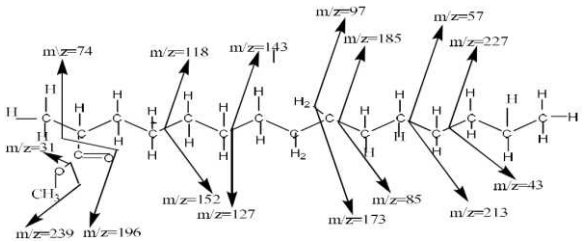

The peak with R_t (37.433 min. 11%) was identified as 2-hydroxypalmitic acid from its MS fragmentation pattern.

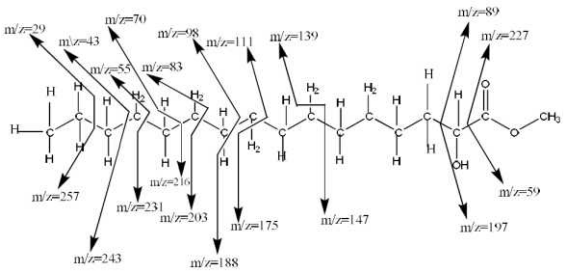

The peak with R_t (38.658, min 19%) was identified as methyl oleate from its MS fragmentation pattern.

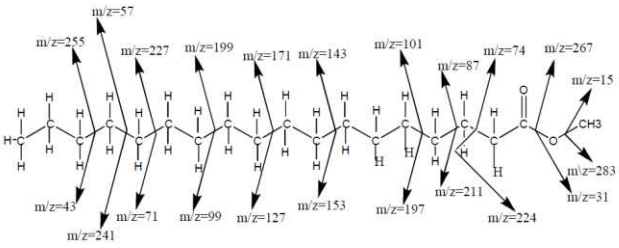

The peak with R_t (38.357 min. 21%) was identified as methyl stearate from its MS fragmentation pattern.

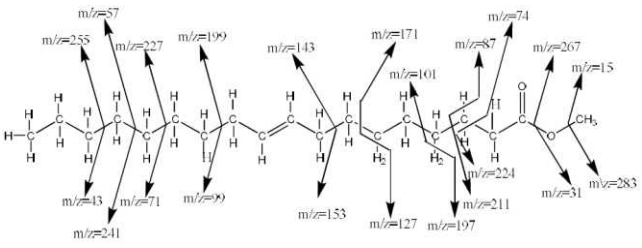

DISCUSSION

The trace amounts of adipocere (hydrogenation of the free fatty acids) detected in the grave soils were characterised by a composition reflecting the usual ratio of myristic, palmitic and stearic acids in this substance. The presence of low concentrations of oleic acid in each sample suggests that the conversion process is not yet stable and hydrogenation of the remaining unsaturated fatty acid is still possible [16]. Total FA concentration in the earthworm gut was about two orders of magnitude greater than in bulk soil. Moreover, several FAs appearing in the gut were not present in bulk soil [17]. The changes in FAME profiles are in agreement to the small differences in the bacteria communities of gut and casts recently suggested by means of molecular profiling of 16S rRNA genes [18].

The predominant FAs in *Eisenia foetida* were C20: 1 and C20: 5 [9]. The FA compositions of the lipid of earthworm *Lumbricus terrestris* were includes cis-vaccenic and eicosapentaenoic acids [10]. Elongation of palmitic acid to stearate and oxidation to CO_2 occurred extensively in the same species [11]. Moreover, the chemical structures of thirty-six volatile components were identified by GC-MS in the lipid composition of *Pheretima aspergillum* [12].

Concerning the biological activity of identified FA, dietary intake of palmitic acid increases risk of developing cardiovascular diseases [19]. However, another study showed that palmitic acid has no hypercholesterolaemic effect if intake of linoleic acid is greater than 4.5% of energy. On the other hand, it was shown that, if the diet contains trans fatty acids, the health effects are negative, causing an LDL-cholesterol increase and HDL cholesterol decrease [20]. Long-acting anti-psychotic medication, palip-eridone palmitate, used in the treatment of schizophrenia, has been synthesized using the oily palmitate ester as a long-acting release carrier medium when injected intramuscularly [21]. Esters of stearic acid with ethylene glycol as glycol stearate and glycol distearate, are used to produce a pearly effect in shampoos, soaps, and other cosmetic products [22]. Moreover, stearic acid has protective effects against cholestasis-related liver damage [23].

Succinic acid has beneficial effect on erythrocyte membrane bound enzymes and antioxidant status

in streptozotocin–nicotinamide induced type 2 diabetes [24]. However, 2-hydroxypalmitic acid has both cell growth inhibiting and cell death inducing actions on human lung adenosquamous carcinoma cell line H596 and adenocarcinoma cell line A549 [25]. Oleic acid alters LDL fatty acid composition and reduces oxidation disability in NIDDM [26]. Diet rich in olive oil decreases the development of atherosclerosis and lowers serum cholesterol by diminishing oxidative stress and inflammatory mediators while promoting antioxidant defenses [27]. Moreover, oleic acid was active against Gram-positive bacteria [28]. Finally, saturated and mono-unsaturated fatty acids increase interleukin-10 production in rat hepatocytes [29].

CONCLUSION

In spite of the two species of earthworms from the same environment, but their content of FAME was different and that may explain why the biological activity of the whole body extract was different.

TRANSPARENCY DECLARATION

The authors declare no conflicts of interest.

REFERENCES

1. Edwards CA, Bohlen PJ. 1996. Biology and ecology of earthworms. London: Chapman and Hall.
2. Torsvik V, Ovreas L. Microbial diversity and function in soil: from genes to ecosystems. Curr Opin Microbiol 2002; 5: 240-245.
3. Zirbes L, Thonart P, Haubruge E. Microscale interactions between earthworms and micro-organisms: a review. Biotechnol Agron Soc Environ 2012; 16(1): 125-131.
4. Ruess L, Schutz K, Hauber D, Haggbiom MM, Kandeler E, Scheu S. Application of lipid analysis to understand trophic interactions in soil. Ecology 2005 86: 2075-2082.
5. Gómez-Brandón M, Lores M, Dominguez J. Comparison of extraction and derivatization methods for fatty acid analysis in solid environmental matrixes. Analyt Bioanalyt Chem 2008; 392: 505-514.
6. Lores L, Gómez-Brandón M, Domínguez J. 2010. Tracking down microbial communities via fatty acids analysis: analytical strategy for solid organic samples. Current Research, Technology and Eduction Topics in applied Microbiology and Microbial Biotechnology. Mendez-Vilas A. (Ed.). pp. 1502-1508.
7. Lores L, Gómez-Brandón M, Perez-Diaz D, Domínguez J. Using FAME profile for the characterization of animal wastes and vermicomposts. Soil Biol Biochem 2006; 38: 2993-2996.
8. Shibahara A, Yamamoto K, Kinoshita A, Miyatani S. Fatty acids of the total lipid from earthworm. J Rehabil Health Sci 2003; 1(23-28): 12-26.
9. Velasquez B, Herrera C, Ibanez B. Earthworm meal. II. Fatty acid composition, antinutritional factors and heat treatment for control of bacteria. Alimentos 1987; 11(4): 9-13.
10. Albro PW, Schroeder JL, Corbett JL. Lipids of the earthworm *Lumbricus terrestris*. Lipids 1992; 27(2): 136-43.
11. Albro PW, Corbett JL, Schroeder JL. Lipids of the earthworm *Lumbricus terrestris*. Biochem Cell Biol 1993; 71(3-4): 220-221.
12. Yang D, Wang F, Peng J, Xiao L, Su W. Study on lipids and other volatile constituents in *Pheretima aspergillum*. Zhong Yao Cai 2000; 23(1): 31-33.
13. Johnson AR, Davenport JB. 1971. Biochemistry and Methodology of Lipids. John Wiley & Sons, INC, New York, pp. 131-136.
14. Nonaka G, Minami M, Nishioka I. Studies on rhubarb (*Rhei* rhizoma). III. Stilbene glycosides. Chem Pharmaceut Bull 1977; 25(9): 2300–2305.
15. Cerbulis J, Ard J. Methods for the isolation of di-octylphthalate from milk lipids. J Assoc Offic Anal Chem 1967; 50: 646.
16. Forbesa SL, Keeganb J, Stuartb BH. Boyd B. Dentc A gas chromatography-mass spectrometry method for the detection of adipocere in grave soils. Eur J Lipid Sci Technol 2003; 105: 761–768.
17. Sampedro L, Whalen JK. Changes in the fatty acid profiles through the digestive tract of the earthworm *Lumbricus terrestris* L. Appl Soil Ecol 2007; 35: 226–236.
18. Egert M, Marhan S, Wagner B, Scheu S, Friedrich MW. Molecular profiling of 16S rRNA genes reveals diet-related differences of microbial communities in soil, gut and casts of *Lumbricus terrestris* L. (*Oligochaeta*: *Lumbricidae*). FEMS Microbiol Ecol 2004; 48, 187–197.
19. WHO. 2003. Technical Report Series 916, Report of a Joint WHO/FAO Expert Consultation, World Health Organization, Geneva, pp. 88.
20. French MA, Sundram K, Clandinin MT. Cholesterolaemic effect of palmitic acid in relation to other dietary fatty acids. Asia Pacific J Clin Nutr 2002; 11(7): S401–S407.
21. Sedky K, Racha N, Nazir MD, Lindenmayer JP, Lippmann S. Paliperidone palmitate: Once-monthly treatment option for schizophrenia. Curr Psychiatry 2010; 9(3): 48-49.
22. Alkan C, Kaya K, Sari A. Preparation and thermal

properties of ethylene glycol distearate as a novel phase change material for energy storage. Materials Lett 2008; 15(6-7): 1122-1125.

23. Pan PH, Lin SY, Ou YC, Chen WY, Chuang YH, Yen YJ, Liao SL, Raung SL, Chen CJ. Stearic acid attenuates cholestasis-induced liver injury. Biochem Biophys Res Commun 2010; 391(3): 1537-1542.
24. Pari L, Saravanan R. Beneficial effect of succinic acid monoethyl ester on erythrocyte membrane bound enzymes and antioxidant status in streptozotocin–nicotinamide induced type 2 diabetes. Chem Biol Interact 2007; 169(1): 15-24.
25. Abe A, Yamane M, Yamada H, Sugawara I. The ω-Hydroxy palmitic acid induced apoptosis in human lung carcinoma cell lines H596 and A54. J Biochem Mol Biol Biophys 2002; 6(1): 37-43.
26. Dimitriadis E, Griffin M, Collins P, Johnson A, Owens D, Tomkin GH. Lipoprotein composition in NIDDM: effects of dietary oleic acid on the composition, oxidisability and function of low and high density lipoproteins. Diabetologia 1996; 39: 667–676.
27. Moreno JJ, Mitjavila MT. The degree of unsaturation of dietary fatty acids and the development of atherosclerosis. J Nutr Biochem 2003; 14(4): 182–195.
28. Dilika F, Bremner PD, Meyer JJ. Antibacterial activity of linoleic and oleic acids isolated from Helichrysum pedunculatum: a plant used during circumcision rites. Fitoterapia 2000; 71(4): 450–452.
29. Nishitani Y, Okazaki S, Imabayashi K, Katada R, Umetani K, Yajima H, Matsumoto H. Saturated and mono-unsaturated fatty acids increase interleukin-10 production in rat hepatocytes. Nihon Arukoru Yakubutsu Igakkai Zasshi 2007; 42(1): 32–35.

Journal of Biology and Earth Sciences

MEDICINE REVIEW

Role of brain glutamic acid metabolism changes in neurodegenerative pathologies

Nina P. Kanunnikova

Yanka Kupala's State University, Grodno, Belarus

ABSTRACT

Glutamic acid is an essential participant of brain metabolism. It is known that the glutamate is a neurotransmitter in a numerous part of the brain synapses and acts through various ionotropic or metabotropic receptors. Multiple alterations of the brain glutamate system are observed in both acute and chronic brain injures. Glutamate metabolism changes take place in many neurodegenerative pathologies, such as brain ischemia, Parkinson's disease, Alzheimer's disease, Huntington's disease, amyotrophic lateral sclerosis etc. These disruptions may be related to changes of glutamate metabolism enzyme activities, alterations of the main energy formation reactions in mitochondria, and shifts of oxidation/redox balance in cells. Potential targets for therapy of neurodegenerative diseases, especially in chronic treatment, can include the drugs for recovery of glutamate metabolism system.

Key words: glutamic acid, glutamate metabolism, neurodegenerative pathologies, enzymes of glutamate metabolism, brain ischemia.

J Biol Earth Sci 2012; 2(1): M1-M10

Corresponding author:
Nina P. Kanunnikova
Department of Zoology and Physiology of Human and Animals, Yanka Kupala's State University,
22 Orzheshko str., Grodno, 230023, Belarus
E-mail: n.kanunnikava@gmail.com
n.kanunnikova@grsu.by

Original Submission: 28 February 2012; Revised Submission: 20 March 2012; Accepted: 21 March 2012

ISSN: 2084-3577
http://www.journals.tmkarpinski.com/index.php/jbes or http://jbes.strefa.pl
e-mail: jbes@interia.eu

INTRODUCTION

Due to many different roles associated with brain glutamate, it is not surprising that the glutamate system is probably the most versatile and complex signalling system in the brain. Glutamic acid is an essential participant of brain metabolism, as well as a main excitatory neurotransmitter in the brain, therefore changes in this process can be observed when studying most cases of neurodegenerative diseases [1-9]. It is known that the glutamate is a neurotransmitter in a numerous part of the brain synapses and acts through various ionotropic or metabotropic receptors (Fig. 1) [3, 8, 10, 11].

Another peculiarity of brain glutamate metabolism is its close relation to the citrate cycle and to energy metabolism [10-12]. Metabolism of glucose in the brain depends on glutamate to a great extent. Glucose and glycogen are essential sources of energy not only for maintaining glutamate homeostasis but also for glutamatergic neurotransmission [13]. Brain glutamate comes from 2-oxoglutarate by means of direct amine incorporation by glutamate dehydrogenase (GDH) or through reamine incorporation by transaminases [8]. These processes help to support levels of citrate cycle metabolites for sufficient energy formation and redox equivalents supply to neuron mitochondria.

Third peculiarity of brain glutamate metabolism is the fact that some of its steps take place in certain types of cells - in neurons or in glial cells, therefore a close and accurate interrelation between neurons and glia is necessary [14]. An injection of radioactively labeled main precursors of glutamate, such as glucose and acetate, showed their participation in the glutamate synthesis through two different citrate cycles in the brain tissue. It seems that glucose is metabolized in neurons [10, 11], whereas acetate is processed in astroglial cells [11], which display a higher glutamine synthase activity [12, 14, 15]. Apart from that, neurons must catch glutamine from glial cells for maintaining the transmitter role of the glutamate, and for maintaining energy metabolism, too. Glutamine is a transport form of glutamate transfer from glial cells into neurons. Since carboxylation of pyruvate to oxaloacetate occurs in astrocytes, net synthesis of 2-oxoglutarate in the TCA cycle can also take place in these cells.

At least a certain rate of glutamate synthesis is necessary for maintaining glutamate level in synaptic vesicules. New molecules of glutamate and GABA are mainly formed from glucose [8, 11, 13]. Oxaloacetic acid is predominantly formed from pyruvate within astrocytes, therefore main synthesis of 2-oxoglutaric acid for the Krebs cycle takes place within astrocyte cells.

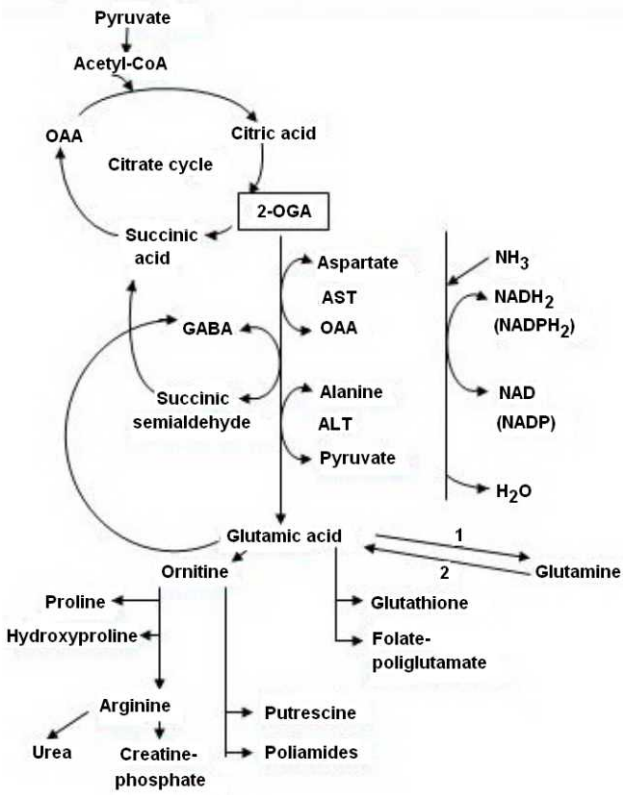

Fig. 1. Some ways for metabolism of glutamate in nervous tissue and its relation to citric acid cycle.
Legend:
1 - glutamine synthetase,
2 - glutaminase,
2-OGA - 2-oxoglutaric acid,
AST - aspartate transaminase,
ALT - alanine transaminase,
OAA - oxaloacetic acid.

Fourth peculiarity of brain glutamate metabolism is its close relation to ammonia metabolism. The urea cycle reactions are considerably slower in the brain tissue, and the main way of binding excessive ammonia ions in the brain is through formation of glutamine. The ammonia ions enter brain by diffusing through the blood-brain barrier or are formed within brain [16]. Excessive levels of ammonia ions are toxic for brain, therefore amount of ammonia is kept low with the help of high activity of the glutamine synthetase.

The influx of glutamate from plasma across the blood-brain barrier is much lower than its efflux from

brain [17, 18], therefore brain metabolism of glutamate plays an important role in the maintenance of normal brain tissue function.

Depolarization of glutamatergic presynaptic nerve endings leads to excretion of glutamate from vesicules by Ca-dependent exocytosis into synaptic cleft (Fig. 2). During excitation glutamate concentration may peak at around 1 mM in the synaptic cleft, but it is then immediately decreased to 1-2 μM. Glutamate acts on ionotropic receptors (i-glu-R, bound with ion channels) or metabotropic ones (m-glu-R, bound with second messengers), after that it is removed from the synaptic cleft by reuptake into nerve endings, or by diffusion and uptake into glial cells by glutamate transporters [9, 19, 20]. Excitatory amino acid transporter EAAT-2 is one of the major glutamate transporters expressed predominantly in astroglial cells and is responsible for 90% of total glutamate uptake. Glutamate transporters tightly regulate glutamate concentration in the synaptic cleft [21].

Within presynaptic nerve endings glutamate enters specialized vesicules with the help of specific vesicular transporter. Amount of glutamate that can be excreted from nerve ending depends on the activity of the transporter. Glutamate is removed from a synaptic cleft by reuptake transporters which are located in neuronal and glial membranes. The transporters carry inside one molecule of glutamate together with one sodium ion and one proton, and transfer outside one potassium ion.

Glutamate inside astrocytes is turned into glutamine by glutamine synthetase. One of the primary roles of astrocytes is to protect neurons from excitotoxicity by taking up excess ammonia and glutamate and converting them into glutamine with the help of enzyme glutamine synthase [5, 14]. After that glutamine is transferred into neurons where it is transformed into glutamate by glutaminase. Then glutamate is preserved within vesicules. Part of resulting glutamate may be immediately transferred to presynaptic nerve ending by special membrane transporter.

Disruption of glutamate removal from synaptic cleft results in glutamate excitotoxicity [3, 9, 20]. In cases of energy shortage (e.g. during ischemia), glutamate level in the synaptic cleft may remain unusually high for a long time which will initiate a cascade of excitotoxic reactions. Excitotoxicity is caused by excessive activation of excitatory amino acid receptors which leads to an uncontrolled

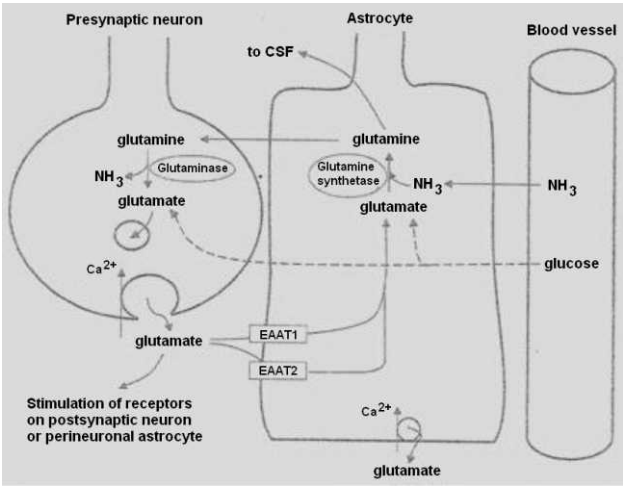

Fig. 2. Schematic representation of the synthesis, metabolism and intracellular transport of glutamate into the brain (based on Vaquero J, Butterworth RF, 2006). EAAT-1, EAAT-2 - high-affinity glutamate transporters localized on astrocytes.

increase of sodium and potassium ion levels in the cell resulting in cell death [21].

Exposure of brain tissue to very high concentrations of potassium (above 20 mM) leads to membrane depolarization and depolarization-dependent increase of free potassium in synaptosomes, neurons and astrocytes. This facilitates removal of glutamate (and GABA) from neurons and CO_2 accumulation within astrocytes. As the result, metabolic exchange between neurons and glial cells is intensified therefore stimulating synthesis of neurotransmitter precursors inside neurons [22-24].

REVIEW

Glutamate metabolism enzymes

Glutamine synthetase (EC 6.3.1.2)

Glutamine synthetase acts as a catalyst in the following reaction:

Glutamate + NH_3 + ATP → Glutamine + ADP + P_i.

The enzyme from mammalian brain has two important functions: assimilation of ammonia and biosynthesis of glutamine. It catalizes the direct and reverse reactions with rate approximately 10:1 (with sufficient level of ATP in a tissue) [25, 26]. Glutamine synthetase is composed of eight identical subunits (44-50 kDa). Distribution of glutamine synthetase is uneven in the central nervous system: the highest activity is observed in the structures where the quantity of glutamatergic neurones is the

highest [14, 15, 18, 30], and the enzyme takes place in cytosole [26, 27, 31]. Induction of the glutamine synthetase expression is the way for protection of neurons against increase of extracellular glutamate concentration, whereas decrease of the expression may lead to disruption of metabolic interrelations between neurons and glia during hyperammonemia [31, 32, 33].

Changes in glutamine synthetase expression may reflect changes in astroglial function, which can affect neuronal functions, especially in astrocytes located in glutamatergic areas. Hyperammonemia is an important factor responsible of hepatic encephalopathy and causes astroglial swelling [1]. The induction of glutamine synthetase expression in these specific areas would balance the increased ammonia and glutamate uptake and protect against neuron al degeneration, whereas decrease of its expression in non-glutamatergic areas could disrupt the neuron-glial metabolic interactions as a consequence of hyperammonemia [18, 34. 35].

In glutamatergic areas, the distribution of both glial glutamate receptors and and glial glutamate transporters parallels the glutamine synthetase location, suggesting a functional coupling between glutamate reuptake and glutamine synthase to attenuate brain injury in these areas.

In hyperammonemia, the astroglial cells located in proximity to blood capillars in glutamatergic areas show increased glutamine synthase protein content in their perivascular tissue. Since ammonia freely crosses the blood-brain barrier and astrocytes are responsible for maintaining the blood-brain barrier, the presence of glutamine synthase in the perivascular tissue could produce a rapid glutamine synthesis to be released into blood, and glutamine synthase could play an important role in removal of ammonia from the brain. Glutamine synthetase is not working at maximum rate in brain and its activity may be increased by blocking i-glu (NMDA) receptors [36, 37]. The activation of glutamate receptors may also favour nitric oxide (NO) formation by activation of NO-synthase (NOS), and NO has been implicated in the pathogenesis of several CNS diseases [36]. Glial cells have carboanhydrase which catalizes conversion of CO_2 into H_2CO_3, too. Consequently, glial cells take part in a regulation of oxidation-reduction balance and of metabolism of glutamate-related amino acids in the CNS. The glutamine synthetase is activated by 2-oxoglutarate in a liver but not in a brain [25, 30, 35]. Glutamine synthetase is irreversibly inhibited by methionine sulfoximine. And this inhibition significantly impairs glutamate uptake and glutamine release [38].

Glutaminase (EC 3.5.1.2)

Glutaminase catalizes reaction of glutamine catabolism to glutamate and ammonia. Its activity can be observed both in neurones and astroglial cells [39], but glutaminase is more active in neurons, predominantly in mitochondria [40, 41]. Mitochondria from pig brain have two main isoforms of the enzyme. One of them is soluble and resides in matrix, while the other is membrane-bound and remains on inner mitochondria membrane. Both isoforms are activated by phosphate [39].

Soluble glutaminase is a dimer of rather low specific activity which easily aggregates into a more active form following incubation in presence of phosphate [39, 42]. It seems that soluble and membrane-bound forms of the enzyme have different functions in brain. Km for glutamine is equal 0.8-1.4 mM and 3.4-9.7 mM. One of the products, glutamate, inhibits glutaminase to a great extent while the other product, ammonia, inhibits the enzyme very weakly. Activity of glutaminase in brain is low. The enzyme becomes free from inhibitory influence of glutamate only when the concentration of glutamic acid falls below normal values [43].

Glutamate dehydrogenase (EC 1.4.1.2-4, GDH)

Glutamate dehydrogenase catalyzes a reversible reaction:

L-glutamic acid + H_2O + NAD(P) ↔ 2-oxoglutarate + NH_3 + NAD(P)H.

GDH is an enzyme central to the metabolism of glutamate. It is encoded by a single gene (GLUD1 in humans) which occurs widely. Humans and other primates also possess a second gene, GLUD2, which encodes a highly homologous GDH isoenzyme (hGDH2) expressed predominantly in retina, brain and testis. hGDH2 localizes mainly to mitochondria and to a lesser extent to the endoplasmic reticulum of these cells [44].

The GDH reaction is reversible but equilibrium is shifted closer to direct reaction (i.e. to synthesis of glutamic acid) [9, 42, 43, 44]. Consequently, GDH in brain takes part in synthesis of glutamate from 2-oxoglutaric acid more than in oxidation of the amino acid. This is the way for continious maintenance for changing of a free ammonia into amino nitrogen of amino acids. On the other hand,

this leads to a loss of 2-oxoglutarate from the pool of citrate cycle intermediates inside mitochondria and to decrease of rate of glucose oxidation which is a main energy source for brain cells. On the contrary, reversion of the GDH reaction is one of the ways for restoration of cytrate cycle intermediate pool. Only optimal ratio of direct and reverse reactions may guarantee normal work of brain cells.

GDH may exist in one of three forms. Each of them can contain NAD/NADH (EC 1.4.1.2), or NADP/NADPH (EC 1.4.1.4), or both the cofactors (EC 1.4.1.3). Neuronal GDH (EC 1.4.1.3) may possess both cofactors but NAD is more effective than NADP [9, 11]. The direction of preferable reaction depends on the balance between NAD(P)/NAD(P)H in the tissue.

Two forms of GDH are present in brain, soluble and insoluble. They differ by their kinetic parameters, stability to heat denaturation, and allosteric properties. Oxidative deamination of glutamate takes place if glucose is absent. In the presence of glucose, redox amination of 2-oxoglutaric acid prevails [9, 11]. GDH from a bull brain can utilise both NAD and NADP cofactors. It has molecular mass of 332 kDa and consists from 6 identical subunits. Vmax of GDH in synaptic mitochondria from a rat brain is 20-40% lower than Vmax of aspartic acid transaminase (AST) but 4-5 times higher than the activity of phosphate-dependent glutaminase [43].

Aspartate transaminase (AST, or glutamate oxaloacetate transaminase, EC 2.6.1.1)

Aspartate transaminase catalizes reversible transfer of amino group to 2-oxoglutarate, as a result oxaloacetate and glutamate are formed. This is the most active transaminase in a brain. Rat brain AST activity is 2.5-10 times higher than activity of GDH [8]. 90% of glutamate is transaminated to aspartic acid within brain mitochondria.

Oxaloacetate is quickly transformed into malic acid which enters from cytoplasma into mitochondria. In this way the aspartate-malate bypath for transfer redox equivalents from a cytosol into mitochondria is formed. This bypath is the main way for transfer redox equivalents into mitochondria in neurons. Influx of aspartate through mitochondria membrane is bound with efflux of a glutamate. In such a way influx of a malate is bound with efflux of 2-oxoglutarate, too.

Mammals have two isoforms of the enzyme - cytoplasmic and mitochodrial. Both forms are dimers containing subunits in 45 and 2 kDa [8, 42]. Functional roles of these forms are different. The mitochondrial form is related to citrate cycle functioning whereas the cytoplasmic form determines gluconeogenesis activity.

Another transaminase, ***alanine transaminase (ALT, EC 2.6.1.2)***, transfers an amino group from alanine to 2-oxoglutarate with forming pyruvate and glutamate. It has cytoplasmic and mitochondrial isoforms.

Macroergic substances play an important role in the regulation of balance between dehydrogenase and transaminase ways of metabolism, which compete for one substrate. Under normal conditions, citrate cycle utilises transaminase way products while dehydrogenase path of glutamate oxidation is suppressed. If the level of macroergic compounds decreases (for example, after addition of 2,4-dinitrophenol which divides oxidative phosphorilation), the transamination way is suppressed but the dehydrogenase path of glutamate oxidation increases to a great extent.

Systemic introduction of ammonia salts cause seazures and increase of glutamine content in a brain [16, 18]. Synthesis of adequate content of glutamate must precede glutamine synthesis because the amount of glutamate received from blood flow may be insufficient if level of ammonia in blood is high. Since 2-oxoglutarate is a direct precursor of glutamate, formation of glutamine from glutamic acid and ammonia may cause rapid decrease of levels of the Krebs cycle intermediates if they are not replenished by transformation of pyruvate into oxaloacetate accompanied with CO_2 fixation. Indeed, significant inclusion of CO_2 into amino acids is observed in brain tissue after possible metabolism of CO_2 in the Krebs cycle. After an injection of ammonia, additional quantity of oxaloacetate goes to a synthesis of glutamine (through a 2-oxoglutarate step). Activation of AST may help with protection from toxic effects of ammonia [1, 8, 33].

Glutamic acid decarboxylase (EC 4.1.1.15, GAD)

Glutamic acid decarboxylase catalyzes separation of a carboxylic group from glutamate with forming of gamma-amino butyric acid (GABA). Cofactor in the reaction is a pyridoxal phosphate, as in AST and ALT. The enzyme has high specificity for substrate, and its activity is found predominantly in

brain tissue. When GAD acts on glutamate which has excitatory influence on neurons, then GABA is formed which is a main inhibitory neurotransmitter in the brain. It is known that the degree of a brain tissue damage depends not only on the level of glutamate, but also on the ratio of excitatory and inhibitory processes, that is on balance between levels of glutamate and aspartate and levels of GABA and glycine [42, 45]. Increase of excitatory/inhibitory index during reperfusion is shown in the regions susceptible to ischemic injury, and the rise correlates with an increasing of a glycine level.

Disruptions of glutamate metabolism in the brain

Glutamate-induced excitotoxicity is responsible for neuronal death in acute neurological conditions as well as in chronic neurodegeneration. The underlying mechanisms through which glutamate excitotoxicity affects neurodegeneration still needs further investigation. Glutamate excitotoxicity has been linked to neurodegenerative disorders such as amyotrophic lateral sclerosis, multiple sclerosis, Parkinson's disease, brain ischemia and reperfusion and others [7-10, 46, 47]. Maintenance of a low level (1-3 μM) of extracellular glutamate is a necessary condition for normal functioning of brain as this restricts excessive stimulation of receptors and excessive formation of ammonia by GDH. These effects of extracellular glutamate may lead to neuron death. Glutamate neurotoxicity may be prevented by glutamate antagonists and weakened by addition of antagonists following exposure to glutamate. Excessive activation of glutamate receptors by excitatory amino acids leads to a number of deleterious consequences, including impairment of calcium buffering, generation of free radicals, activation of the mitochondrial permeability transition and secondary excitotoxicity [48-53].

Dysfunction of EAAT2 and accumulation of excessive extracellular glutamate are among the causes of development of several neurodegenerative diseases including Alzheimer's disease, Huntington's disease, and amyotrophic lateral sclerosis [21].

Presence of increased level of extracellular glutamate during neurodegenerative diseases (including diseases with brain hypoxia/ischemia) was described in many articles. Excessive extracellular glutamate accumulation during hypoxia may be related to activation of Ca-independent mechanism disrupting glutamate transport into neurons [22, 30, 52, 53]. This increase of extracellular glutamate acts predominantly on postsynaptic structures and leads to increase of intracellular calcium concentration, resulting in cell death.

Mechanisms for increase of glutamate level during neurodegenerative diseases have not been fully studied. Increase of extracellular glutamate levels may be caused by inhibition of GDH activity (e.g. in Parkinson's disease) [49, 54] or because of a reduction of Na-dependent glutamate transporters (in lateral amyotrophic sclerosis, Huntington's disease) [55-59].

In Alzheimer's disease death of cells may be caused by excessive synthesis or excretion of glutamate, or insufficiently active reuptake, weakened degradation or decreased inhibition of excitatory neurons. Each of these processes, particularly in the beginning of a disease, may promote local increase of glutamate level and therefore initiate slowly progressing neurodegeneration and probable death of a neuron [45, 50, 51].

Postmortal study of brains of patients with Alzheimer's disease showed lower glutamate content in frontal and parietal lobes, but level of free glutamate in cerebrospinal fluid was significantly higher than in samples taken from control group [45, 59].

In Huntington's disease glutamate and GABA contents are lower in brain basal ganglia but not in the frontal lobes. This decline may be caused by disruption of glutamate reuptake from a synaptic cleft but not by lowered secretion as significant decrease of the high-affinity sites for glutamate binding is observed in autopsy tissue of basal ganglia of patients with Parkinson's disease [59]. High concentration of glutamate in synaptic cleft causes damage of neurons. Excess glutamate enters into liquor, and level of the amino acid in the basal ganglia is decreased. Altered glutamatergic neurotransmission and neuronal metabolic dysfunction appear to be central to the pathophysiology of Parkinson's disease [9].

Decline of an activity of the mitochondrial respiratory chain complex I in substantia nigra was found at Parkinson's disease [56]. Failure of complexes II and IY was observed in biopsy muscle tissue in patients with Parkinson's disease, as well

as decreased activity of GDH but not of pyruvate dehydrogenase complex. Intake of redox equivalents (NADH) into respiratory chain takes place at the complex I level, therefore its decrease may cause inhibition of GDH caused by feedback mechanism, which in turn would result aggravation of glutamate excitotoxicity through NMDA-receptors at dopaminergic nerve endings within corpus striatum and contribute to degeneration of neurons.

Amyotrophic lateral sclerosis is characterized by neuron degeneration in motor cortex, brain stem and spinal cord. It seems that change of glutamate transporter function presented within astrocytes [57] is the main reason of such neurodegeneration, but weakening of glutamate uptake is not accompanied by decrease of expression of the transporter synthesis, so data on gene mutations of the synthesis of the protein is absent. Studies have shown an important role of free radicals and disruptions of superoxide dismutase function in development of an amyotrophic lateral sclerosis. It is possible that these changes cause injures to glutamate transporters. It was shown that changes of glutamate level in amyotrophic lateral sclerosis, and these disruptions were associated to glutathione decrease in the brain [60].

Now we have strong proof for the important role of changes of glutamate transport in development of ischemic injuries in brain tissue. In the first minutes of ischemia slow shift of pH to acid side accompanied with slow increase of extracellular cobcentration of a potassium and following decrease of extracellular levels of calcium and sodium is observed. The elevation of potassium level leads to depolarization of surrounding cells by -20 mV (anoxic depolarization) and release of glutamate [24, 42]. Explanations for the disruptions of glutamate release mechanisms are rather contradictory. On the one hand, there is evidence that this release is Ca-dependent (i.e. glutamate excreted from vesicules), but on the other hand we know that the release does not depend on Ca. Latter information supports the suggestion of an important role that is played by glutamate reuptake disruption [42]. It was shown that increased level of glutamate release induces apoptotic cell death in the 11 vessel occlusion ischemic model [61].

AST which metabolizes glutamate into citric cycle intermediates may be useful to harness excess neurotoxic extracellular glutamate during brain ischemia. And delivery of AST minimized lesion volume, whereas AST knockdown worsened stroke outcomes [62]. Superfusate aspartate, glutamate, phosphoethanolamine, taurine, and GABA were significantly elevated by cerebral ischemia, then declined during reperfusion. The ischemia-evoked accumulations of aspartate, glutamate, taurine and GABA were all significantly depressed by glucose, while phosphoethanolamine levels were elevated [63].

Glutamate toxicity and cellular calcium overload are thought to be pathophysiological key factors not only in gray matter but also in white matter during ischemia and reperfusion [45, 51]. Glutamate, aspartate, GABA, and taurine are increased in gray matter but not in white. Deleterious processes such as glutamate accumulation and cellular Ca^{2+} influx occur in gray matter only.

Glutamate excitotoxicity is closely bound with energy metabolism disruptions and changes of antioxidant activity in the brain tissue. Oxidative stress and unbalanced cellular energy homeostasis are key aspects in many neurodegenerative pathologies [13, 64].

Free radicals decrease activity of the reactions of transamination in the brain that exacerbate disruptions of energy-dependent transport of ions, inhibit glutamine synthetase, and activate synthesis of glutamate in GDH reaction [4, 34].

Brain lacks a complete urea cycle and glutamine represents a temporary storage form of excess ammonia which is neurotoxic. Hyperammonemia results in increased formation of glutamine directly in astrocytes, thereby generating an osmotic stress in these cells, which in turn leads to neuronal disfunction. Syndromes which result in increased level of ammonia (e.g. liver failure, inborn defects of an urea cycle, Reye disease) lead to astrocyte damage. Harm is done directly by increased glutamine synthesis inside astrocytes an also induced by osmotic stress.

Chronic treatment of rats with the anti-epileptic drug sodium valproate leads to dose-dependent increase in glutamate uptake capacity in hippocamp, but not in hemispheres or cerebellum, by increasing of the levels of glutamate transporters EAAT1 and EAAT2 [11]. And this effect is the result of inhibition of phosphate-activated glutaminase. It seems that valproate may have a role in the treatment of excitotoxical effects of glutamate in the hippocampus.

Immediately following the hypoxic stroke there

was a rapid transient elevation of glutamate level in neonatal rat brain followed by a fall. Glutamine content and glutamine synthetase activity were decreased immediately after hypoxia and returned to normal values within 6 hours [12].

Changes in astrocytes glutamine synthetase in some regions of postischemic rat brain were correlated with regional neuronal vulnerability or resistance of the regions to ischemia. Immediately after ischemia activity of glutamine synthetase was increased in cortex, striatum and hippocampus but not in other brain regions [13]. These changes may be important in normalizing extracellular glutamate following ischemia and protecting brain from neurotoxic effects of the amino acid. Brain glutamine and glutamate loss is correlated with deteriorated social functioning and gray matter losses in schizophrenia, consistent with neuro-degeneration [65]. Glutamatergic neurotransmission has also been implicated in mechanisms of alcohol-induced neurodegeneration and cognitive impairment [66].

Changes in glutamate levels as well as correlation between glutamate and glutamine in the whole brain of newborn rats were not found despite 2-fold decrease of glutamine synthetase activity. This fact testifies that significant changes in glutamate metabolism take place only in separate important brain structures [45].

CONCLUSIONS

Multiple alterations of the brain glutamate system are observed in both acute and chronic brain injures. Glutamate metabolism changes take place in many neurodegenerative pathologies, such as brain ischemia, Parkinson's disease, Alzheimer's disease, Huntington's disease, amyotrophic lateral sclerosis etc. These disruptions may be related to changes of glutamate metabolism enzyme activities, alterations of the main energy formation reactions in mitochondria, and shifts of oxidation/redox balance in cells. Potential targets for therapy of neurodegenerative diseases, especially in chronic treatment, can include the drugs for recovery of glutamate metabolism system.

TRANSPARENCY DECLARATION

The author declare no conflicts of interest.

REFERENCES

1. Vaquero J, Butterworth RF. The brain glutamate system in liver failure. J Neurochem 2006; 98: 661-669.
2. Benveniste H, Drejer J, Schousboe A, Diemer NH. Elevation of the extracellular concentrations of glutamate and aspartate in rat hippocampus during transient cerebral ischemia monitored by intracerebral microdialysis. J Neurochem 1984; 43: 1369-1374.
3. Rothman SM, Olney JW. Glutamate and the pathophysiology of hypoxic-ischemic brain damage. Ann Neurol 1986; 19(2): 105-111.
4. Coyle JT, Puttfarcken P. Oxidative stress, glutamate and neurodegenerative disorders. Science 1993; 262: 689-695.
5. Palmada M, Centelles JJ. Excitatory amino acid neurotransmission. Pathways for metabolism, storage and reuptake of glutamate in brain. Front Biosci 1998; 3: d701-718.
6. Telushkin PK. Glutamate and lipoperoxidation in CNS disease pathogenesis. Vopr Med Chem 1998; 44(6): 520-526 (Rus).
7. Choi DV. Glutamate neurotoxicity and disease of the nervous system. Neuron 1988; 1: 628-634.
8. Thomas RJ. Excitatory amino acids in health and disease. J Am Geriatr Soc 1995; 43(11): 1279-1289.
9. Blandini F, Porter RH, Greenamyre JT. Glutamate and Parkinson's disease. Mol Neurobiol 1996; 12(1): 73-94.
10. Lau A, Tymianski M. Glutamate receptors, neurotoxicity and neurodegeneration. Pflugers Arch 2010; 460(2): 525-542.
11. Erecinska M, Silver IA. Metabolism and role of glutamate in mammalian brain. Progr Neurobiol 1990; 35: 245-296.
12. Obel LF, Andersen KM, Bak LK, Schousboe A, Waagepetersen HS. Effects of Adrenergic Agents on Intracellular Ca(2+) Homeostasis and Metabolism of Glucose in Astrocytes with an Emphasis on Pyruvate Carboxylation, Oxidative Decarboxylation and Recycling: Implications for Glutamate Neurotransmission and Excitotoxicity. Neurotox Res. 2012; 21(4): 405-417.
13. Genius J, Geiger J, Bender A, Möller HJ, Klopstock T, Rujescu D. Creatine protects against excitoxicity in an in vitro model of neurodegeneration. PLoS One 2012; 7(2): e30554.
14. Hertz L, Dringen R, Schousboe A, Robinson SR. Astrocytes: glutamate producers for neurons. J Neurosci Res 1999; 57(4): 417-428.
15. Hertz L, Schousboe A. Metabolism of glutamate and glutamine in neurones and astrocytes in primary cultures. In: Glutamine and glutamate in mammals. Eds: Kvamme E. CRC Press. Boca Raton, Fla. 1988,

2: 39-55.
16. Cooper FJ. Role of glutamine in cerebral nitrogen metabolism and ammonia neurotoxicity. Mental Retard Dev Disabil Res Rev 2001; 7(4): 280-286.
17. Oldendorf WY, Szabo J. Amino acid assignment to one of three blood-brain barrier amino acid carriers. Am J Physiol 1976; 230(1): 94-98.
18. Suarez I, Bodega G, Fernandez B. Glutamine synthetase in brain: effect of ammonia. Neurochem Int 2002; 41(2-3): 123-142.
19. Hassel D, Iversen EC, Gjerstad L, Tauboll E. Up-regulation of hippocampal glutamate transport during chronic treatment with sodium valproate. J Neurochem 2001; 77(5): 1285-1292.
20. Pratt OE. The transport of metaboliable substances into the living brain. Adv Exp Med Biol 1976; 69: 55-75.
21. Kim K, Lee SG, Kegelman TP, Su ZZ, Das SK, Dash R, et al. Role of excitatory amino acid transporter-2 (EAAT2) and glutamate in neurodegeneration: opportunities for developing novel therapeutics. J Cell Physiol 2011; 226(10): 2484-93.
22. Lazarewicz J, Salinska E. Ekscytotoksyczność jako mechanizm neurodegeneracji i cel dla strategii terapeutycznych. Neuroprotekcja. XX Zimowa Szkoła Instytutu Farmakologii PAN. Mogilany 2003. Kraków 2003: 9-28.
23. Ancarcrona M, Dypbukt JM, Bonfoco E, Zhivotovsky B, Orrenius S, Lipton SA, Nicotera P. Glutamate-induced neuronal death; a succession of necrosis or apoptosis depending on mitochondrial function. Neuron 1995; 15: 961-973.
24. Erecinska M, Nelson D, Chance B. Depolarization induced changes in cellular energy production. Proc Natl Acad Sci USA 1991; 88: 7600-7604.
25. Boksha IS, Tereshkina EB, Burbayeva GS. Isolation and some properties of glutamine synthetase from human brain. Biokhimia (Mosc) 1995; 60(10): 1697-1705 (Rus).
26. Deuel TF, Louie M, Lerner A. Glutamine synthetase from rat liver. Purification, properties, and preparation of specific antisera. J Biol Chem 1978; 253(17): 6111-6118.
27. Krajnc D, Neff NH, Hadjiconstantinou M. Glutamate, glutamine and glutamine synthetase in the neonatal rat brain following hypoxia. Brain Res 1996; 707(1): 134-137.
28. Petito CK, Chung M, Verkhovsky LM, Cooper A. Brain glutamine synthetase increases following cerebral ishemia in the rat. Ibid 1992; 569(2): 275-280.
29. Schor NF, Barmada MA, Nemoto E. Brain glutamine synthetase activity and hyperoxia in neonatal rats. Ibid 1991; 566(1-2): 342-343.
30. Boksha IS, et al. Glutamine synthetase isolated from human brain: octameric structure and homology of partial primary structure with human liver glutamine synthetase. Biochemistry (Mosc) 2002; 67(9): 1012-1020.
31. Ward HK, Bradford HF. Relative activities of glutamine synthetase and glutaminase in mammalian synaptosomes. J Neurochem 1979; 33: 339-342.
32. Almeida A, Delgado-Esteban M, Bolaños JP, Medina JM. Oxygen and glucose deprivation induces mitochondrial dysfunction and oxidative stress in neurones but not in astrocytes in primary culture. J Neurochem 2002; 82: 207-217.
33. Norenberg MD, Martinez-Hernondez A. Fine structural localization of glutamine synthetase in astrocytes of rat brain. Brain Res 1979; 161: 303-310.
34. Oliver CN, Starke-Reed PE, Stadtman ER, Liu GJ, Carney JM, Floyd RA. Oxidative damage to brain proteins loss of glutamine synthesis activity and production of free radicals during ischemia-reperfusion induced injury to gerbil brain. Proc Natl Asad Sci USA 1990; 87: 5144-5147.
35. Boksha IS, Tereshkina EB, Burbaeva GS. Glutamine synthetase and glutamine synthetase-like protein from human brain: purification and comparative characterization. J Neurochem 2000; 75(6): 2574-2582.
36. Dawson VL, Dawson TM, London ED, Bredt DS, Snyder SH. Nitric oxide mediates glutamate neurotoxicity in primary cortical cultures. Proc Natl Acad Sci USA 1991; 88: 6368-6371.
37. Kosenko E, Llansola M, Montoliu C, Monfort P, Rodrigo R, Hernandez-Viadel M. et al. Glutamine synthetase activity and glutamine content in brain: modulation by NMDA receptors and nitric oxide. Neurochem Int 2003; 43(4-5): 493-499.
38. Zou J, Wang YX, Dou FF, Lü HZ, Ma ZW, Lu PH, Xu XM. Glutamine synthetase down-regulation reduces astrocyte protection against glutamate excitotoxicity to neurons. Neurochem Int 2010; 56(4): 577-584.
39. Nimmo GA, Tipton KF. The distribution of soluble and membrane-bound forms of glutaminase in pig brain. J Neurochem 1979; 33: 1089-1094.
40. Collins RM, Zielke HR, Woody RC. Valproate increases glutaminase and decreases glutamine synthetase in primary cultures of rat brain astrocytes. J Neurochem 1994; 62: 1137-1143.
41. Kvamme E, Torgner IA, Roberg B. Kinetics and localization of brain phosphate activated glutaminase. J Neurosci Res 2001; 66(5): 951-958.
42. Dennis SC, Clarke JB. The pathway of glutamate metabolism in rat brain mitochondria. Biochem J 1977; 168: 521-427.
43. Plaitakis A, Berl S, Yahr MD. Neurological disorders associated with deficiency of glutamate dehydrogenase. Ann Neurol 1984; 15: 144-153.
44. Zaganas I, Kanavouras K, Mastorodemos V,

Latsoudis H, Spanaki C, Plaitakis A. The human GLUD2 glutamate dehydrogenase: localization and functional aspects. Neurochem Int 2009; 55(1-3): 52-63.

45. Globus MY, Busto R, Martinez E, Valdés I, Dietrich WD, Ginsberg MD. Comparative effect of transient global ischemia on extracellular levels of glutamate, glycine and γ-aminobutyric acid in vulnerable and nonvulnerable brain regions in the rat. J Neurochem 1991; 57(2): 470-478.
46. Bashun NZ, Raduta HF, Balash ZI, Kirvel PC, Sushko LI, Kanunnikova NP, Moiseenok AG. Correction of postischemic disturbances in the hemispheres of the brain using precursors of succinyl-CoA biosynthesis. Neurochemical J 2007; 1(3): 249-252.
47. Kanunnikova NP, Omelyanchik SN, Bashun NZ, et al. GABA and glutamate metabolism in the rat brain following experimental ischemia. Neirochimia 2003; 20(3): 196-200 (Rus.).
48. Castegna A, Palmieri L, Spera I, Porcelli V, Palmieri F, Fabis-Pedrini MJ, et al. Oxidative stress and reduced glutamine synthetase activity in the absence of inflammation in the cortex of mice with experimental allergic encephalomyelitis. Neurosci 2011; 30(185): 97-105.
49. Blandini F. An update on the potential role of excitotoxicity in the pathogenesis of Parkinson's disease. Funct Neurol 2010; 25(2): 65-71.
50. Pomara N, Singh R, Deptula D, Chou JC, Schwartz MB, LeWitt PA. Glutamate and other CSF amino acids in Alzgeimer's disease. Am J Psychiatry 1992; 149: 251-254.
51. Dohmen C, Kumura E, Rosner G, Heiss W-D, Graf R. Extracellular correlates of glutamate toxicity in short-term cerebral ischemia and reperfusion: a direct in vivo comparison between white and gray matter. Brain Res 2005; 1037(1-2): 43-51.
52. Paschen W. Glutamate excitoxicity in transient global cerebral ischemia. Acta Neurobiol Exp 1996; 56: 313-322.
53. Dong XX, Wang Y, Qin ZH. Molecular mechanisms of excitotoxicity and their relevance to pathogenesis of neurodegenerative diseases. Acta Pharmacol Sin 2009; 30(4): 379-387.
54. Schapira AH, Cooper JM, Dexter D, Jenner P, Clark JB, Marsden CD. Mitochondrial complex I deficiency in Parkinson's disease. Lancet 1989; 1: 1269-1271.
55. Rothstein JD, Dykes-Hoberg M, Pardo CA, Bristol LA, Jin L, Kuncl RW. Knockout of glutamate transporters reveals a major role for astroglial transport in excitotoxicity and clearance of glutamate. Neuron 1996; 16: 675-686.
56. Rothstein JD, Jin L, Dykes-Hoberg M, Kuncl RW. Chronic inhibition of glutamate uptake produces a model of slow neurotoxicity Proc Natl Acad Sci USA 1993; 90: 6591-6595.
57. Perry T, Hansen S. What excitotoxin kills striatal neurones in Huntington's disease? Clues from neurochemical studies. Neurology 1990; 40: 20-24.
58. Rothstein JD, Van Kammen M, Levey AI, Martin L, Kunel RW. Selective loss of glial glutamate transporter GLT-1 in amyotrophic lateral sclerosis. Ann Neurol 1995; 38: 73-84.
59. Bristol LA, Rothstein JD. Glutamate transporter gene expression in amyotrophic lateral sclerosis motor cortex. Ann Neurol 1996; 39: 676-679.
60. D'Alessandro G, Calcagno E, Tartari S, Rizzardini M, Invernizzi RW, Cantoni L. Glutamate and glutathione interplay in a motor neuronal model of amyotrophic lateral sclerosis reveals altered energy metabolism. Neurobiol Dis 2011; 43(2): 346-55.
61. Park E, Lee GJ, Choi S, Choi SK, Chae SJ, Kang SW, Park HK. Correlation between extracellular glutamate release and neuronal cell death in an eleven vessel occlusion model in rat. Brain Res 2010; 25(1342): 160-166.
62. Rink C, Gnyawali S, Peterson L, Khanna S. Oxygen-inducible glutamate oxaloacetate transaminase as protective switch transforming neurotoxic glutamate to metabolic fuel during acute ischemic stroke. Antioxid Redox Signal 2011; 14(10): 1777-1785.
63. Phillis JW, Ren J, O'Regan MH. Studies on the effects of lactate transport inhibition, pyruvate, glucose and glutamine on aminoacid, lactate and glucose release from the ischemic rat cerebral cortex. J Neurochem 2001; 76(1): 247-257.
64. Kosenko E, Kaminsky Y, Lopata O, Muravyov N, Felipo V. Blocking NMDA-receptors prevents the oxidative stress induced by acute ammonia intoxication. Free Radical Biol Med 1999; 26: 1369-1374.
65. Aoyama N, Théberge J, Drost DJ, Manchanda R, Northcott S, Neufeld RW, et al. Grey matter and social functioning correlates of glutamatergic metabolite loss in schizophrenia. Br J Psychiatry 2011; 198(6): 448-456.
66. Cippitelli A, Damadzic R, Frankola K, Goldstein A, Thorsell A, Singley E, et al. Alcohol-induced neurodegeneration, suppression of transforming growth factor-beta, and cognitive impairment in rats: prevention by group II metabotropic glutamate receptor activation. Biol Psychiatry 2010; 67(9): 823-830.

Journal of Biology and Earth Sciences

EARTH SCIENCES ORIGINAL ARTICLE

The Pan-African calc-alkaline granitoids and the associated mafic microgranular enclaves (MME) around Wadi Abu Zawal area, North Eastern Desert, Egypt: geology, geochemistry and petrogenesis

Asran M. Asran[1], Ezzat M. Abdel Rahman[2]

[1]Geology Department, Faculty of Science, Sohag University, Egypt

[2]Geology Department, Faculty of Science (Aswan), South Valley University, Egypt

ABSTRACT

Introduction: The area around Wadi Abu Zawal is occupied by gneisses-migmatites, island arcs metavolcanics, Dokhan volcanics, Hammamat sediments, intrusive rocks of granitic and gabbroic composition and dyke swarms.

Materials and Methods: The present work concerning on the geology, geochemistry and petrogenesis of the MME and the host granitoid rocks of that area. The analytical methods for major and trace elements of some representative samples were carried out by XRF technique at the Institute of BGR in Hannover, Germany.

Results: Mineralogically, MME are composed mainly of plagioclase, hornblende, biotite and quartz with accessory of sphene, acicular apatite and opaque oxides, while chlorite and epidote are secondary ones. Whereas Abu Zawal granitoid rocks are subsolvus and consist of variable contents of plagioclase, K-feldspar, quartz, and biotite, with accessory sphene, zircon and opaque oxides, typical of I-type granites. The studied Abu Zawal area represents part of the northeastern Egypt which formed by regional crustal extension and magmatic-arc regimes during Pan-African orogenic event. The MME display major, trace element contents and tectonic setting comparable with the end members of (GDT) and (IAG) of the Eastern Desert which produced (by fractionation) from a mantle-derived tholeiitic magma in an island-arc tectonic environment. Abu Zawal granitoid rocks exhibit trace element characteristics of volcanic-arc granites, and formed in an Andean-type setting.

Conclusions: On the variation diagrams, major and trace element contents of the MME and granitoid rocks display conspicuous gap and two distinct trends one for the MME, (IAG) and the other for the Abu Zawal granitoid rocks, which indicates that they are not genetically related and suggest the crustal source for the host granitoid rocks.

Key words: granitoids, gabbro, gneisses, metavolcanics, mafic microgranular enclaves, Egypt.

J Biol Earth Sci 2012; 2(1): E1-E16

Corresponding author:
Prof. Asran M. Asran
Geology Department, Faculty of Science,
Sohag University, Sohag, 82524, Egypt
e-mail: asran_58@yahoo.com

Original Submission: 16 February 2012; Revised Submission: 08 March 2012; Accepted: 09 March 2012

ISSN: 2084-3577
http://www.journals.tmkarpinski.com/index.php/jbes or http://jbes.strefa.pl
e-mail: jbes@interia.eu

INTRODUCTION

The western part of Saudi Arabia, Sinai peninsula, Egyptian Eastern Desert and Northern Sudan have been termed collectively as the Arabian-Nubian Shield (ANS), which is characterized by four main rock assemblages:

1) a gneiss assemblage,
2) an ophiolite assemblage,
3) an arc assemblage,
4) igneous intrusions.

The ANS represents the best example of crustal growth which involves progressive cratonization by formation of oceanic crust, subduction, magmatic arc development and collision between arc complexes to assemble a continental shield during the period 900-550 Ma.

The Precambrian of the Eastern Desert of Egypt was divided into North Eastern Desert (NED), Central Eastern Desert (CED) and South Eastern Desert (SED) where the igneous activity began prior to 765 Ma and ended by 540 Ma [1]. They (op.cit.) postulated that the Precambrian rocks of the Eastern Desert display negative εSr and positive εNd values which used as evidence against the interaction with the old continental crust. This assumption was based on relative abundance of the rock units, where the younger rocks predominate northward and the older ones southwards. The proposed two tectonic models for the evolution of northern part of the Nubian shield that exposed in northeastern Egypt are:

1) progressive cratonization through the development of oceanic crust, subduction, magmatic arc and collision between arc complexes into continental shield [2]. This model was suggested to entire Arabian – Nubian Shield (ANS) [3-5].

2) crustal extension regime between 670 and 500 Ma [6-9] concluded that, the crustal block of northeastern Egypt is not a remobilized (ensialic) Archean continental crust, nor was it entirely formed in an extensional tectonic regime [9].

He added (op.cit.) that it formed by early multiple (intra-oceanic) arc subduction and progressive development with late Andean-type continental margin magmatism (880-550 Ma), followed by regional inversion from arc tectonics to continental extension due to crustal relaxation, cooling and fracturing of the newly formed Pan- African crust around the Neoproterozoic-Paleozoic boundary (~ 550 Ma), and extended to about 90 Ma (Table 1). Granitoids constituents about 40% of the basement complex and classified in several ways (Fig. 1). The Egyptian granites have long been known, based on relative age and composition, to pertain to an older and younger granitoids [10-11]. Depending on tectonic events, El-Gaby [12] divided the Egyptian granites into two groups: a) The synorogenic granitoids and b) The younger granites. He also concluded (op.cit) that the two aforementioned major granite groups constitute one continuous granite series. Hussein *et al.* [13] proposed three groups for the Egyptian granites:

1) G-1 granites: comprised most of the granites for which the names “old”, “Shaitian”, “Grey” or “synorogenic” granites and based on their characteristics, it is believed that these are subduction - related granites formed by the partial fusion of the mantle wedge, with little or no crustal melt contribution,

2) G-2 granites: include most of the granites previously referred to as “younger”, “Gattarian”, “Pink”, “Red” or “Post –orogenic”. These granites therefore appear to have been formed by the partial melting of the lower crust probably with some

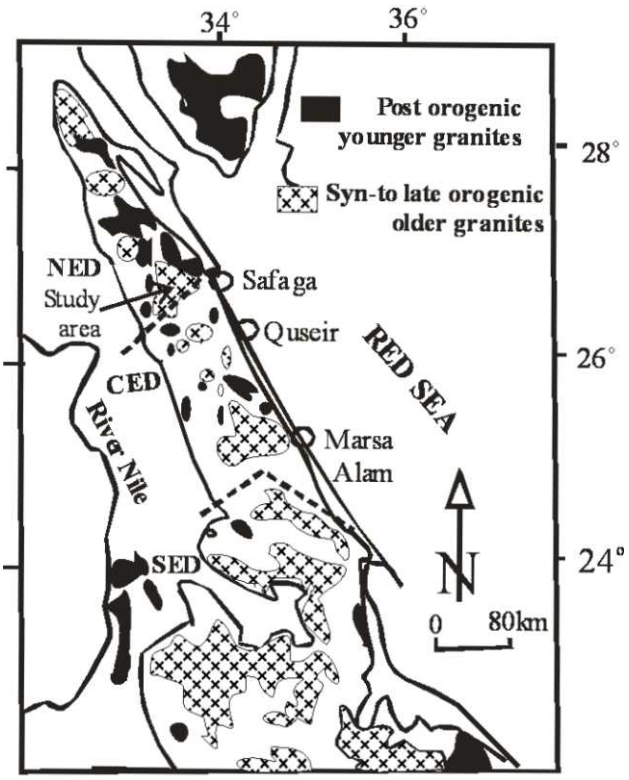

Fig. 1. Map of distribution of Egyptian granitoids, location of Abu Zawal area and terms NED (Northeastern Desert), CED (Central eastern Desert) and SED (Southeastern Desert). Based on [1] and [17].

Table 1. Geochronology of the Pan-African rocks of Egypt.

Tectonic setting	Rock units	Rock names	Age (Ma)	References
Post-orogenic stage	Younger granites	Monzogranite, syenogranite and alkali feldspar granite	610 - 550	[1, 15, 16]
	Hammamat Group	Sandstone, conglomerate, greywacke and volcaniclastics	600 - 585	[8]
Orogenic stage	Dokhan volcanics	Andesite and rhyolite flows, pyroclastics and dyke swarms	600 - 550	[1]
	Older granitoids	Quartz diorite-trondhjemite-tonalite-granodiorite	800 - 614	[1, 15, 16]
	Island arc assemblage	Calc-alkaline metavolcanics (basalt, andesite and rhyolite flows, together with metapyroclastics) and gabbro-diorite complexes	850 - 620	[1, 18]
	Ophiolitic group	Serpentinites, gabbros, and pillow lavas of basalt composition	810 - 730	[19]

addition from the mantle, by collision (suturing) at plate boundaries,

3) G-3 granites that include the alkaline or peralkaline granites as well as a considerable proportion of those treated as “Younger granites” by El-Gaby [12] or by Hussein *et al.* [13]. It is suggested that these granites are intraplate, anorogenic granites, formed by melting of pre-existing crustal rocks.

Generally, the older granites have quartz diorite to granite and were emplaced during the orogeny between 810 and 614 Ma [1, 15, 16]. The Precambrian rocks, where the area under consideration represents part of them, around the asphaltic roads (traversed by both Qena – Safaga, from the southern part, and Sohag – Safaga, from the northern part) are located in the North Eastern Desert and comprised infracrustal rocks (amphibolites, migmatites and gneisses), supracrustal rocks that represented by island arcs metavolcanis of calc-alkaline nature, Dokhan volcanics of basaltic andesites to rhyolite composition, Hammamat sediments, intrusive rocks of granitic and gabbroic composition and finally dyke swarms of basic, intermediate and acidic composition.

Vernon [20] and Didier [21] mentioned that xenoliths are enclaves older than their hosted granite. With regard to the xenoliths occurrences in Precambrian rocks of Egypt, it is not only restricted to the granite plutons. The mafic microgranular enclaves (MME) are widely distributed in Egyptian Precambrian rocks and described in some localities.

El-Aref *et al.* [22] investigated diorite and amphibolite enclaves in the older granitoids of western Sinai. Migmatites at Wadi Dafai, southwestern Sinai, contain migmatized amphibolites that characterized by schlieren structure [23]. Khalid [24] described amphibolites enclaves in diorite gneisses of Wadi Watir, Southeast Sinai. Amphibolite enclaves were described in granite gneisses of Wadi Ghadir, Southeastern Desert [25]. The microgranular enclaves are recorded in the granitoids of Southwestern Sinai and it is formed by mingling model of mafic globules of different compositions [26]. Katta *et al.* [27] described dioritic, hornblende gneiss and amphibolite enclaves within granodiorites and tonalities of Qaret El Maiyit, Southeastern Desert. Sorour and Kabesh [28] described quartz diorite enclaves in calc-alkaline granite of Wadi Risasa, Southeastern Sinai. Asran and Mohamed [29] described andesite enclaves within Kadabora granite, Central eastern Desert.

The study area has been the subject of several studies due to its accessibility. The granitoid rocks are differentiated into autochthonous, parautochthonous and intrusive varieties as well as porphyritic adamellite, red granites and later alkaline granites [30, 31]. The area around Wadi Abu Zawal was studied by Soliman [32] as granite gneisses, arc ophiolite fragments, synkinematic granitoids, post kinematic granites and post granite dykes. Sharara *et al.* [33] mentioned that the area around Abu Zawal is occupied by metavolcanics, metagabbros, synkinematic granitoids and post

kinematic granites. Asran *et al.* [34] mentioned that the Pan-African granitoid rocks of Wadi Fatirah area are differentiated into two distinct assemblages, viz. the older granites and younger granites. The older granites are calc-alkaline in character and of I-type and were emplaced under compressional tectonic regime, while the younger granites were formed under an extensional tectonic regime.

The present Abu Zawal area is very important due to its occurrence approximately along the boundary between NED and CED, beside its intrusive rocks have different tectonomagmatic stages [35] which may play significant role in crustal growth of NED. Therefore, the present study concerning on the petrogenesis of the mafic microgranular enclaves (MME) and the hosted granitoids that occupied the area around Wadi Abu Zawal.

Geological setting

The area surrounding Wadi Abu Zawal comprised the following rock units:

1) gneisses and migmatites,
2) calc-alkaline metavolcanics,
3) older granitoids,
4) Dokhan volcanics,
5) younger gabbros,
6) younger granitoids and finally dyke swarms (Fig. 2).

Gneisses and migmatites occupied the eastern part of the mapped area and intruded by both older and younger granites. The calc-alkaline island arcs metavolcanics, besides the Dokhan volcanics, are occupied the extreme western part of the mapped area and extend beyond the limit of the present area. It is commonly intruded by intrusive rocks and the dyke swarms.

The older granitoids constituent the major rock units which covering about 120 km^2. It is intruded into gneisses–amphibolites-migmatites associations and calc-alkaline metavolcanics, where the contact in between is gradational and dip away from the granite intrusions. The older granitoids have mainly granodiorites with subordinate monzogranites composition, low to moderate relief, intensely weathered and consequently occupied by wide Wadi sands. It is characterized by spheroidal exfoliation, contains numerous dioritic microgranular enclaves and dissected by younger gabbros and younger granites. The later sends off-shoots, apophyges and enclosed large xenoliths from them.

Wadi Abu Zawal area was affected by the Pan-African orogeny which indicated by:

1) The gneisses-amphibolite-migmatiotes association are metamorphosed up to amphibolite facies,
2) The calc-alkaline metavolcanics are metamor-

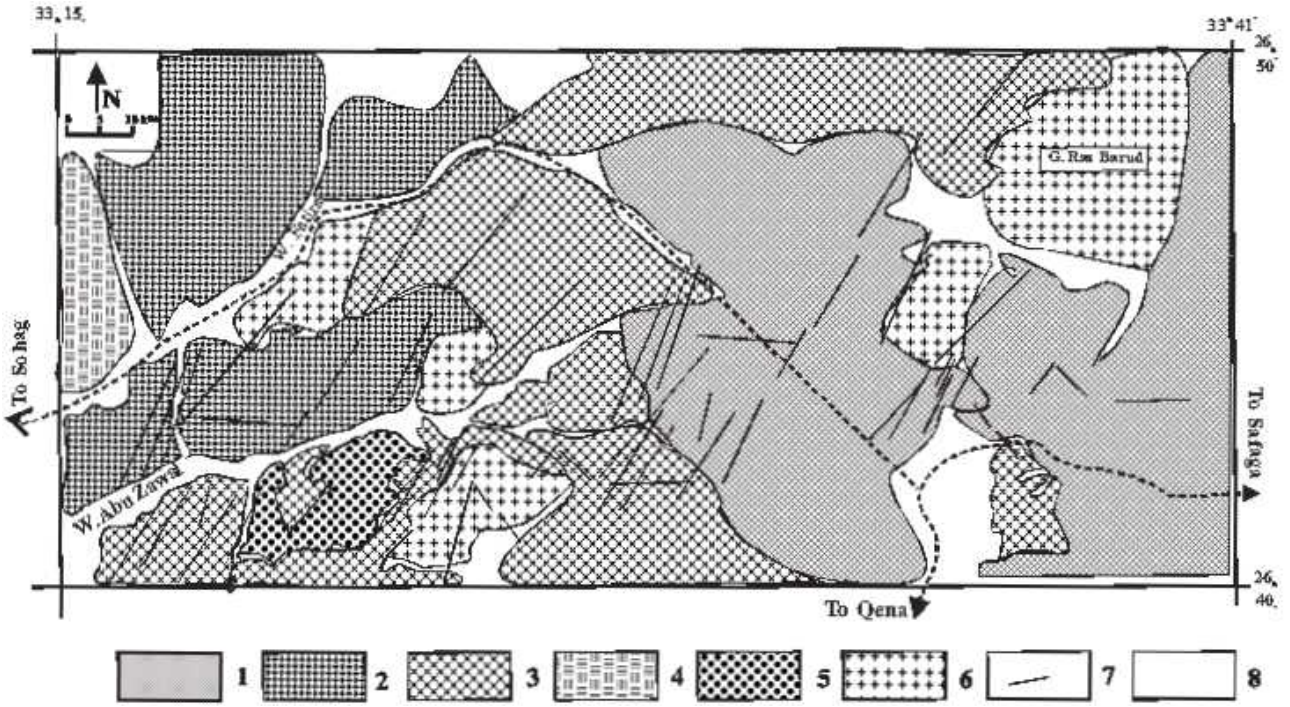

Fig. 2. Geological map of Wadi Abu Zawal area (modified after Asran 2001).
Legend: 1 - gneisses and migmatites, 2 - calc-alkaline metavolcanics, 3 - older granitoids, 4 - Dokhan volcanics, 5 - gabbros, 6 - younger granites, 7 - dikes, 8 - Wadi deposits.

phosed up to green-schist facies and foliated, and 3) The peripheries of the older granitoids are foliated that is pronounced by the presence of undulose extinction in quartz and the displacement of plagioclase twin planes.

The mafic microgranular enclaves (MME) range in size from less than 3 cm to more than 0.5 m in diameter, but most of them are in the range of 20-40 cm. The MME display various shapes ellipsoidal, irregular, spheroidal and wedge shaped. In some observation points, the MME are subangular which indicate that they were rigid before and when entering magma [36]. The MME have diffuse or transitional boundary with the host granites, but others display sharp contact with them.

Petrography

Abu Zawal granitoids:

1 - Granodioites

These rocks are coarse-grained, greyish pink in colour and massive, however some varieties display feeble foliation particularly along the peripheries of the pluton. In thin section, they are composed mainly of quartz, plagioclase, microcline and biotite. Hypidiomorphic textures is characteristic. The accessory minerals include sphene, zircon and opaque oxides. Quartz forms subhedral to anhedral crystals, enclosed some of the accessories and sometimes displays wavy extinction. Plagioclase is commonly kaolinitized and saussuritized and displays zoning with altrered core and fresh rim. Biotite is frequently altered to chlorite with liberation of opaque oxides along the inherited cleavage planes. Microcline fills the interstices between quartz and plagioclase. Zircon and sphene are commonly enclosed within biotite.

2 - Monzogranites

Monzogranites are coarse grained, massive and pink in colour. They are composed mainly of plagioclase, k-feldspars, quartz and biotite. Zircon, opaque oxides and sphene are accessories, whereas chlorite, kaolinite and saussurite are secondary ones. Hypidiomorphic and myrmekitic textures are common. Plagioclase occurs as small laths enclosed within k-feldspars and quartz, while large plagioclase crystals form tabular ones, up to 1.2x2.1 mm, kaolinitized and some of them corroded k-feldspars with the formation of myrmekitic texture. K-feldspars are represented by microcline, microcline perthite, orthoclase and orthoclase perthite. It is commonly subhedral to anhedral, rarely altered and encloses partially and completely plagioclase crystals. Quartz forms anhedral crystals that are commonly filling the spaces between the other constituents. Biotite occurs as subhedral flakes, up to 1.3 mm long, brown in colour and strongly pleochroic from yellowish brown to dark brown. It is frequently altered partially and completely to chlorite.

Mafic microgranular enclaves (MME):

Petrographic description of the enclaves display that they medium to coarse grained, grayish green in colour and massive. In thin section, they are composed mainly of plagioclase, hornblende, biotite and quartz. The accessory minerals include sphene, acicular apatite and opaque oxides, while chlorite and epidote are secondary ones. The studied microgranular enclaves are thermally metamorphosed which evidenced by the presence of granoblastic hornblende and the disoriented biotite small flakes which in turn confirming the decussate texture. However, the hypidiomorphic texture is faithfully still preserved.

MATERIALS AND METHODS

Analytical technique

Eight representative samples from the different granitic rocks and three samples from the enclaves were petrographically selected for chemical analyses. Major and trace elements were determined by XRF technique at the Institute of BGR (Bundesanstalt für Geowissenschaften und Rohstoffe) in Hannover, Germany. The X-ray fluorescence data was done by Philips PW1480 and PW2400.

Object and Area of Application

The samples were analysed for the following determinands: SiO_2, TiO_2, Al_2O_3, Fe_2O_3, MnO, MgO, CaO, Na_2O, K_2O, P_2O_5, SO_3, chlorid, fluorid, As, Ba, Bi, Ce, Co, Cr, Cs, Cu, Ga, Hf, La, Mo, Nb, Nd, Ni, Pb, Pr, Rb, Sb, Sc, Sm, Sn, Sr, Ta, Th, U, V, W, Y, Zn, and Zr.

Samples were ignited at 1030°C, the loss on ignition (LOI) was calculated and the residue was fused to a glass bead using a borate flux material. The beads were analyzed by wavelength dispersive x-ray fluorescence spectrometry (WD-XRF).

Instrumentation and Reagents

The flux used for producing glass beads was

lithium metaborate (Alfa Flux no. 100 A Spectroflux coarse $LiBO_2$ 100%) and lithium tetraborate (Merck Spectromelt A 10, $Li_2B_4O_7$).

The beads were analysed using Philips PW1480 and PW2400 spectrometers.

The PW1480 spectrometer was fitted with a 102 position sample changer and a 3 kW chromium anode x-ray tube operated at 2.5 kW and was controlled by Philips SuperQ software. This spectrometer was used to determine TiO_2, CaO, K_2O, chlorid and Ba, Cs, Sb, Sc, and Sn.

The PW2400 spectrometer was fitted with a 91 position sample changer and a 3 kW/60 kV rhodium anode x-ray tube operated at 2.7 kW and was controlled by Philips SuperQ software. This spectrometer was used to determine SiO_2, Al_2O_3, Fe_2O_3, MnO, MgO, Na_2O, P_2O_5, SO_3, fluorid and As, Bi, Ce, Co, Cr, Cu, Ga, Hf, La, Mo, Nb, Nd, Ni, Pb, Pr, Rb, Sr, Sm, Ta, Th, U, V, W, Y, Zn, and Zr.

RESULTS

Whole rock chemistry

Chemical classification and magma type:

On the Q-ANOR diagram (Fig. 3a) [37], Abu Zawal granitoids fall within the granodiorite and straddle the boundary between the granodiorite and monzogranite fields, while two samples (Nos. 2 & 5) fall within the syenogranites field which may represent the more differentiated types. The mafic microgranular enclaves (MME) fall within the diorite field. The dioritic composition is again confirmed, beside the composition of the granitoid rocks, on the Or-Ab-An ternary diagram (Fig. 3b) [38]. On the Q-Ab-Or – H_2O ternary diagram [39] (Fig. 3c), the MME fall close to the high water vapour pressure, while the granitoid rocks fall close to the moderate water vapour pressure. This feature indicates that the MME emplaced at greater depth

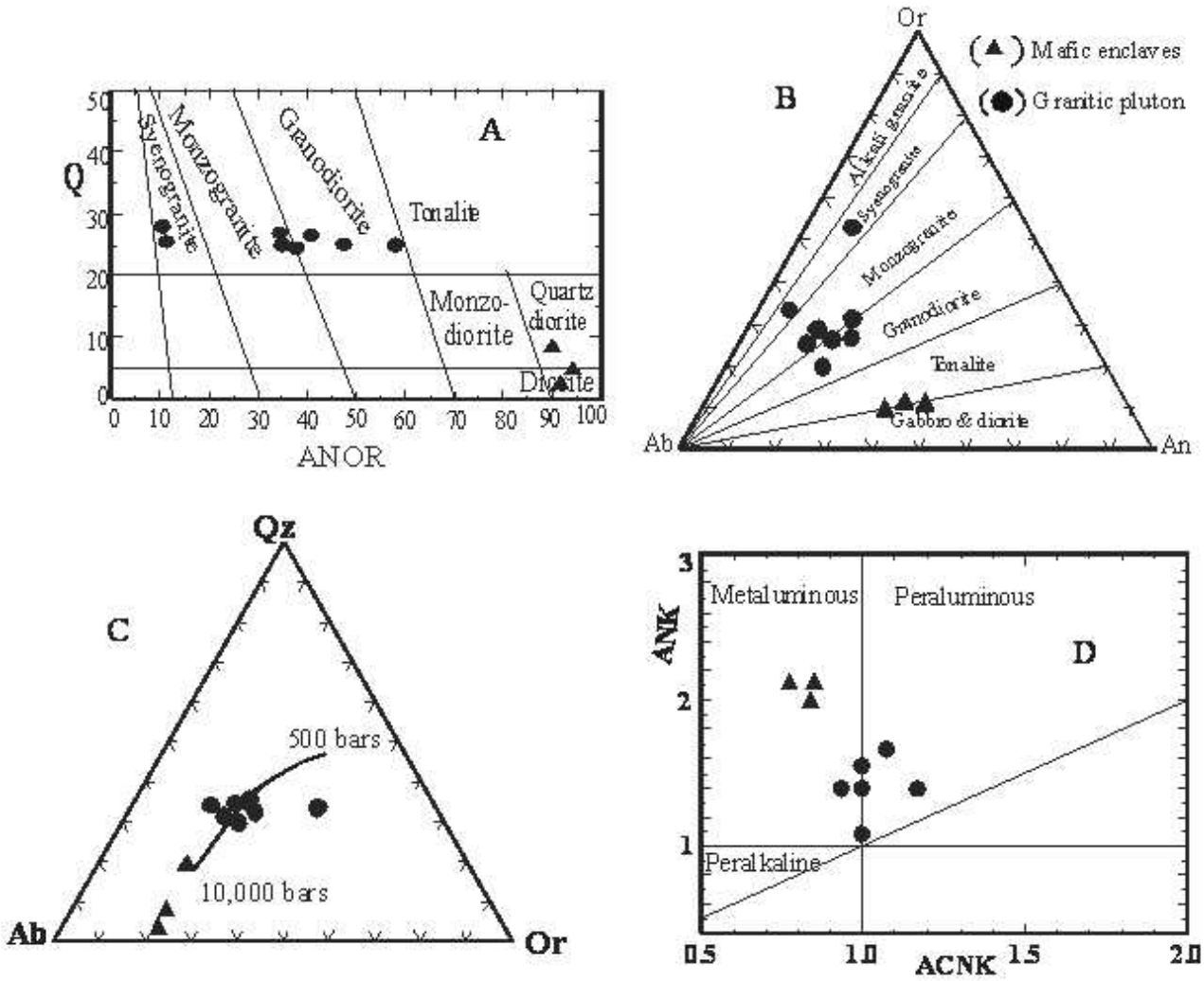

Fig. 3. A) Q=Qz/(Qz+Or+Ab+An), ANOR=An/(Or+An) [37]. B) Or-Ab-An ternary diagram [38]. C) Qz-Ab-Or-H_2O system [39]. D) Plots of Shand index for the studied rocks, fields after [40]. Symbols as follows: Abu Zawal granitoids (●) and the associated mafic enclaves (▲).

than the host granitoid rocks.

The studied MME and the granitoid rocks of Abu Zawal area are plotted on the ANK-ACNK diagram (Fig. 3d) [40]. The MME fall mostly within the metaluminous field, whereas the granitoid rocks straddle the boundary between the metaluminous and peraluminous fields. On the K_2O-Na_2O-CaO ternary diagram (Fig. 4a), compared to the Egyptian granitoid rocks as defined by Hassan and Hashad [16], the granitoid rocks similar to the highly evolved calc-alkaline older granites, while the more differentiated types (samples Nos. 2 & 5) plot within the Egyptian younger granites field. The mafic microgranular enclaves (MME) fall within and close to early members of calc-alkaline older granites. The calc-alkaline nature of the MME and the granitoid rocks was displayed on the SiO_2 – alkalinity ratio diagram (Fig. 4b) [41]. The calc-alkaline character of the MME and the granitoid rocks is also confirmed by plotting the analyzed samples on the SiO_2 – log (K_2O/MgO) diagram (Fig. 4c) [42], however, one sample No.2 falls within the alkaline field.

Sylvester [43] classified the granitic rocks into: calc-alkaline granitoids, strongly peraluminous leucogranites, alkaline granites and highly fractionated calc-alkaline granites. Therefore, the analyzed MME and granitoid rocks are plotted on the $(Al_2O_3+CaO)/(FeO+Na_2O+K_2O)$ – $100(MgO+FeO+TiO_2)/SiO_2$ diagram (Fig. 4d) [43] and adopted this classification, the analyzed samples fall within the calc-alkaline and peraluminous field, except two samples Nos. 2 and 5 fall within the highly fractionated calc-alkaline granites field (HFCAG).

Major and trace elements chemistry:

The authors are concerned on the study of differentiation trends within the enclaves and the host granitoids which gave best indication for the processes of magma generation and evolution. Abu Zawal granitoids have SiO_2 range from 69.97 to 71.87, and K_2O range from 3.11 to 3.46, except sample (No. 2) contains 6.06 that may represent younger granites off-shoots and/or the more

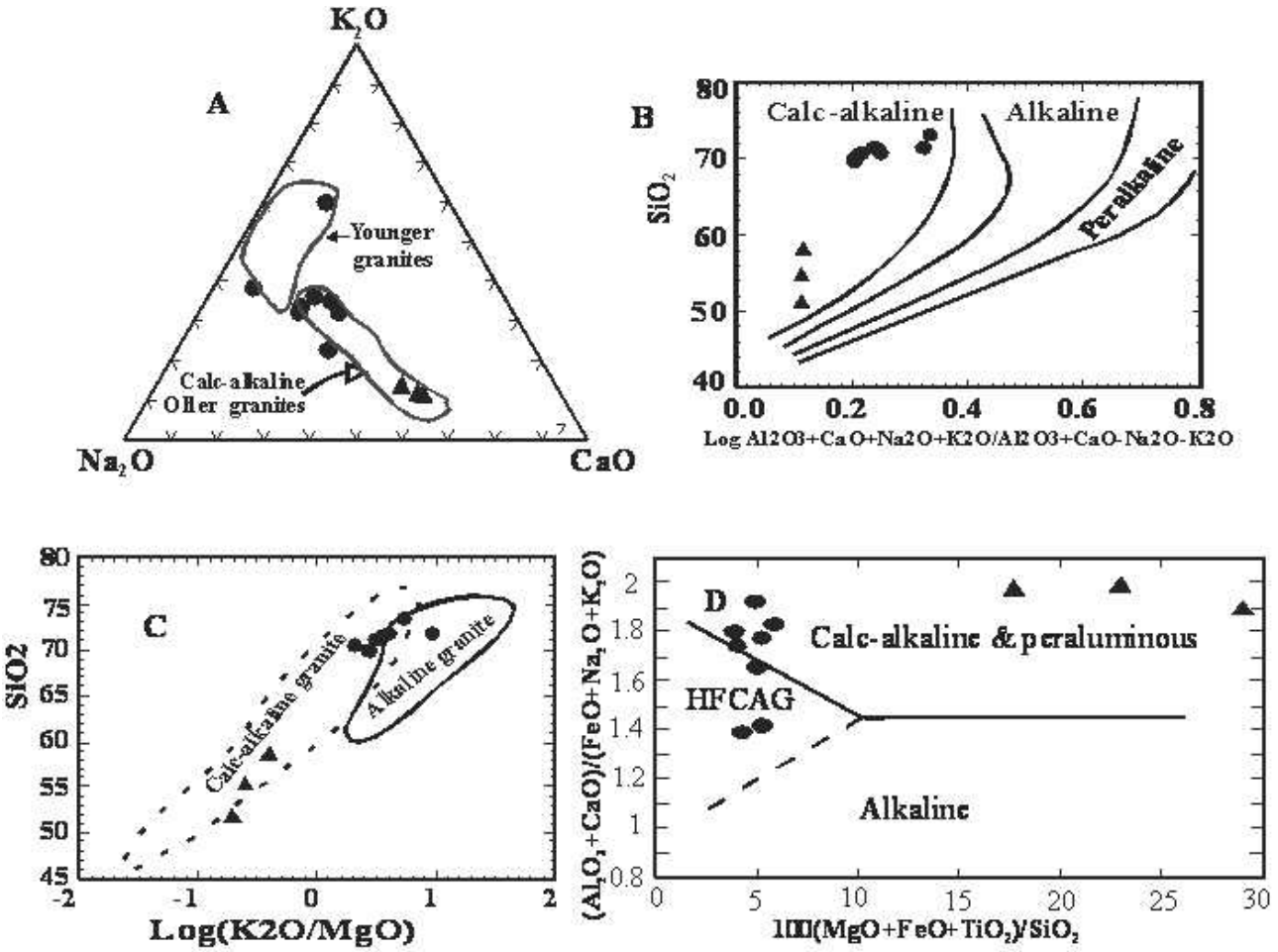

Fig. 4. A) K_2O-Na_2O-CaO ternary diagram. Fields of calc-alkaline older granites and younger granites from [16]. B) SiO_2-alkalinity ratio diagram [41]. C) SiO_2-log(K_2O/MgO) [42]. D) $(Al_2O_3+CaO)/(FeO+Na_2O+K_2O)$ vs. $100(MgO+FeO+TiO_2)/SiO_2$ [43]. Symbols as in Fig. 3.

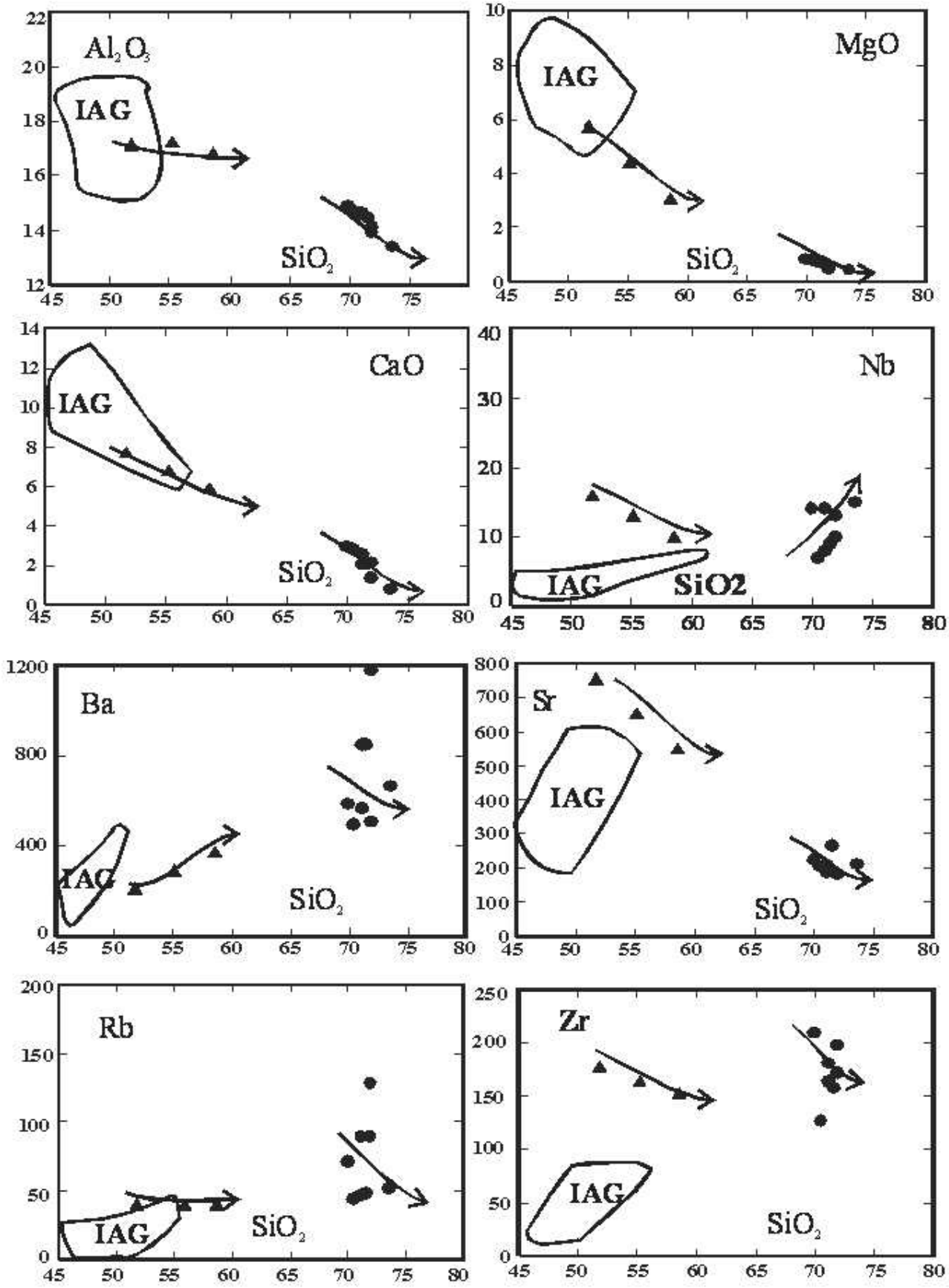

Fig. 5. Harker variation diagrams of some major and trace elements for the studied Abu Zawal granitoids and the associated mafic enclaves. The field labeled (IAG) are from [45]. Symbols as in Fig. 3.

differentiated types, which higher than the MME. The MME have dioritic composition with relatively higher in TiO_2, Al_2O_3, FeO, MgO, CaO and P_2O_5, but lower in SiO_2 and K_2O than the granitic host. The analyzed MME and the granitoid rocks of Abu Zawal area are plotted on the Harker variation diagram. From the plotted samples we can detect the following patterns:

1) The plots display well defined trends with increasing SiO_2 which established by decrease in Al_2O_3, FeO, MgO, CaO, Nb and Sr and increase in Ba and K_2O.

2) Most of the major elements in the enclaves (MME) are higher than the host granites, both the plots (enclaves and granites) have distinct different trends as shown by the drawn arrows, however, the mafic enclaves data lie on the extension of the host granite trends.

3) The MME display most of major and trace elements contents overlap and/or close to the more differentiated parts of the island arc gabbro-diorite association from the Eastern Desert of Egypt (Fig. 5).

4) The presence of a wide gap between the enclaves and the host granites indicates the MME and the host granitoids are not genetically related.

5) For some elements, the granitoid rocks data have restricted variations and slightly scattered, while the MME have a distinct trends.

The trace elements such as Sr, Ba and Rb are very important to deduce the course of fractional crystallization in granitoid rocks where their concentration is controlled by feldspars and mica. Therefore, the visual estimation of the data (Table 2) and the plotted data indicate that Sr decreases while Ba and Rb show variable trends with increasing SiO_2 as passing from MME to granitoid rocks (see Fig. 5); this may be due to plagioclase fractionation. Plotting the analyzed samples on the Rb-Ba-Sr ternary diagram (Fig. 6a) [44] indicate that the MME fall within the diorite field and substantiate their higher Sr content than the host granitoid rocks.

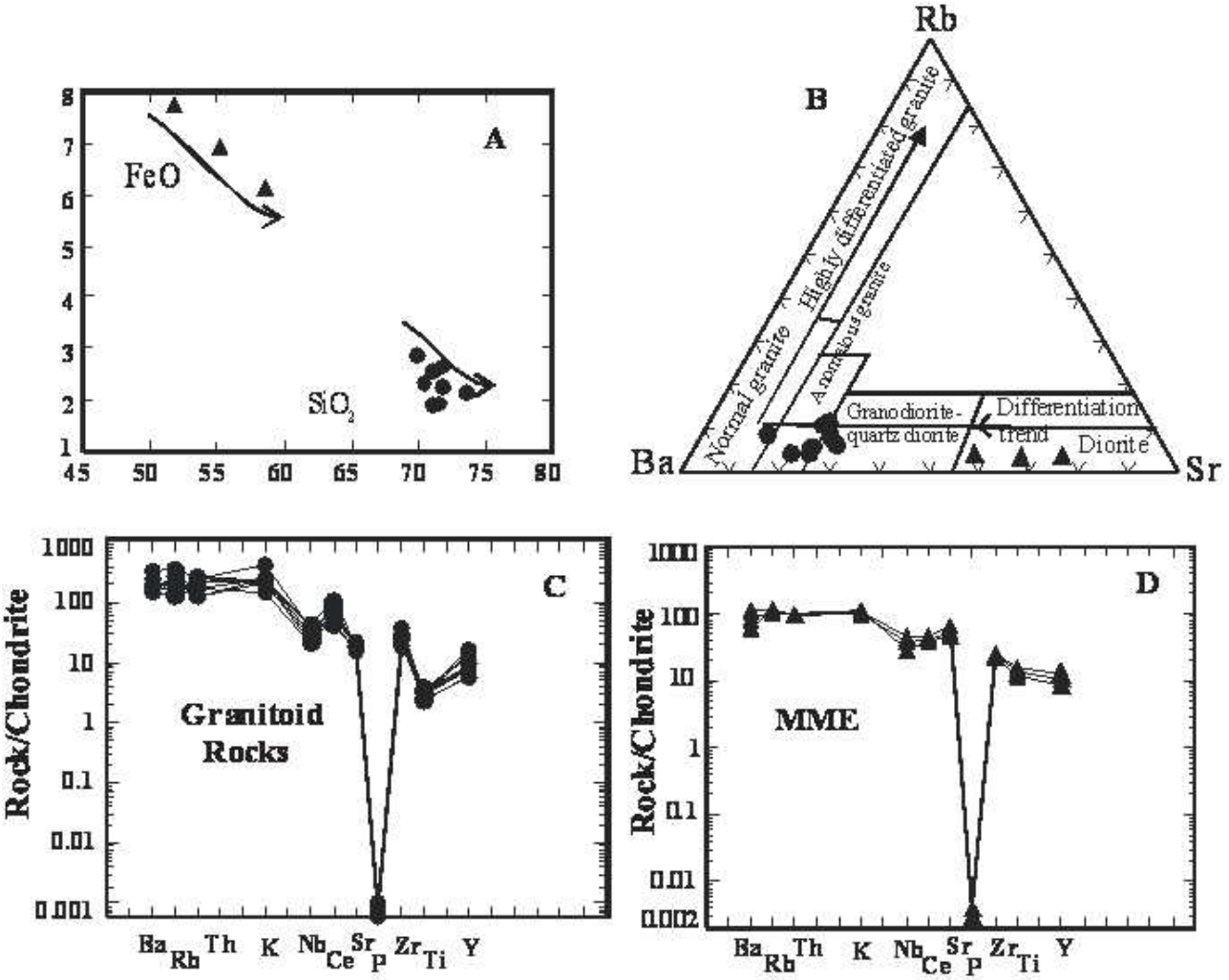

Fig. 6. A) FeO-SiO2. B) Rb-Ba-Sr ternary diagram [44]. C) and D) Chondrite- normalized trace elements diagram for Abu Zawal granitoids and the associated MME. Normalized factors by [46]. Symbols as in Fig. 3.

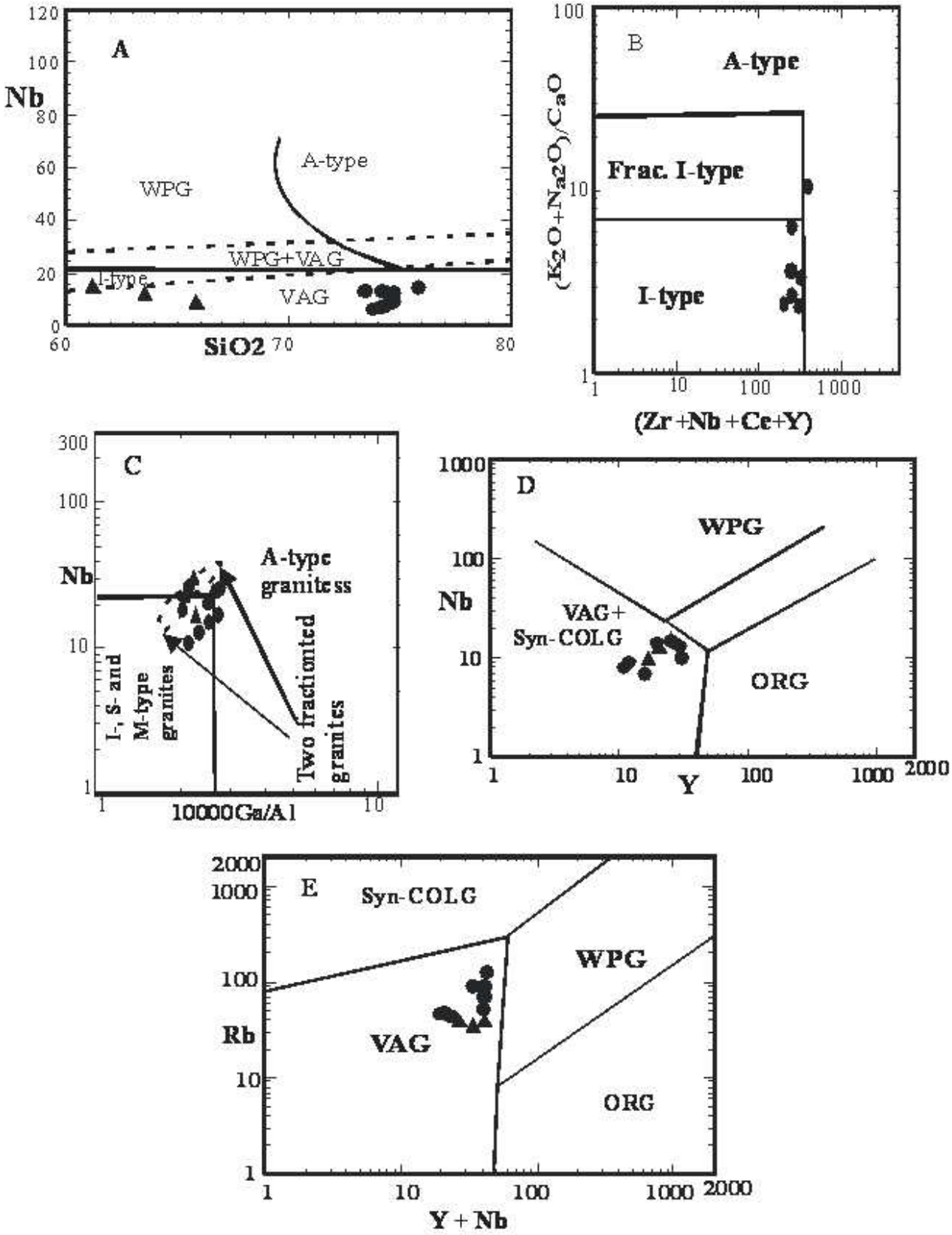

Fig. 7. A) Nb-SiO_2 [52]. B) $(Na_2O+K_2O)/CaO$-(Zr+Nb+Ce+Y), and C) Nb-10000Ga/Al [48]. D) Nb-Y and E) Rb-(Y+Nb) [47]. Symbols as in Fig. 3.

On the other hand, the Abu Zawal granitoid rocks straddle the boundary between granodiorite and anomalous granite fields and confirmed the feature of higher Ba content.

To detect the behavior of the trace elements in the studied MME and granitoid rocks, the chondrite normalized spider diagrams are constructed (Figs. 6c, d). Generally, the MME and granitoid rocks display enrichment in trace elements contents relative to the chondrite. In the MME, there is slightly depletion of Nb, Ti and Sr and distinct depletion in P, while in the granitoid rocks there is a pronounced negative Nb, P and Ti anomaly. Therefore, pronounced depletion in P indicates apatite fractionation. Ti anomaly may be related to ilmenite and/or sphene fractionation. The observed depletion in Sr suggests plagioclase fractionation. The slightly depletion in Zr is probably due to zircon fractionation. Generally, the pronounced Nb negative anomaly is a characteristics feature of subduction-related magmatism (i.e. it is common in arc granitoids and in the study area is represented by Abu Zawal arc-granitoid rocks).

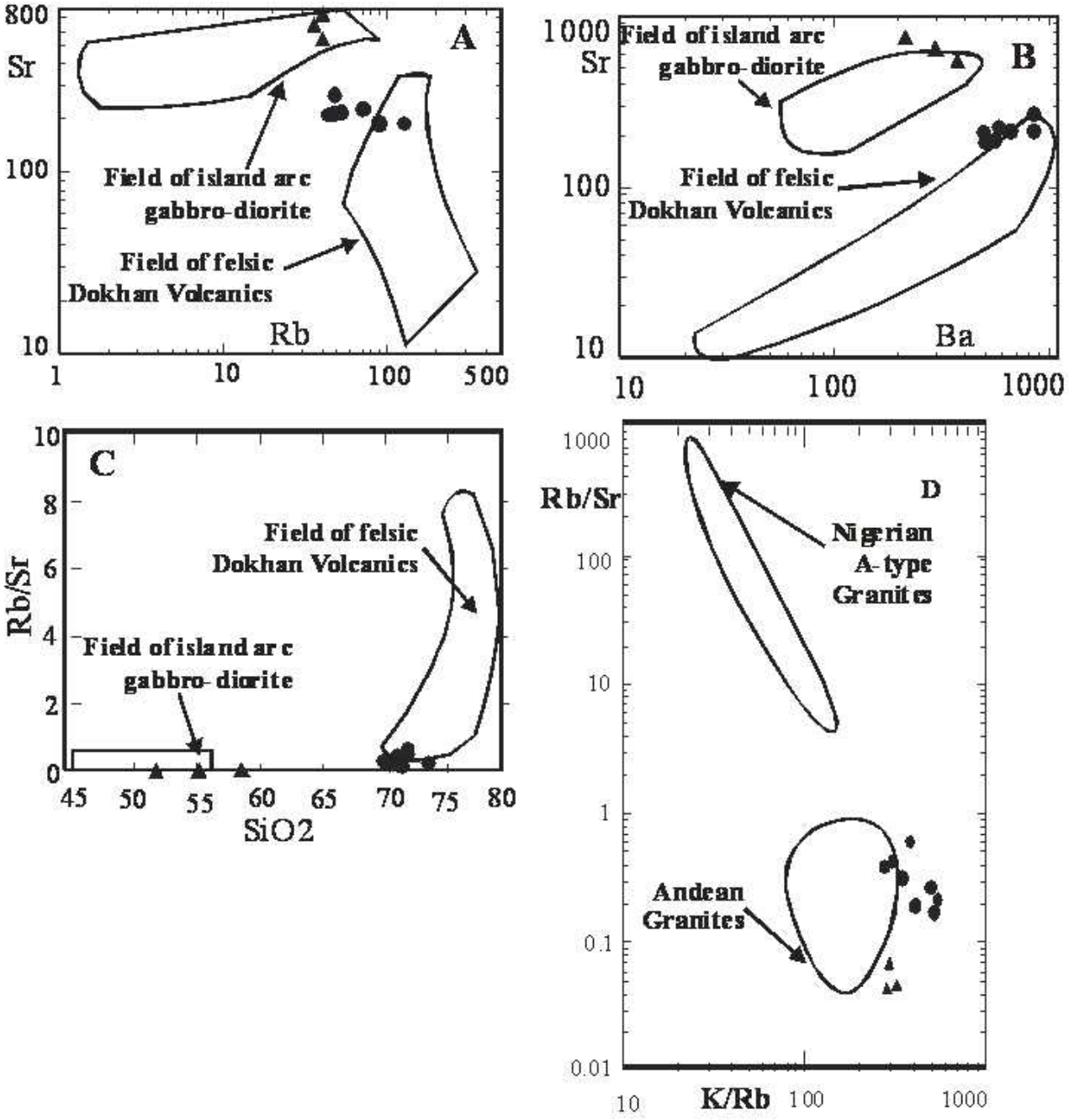

Fig. 8. A) Binary variation diagrams of Sr-Rb-Ba and Rb/Sr-SiO_2 for Abu Zawal granitoids and the MME. Symbols as in Fig. 3. Field of island arc gabbro-diorite (by [49, 50]). Field of Dokhan volcanics from the Eastern Desert of Egypt (see, [7]). D) Rb/Sr vs. K/Rb. Andean granite field [53] and A-type granite field from Nigerian [54].

Table 2. Chemical analyses of Abu Zawal granitoid rocks and MME.

Ser. No.	1	2	3	4	5	6	7	8	9	10	11
Sam. No	G 1	G 8	G 12	G 19	22	26	26a	28	X3	X 8	X 13
SiO_2	71.86	71.87	69.97	71.10	73.52	71.50	71.13	70.46	55.16	58.61	51.70
TiO_2	0.329	0.289	0.334	0.285	0.380	0.244	0.259	0.304	1.33	1.143	1.525
Al_2O_3	14.17	13.94	14.89	14.58	13.41	14.4	14.64	14.68	17.22	16.82	17.18
FeO	2.66	2.27	2.89	2.56	2.14	1.92	1.90	2.33	6.95	6.15	7.74
MgO	0.62	0.50	0.87	0.80	0.48	0.68	0.73	0.82	4.40	3.08	5.72
CaO	2.179	1.366	2.961	2.591	0.802	2.069	2.092	2.817	6.82	5.910	7.728
MnO	0.057	0.049	0.059	0.058	0.034	0.032	0.032	0.045	0.125	0.106	0.145
Na_2O	3.84	2.66	3.68	3.64	4.83	4.32	4.48	4.55	3.66	3.72	3.87
K_2O	3.371	6.064	3.151	3.340	3.468	3.221	3.111	2.194	1.44	1.592	1.504
P_2O_5	0.100	0.080	0.112	0.092	0.091	0.081	0.084	0.109	0.32	0.309	0.427
L.O.I.	0.47	0.53	0.74	0.61	0.59	1.21	1.26	1.48	1.88	2.02	1.94
Total	99.78	99.72	99.69	99.75	99.76	99.76	99.74	99.79	99.30	99.59	99.58
Trace elements (ppm)											
Ba	509	1172	585	564	662	848	849	494	295	376	213
Ce	77	37	53	34	91	59	71	49	36	32	40
Ga	19	16	16	16	20	18	18	19	18	19	19
Hf	6	8	<6	<6						<6	10
La	30	30	17	20	34	31	55	41	20	25	<15
Nb	10	13	14	14	15	9	8	7	18	10	16
Rb	90	128	71	90	52	48	47	44	36	40	40
Sr	183	185	224	190	213	267	211	208	653	550	756
Th	7	10	5	5	9	11	11	7	<4	<4	<4
Y	31	30	27	20	25	12	12	16	21	17	25
Zr	198	172	210	181	255	158	164	127	165	153	178
Zn	59	163	62	45	46	32	35	44	74	76	77
Ni	4	3	7	6	<2	5	3	17	60	42	79
V	26	25	36	31	17	12	22	32	100	119	109
Pb	28	36	19	13	15	7	10	7	7	6	8
Cu	18	14	27	22						80	22
Cr	85	74	137	81	110	102	94	109	124	14	235

1- 8 Abu Zawal Granitoid rocks 9-11 Enclaves

Tectonic setting:

To define the tectonic setting of the MME and the granitoid rocks, several discrimination diagrams are adopted. On the Nb - SiO_2 diagram (Fig. 7a) [47], both the MME and the granitoid rocks fall within the I-type field and the volcanic arc granites (VAG) field. The I-type characters for MME and the granitoid rocks is again confirmed on the (K_2O +Na_2O)/CaO versus (Zr+Nb+Ce+Y) and Nb – 10000*Ga/Al diagrams (Figs. 7b, c) [48]. Moreover, the analyzed samples are plotted on the Nb – Y and Rb – (Y+Nb) diagrams (Figs. 7d & e) [47], where the plots fall mostly within the VAG field and comparable to the orogenic calc-alkaline older granites (CAG) of the Eastern Desert of Egypt (see, [49, 50]).

Reverting back to the tectonic setting of the Arabian-Nubian shield (ANS) proposed by Stern (1994) that there are three tectonomagmatic stages, viz.: Arc stage which began early about 850 Ma [51], Collision stage and finally post-collision stage. During the three stages, the Pan-African rocks of the Eastern Desert of Egypt are metamorphosed. According to the deduced field setting and geochemical data, the studied Abu Zawal granitoid rocks may be emplaced during the arc stage.

DISCUSSION

The Arabian-Nubian shield displays an example of plate tectonics during the Pan-African orogenic event (ca. 950-550 Ma). It is considered that the northeastern Egypt was evolved by regional crustal extension and magmatic-arc regimes [9]. Moreover, in this segment, large gabbro-diorite-tonalite complex (GDT, 881 Ma) was emplaced during the early stage of the Pan-African orogeny and produced (by fractionation) from a mantle-derived tholeiitic magma formed within an island-arc tectonic environment. Thus, subduction-related magmatism in synorogenic belts could be formed by several processes. The most predominate types are the fractional crystallization of mantle-derived basaltic magma [55] and partial melting of lower crust with intrusion of basaltic magma [56].

The mafic microgranular enclaves that hosted in Abu Zawal granitoid rocks (MME) are characterized by their enrichment in Mg, Ca, Fe, Al, Sr and depleted in K, Rb, Y, Nb, and it was emplaced in VAG field, beside their plotting in and/or close to the field of island arc gabbro-diorite (IAG). Therefore, the MME are comparable with the GDT of the northeastern Egypt which represents the oldest crustal component in this region; it was emplaced (881 Ma; Rb-Sr age, [57] during the early stage of the evolution of the shield area and the island arc gabbro-diorite (IAG) of the eastern Desert of Egypt. Abu Zawal granitoid rocks represent part of the late orogenic magmatism in the northeastern Desert of Egypt which in turn constitute and represent a major component of more than 70% of the crust in northeastern Egypt. It exhibits typical features of I-type granites, trace element characteristics of volcanic-arc granites, and have been formed in an Andean-type setting.

The northeastern Desert (NED) of Egypt, in contrast to SED, is characterized by: (a) the predominant of calc-alkaline granitic rocks of the "Gattarian" or "Younger" granites and coeval "Dokhan" volcanics; (b) the scarcity of the older metasedimentary, metavolcanic and ophiolitic rocks; and (c) the apparent absence of igneous activity younger than ca. 345 Ma (e.g., [58-61]). There is no convincing evidence to indicate the existence of any older (e.g., Mesoproterozoic to Archean) sialic crust in northeastern Egypt [9]. Therefore, Abu Zawal granitoid rocks were produced above a subduction system in an island-arc setting similar to the diorite-tonalite assemblages in the Caribbean [62] and in the Philippines [63].

Mineralogically, Abu Zawal granitoid rocks are subsolvus and consist of variable contents of plagioclase, K-feldspar, quartz, and biotite, with accessory titanite (sphene), zircon and opaque magnetite, typical of I-type granites. The rocks also exhibit major and trace elements characteristic of calc-alkaline orogenic suites (Fig. 4) and volcanic-arc granites (Fig. 7) that resemble younger examples characteristic of orogenic zones at continental plate margins. We suggested that the magma source for Abu Zawal granitoid rocks was formed by partial melting of a modified oceanic crust at an active (Andean-type) continental margin (Fig. 8d) that run in harmony with the result obtained by [61] for the northeastern Egypt.

CONCLUSIONS

Such as other MME in the world [64, 65], most of the studied MME in Abu Zawal granitoids are rich in hornblende and plagioclase and the next common minerals in order of decreasing abundance, are quartz and biotite.

Subduction related magmatism in orogenic belts

could be formed by several processes. The most plausible types are the fractional crystallization of mantle derived basaltic magma [55] and partial melting of lower crust with intrusion of basaltic magma [56]. The studied Abu Zawal granitoid rocks have chemical characteristics (e.g. high K_2O and Rb) which preclude their derivation via fractional crystallization of mantle derived basaltic magma. It is established that the island arc gabbro-diorite complex of the Eastern Desert of Egypt could be formed from mafic magma source by fractional crystallization of pyroxene, plagioclase and amphibole [50, 66]. On Fig. 6. it is indicated that studied Abu Zawal granitoid rocks and the island arc gabbro-diorite are not genetically related. However, the mafic microgranular enclaves (MME) fall within and/or close to the field of island arc gabbro-diorite (IAG), suggesting that they are genetically related (Figs. 6 & 8). This feature is again confirmed on the Rb/Sr – SiO_2, Sr – Rb and Sr – Ba diagrams (Fig. 8). In Sr – Rb and Sr – Ba diagrams (Fig. 8a & b). Abu Zawal granitoid rocks are depleted in Rb, Sr and Ba relative to the island arc gabbro-diorite field, which used as evidences against their derivation from mantle derived magma by fractional crystallization of pyroxene, amphibole and plagioclase.

Plot of the studied Abu Zawal granitoid rocks Rb/Sr vs. K/Rb, (Fig. 8d). Andean granites from the Coastal Batholith of Peru [53], whereas A-type granites from Nigeria [54]. We can notice that the studied Abu Zawal granitoid rocks fall close to the Andean granites field and dissimilar to the within-plate Nigerian granites.

ACKNOWLEDGMENTS

We would like to express our appreciation and gratitude for Dr. Rammlmair and Frank Melcher, Institute of BGR (Bundesanstalt für Geowissen-schaften und Rohstoffe) in Hannover, Germany, for performing the analytical work.

TRANSPARENCY DECLARATION

The authors declare no conflicts of interest.

REFERENCES

1. Stern RJ, Hedge CE. Geochronologic and isotopic constraints on Late Precambrian crustal evolution in the Eastern Desert of Egypt. Am J Sci 1985; 285: 97-127.
2. Shimron AE. The Dahab mafic-ultramafic complex, southern Sinai Peninsula-a probable ophiolite of late Proterozoic (Pan-African) age. Ofioliti 1981; 6: 461-471.
3. Gass IG. Evolution of the Pan-African crystalline basement in north-east Africa and Arabia. J Geol Soc London 1977; 134: 129-138.
4. Kroner A. Ophiolites and the evolution of tectonic boundaries in the Late Proterozoic Arabian-Nubian shield of northeast Africa and Arabia. Precambrian Res 1985; 27: 277-300.
5. Kroner A, Reischmann T, Wust HJ, Rashwan AA. 1988. Is there any Pre-Pan-African > 950 Ma Basement in the Eastern Desert of Egypt? In: El-Gaby S, Greiling RO. (Eds.): The Pan-African Belt of Northeast Africa and Adjacent areas. 95-119. Vieweg, Braunschweig/Wiesbaden.
6. Stern RJ, Sellers G, Gottfried D. 1988. Bimodal dike swarms in the North Eastern Desert of Egypt: Significance for the origin of late Precambrian "A-type" granites in northern Afro-Arabia. In: El-Gaby S, Greiling R.O. (Eds.): The Pan-African Belt of Northeast Africa and Adjacent areas: 147-177. Vieweg, Braunschweig/Wiesbaden.
7. Stern RJ, Gottfried DG. Petrogenesis of a Late Precambrian (575-600 Ma) bimodal suite in northeast Africa. Contrib Mineral Petrol 1986; 92: 492-501.
8. Willis KM, Stern RJ, Clauer N. Age and geochemistry of late Precambrian sediments of the Hammamat Series from the northeastern Desert of Egypt. Precambrian Res 1988; 42: 173-187.
9. Abdel Rahman AM. Tectonic magmatic arc of shield evolution: the Pan-African belt in northeastern Egypt. Tectonophysics 1995; 242: 223-240.
10. Hume WF. 1935. Geology of Egypt. vol. II, part II. Survey of Egypt, Cairo.
11. Schurmann H.M.E. The Pre-Cambrian of the Gulf of Suez area. 19th Int Geol Cong CR 1953; 1: 115-135.
12. El-Gaby S. Petrochemistry and geochemistry of some granites from Egypt. N Jb Miner Abh 1975; 124: 147-189.
13. Hussein AA, Monir MA, E1-Ramly MF. A proposed new classification of the granites of Egypt. J Volcanol Geotherm Res 1982; 14: 187-198.
14. El-Ramely MF. A new geological map for the basement rocks in the Eastern and South-Western Desert of Egypt. Ann Geol Surv Egypt 1972; 2: 1-18.
15. Hashad AH. Present status of geochronological data on the Egyptian basement complex. Inst Appl Geol Bull Jeddah 1980; 3: 31-46.

16. Hassan MA, Hashad AH. 1990. Precambrian of Egypt. In: Said R. (Ed.) The geology of Egypt. Balkema, Rotterdam, 201-245.
17. Geological Map of Egypt. 1981. Scale 1:2.000.000. Egyptian Survey and Mining Authority, Abbbassiya, Cairo.
18. Stern RJ. Petrogenesis and tectonic setting of late Precambrian ensimatic volcanic rocks, central Eastern Desert of Egypt. Precambrian Res 1981; 16: 195-230.
19. Kroner A, Todt W, Hussein IM, Mansour M, Rashwan A. Dating of late Proterozoic ophiolites in Egypt and the Sudan using single zircon evaporation technique. Precambrian Res 1992; 59: 15-32.
20. Vernon RH. Restite, xenoliths and microgranitoid enclaves in granites. J Proceed Roy Soc New S Wales 1983; 116: 77-103.
21. Didier J. Contribution of enclaves studies to the understanding of origin and evolution of granitic magmas. Geol Rund 1987; 76: 41-50.
22. El-Aref MM, Abdel Wahed M, Kabesh M. On the geology of the basement rocks, east of Abu Zenima, west central Sinai, Egypt. Egypt J Geol 1988; 32: 1-25.
23. El-Aref MM, Abdel Wahed M, Kabesh M. Fabric evolution and geochemical characters of the migmatites and associated gneisses at Wadi Baba and Wadi Dafari, west central Sinai, Egypt. Egypt Mineral 1989; 1: 27-53.
24. Khalid AAM. 1988. Geological, petrological and geochemical studies on the basement rocks of Wadi Watir area, Sinai. p. 250. M.Sc. Thesis, Cairo Univ., Egypt.
25. Takla MA, Basta FF, El-Maghraby A. Contribution to the geology of Wadi Ghadir area, south Eastern Desert, Egypt. Egypt J Geol 1992; 36 (1-2): 373-3392.
26. El-Mettwaly AA. Microgranular enclaves in the Pan-African I-type granites from the Sinai Massif: petrology, mineralogy and geochemistry. J Afr Earth Sci 1993; 17 (1): 95-110.
27. Katta LA, Mashaal SE, El Tokhi MM. Geochemistry and tectonic evolution of Pan-African granitoid rocks in the east Sahara craton, Qaret El Maiyit, southwestern Desert, Egypt. Egypt Mineral 1994; 6: 95-117.
28. Surour AA, Kabesh ML. Calc-alkaline magmatism and associated mafic microgranular enclaves of Wadi Risasa area, Southeastern Sinai, Egypt. Ann Geol Surv Egypt 1998; XXI: 35-54.
29. Asran MHA, Mohamed MM. Geochemistry, petrogenesis and fluid inclusion studies of the Kadabora granite pluton and associated enclaves, Central Eastern, Egypt. 5th Intern. Conf. on Geology of the Middle East, Cairo, Egypt. 2003: 139-154.
30. Sabet AH, El Gaby S, Zalata AA. Geology of the basement rocks in the northern parts of El-Shayib and Safaga sheets, Eastern Desert. Ann Geol Surv Egypt 1972; 2: 111–128.
31. Zalata AA. 1997. Geology of the area around Gabal El Shayib, Eastern Desert, Egypt. p. 350. Ph.D. Thesis, Ain Shamis Univ.
32. Soliman MF. 1988. Geologic studies on the basement complex of El-Urf area, Eastern Desert, Egypt. p. 112. M.Sc. Thesis, Assiut Univ., Egypt.
33. Sharara NA, Abu El Ela F, El Nady OM, Soliman MF. Geology and geochemistry of the island arc association of the area around Gabal El Urf Eastern Desert, Egypt. Bull Fac Sci Assiut Univ 1990; 19 (1-F): 97-122.
34. Asran AM, Ibrahim ME, El-Mansi MM, Abdel Ghani IMM. Geochemistry, petrogenesis and radioactivity of Pan-African granitoids, Fatirah area, Eastern Desert, Egypt. 5th intern. Conf. Geochemistry, Alex. Univ., Egypt. 2001: 599-626.
35. Asran AMH, Ibrahim MA, El Mansi MA, Abdel Ghani IM. Back-arc to active continental margin Pan-African volcanicity along Wadi Fatirah, Central Eastern Desert, Egypt. 5th International Conference on the Geology of the Tethys, Cairo Univ. 2008: 23-34.
36. KuirongY, Liankun S. 1991. A two stage crust-mantle interaction model for mafic micrgranular enclaves in the Daning granodiorite pluton, Guangexi, China: In: Didier J, Barbarin B. (Eds.): Enclaves and granite petrology. Elsevier, New York: 95-112.
37. Streckeisen A, Le Maitre RW. A chemical approximation to the modal QAPF classification of the igneous rocks. N Jb Mineral Abh 1979; 16: 169-206.
38. Streckeisen AL. Classification of the common igneous rocks by means of their chemical ccomposition. A provisional attempt. N Jb Min J 1976: 1-15.
39. Tuttle OF, Bowen NL. origin of granite in the light of experimental studies in the system Na Al Si_3O_8- K Al Si_3O_8- SiO_2 H_2O. Geol Soc Amer Mem 1958; 24: 1-53.
40. Maniar PD, Piccoli PPM. Tectonic discrimination of granitoids. Bull Geol Soc Am 1989; 101: 635–643.
41. Wright JB. A simple alkalinity ratio and its application to questions of non-orogenic granite gneiss. Geol Mag 1969; 106: 370-384.
42. Greenberg JK. Characteristic and origin of Egyptian younger granites. Bull Geol Soc Am 1981; 92 (Part 1): 224-232.
43. Sylvester PJ. Post-collisional alkaline granites. J Geol 1989; 97: 261-281.
44. El-Bouseily AM, El-Sokkary AA. The relation between Rb, Ba and Sr in the granitic rocks. Chem Geol 1975; 16: 207-219.
45. Moghazi AM. Petrology and geochemistry of Pan-African granitoids, Kab Amiri area, Egypt-implications

for tectonomagmatic stages in the Nubian Shield evolution. Mineral Petrol 2002; 75: 41-67.
46. Thompson RN, Morrison MA, Hendry GL, Parry SJ. An assessment of the relative roles of crustal and mantle in magma genesis: an elemental approach. Phil Trans Roy Soc Lond 1984; A310: 549-590.
47. Pearce JA, Harris NBW, Tindle AG. Trace element discrimination diagrams for the tectonic interpretation of granitic rocks. J Petrol 1984; 25 (part 4): 956-983.
48. Whalen JB, Currie KL, Chappell BW. A-type granites: geochemical characteristics, discrimination and petrogenesis. Contrib Mineral Petrol 1987; 95: 407-419.
49. Mohamed FH, Hassanen MA. Geochemical evolution of arc-related mafic plutonism in the Um Naggat district, Eastern Desert of Egypt. J Afr Earth Sci 1996; 22: 269-283.
50. Moghazi AM. Magma source and evolution of Late Neoproterozoic granitoids in the Gabel El-Urf area, Eastern Desert, Egypt: geochemical and Sr-Nd isotopic constraints. Geol Mag 1999; 136: 285–300.
51. Kroner A, Eyal M. Early Pan-African evolution of the basement around Elat, Israel, and the Sinai Peninsula revealed by single zircon evaporation dating and implication for crustal accretion rates. Geology 1990; 18: 545-548.
52. Pearce TH, Gale GH. Identification of ore-deposition environments from trace element geochemistry of associated igneous rocks. J Geol London Sp Pub 1977; 134: 14-24.
53. Atherton MP, McCourt WJ, Sanderson LM, Taylor WP. The geochemical character of the segmented Peruvian coastal batholith and associated volcanics 1979. In: Atherton MP, Tarney J. (Eds.): Origin of Granite Batholiths: Geochemical Evidence. Shiva, Cheshire: 45-64.
54. Imeokparia EG. Geochemical aspects of the evolution and mineralization of the Amo Younger granite complex (northern Nigeria). Chem Geol 1983; 14: 187-198.
55. Bacon CR, Druitt TH. Compositional evolution of the zoned calc-alkaline magma chamber and trondhjemite magmas. J Petrol 1988; 19: 289-316.
56. Guffanti M, Clynne MA, Muffler LJP. Thermal and mass implications of magmatic evolution in the Lassen volcanic region, California and constraints on basalt influx to the lower crust. J Geophys Res 1996; 101: 3001-3013.
57. Abdel-Rahman AM, Doig R. The Rb-Sr geochronological evolution of the Ras Gharib segment of the northern Nubian shield. J Geol Soc London 1987; 144: 577-586.
58. Engel AEJ, Dixon TH, Stern RJ. Late Precambrian evolution of Afro-Arabian crust from ocean arc to craton. Geol Soc Am Bull 1980; 91: 699-706.
59. Burollet PF, Bolze J, Ott d'Estevou P. Sedimentology and tectonics of the Gharamul area, west of Suez Gulf. 6th E.G.P.C. Explor. Sem., Cairo 1982; 1: 17.
60. Ries AC, Shackleton RM, Graham RH, Fitches WR. Pan-African structures, ophiolites and melange in the Eastern Desert of Egypt: a traverse at 26°N. J Geol Soc London 1983; 140: 75-95.
61. Abdel-Rahman AM, Martin RF. Late Pan-African magmatism and crustal development in northeastern Egypt. Geol J 1987; 22: 281-301.
62. Kesler SE, Jones LM, Walker RL. Intrusive rocks associated with porphyry copper mineralization in island-arc areas. Econ Geol 1975; 70: 515-526.
63. Wolfe JA, Manuzon MS, Divis AF. The Taysan porphyry copper deposit, southern Luzon Island, Philippines. Econ Geol 1978; 73: 608-617.
64. Barbarin B. Plagioclase xenocrysts and mafic magmatic enclaves in some granitoids of th Sierra Nevada Batholith, California. J Geophys Res 1990; 95: 17747-17756.
65. Barbarin B, Didier J. Genesis and evolution of mafic granular microgranular enclaves through various types of interaction between coexisting felsic and mafic magmas. Trans R Soc Edinburg Earth Sci 1992; 83: 145-153.
66. Abdel Rahman AM. Petrogenesis of early orogenic diorites, tonalities and post-orogenic trondhjemites in the Nubian Shield. J Petrol 1990; 31: 1285-1312.

Journal of Biology and Earth Sciences

EARTH SCIENCES ORIGINAL ARTICLE

Evolution and geochemical studies on a stromatic migmatite-amphibolite association in Hafafit area, Central Eastern Desert, Egypt

Asran M. Asran[1], Mona Kabesh[2]

[1]Geology Department, Faculty of Science, Sohag University, Sohag, Egypt

[2]Geology Department, Faculty of Science, Cairo University, Cairo, Egypt

ABSTRACT

The infrastructural rocks exist in the form of the gneiss domes that constituting 7% of the surface outcrops of the basement rocks of the Eastern Desert of Egypt. This study is a closer look on the mesoscopic and microscopic characteristics and the chemical behaviour of typestromatic migmatites, associated with amphibolite bands and boudins that are exposed in the northeastern part of the Migif dome, Hafafit area. Therefore, the major oxides for the studied rocks were analyzed by using the wet chemical analysis technique, whereas the trace elements analyses were carried out by XRF technique. Microprobe analyses of the investigated minerals (amphiboles, plagioclase, biotite and muscovite) were carried out with a scanning microscope and wave length dispersive spectrometers. The paragenesis and microfabric evolution of these migmatites show that they are affected by three phases of deformation. These are associated with metamorphic differentiation, crystallization and segregation. Geochemical variation between mesosomes and leucosomes reflect original compositional variations, enhanced by metamorphic differentiation and short-range migration resulting in segregation of bands. This is followed by partial melting and in-situ formation of leucosomes. Geochemical data of the associated amphibolite show that they represent para- and ortho-amphibolites. Mineral chemistry show that hornblende of the migmatites is of ferro-tschermakitic, while from the amphibolites has magnesio-hornblende composition. Plagioclase of the amphibolite has An_{36-44}, while of the migmatites has An_{25-32} in the leucosomes and An_{51-60} in the mesosomes and melanosomes. The amphibolites were formed at temperature ranges from 720-740ºC, whereas the migmatites at temperature ranges from 800-820ºC.The mineral chemistry support their formation in the upper amphibolite facies.

Key words: migmatite, amphibolite, mesosomes, leucosomes, Eastern Desert, Egypt.

J Biol Earth Sci 2012; 2(1): E17-E33

Corresponding author:
Prof. Asran M. Asran
Geology Department, Faculty of Science,
Sohag University, Sohag, 82524, Egypt
e-mail: asran_58@yahoo.com

Original Submission: 16 February 2012; Revised Submission: 26 March 2012; Accepted: 27 March 2012

ISSN: 2084-3577
http://www.journals.tmkarpinski.com/index.php/jbes or http://jbes.strefa.pl
e-mail: jbes@interia.eu

INTRODUCTION

The Migif-Hafafit gneisses of Wadi Hafafit area are located near the boundary between the South Eastern Desert (SED) and the Central Eastern Desert (CED), (Fig. 1). These basal gneisses were previously considered as the structurally lowest, autochthonous pre-orogenic unit [1]. Recently these gneisses are viewed as thrust units representing tectonic windows beneath low grade successions of ophiolitic melange, Calc-alkaline igneous rocks and metasediments [2-4]. These thrust units are part of the thrust and fold belt at the margin of the pre-Panafrican craton in the west [5]. El Ramly et al. [3] suggested a NW directed regional tectonic transport.

The domal structure of Migif is mainly occupied by granitic to tonalitic gneisses in the core followed outwards by biotite, hornblende, hornblende-biotite gneisses with garnet-biotite schist and garnet-biotite gneisses and rimed by a zone of psammitic gneiss. The gneisses show local migmatization specially in the eastern side of the domal structure [6-7]. The multi-phase deformation and metamorphic evolution of the Hafafit area suggest three phases of deformation namely D_1, D_2 and D_3 coeval with three metamorphic events [6]. The first phase of metamorphism (M_1) is a multi-stage phase in the high grade upper amphibolite facies. The following events (M_2 and M_3) took place within the greenschist to low amphibolite facies. The high grade gneisses are separated from the melange rocks by major thrust faults. More phases of deformation were recognized and described by Rashwan [8], El Ramly et al., [9] and Greiling et al. [10]. Fowler & El Kalioubi [11] concluded that the structures of the Hafafit area are the result of interference of four macroscopic fold phases:

1) sheath-like fold nappes transported to the N or NW on gently dipping mylonite zones;
2) NE-SW trending small upright open folds;
3) NE trending large macroscopic monoclinal folds and thrusts;
4) NE-SW shortening producing NW-SE trending upright gently plunging folds.

The present study presents a closer look on the mesoscopic, microscopic and geochemical characteristics of the stromatic migmatites and associated amphibolites. It is an attempt to clarify their metamorphic and microstructural evolution, and discusses the effect of deformation on the rocks and their response to recovery and recrystallization stages following the migmatization and deformation phases.

Field and megascopic observations

The basement rocks exposed in the Migif dome in the Hafafit area [9] include migmatites and amphibolites units among the succession.

Migmatites occupy a narrow zone between the granite gneiss and the hornblende and biotite gneisses, within the inner parts of the domal structure. Because of the heterogeneity and complexity of the gneiss and migmatite belt, a small sector was chosen in the northeastern part of the Migif dome for a more detailed study (Fig. 1).

The migmatites exhibit different fabrics and structures such as banded, agmatic and boudinage. The stromatic (banded) structure is the most prevalent where the migmatites show alternating bands of dark grey to black mesosome and light coloured coarse quartzofeldspathic leucosome, with or without discontinuous melanosome along their contact. Leucosomes commonly form straight regular and rhythmic bands, but they may also form patches, pockets and concordant or discordant veins.

The studied banded migmatites are considered metatexites, as those described by Mehnert [12],

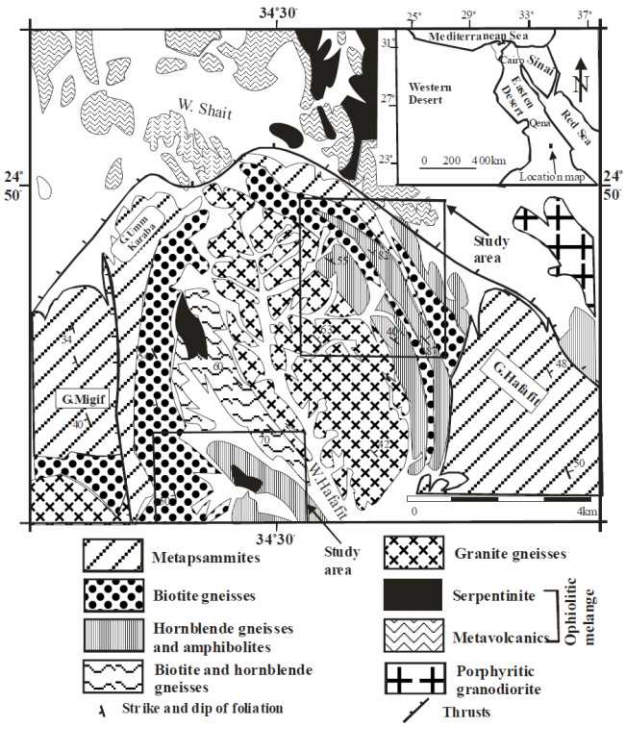

Fig. 1. Geological map of the northern part of Wadi Hafafit area (modified after El-Ramly et al. 1993).

Brown [13-15] and Sawyer [16], as the characteristic banded fabric is well preserved. But locally where the amount of leucosome increases, the migmatites grade into diatexites, where the original fabrics and composition are nearly obliterated.

The banded migmatites are affected by more than one phase of deformation, equivalent to those affecting the surrounding gneisses. The present authors prefer to use the terminology first, second and third phases of deformation that are probably conformable with D_1, D_2 and D_3 and the associated folding phases of Abdel Wahed [6].

The mesosome bands are schistose, reflecting the first phase of deformation D_1, as rock foliation is parallel to the lithological layering ($S_1//S_0$) and parallel to the mesosome/leucosome contact. They also show L_1 mineral lineation due to the strong preferred orientation of biotite and hornblende. Formation of leucosome bands parallel to the S_1 foliation may suggest that they are syn-kinematic with the D_1 deformational phase. Rootless folds (F_1) are formed at later stages in this phase.

In the second phase of deformation D_2, the banded migmatites are folded into F_2, tight, isoclinal and asymmetric folds; disharmonic folds are also observed. Commonly these folded banded migmatites show passive flow folds with thick leucosomes at the crests and thin leucosomes along the limbs. This feature suggests deformation in semi-viscous conditions as the leucosome is rather mobile and migrates to lower pressures zones, indicating syn-migmatization deformation. When the F_2 folding phase continued after migmatization and leucosome formation, F_2 folds possess leucosome bands with rather uniform thickness due to deformation after the crystallization of solid phases, ptygmatic folding is also observed. In this phase S_2 schistosity is formed as axial plane foliation and L_2 is observed as mineral lineation and crenulation lineation.

With continuous tightening and change in the folding axes direction during the late stage of F_2 folding phase, refolding and formation of complicated interference patterns were generated. The third phase of deformation D_3 produced F_3 open, symmetrical and asymmetrical folds. Weak S_3 schistosity as strain-slip cleavage and L_3 kinking and crenulation lineation are observed.

Later pegmatitic veins of granitic composition cut across the migmatized rocks. Some leucosome bands show dilation or displacement at the contact with pegmatitic veins.

Amphibolites, represent para- and ortho-amphibolites, they are distinguished into; foliated amphibolites which are more prominent and devoid of banding and banded amphibolites.

The foliated amphibolites constitute a continuous belt along the outer core of the dome between the garnet-biotite schist and the granite gneiss which forms the core. Generally, they have moderate relief. They are foliated, with foliation running conformable with the surrounding rocks and the regional structure. They possess grayish green to dark green colour and are locally migmatized.

The banded amphibolites occur as continuous beds intercalating the foliated amphibolites; they possess gradational contacts against the massive amphibolites. They are more well-developed in the southwestern part of the dome. Megascopically, they are built up of felsic bands, up to 5 cm thick, alternating with mafic bands, up to 10 cm thick, with distinct sharp contacts. The amphibolite bands run conformable with the regional structure and are affected by ductile and brittle deformations. The ductile behavior of the amphibolite is manifested by the well-developed foliation, folds and pinching out of the bands. The brittle deformations are expressed in the fragmentation of the solid amphibolite bands into angular blocks and boudins. They may be broken by faults with displacement of the amphibolite bands.The amphibolite bands are dissected by aplite and pegmatite veins, formed mainly of quartz and feldspars, that are discordant and rarely concordant to the bands.

Petrographic Characteristics

The banded migmatites in the studied sector are differentiated according to mesosome composition into: hornblende-biotite, biotite and hornblende migmatites. The different varieties are microscopically studied for their mineralogical composition, microtextures and microstuctures reflecting deformation and recrystallization processes. Intracrystalline deformation structures and post deformational recovery features are highlighted.

1) Hornblende-biotite migmatites:

The hornblende-biotite gneiss in the area progressively shows the beginning of segregation of felsic lenses and bands, which grew thicker and

coarser forming leucosomes with or without melanosomes along their contacts. It shows a well-developed banded structure with a gneissose mesosome and a coarse-grained leucosome separated by a dark discontinuous melanosome. The rocks are probably derived from impure marl (calc-pelitic rocks).

The mesosome is a medium-grained gneiss formed mainly of biotite, quartz and plagioclase and less abundant dark green hornblende. The main accessories are coarse apatite and few opaque grains.

The S_1 schistosity is represented by perfectly oriented medium-grained sub- idiomorphic biotite crystals, 1 to 1.5 mm long, fine plagioclase, quartz and less frequent sub-idiomorphic to xenomorphic green hornblende, up to 4 mm long. The second episode of crystallization is expressed by a less prominent foliation S_2, traced by oriented biotite flakes, smaller in size and intersecting S_1 biotite.

Medium-grained sub-idiomorphic plagioclase crystals, up to 3 mm long, sometimes enclosing older S_1 fine plagioclase crystals or S_1 and S_2 biotite. Quartz forms coarse crystals, which may also enclose S_1 biotite crystals. Hornblende is xenomorphic and increases in size and abundance towards the melanosome. They form poikiloblasts enclosing S_1 biotite, quartz and apatite.

The third phase of crystallization shows a weak foliation (S3) marked by thinner biotite crystals. Some plagioclase crystals enclose S_3 biotite. The S_2 and S_3 foliation trends are nearly normal to each other.

Deformation of mesosome is manifested by deformation twin lamellae in plagioclase tapering inwards, and by the undulose extinction in quartz crystals mainly of S_1 schistosity, during the D_1 and D_2 deformational episodes. During the recovery phase quartz commonly forms subgrain boundaries. This is followed by partial dynamic recrystallization of quartz, forming new fine-grained strain-free crystal aggregates; biotite commonly exhibits wavy extinction, twinning and kinking. Later brittle deformation forms microfractures in biotite and plagioclase. Bands of fine, dynamically recrystallized quartz are sometimes observed parallel to the S_2 and S_3 trends, transecting the minerals.

The melanosome is formed of idiomorphic biotite crystals larger than those in the mesosome. The biotite crystals are aligned mainly along the contact between the mesosome and leucosome. Coarse, dark green hornblende crystals, 3 mm long, form poikiloblasts enclosing quartz, plagioclase and apatite. They may partly enclose biotite crystals or push them aside around their contacts. Some biotite crystals are oriented parallel to the S_2 and S_3 trends in the mesosome. This orientation could be due to deformation affecting the mesosome or partly due to local pressure of hornblende poikiloblasts during their growth.

The leucosome band is coarse-grained, and composed of large xenomorphic quartz and sub-idiomorphic to xenomorphic plagioclase and few biotite flakes. Orthoclase sometimes fills the interstices between the plagioclase crystals, and sometimes corroding them. The leucosome is also deformed, probably during D_2 and D_3, since quartz and plagioclase sometimes show evidences of deformation, recovery and recrystallization. Quartz forms large crystals with undulose extinction and forms crystals with subgrain boundaries during recovery. It also occurs as aggregates of fine new grains of dynamically recrystallized quartz with irregular boundaries, reflecting a bimodal size distribution characteristic of grain boundary migration recrystallization (GBM). The dynamically recrystallized quartz may also form fine-grained bands correlated to those in the mesosome following the two deformation directions (S_2 and S_3).

Plagioclase shows tapered deformation twin lamellae; bent crystals with undulose extinction and broken crystals with sharp termination of twinning. Some plagioclase crystals are surrounded by aggregates of small dynamically recrystallized plagioclase grains along their rims forming a core and mantle structure (mortar structure).

2) Biotite migmatites:

The biotite migmatites are mainly derived from greywackes (semi-pelitic sediments). Two varieties are distinguished:

a) Biotite-plagioclase migmatite: it has a medium-grained gneissose mesosome and a coarse-grained leucosome, separated by a symmetrical or asymmetrical thick dark melanosome.

The mesosome is composed mainly of biotite, plagioclase and quartz with accessory zircon and opaques. The earliest phase of crystallization is mainly represented by fine biotite flakes and small rounded quartz crystals. The prominent schistosity S_1 is expressed by oriented biotite flakes, up to 1.5

mm long, commonly stacked in short streaks marking the main rock foliation developed during the first phase of deformation D_1. Plagioclase is mainly subidiomorphic to xenomorphic, 0.6 mm long, and may enclose earlier rounded quartz and few biotite flakes. Quartz forms medium to coarse-grained crystals.

Later deformation D_2 is manifested by the development of a less prominent S_2 biotite foliation inclined to the S_1 foliation of biotite. It is also reflected by wavy extinction in the large quartz crystals and deformation twin lamellae in plagioclase that are tapered, and sometimes bent or broken. During the stage of recovery, quartz crystals with subgrain boundaries were formed followed by the formation of fine recrystallized crystal aggregates.

The melanosome occurs as a thick dark band consisting of coarse biotite flakes, up to 7 mm long with abundant quartz and plagioclase mainly arranged parallel to the leucosome/mesosome contact and S_1 foliation. Coarse apatite crystals are concentrated in the melanosome and are sometimes partly enclosed in biotite. Biotite deforms mainly by slip mechanism as it shows undulose extinction and kinking reflecting the D_2 and D_3 deformational phases. The melanosome bands may be disturbed by light coloured lenticular bodies formed of quartz with or without plagioclase. This seems to be stripping off parts of the melanosome towards the leucosome layer. This could represent a stage in the process of mechanical formation of relict melanosome, as dark streak within light leucosome band.

The leucosome is formed mainly of plagioclase, quartz, few biotite and K-feldspar crystals. The main schistosity S_1 is not observed in the leucosome band, suggesting that it was formed during or later than D_1 deformation but were affected by D_2 and D_3 deformations. Plagioclase forms large xenomorphic crystals. Some plagioclase crystals show deformational twin lamellae, while others are broken by microfaults displacing the twin lamellae and microfractures that are sometimes filled by later quartz. Quartz forms coarse crystals, commonly showing wavy extinction and subgrain boundaries. It may also form small recrystallized aggregates. Orthoclase and microcline crystallize interstitially corroding and partly enclosing plagioclase crystals.
b) Biotite–plagioclase-K, feldspar-muscovite migmatite: the mesosome consists mainly of biotite, plagioclase and quartz. Plagioclase forms subidiomorphic crystals. Quartz shows large crystals with wavy extinction, but fine recrystallized crystals are not common. In this mesosome, biotite is partly altered to chlorite and sometimes replaced by muscovite. Some muscovite flakes occur along fractures in plagioclase. Potash feldspars occur as orthoclase and microcline growing interstitially and partly or completely enclosing plagioclase.

An asymmetrical melanosome is observed on one side of the leucosome band. It is mainly formed of coarse biotite and few hornblende crystals.

3) Hornblende migmatites:

The hornblende gneiss grades into migmatites through the development of segregated leucocratic lenses and bands conformable with the main foliation. This migmatite is composed of a medium to coarse-grained mesosome alternating with coarse-grained leucosome without melanosome inbetween.

The mesosome is formed mainly of hornblende, quartz and plagioclase with accessory apatite and secondary chlorite. Almost no opaques are found, except for very minute crystals in hornblende. The first phase of metamorphic crystallization was contemporaneous with the earliest deformational phase D_1. This phase is characterized by parallel oriented hornblende crystals marking the S_1 foliation. The hornblende crystals are, 0.5-1 mm long and may reach up to 2 mm in the coarser variety. Hornblende commonly encloses drop-like quartz and partly or completely encloses plagioclase. Plagioclase shows slightly elongated subidiomorphic crystals sometimes enclosing earlier, very small rounded quartz and hornblende crystals. Quartz forms xenomorphic crystals mostly elongated along S_1. The second phase of deformation (D_2) is accompanied by less developed S_2 foliation inclined to S_1. It is formed of finer hornblende crystals and some thin biotite flakes. The third phase of crystallization accompanying deformation D_3, is marked by the weak foliation S_3 (almost normal to S_2) marked by some hornblende and few biotite.

Deformations are expressed in the different minerals. Plagioclase shows undulose extinction, tapering deformational twin lamellae, or bent twin lamellae that are sometimes broken and displaced. Quartz commonly exhibits undulose extinction and less developed recrystallization features.

The leucosome bands are coarse-grained and composed of quartz and plagioclase. Plagioclase occurs as large xenomorphic crystals that are mostly deformed exhibiting wavy extinction, and tapered and bent twin lamellae. Quartz forms large crystals showing wavy extinction and subgrain boundaries. They exhibit recovery texture formed of finer recrystallized aggregates which is more frequent than in the mesosome.

4) Amphibolites:

The amphibolite layers and bands exhibit foliated and banded fabric. The layers are affected by brittle and ductile deformation. Brittle deformation broke the layers into angular blocks and boudins, the ductile behavior of the amphibolite is manifested by the development of foliation running parallel to the surrounding gneissosity. Microscopically the foliated amphibolites are mainly fine-grained, foliated and consist mainly of hornblende, plagioclase and few quartz grains, with fine sphene and few minute opaques as accessories. Hornblende forms subhedral crystals preferably oriented along the bedding plane foliation while plagioclase forms subhedral crystals showing lamellar twinning. The foliated amphibolites may exhibit vertical and lateral variation in grain size.

The banded amphibolites is composed of dark bands made up of fine preferred oriented hornblende and plagioclase similar to the foliated amphibolite; alternating with light colored bands constituted mainly of plagioclase, sphene and may contain small skeletal crystals of clinopyroxene (diopside) concentrated in thin streaks parallel to the rock foliation.

MATERIALS AND METHODS

Analytical technique

The major oxides for the studied rocks were analyzed at the Geology Department, Faculty of Science, Sohag University by using the wet chemical analysis technique, whereas the trace elements analyses were carried out at the Central laboratories of the Geological Survey of Egypt. Therefore, twenty nine representative samples were collected from the different rock types.

Microprobe analyses of the investigated minerals (amphiboles, plagioclase, biotite and muscovite) were carried out at the institute of Mineralogy and petrology at Karl-Franzens University, Graz, Austria with a JEOL JSM-6310 scanning microscope using an acceleration voltage of 15 kv and oxford energy and wave length dispersive spectrometers.

RESULTS

Whole Rock Chemistry:

Geochemical characteristics

To exhibit and discuss the geochemical characteristics of the studied amphibolites and

Table. 1. Chemical analyses of the studied Hafafit migmatites.

Ser.No.	1	2	3	4	5	6	7	8	9	10	11	12	13	14	15	16	17	18	19	20
SiO_2	57,25	58,21	56,4	60,71	59,47	57,83	67,32	66,3	73,18	71,23	67,91	70,12	66,61	68,43	64,73	69,32	68,76	53,82	51,64	54,94
TiO_2	0,79	0,37	0,38	0,56	1,16	0,59	0,14	0,15	0,07	0,09	0,22	0,24	0,24	0,21	0,23	0,28	0,25	0,4	0,43	0,61
Al_2O_3	12,08	15,09	13,08	15,08	14,09	13,09	13,42	14,19	13,58	16,1	16,1	13,06	16,09	15,09	16,01	15,09	16,08	14,09	16,1	14,09
FeO	10,67	8,39	9,15	8,39	11,43	9,34	5,81	6,86	1,53	3,04	3,03	2,81	1,51	1,52	1,48	3,05	2,29	9,91	9,91	10,29
MgO	5,29	4,23	4,23	4,34	4,23	5,82	4,41	5,88	4,3	2,94	1,06	3,17	3,23	2,11	3,17	2,11	2,29	7,41	6,29	5,29
CaO	5,88	7,8	10,31	4,42	4,42	4,96	1,06	1,01	1,03	0,98	4,41	4,42	5,87	5,88	6,62	4,67	5,88	8,83	8,83	5,86
Na_2O	5,73	3,59	4,23	3,19	2,18	4,12	4,76	2,7	3,19	3,84	5,29	4,21	4,71	5,1	4,91	3,94	2,78	3,6	4,36	5,04
K_2O	1,15	1,38	1,22	1,76	0,91	1,96	1,13	0,92	0,72	0,71	0,6	0,81	1,07	0,84	0,96	0,89	0,72	1,1	1,19	1,17
MnO	0,22	0,18	0,18	0,14	0,16	0,17	0,13	0,12	0,06	0,04	0,01	0,03	0,01	0,003	0,01	0,02	0,02	0,16	0,15	0,19
P_2O_5	0,14	0,09	0,19	0,27	0,11	0,29	0,32	0,22	0,14	0,13	0,02	0,18	0,01	0,15	0,08	0,06	0,28	0,06	0,47	0,31
L.O.I.	0,79	0,59	0,62	0,92	0,83	0,79	0,92	0,83	0,61	0,73	0,33	0,81	0,73	0,66	0,94	0,45	0,48	0,57	0,52	0,66
Total	99,99	99,97	99,99	99,78	98,99	99,14	99,42	99,18	98,41	99,83	98,98	99,86	99,98	99,99	99,14	99,85	99,88	99,88	99,89	98,45
Pb	15	42	62	34	32	24	38	40	22	25	10	20	22	18	20	8	13	56	16	14
Ni	69	40	35	24	44	32	24	18	14	8	13	21	11	28	18	16	5	39	35	40
Co	154	58	86	56	68	89	12	18	10	8	68	64	36	52	42	38	12	74	92	123
Cu	55	66	52	50	62	58	30	38	20	18	18	19	20	16	33	12	33	48	46	65
Sr	210	410	320	370	230	355	220	200	160	140	140	128	150	10	98	120	155	290	260	238

1-8 Mesosomes 9-17 Leucosomes 18-20 Melanosomes

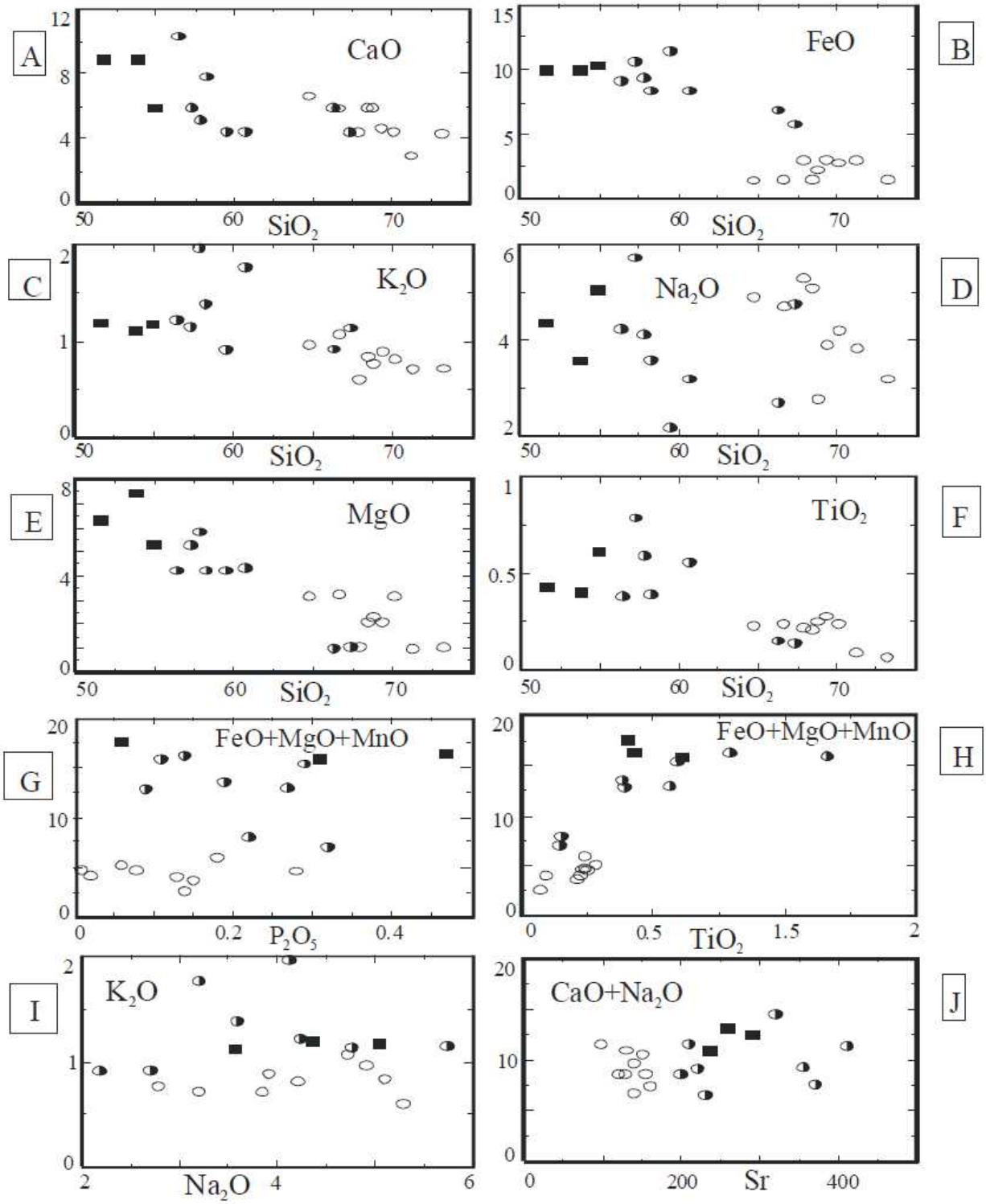

Fig. 2. A-F) - variation plots of CaO, FeO, K_2O, Na_2O, MgO, and TiO_2 vs. SiO_2, respectively, whereas G) and H) are P_2O_5 and TiO_2 vs. FeO+MgO+MnO, respectively, I) Na_2O vs. K_2O, J) $CaO+Na_2O$ vs. Sr.
Symbols as follows: ■ Melanosomes, ◑ Mesosomes, ○ Leucosomes.

migmatite rocks, twenty nine samples are analysed for major and some trace elements (Table 1). The analyses comprise nine amphibolites of foliated and banded types and twenty samples representing the melano- meso- and leucosomes of the migmatites.

The leucosomes possess higher SiO_2, rather similar Na_2O, slightly lower K_2O and CaO and clearly lower FeO, MgO and TiO_2 contents than the associated mesosomes and melanosomes (Figs. 2 a-f).

Plots of the $FeO+MgO+MnO/P_2O_5$ and TiO_2 (Figs. 2g, h) exhibit a good separation of leucosomes with lower femic oxides from the mesosomes and melanosomes. The leucosomes show a very limited variation in TiO_2 but a wider range for the P_2O_5 content.

Plotting of K_2O/Na_2O (Fig. 2i) shows slightly lower K_2O content of the leucosomes than the mesosomes, mainly due to the absence of biotite and the low amounts of K-feldspars in the former. The leucosomes and mesosomes exhibit a rather similar range of Na_2O suggesting either a similar proportion of plagioclase or a rather limited variation in plagioclase composition of the two bands.

The low Sr content of the leucosomes relative to the associated mesosomes and melanosomes on the $CaO+Na_2O$ versus Sr (Fig. 2j) support the idea that the leucosomes contain lower An content compared to the mesosomes and melanosomes.

Plotting Sr, Cu, Co, Ni and Pb against the femic oxides (FeO+MgO+MnO) (Figs. 3a-e) shows that the mesosomes have higher values due to higher

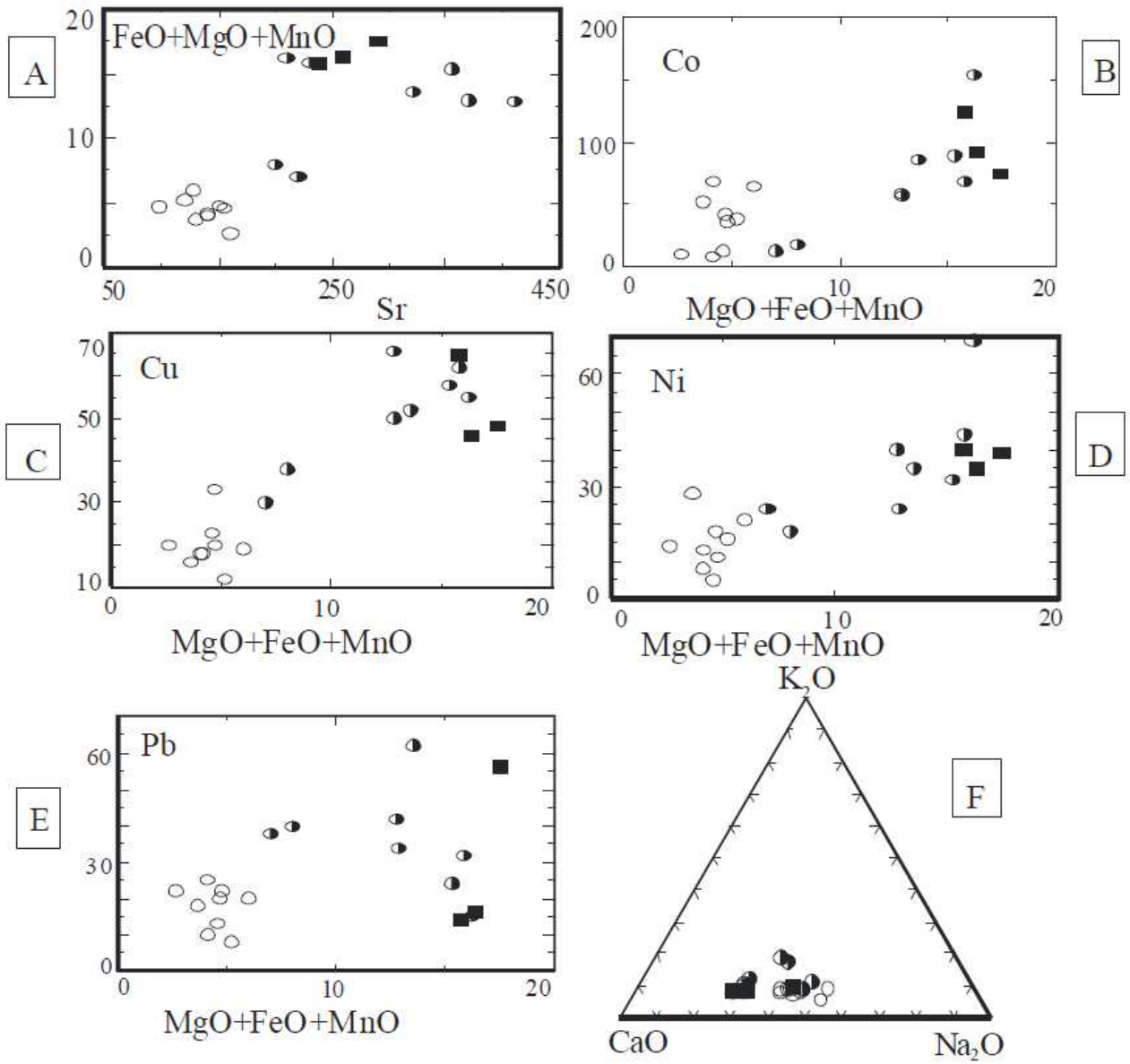

Fig. 3. A-E) Plots of Sr, Co, Cu, Ni and Pb vs. MgO+FeO+MnO, respectively, F) K_2O-CaO-Na_2O ternary diagram for the analysed migmatite. Symbols as in Fig. 2.

contents of mafics and higher concentrations of accessories and opaques.

On the K_2O-CaO-Na_2O ternary diagram (Fig. 3f), the plotted samples have slightly higher alkalies than the mesosomes and melanosomes.

From the previous variation diagrams, we can conclude that the mesosomes always occupy an intermediate position between the associated leucosomes and melanosomes. This feature suggests that the studied migmatites could be formed by metamorphic differentiation aided by partial melting [12, 17].

On the Niggli c-mg diagram [18] which is commonly used to distinguish between ortho- and para- amphibolites, some amphibolites plot along the Karoo dolerite trend (Fig. 4a) whereas some other amphibolites plot in the fields of limestone mixture and pelite-dolomite mixture. This suggests that the amphibolites comprise ortho-amphibolites and para-amphibolites. On the al-alk versus c

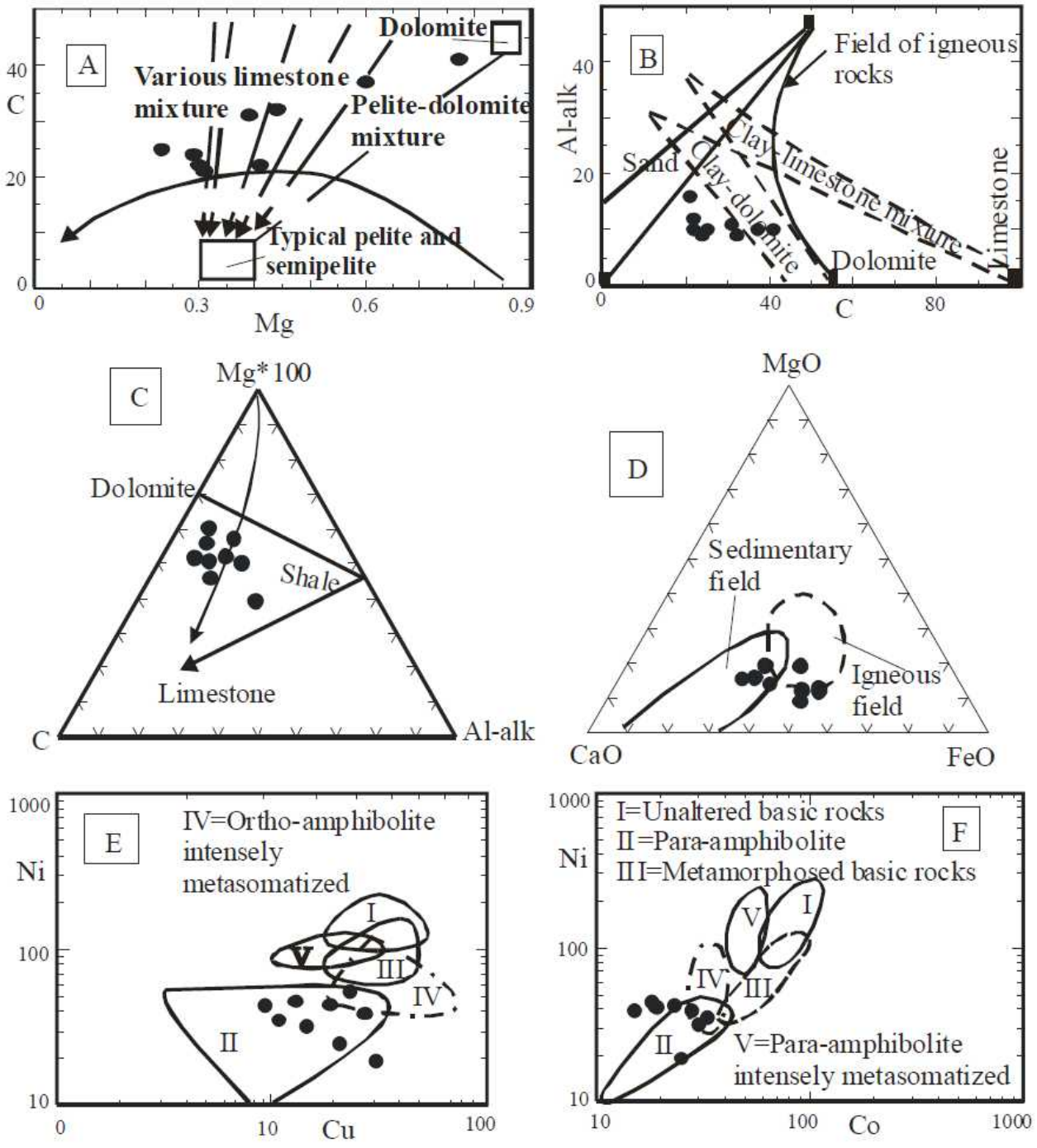

Fig. 4. Variation diagram for the studied amphibolites: A) Niggli c vs. Mg (Leake, 1964), B) Niggli c vs. Al-alk (Leake and Singh, 1989), C) Niggli c-Mg-(Al-alk) ternary diagram (Leake, 1964), D) CaO-Mg-FeO ternary diagram (Walker et al., 1960), E-F) plots of Ni vs. Cu and Ni vs. Co, respectively (Walker et al., 1960).

Table 2. Chemical composition of hornblende, biotite, plagioclase and muscovite.

Ser.No.	1	2	3	4	5	6	7	8	9	10	11	12
SiO_2	41,81	42,27	42,6	42,2	44,44	43,8	45,1	43,91	36,95	38,95	35,88	37,9
TiO_2	0,77	0,85	0,62	0,55	0,65	0,65	0,56	0,59	2,69	2,44	2,31	2,57
Al_2O_3	14,19	14,18	13,6	14,8	11,07	10,7	10,7	11,09	17,24	16,2	18,66	16,72
Cr_2O_3	0,06	0,04	0,03	-	-	-	-	-	-	-	0,04	0,02
Fe_2O_3	0,82	-	-	-	-	0,5	0,69	1,07	-	-	-	-
FeO	17,91	18,8	19,1	19,4	17,49	16,87	15,9	16,8	19,74	19,73	17,78	20,84
MnO	0,53	0,48	0,47	0,55	0,27	0,31	0,48	0,44	0,21	0,24	0,12	0,23
MgO	8,12	7,99	7,83	7,09	9,8	9,89	10,7	9,9	9,27	10,24	11,13	9,78
CaO	10,69	10,6	10,6	10,7	11,27	11,34	11,4	11,13	-	-	-	-
Na_2O	1,14	1,19	1,26	1,18	1,32	1,3	1,11	1,25	0,09	0,11	0,13	0,1
K_2O	0,76	0,75	0,7	0,8	0,69	0,8	0,67	0,75	9,71	8,71	10,4	9,21
H_2O	1,97	1,98	1,97	1,98	1,99	1,97	2,01	1,99	3,85	3,4	3,51	2,33
Total	98,75	99,06	98,8	99,3	99,08	98,16	99,4	98,96	99,75	100	99,92	99,08
Number of ions bases on 23 oxygen								calculation on the bases of 22 oxygen				
Si	6,35	6,41	6,49	6,4	6,69	6,66	6,72	6,63	5,61	5,91	5,44	5,75
Ti	0,08	0,09	0,07	0,06	0,07	0,07	0,06	0,06	0,31	0,28	0,27	0,3
Al	2,54	2,53	2,44	2,65	1,96	1,92	1,89	1,97	3,08	2,89	3,34	2,99
Cr	0,006	0,005	0	-	-	-	-	-	-	-	-	-
Fe^{3+}	0,09	-	-	-	-	0,06	0,07	0,12	-	-	-	-
Fe^{2+}	2,28	2,38	2,43	2,46	2,2	2,15	1,98	2,12	2,504	2,77	2,25	2,64
Mn	0,06	0,06	0,06	0,07	0,03	0,04	0,06	0,06	0,027	0,02	0,009	0,018
Mg	1,84	1,79	1,78	1,6	2,2	2,24	2,36	2,23	0,096	2,31	2,52	2,21
Ca	1,74	1,72	1,72	1,74	1,81	1,85	1,83	1,8	_	0,004	0,004	0,002
Na	0,33	0,35	0,37	0,34	0,38	0,38	0,32	0,37	0,026	0,04	0,04	0,03
K	0,15	0,15	0,13	0,15	0,13	0,16	0,13	0,14	1,82	1,63	1,95	1,73
Al^{iv}	1,649	`1.59	1,51	1,6	1,306	1,334	1,27	1,372				
Al^{vi}	0,892	0,941	0,93	1,06	0,66	0,585	0,62	0,601				

1-4 amphiboles from migmatites. 5-8 amphiboles from amphibolites. 9-12 biotites

Ser.No.	13	14	15	16	17	18	19	20	21	22	23	24	25
SiO_2	63,975	56,155	54,51	56,495	61,265	57,95	58,82	58,76	59,61	47,33	48,36	47,055	48,645
TiO_2	_	_	0,01	0,03	0,05	_	0,01	0,01	0,14	0,03	0,07	_	0,03
Al_2O_3	22,775	28,065	29,14	27,855	24,605	26,96	26,3	26,16	25,8	36,44	33,22	37,395	35,245
FeO	0,28	0,15	0,18	0,06	0,19	0,11	_	0,18	0,06	0,87	2,18	0,1	0,78
MnO	_	0,12	0,05	0,07	_	_	_	_	_	_	_	0,05	_
MgO	_	_	_	_	_	_	_	_	_	_	1,23	0,11	_
CaO	4,97	10,53	11,7	10,14	6,38	8,74	8,01	8,2	7,24	0,06	0,08	0,2	0,01
Na_2O	7,92	4,97	4,2	5,28	7,45	6,17	6,73	6,62	7	0,41	0,3	0,45	0,38
K_2O	0,08	0,01	0,09	0,07	_	0,06	0,09	0,06	0,01	10,83	10,33	10,64	11,71
H_2O	_	_	_	_	_	_	_	_	_	3,95	4,06	4	3,2
Total	100	100	99,88	100	99,94	99,99	99,96	100	99,86	99,92	99,83	100	100
Normalization on the basis of 5 cations and 16 oxygen								Calculation on 22 oxygen 14 cations					
Si	2,84	2,54	2,47	2,55	2,73	2,59	2,63	2,63	2,66	6,22	6,38	6,16	6,36
Ti	_	_	0,0005	0,0009	0,001	_	0,0003	0,0003	0,004	0,003	0,007	_	0,003
Al	1,24	1,53	1,59	1,51	1,32	1,45	1,4	1,41	1,37	5,66	5,24	5,79	5,44
Fe^{2+}	0,01	0,005	0,007	0,002	0,007	0,004	_	0,006	0,002	0,094	0,233	0,011	0,085
Mn	_	0,004	0,002	0,003	_	_	_	_	_	_	_	0,005	_
Mg	_	_	_	_	_	_	_	_	_	_	0,23	0,02	_
Ca	0,23	0,49	0,55	0,47	0,3	0,41	0,38	0,38	0,35	0,008	0,011	0,028	0,001
Na	0,67	0,43	0,36	0,45	0,64	0,53	0,58	0,56	0,6	0,103	0,074	0,112	0,096
K	0,004	0,0008	0,005	0,004	_	0,003	0,005	0,003	0,0007	1,79	1,68	1,74	1,94
An%	25,6	5,39	60,3	51,2	32,1	43,7	39,4	40,5	36,3				
Ab%	73,9	46	39,1	48,3	67,9	55,9	60	59,1	63,6				
Or%	0,5	0,1	0,6	0,4	_	0,4	0,5	0,4	0,1				

13-17 Plagioclase from migmatites 18-21 Plagioclase from amphibolites 22-25 Muscovit

diagram [19] all plots fall in the overlap area between igneous and sedimentary rocks (Fig. 4b). Leake [18] diagram of c-(al-alk)-100 mg shows that some amphibolites plot on or close to the igneous trend while others are scattered away but nearer to the dolomite rocks (Fig. 4c). Some amphibolites plot in or near the ortho-amphibolite field whereas others plot within the para-amphibolite field on the MgO-CaO-FeO(t) diagram of Walker et al. [20] (Fig. 4d) supporting the idea that some amphibolites are of igneous parentage while others are of sedimentary parentage.

Due to the high mobility of most major elements under the effect of metamorphism some less mobile elements as Ni, Co and Cu are used. Plotting of these amphibolites on the Ni- Cu and Ni- Co diagrams (Figs. 4e,f) show that most of the plots fall in the field of para-amphibolites, few fall in the overlap area with ortho-amphibolites [20].

Mineral chemistry:

The Microprobe analyses of the amphiboles, plagioclase, biotite and muscovite from migmatites and amphibolites are listed in Table 2.

1) Amphiboles:

Chemical composition of the analysed amphiboles from amphibolites and migmatites is given in Table 2. Generally, all amphiboles in the data set are calcic-amphiboles according to the terminology of Leake [21] with more than 1.3 atoms Ca per formula unit (pfu).

According to the nomenclature given by Leake [21] for the amphiboles (Fig. 5a), it is obvious that the analysed amphiboles from the amphibolites are magnesio-hornblende composition and close to the ferro-hornblende field, whereas the amphiboles from the migmatites are of ferro-tschermakitic hornblende composition.

Based on the chemical composition of the amphiboles from the mafic schist of Vermont, Laird and Albee [22] distinguished three metamorphic zones, namely biotite, garnet and staurolite-kyanite zones, which corresponding to greenschist, epidote-amphibolite and amphibolite facies, respectively.

Thus, the analysed amphiboles from the amphibolites and from the migmatites fall within and close to the garnet and staurolite-kyanite zones, respectively (Figs. 5b-d). This conclusion is seem reasonable, since the studied amphibolites and migmatites are associated with biotite-garnet-schist and biotite-garnet-gneiss in which the analysed garnet falls within the staurolite/kyanite zone [8].

The average Fe^{2+}/Mg is 0.93 in amphibole from amphibolites which is lower than those from migmatites (average=1.36). This value confirmed the increasing Fe^{2+}/Mg with prograde metamorphism [23]. Higher Ti contents generally indicate higher temperature [24]. A higher temperature for the migmatites as compared to that for the amphibolites is indicated by low Si and high Ti values (Fig. 5e).

On the Al-Ti diagram of Hynes [25], it is obvious that the Ti in amphibole is (0.06-0.07) and (0.06-0.09) from amphibolites and migmatites, respectively. Thus, they plot in the field of medium-pressure amphibole (Fig. 5f). On the $Na^{(M4)}$ - Al^{iv} diagram (Fig. 5g) [14], the plotted amphibole analyses from amphibolites and migmatites fall at extension of the higher pressure trend, which is characteristic of 6-7 kbar metamorphic pressure. On the $Na_2O+K_2O-TiO_2$ diagram (Fig. 5h) [26], the analysed samples fall within the amphibolite facies.

2) Plagioclase:

The chemical composition of the studied plagioclase from amphibolites and migmatites is listed in Table 2, where the analyses has been calculated on the basis of 8 oxygen atoms contained in the unit cell. The plotted electron microprobe data for the studied plagioclase on the Or-Ab-An diagram (Fig. 6a) [27] indicate that plagioclase of the amphibolites is of andesine composition (An_{36-44}), whereas plagioclase of the migmatites range from sodic oligoclase (An_{25-32}) in the leucosomes, to labradorite (An_{51-60}) in the melanosomes and mesosomes. From these results, it is clear that the An content is increased from amphibolites to migmatites (except plagioclase from the leucosomes), a conclusion confirmed with increasing temperature. The composition of the plagioclase could be used as indicators for the grade of metamorphism where greenschist facies contains albite, while amphibolite facies contain plagioclase range from albite to more calcic plagioclase with anorthite content more than 17 [28]. Accordingly, the studied rocks belong to the amphibolite facies.

3) Biotite:

On the Mg-Al+Ti-Fe+Mn ternary diagram (Fig. 6b) of Foster [29] the analysed biotites from the migmatite are ferrous iron-rich (i.e. fall close to Fe-biotite). In the $MgO-Al_2O_3$-FeO ternary diagram (Fig.

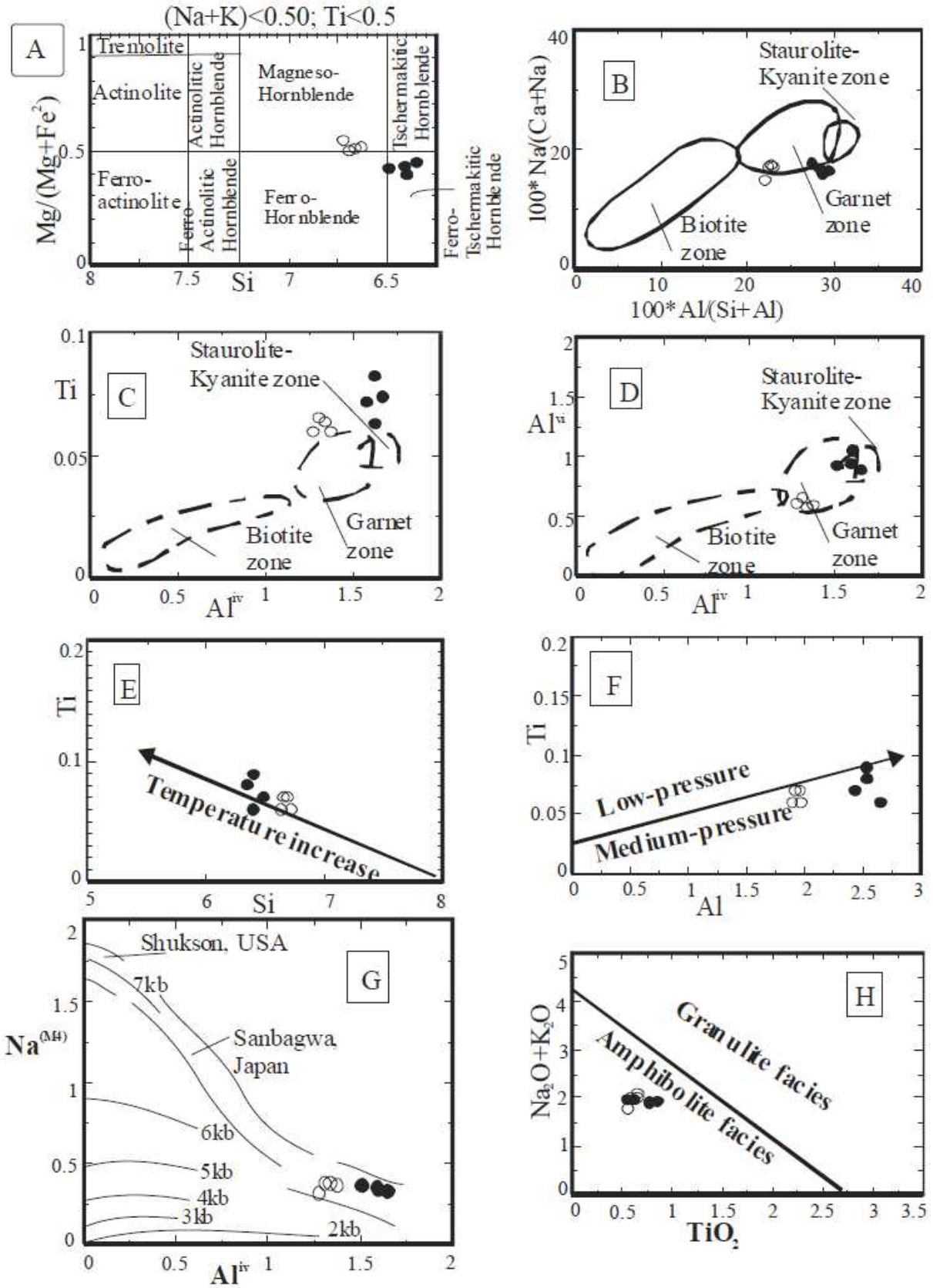

Fig. 5. A) Nomenclature of amphibole after Leake (1978), B, C and D) are Na/Ca+Na vs. Al/Si+Al, Ti vs. Al^{vi} and Al^{iv}, respectively (Laid and Albee, 1981), E) Ti vs. Si, F) Ti vs. Al (Hynes, 1982), G) Na vs. Al^{vi} (Brown, 1978) and H) Na_2O+K_2O vs. TiO_2 (Zakrutin and Grigorenko, 1968).
Symbols as follows: ○ Hornblende from amphibolites, ● Hornblende from migmatites.

6c), the two solid lines parallel to the base FeO-MgO was demarcated by Nockolds [30] for igneous rocks, while the dashed line was drawn by Gokhale [31] to separate between biotite of magmatic rocks from those of metamorphic-metasomatic rocks. Accordingly, the plotted biotite analyses from the migmatites fall mostly within the metamorphic-metasomatic field.

Studies have been done to the chemical behavior of biotite in relation to the grade of metamorphism [32]. Increasing Ti contents pfu with rising PT is one of the most reliable evidence for determing the mineral facies [33]. According to Zakrutkin and Grigorenko [26], the average Ti contents is 0.22 atoms pfu in the amphibolite facies and 0.48 atoms pfu in the granulite facies. Thus, the studied biotite from migmatites (contains Ti 0.27-0.31 atoms pfu; average 0.29) occupy intermediate position between amphibolite and granulite facies. This feature is again confirmed by using K content of biotite which in increased with increasing metamorphism. Zakrutkin and Grigorenko [26] stated that the average K content of biotite is 1.61 and 1.85 atoms pfu for amphibolite and granulite facies, respectively. Accordingly, the investigated biotite from migmatites has average 1.78 atoms pfu that is intermediate position between amphibolite and granulite facies.

4) Muscovite:

Muscovite frequently forms subhedral flakes and shreds that are replaced feldspars and sometimes biotite. Microprobe analyses (Table 2) revealed that muscovite has a limited range of composition. On the Al-(Fe+Mg+Mn)-Si, the analysed muscovite fall along muscovite-phengite join line [34] (Fig. 6d).

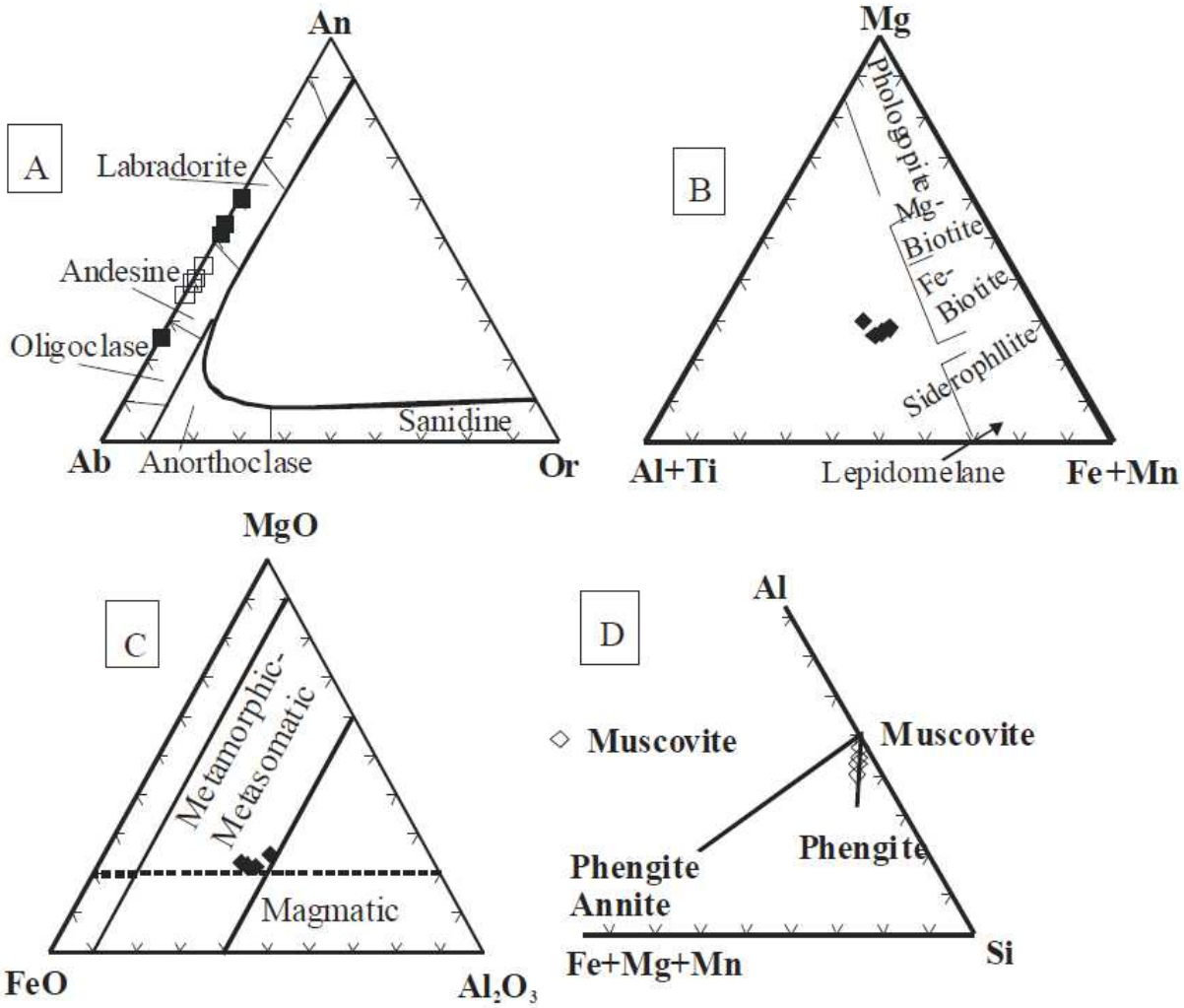

Fig. 6. A) Ternary Or-Ab-An diagram (King, 1989), B) Mg-Al+Ti-Fe+Mn ternary diagram (Foster, 1960), C) MgO-FeO-Al2O3 ternary diagram (Nockolds, 1947), D) (Fe+Mg+Mn)-Al-Si (Butler, 1977).
Symbols as follows: □ Plagioclase from amphibolites, ■ Plagioclase from migmatites, ♦ Biotite from migmatites, ◇ Muscovite from migmatites.

Amphibole-plagioclase thermometry:

According to the new thermometer proposed by Blundy and Holland [35] is used for a number of samples from amphibolites and migmatites to measure their crystallization temperature. The obtained results display that the temperature for amphibolites ranges from 720-740ºC, whereas for migmatites ranges from 800-820ºC.

The appearance of granular clinopyroxene in some amphibolite bands suggest that they reach the upper limit of the amphibolite facies and are most probably formed due to breakdown of hornblende in bands of favorable compositions [36].

The equation of geothermometer proposed by Blundy and Holland [35] which is:

$T=0.673P-48.98+Y/-0.0429-0.00841\ lnk$

and $K=Si-4/8-Si*X_{ab}^{Pl}$.

Where Si is the number of atoms per formula unit in amphiboles, with P in kbar and T in k, the term Y represents plagioclase non-ideality, RT ln Y_{ab} from Darken,s Quadratic formalism (DQF) with Y=0 for $X_{ab}>0.5$ and $Y=-8.06+25.5(1-X_{ab})^2$ for $X_{ab}<0.5$.

Mineral chemistry displayed that:

1) Amphibolites and migmatites were formed at 720-740ºC and 800-820ºC, respectively. Both were formed under medium pressure (6-7 kbar);

2) With respect to the grade of metamorphism of the studied amphibolites and migmatites, it is clear that they belong to the garnet and staurolite-kyanite zones, respectively;

3) The increased in An content of plagioclase (An_{36-44}) in amphibolites to plagioclase (An_{25-60}) in the migmatites support the increasing temperature.

DISCUSSION

The studied area is occupied by migmatites and amphibolites, associated with garnet-biotite schists and garnet-biotite gneisses in the inner part of the northern Hafafit dome. The migmatites are most probably derived from originally banded hornblende, hornblende-biotite and biotite gneisses and amphibolites subjected to upper amphibolite facies metamorphism.

The Hafafit migmatites exhibit well developed banded structure (stromatic); agmatic, ptygmatic, schlieren and nebulitic structures are also observed. These banded migmatites are considered as metatexites with low melt fraction (leucosome) that form during deformation and is controlled by the anisotropic fabric of the rocks as bedding plane foliation, forming alternating mesosome and leucosome bands surrounded by residual melanosome. This relation between the formation, squeezing out of melt and its segregation in dilatant sites was discussed by McLellan [37] and Sawyer [16, 38, 39].

The mesoscopic features of the deformation phases as well as the migmatization processes are summarized in:

1) formation of the banded migmatite with alternating leucosomes and mesosomes and some rootless intrafolial folds parallel to the S_1 foliation (D_1, M_1);

2) major thrust unit;

3) late syn-migmatization folds (D_2, M_2);

4) post-migmatization folding (D_3).

Microscopically, on a grain-scale, intracrystalline deformation stresses form dislocations in the crystals. Crystals with a large number of dislocations reflect bent crystals that exhibit undulose extinction. At a higher degree of deformation where sites of dislocations show cataclastic failure microkinks develop indicating dislocation glide. Intracrystalline deformation also results in deformation twin lamellae that commonly taper towards the core and are concentrated at high strain areas as crystal boundaries commonly described in the plagioclase crystals. After deformation stops, recovery as ordering mechanisms act towards an equilibrium. During the recovery process, dislocations that were distributed over the crystal, start to concentrate in planar zones forming deformation bands and then subgrain boundaries very well observed in quartz, similar to that described by Trepied et. al., [40]; White and Mawer [41]. Another process acting to restore order in crystals is dynamic recrystallization forming aggregates of new small grains of uniform size surrounding large grains suggesting partial recrystallization. To reduce the internal free energy after deformation stops and mostly at high temperatures, crystals tend to decrease the total surface area of grain boundaries by a grain boundary area reduction mechanism (GBAR) [42, 43]. This static recrystallization produces large polygonal grains with straight boundaries as strain-free crystals.

Amphibolites commonly occur as continuous belts and/ or bands with the migmatites. Locally they are migmatized with the production of leucosomes. The melt produced is transferred either along the foliation planes or along fault planes and fractures.

Geochemistry of the stromatic migmatites reflects that the mesosomes ocuppy intermediate position between the leucosomes and melanosomes suggesting formation by metamorphic differentiation. The amphibolites show impure marl protolith with some tendency towards basaltic composition (i.e. mixture of para- and ortho-amphibolites.

Mineral chemistry of hornblende, plagioclase, biotite and muscovite suggest that:

1) these rocks are metamorphosed under upper amphibolite facies, pressure ranges from 6-7 Kbar (i.e. medium pressure) by using variation plots of hornblende;

2) the An contents of plagioclase from migmatite mesosomes are higher than those from the amphibolites, suggesting a higher temperature for the migmatites;

3) plagioclase of the amphibolites are of andesine composition (An_{36-44}), where as migmatites have (An_{25-32}) in the leucosomes and (An_{51-60}) for plagioclases in the mesosomes and melanosomes. This support increased temperature and partial melting from amphibolites to migmatites;

4) biotite is commonly of metamorphic-metasomatic origin and muscovite has a muscovite-phengite composition thus of secondary origin.

In discussing the origin of these banded migmatites, the regular geometry of the leucosomes, the separation of melanosomes at their contacts, the original metamorphic textures of the mesosome and the coarse grain size of the associated leucosome bands and the intermediate chemical composition of the mesosomes between the leucosomes and melanosomes, suggest that the stromatic migmatite is probably formed by metamorphic differentiation and segregation in a locally closed system as discussed by Yardley [44]; McLellan [37]; Johannes [45]; Ashworth and McLellan [46].

Yet a main role was played by partial melting and the formation of melt which is evidenced on microscopic and mesoscopic scales.

Microscopically, recrystallization of quartz and sometimes plagioclase forming new small crystal aggregates, embayed and corroded crystals and filling of fractures in crystals by quartz melt indicate the presence of melt that starts at grain boundaries and crystal junctions, then form melt pools as described by Busch et al. [47]; and Sawyer [39]. Melt is then drained from the layers where they are formed along layering or foliation planes forming leucosome bands, they are then deformed with the mesosomes into folds with crests thicker than limbs, followed by formation of leucosome veins and migration through a network of channels to leave the source layers. Thus a process of partial melting acting on originally banded gneisses as that discussed by Johannes and Gupta [17], Johannes [48] and Sawyer [16, 38, 39, 49] interacts in the formation of the present migmatites.

CONCLUSIONS

Finally, we can conclude from the field observations, mesoscopic structures, microscopic examinations and geochemical characters as well as mineral chemistry that the study migmatites and amphibolites association were formed by metamorphic differentiation aided by partial melting of original gneisses mostly of sedimentary protoliths, at temperature ranging from 800-820ºC to 700-740ºC respectively.

TRANSPARENCY DECLARATION

The authors declare no conflicts of interest.

REFERENCES

1. El-Ramly MF. A new geological map for the basement rocks in the Eastern and Southwestern Deserts of Egypt. Annals Geol Surv Egypt 1972; 2: 1-18.
2. Shackelton RM, Ries AC, Graham RH, Fitches WR. Late Precambrian Ophiolitic melange in the eastern desert of Egypt. Nature 1980; 285: 472-474.
3. El-Ramly MF, Greiling R, Kroner A, Rashwan AA. On the tectonic evolution of the Wadi Hafafit area environs, Eastern Desert of Egypt. Bull Fac Earth Sci King Abdulaziz Univ. 1984; 6: 113-126.
4. El-Gaby S, List FK, Tehrani R. Geology, evolution and metallogenesis of the Pan-African Belt in Egypt. In: El-Gaby S, Greiling RO. (eds.), The Pan-African Belt of NE Africa and adjacent areas. Earth Evol Sci. Viewing and Sohn, Braunschweig, Wiesbaden 1987: 17-68.
5. El-Gaby S. Tectonic evolution of the Basement Complex in the Central Eastern Desert of Egypt. Geol Rundschau 1984; 73(3): 1019-1036.
6. Abdel Wahed M. 1985. Structural and petrological studies on the Migif-Hafafit gneisses, Eastern Desert, Egypt. Ph.D. Thesis, Cairo University, Egypt: pp. 298.
7. Abdel Wahed M, Abdel Khalek ML, Hafez AMA. Structural evolution of the gneisses and ophiolitic melange rocks in the northern Migif-Hafafit area, Southeastern Desert, Egypt. Annals Geol Surv Egypt

1984; 14: 279-307.
8. Rashwan AA. 1988. Petrography, geochemistry and petrogenesis of the Migif-Hafafit gneisses at Hafafit Mine area, South Eastern Desert, Egypt. Ph.D. Thesis, Ain Shamis Univ., Cairo: pp. 355.
9. El-Ramly MF, Greiling R, Rashwan AA, Rasmy AH. Explanantory note to accompany the geological and structural maps of Wadi Hafafit area environs, Eastern Desert of Egypt. Geol Surv Egypt 1993; 68: 1-53.
10. Greiling RO, Abdeen MM, Dardir AA, El Akhal H, El Ramly MF, Kamal El Din GM, et al. A structural synthesis of the Proterozoic Arabian-Nubian Shield in Egypt. Geol Rundschau 1994; 83: 484-501.
11. Fowler AA, El Kalioubi B. The Migif-Hafaait gneissic complex of the Egyptian Eastern Desert: fold interference patterns involving multiply deformed sheath folds. Tectonophysics 2002; 346: 247-275.
12. Mehnert KR. 1968. Migmatites and the origin of granitic rocks. Elsevier, Amsterdam: pp. 344.
13. Brown M. The definition of metatexites, diatexites and migmatite. Proc Geol Ass 1973; 84: 371-382.
14. Brown EH. The crossite content of Ca-amphibole as a guide to pressure of Metamorphism. J Petrol 1977; 18: 53-72.
15. Brown M. Petrogenesis of the St.Malo migmatite belt, Armorican Massif, France, with particular reference to the diatexites. Neues Jb Miner Abh 1979; 135: 48-74.
16. Sawyer EW. Disequilibrium melting and the rate of melt residium separation during migmatisation of mafic rocks from the Grenville Front, Quebec. J Petrol 1991; 32: 701-738.
17. Johannes W, Gupta LN. Origin and evolution of a migmatite. Contrib Miner Petrol 1982; 79: 114-123.
18. Leake BE. The chemical distinction between ortho- and para- amphibolites. J Petrol 1964; 5: 238-253.
19. Leake BE, Singh D. The Delaney Dome formation, Connemara, W. Ireland and the geochemical distribution of ortho- and para-quartzofeldspathic rocks. Mineral Mag 1986; 50: 205-215.
20. Walker KR, Joplin GA, Lovering JF, Green R. Metamorphic and metasomatic convergence of basic igneous rocks and lime-magnesia sediments of the Pre-Cambrian of northwestern Qeenland. J Geol Soc Australia 1960; 6: 147-178.
21. Leake BE. Nomenclature of amphiboles. Am Mineral 1978; 63: 1023-1052.
22. Laird J, Albee AL. Pressure, temperature and time indicators in mafic Schist: their application to reconstructing the polymetamorphic history of Vermont. Am J Sci 1981; 281: 127-175.
23. Liou JG, Kuniyoshi S, Ito K. Experimental studies of the phase relations between greenschist and amphibolite in a basaltic system. Am J Sci 1974; 274: 613-632.
24. Rasse P. Al and Ti contents of hornblende, indicators of pressure and temperature of regional metamorphism. Contr Miner Petrol 1974; 45: 321-336.
25. Hynes A. A comparison of amphiboles from medium and low pressure metabasits. Contrib Mineral Petrol 1982; 81: 119-125.
26. Zakrutkin VV, Grigorenko MV. Titanium and alkalies in biotite in metamorphic facies. Dokl Akad Nauk SSSR 1968; 3: 683-686.
27. Deer WA, Howie RA, Zussman J. An introduction to the rock forming Minerals. Longman and Green, London 1966: pp. 528.
28. Winkler HGF. Petrogenesis of metamorphic rocks. 5th ed. New York, Heidelberg, Berlin. Springer Verlag. 1979: pp. 342.
29. Foster MD. Layer charge relation in the dioctahedral and trioctahedral Micas. Am Mineral 1960; 45: 383-398.
30. Nockolds SR. The relation between chemical composition and paragenesis in the biotite micas of igneous rocks. Am J Sci 1947; 245: 401-420.
31. Gokhale NW. Chemical composition of biotites as a guide to ascertain the Origin of granites. Bull Geol Soc Finl 1968; 40: 107-111.
32. Dietvorst EJL. Pelitic gneisses from Kenio, southwest Finland: a study of retrograde zoning in garnet and spinel. Ph.D. Thesis, Free Univ. Amsterdam 1981: pp. 233.
33. Lebeder VI. Vopr. Magmatizma: metamorfizma (Igneous activity and metamorphism). Leningrade 1964; 2: pp. 440.
34. Butler BCM. Chemical study of minerals from Moine schist of the Ardnamurchan area, Argyllshire, Scotland. J Petrol 1967; 8: 233-267.
35. Blundy JD, Holland TJB. Calcic amphibole equilibria and a new Amphibole-plagioclase geothermometer. Contrib Mineral Petrol 1990; 104: 208-224.
36. Spear F. An experimental study of hornblende stability and compositional variability in amphibolite. Am J Sci 1981; 281: 697-734.
37. McLellan EL. Migmatite structures in the Central Gneiss Complex, Boca de Quadra, Alaska. J Metam Geol 1988; 6: 517-542.
38. Sawyer EW. Melt segregation in the continental crust. Geol 1994; 22: 1019-1022.
39. Sawyer EW. Criteria for the recognition of partial melting. Phys Chem Earth 1999; 24: 269-279.
40. Trepied L, Doukhan JC, Paquet J. Subgrain boundaries in quartz: theoretical analysis and microscopic observations. Phys Chem Miner 1980; 5: 201-218.
41. White JC, Mawer CK. Dynamic recrystallization and associated Exsolution in perthites: evidence of deep crystal thrusting. J Geophys Res 1988; 93: 325-337.
42. Vernon RH. 1976. Metamorphic processes. pp. 350. Allen Unwin, London.

43. Bons PD, Urai JL. Syndeformational grain growth: microstructures and kinetics. J Struct Geol 1992; 14: 1101-1109.
44. Yardley BWD. Genesis of the Skagit Gneiss migmatites, Washington, and the distinction between possible mechanisms of migmatization. Geol Soc Am Bull 1978; 89: 941-951.
45. Johannes W. 1983. On the origin of stromatic (layered) migmatites. In: Migmatites Melting and Metamorphism. Atherton MP, Gribble CD (Edts.). Shiva, Nantwich: 234-248.
46. Ashworth JR, McLellan EL. 1985. Textures. In: Migmatites. Ashworth JR. (Ed.). Blackie and Son Ltd. 180-203.
47. Busch W, Schneider G, Mehnert KR. Initial melting at grain boundaries. Part II: Melting in rocks of granodioritic, quartzdioritic and tonalitic composition. Neues Jb Miner Mh 1974; 345-370.
48. Johannes W. What controls partial melting in migmatites? J Metam Geol 1988; 6: 451-465.
49. Sawyer EW. Melt segregation in the continental crust: distribution and movement of melt in anatectic rocks. J Metam Geol 2001; 19: 291-309.

Journal of Biology and Earth Sciences

EARTH SCIENCES ORIGINAL ARTICLE

Investigations of garnets from polymetamorphic rocks of the Lapland Granulite Belt of the Kandalaksha Region

Miłosz A. Huber[1], Wiesław Heflik[2], Agnieszka Pattek-Janczyk[3], Mateusz Pitak[3], Katarzyna Stadnicka[3], Siergiey G. Skublov[4]

[1]Maria Curie-Skłodowska University, Department of Geology and Protection of Litosphere, Lublin, Poland
[2]University of Science and Technology, Department of Mineralogy, Petrography and Geochemistry, Kraków, Poland
[3]Jagiellonian University, Faculty of Chemistry, Kraków, Poland
[4]Russian Academy of Sciences, Institute of Precambrian Geology and Geochronology, Sankt Petersburg, Russia

ABSTRACT

Introduction: The Lapland Granulite Belt is placed on the Kandalaksha region (Kola Peninsula, Russia). The rocks of this Belt are composed mainly of amphibolites and granulites.

Materials and methods: The research were focused on the garnets from the amphibolite and granulite rocks of Lapland Granulite Belt. The petrological methods like polarizing microscopy (PM), SEM-EDS, XRD for powdered samples and single crystal diffraction were used together with IR and Mössbauer spectroscopy and REE analysis by ion–microprobe.

Results: It was found that the garnets from studied amphibolite and granulite rocks could be classified to pyralspite group without hydrogarnets components, so they were formed in high metamorphic facies.

Conclusions: The joint geological observations and results of the performed experiments suggest that the garnets were subject of a blastesy, i.e. there were formed in long lasting metamorphic processes of low dynamics, except of those garnets from tectonic zones, found in the vicinity of mineral veins.

Key words: Lapland Granulite Belt; Kandalaksha; amphibolites; granulites; garnets; IR spectroscopy; Mössbauer spectroscopy; XRD; EDS-SEM; REE analysis; crystal structure.

J Biol Earth Sci 2012; 2(1): E34-E44

Corresponding author:
Miłosz A. Huber
Maria Curie-Skłodowska University
Department of Geology and Protection of Litosphere,
Institute of Earth Science
Al. Kraśnicka 2cd, 10-718 Lublin, Poland
e-mail: miloh@interia.pl

Original Submission: 20 December 2011; Revised Submission: 06 April 2012; Accepted: 25 April 2012

ISSN: 2084-3577
http://www.journals.tmkarpinski.com/index.php/jbes or http://jbes.strefa.pl
e-mail: jbes@interia.eu

INTRODUCTION

Near 10 km on East from Kandalaksha at White Sea (Kola Peninsula, Russia) there are exposures of metamorphic basic rocks of the Lapland Granulite Belt (Fig. 1) [1, 2]. The rocks are composed mainly of amphibolites and granulites, rich with pyroxenes, garnets, amphiboles, quartz and plagioclases [3, 4]. Fig. 2 shows the representative exposures of Kandalaksha region, and amphibolite and granulite rocks, from which the garnet samples were collected [5]. The samples were collected during the science expeditions to Kola Peninsula (1999-2004). The localisation of the samples is given in Fig. 3.

The petrographic analyses were performed by means of scanning microscope technique coupled with an EDS and combined with IR and Mössbauer spectroscopies. Additionally, X-ray diffraction was used as the complementary technique to determine mineral phases in the samples as well as 3-D structure of the selected single garnet crystals.

The aim of the garnet analysis was to determine their chemical composition and crystal structure, which could indicate the dynamics of metamorphic processes. The precise analysis of garnet components should illustrate the blastesy conditions of these minerals formations.

MATERIALS AND METHODS

Microscopic observation for thin sections of studied rocks were performed with Carl Zeis Jena PolMi–A polarizating microscope in transmitted and reflected light. X-ray diffraction (XRD) patterns for powdered samples were obtained using Philips X'PERT diffractometer with graphite monochromated CuK(alpha) radiation; scanning speed 0.02 (2theta)/1s, recorded range 5-75° of theta angle. Infrared spectra were recorded on BIO-RAD FTS 165 spectrometer. XRD and IR measurements were carried out at Faculty of Geology, Geophisics and Environmental Protection UST, Kraków.

SEM–EDS microanalyses were made using electron scanning microscope HITACHI-S-4700 equipped with EDS detector at the Geological Institute of Jagiellonian University, Kraków.

Mössbauer spectra of the samples were recorded at room temperature using a conventional spectrometer with a ^{57}Co(Rh) source (Institute of

Fig. 1. Photograph of the Kandalakshskye Tundry Mountains.

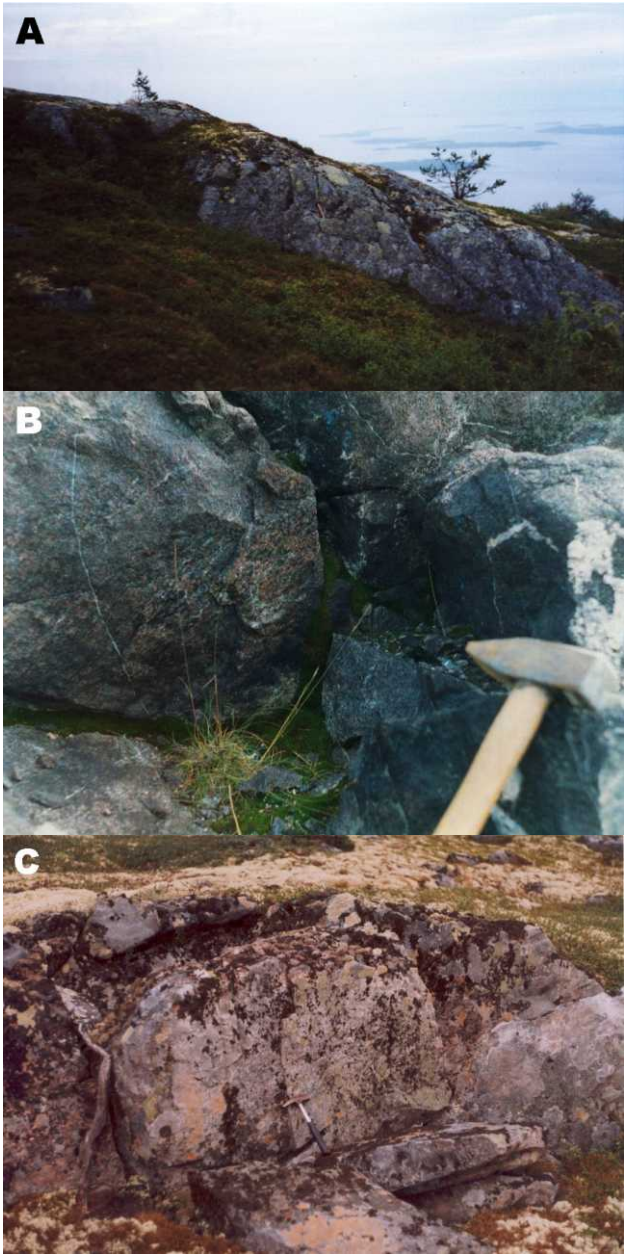

Fig. 2. Kandalakshskye Tundry Moutains:
A - amphibolite rocks exposure in the Volosianaya Mt.
B - amphibolite rocks exposure in the Zhielieznaya Mt.
C - granulite rocks exposure in Siennaya Kurtiazhnaya Mt.

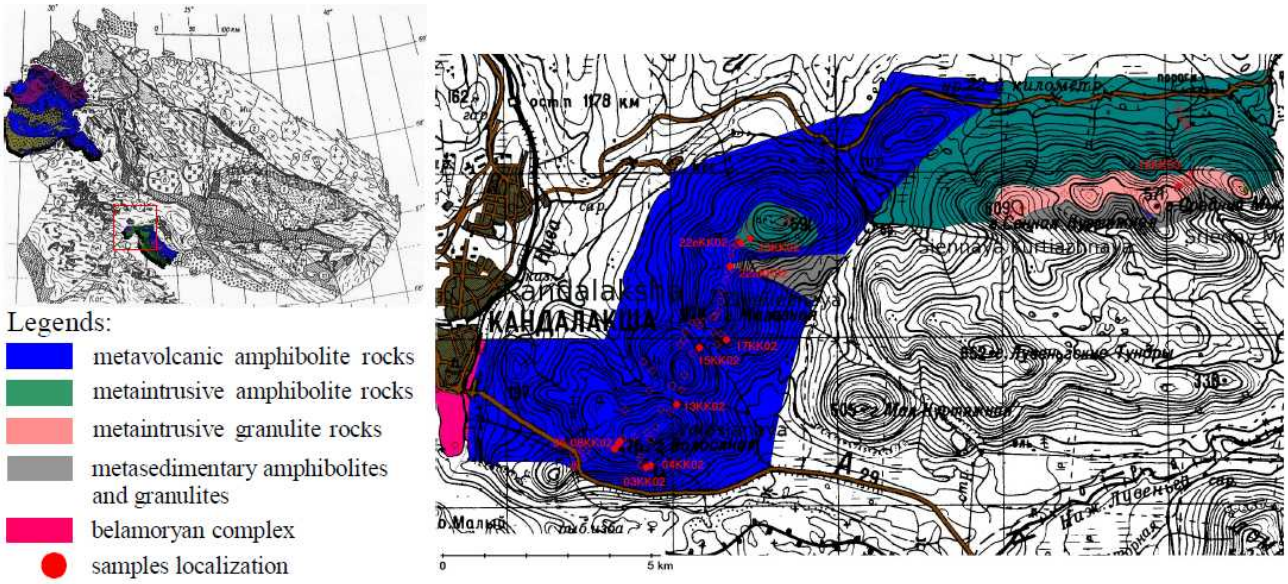

Fig. 3. Situation sketch of Kandalaksha region (maked by authors).

Physics, Jagiellonian University, Kraków). The samples were powdered, mixed with Al_2O_3 and pressed into pellets with the thickness of about 10 mg Fe/cm^2. The Mössbauer spectra were numerically analysed by means of a linear least squares procedure assuming Lorentzian shape of the absoption lines. The isomer shift values are quoted with respect to α - Fe at room temperature.

The REE and rare element contents of minerals were analyzed at Cameca IMS-4f ion microprobe installed at the Institute of Microelectronics and Informatics (IMI) RAS, Yaroslavl (by S.G. Simakin and E.V. Potapov). Single crystal diffraction measurements were carried out using Nonius KappaCCD Difractometer and monochromated MoK(alpha) radiation at Joint X-ray Diffraction Laboratory, Faculty of Chemistry and Regional Labolatory, Jagiellonian University, Kraków.

RESULTS AND DISCUSSION

MICROSCOPIC OBSERVATIONS

Amphibolite rocks (samples 01KK00 -17KK02 and 22dKK02, 23KK02 in Table 1) have grano-, nematoblastic massive structure with disordered texture. They are constructed usually by common hornblende (older rich with Ti and younger rich with Mg), garnets, plagioclases (labradore-bytownite), quartz, rarely biotite, with an accessory accompanion of rutile, titanite, ilmenite and pyrite (Fig. 4, 5). Garnets account for 25-30% volume of rocks. The amphibolite rocks are mixedv old (2,4-2,8 Ga) metavolcanic extrusive-lavas (samples 03KK03-15KK02, Fig. 6A), metasedimentary complexes (sample 23KK02) and metamorphosed intrusive gabbroid complexes (sample 17KK02, Fig. 6B).

Granulite rocks (samples 22aKK02, 22eKK02, 14KK03-45KK03 in Table 1, Fig. 7) have a granoblastic massive structure with disordered, rarely oriented, texture rich with garnets, piroxenes (diopside and hyperstene), quartz, plagioclases (andezine-labradore), with an accessory accompanion of rutile, chromite, amphibole (rich with common hornblende in diaphtoretic zone), and also ilmenite, ülvite, magnetite and pyrite (Fig. 8). Garnets in these rocks account for 30-45% volume of rocks. The granulite rocks are metagabro (sample 22aKK02, 22eKK02, 14KK03-18KK03) and metasedimentary complexes (sample 30KK03, 45KK03).

The observed presence of minerals such as plagioclases rich with albite units (>70%Ab), epidote and carbonates (saussuritization processes), as well as the presence of prehnite prove the advanced retrogressive processes.

SEM-EDS ANALYSIS

Garnet samples from the studied area investigated using scanning electron microscopy equipped with EDS detector show relative similarity of composition for whole population (Table 2). The highest amount of Mg^{2+} (in X position), which is typical for granulite conditions [6], was found in the

Table 1. List of samples with indication of performed analyses.

No. of samples	Name of rocks	performed analysis						
		PM	EDS	XRD	IR	M	SCXD	REE
01KK00	garnet amphibolite	+	+	+	-	-	-	+
03KK02	garnet amphibolite	+	+	+	-	+	+	-
04KK02	amphibolite	+	-	+	+	-	-	-
05KK02	garnet amphibolite	+	-	+	+	+	-	-
06KK02	garnet amphibolite	+	+	+	+	-	-	-
08KK02	garnet amphibolite	+	-	+	+	-	-	-
13KK02	garnet amphibolite	+	-	+	+	-	+	-
15KK02	garnet amphibolite	+	-	+	+	-	-	+
17KK02	garnet plagioclase rocks (metagabbro)	+	-	+	-	+	-	-
22aKK02	garnet - pyroxene rocks	+	+	+	+	+	+	-
22dKK02	garnet amphibolite	+	+	+	-	-	-	+
22eKK02	garnet - pyroxene - plagioclase rocks	+	+	+	+	+	+	+
23KK02	garnet amphibolite schists	+	+	+	-	-	+	-
14KK03	garnet - two pyroxene - granulite	+	+	+	-	-	-	-
17KK03	garnet - two pyroxene - granulite	+	+	+	-	-	+	-
18KK03	garnet - two pyroxene - granulite	+	+	+	+	-	+	-
30KK03	garnet – quartz - pyroxene - schist	+	+	+	+	-	+	-
45KK03	garnet - two pyroxene - granulite	+	-	+	-	-	+	-

Table 2. Electron microprobe analysis of selected garnet samples (EDS). Elements contents are given in wt.%.

No. of samples	Si	Al	Fe	Ti	Ca	Mg	Mn	O	Proposed composition $(X_3)(Y_2)(Z_3)O_{12}$
03KK02	16,56	9,94	17,79	0,40	7,21	1,46	0,32	45,84	(Ca0.91Fe1.27Mg0.31Mn0.03)(Al1.87Fe0.13)(Si3.00)O12
06KK02	18,00	9,84	18,00	0,04	8,01	2,65	0,95	41,80	(Ca0.92Fe1.15Mg0.50Mn0.03)(Al1.67Fe0.33)(Si2.94)O12
22aKK02	17,70	10,70	16,40	0,00	6,14	5,63	0,44	43,00	(Ca0.73Fe1.13Mg1.10Mn0.04)(Al1.89Fe0.11)(Si3.00)O12
22eKK02	18,30	9,20	15,90	0,30	9,14	3,52	0,26	42,30	(Ca1.03Fe0.84Mg0.66)(Al1.55Fe0.45)(Si2.96Ti0.03)O12
23KK02	14,30	8,58	27,80	0,19	5,37	3,00	0,64	40,30	(Ca0.78Fe1.41Mg0.72Mn0.06)(Al1.87Fe0.13)(Si3.00)O12
14KK03	16,48	9,90	17,92	4,15	4,45	3,98	0,53	42,60	(Ca0.57Fe1.51Mg1.07)(Al1.88Fe0.12)(Si3.00)O12
17KK03	18,79	11,34	15,57	0,00	6,23	5,80	0,00	42,26	(Ca0.70Fe1.13Mg1.03Mn0.03)(Al1.88Fe0.12)(Si3.00)O12
18KK03	18,79	10,88	16,10	0,00	6,07	6,06	0,00	42,11	(Ca0.69Fe1.15Mg1.13)(Al1.84Fe0.16)(Si3.00)O12
30KK03	17,95	10,58	18,39	0,00	8,94	3,27	0,00	40,86	(Ca1 05Fe1.39Mg0.63)(Al1.84Fe0.16)(Si3.00)O12

The observed excess of Fe and Ti observed for the samples 22aKK02, 23KK02 and 14KK03, respectively, is due to the presence of inclusions such as ilmenite and rutile.

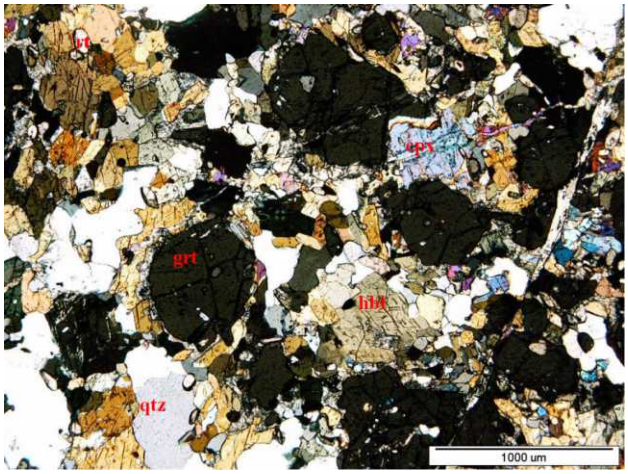

Fig. 4. Microphotographs of metavolcanic amphibolite rocks in crossed-pollars thin-sections.
Legends: hbl – common hornblende, grt – garnets, qtz – quartz, pl – plagioclases, rt – rutile, tit – titanite, cpx – clinopyroxene, opx – orthopyroxene.

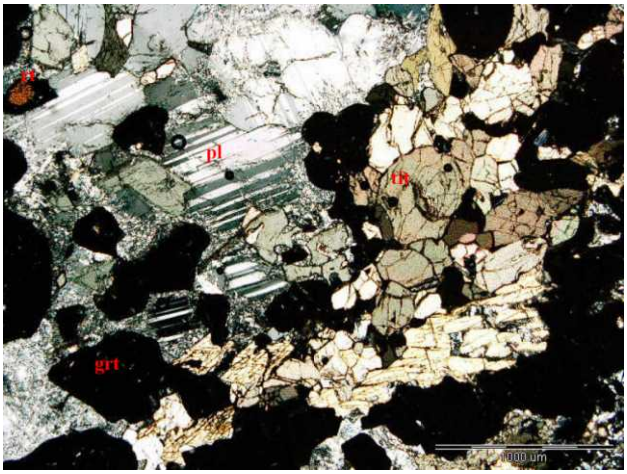

Fig. 5. Microphotographs of metaintrusive amphibolite rocks in crossed-pollars thin-sections. Legends is the same like in the Fig. 4.

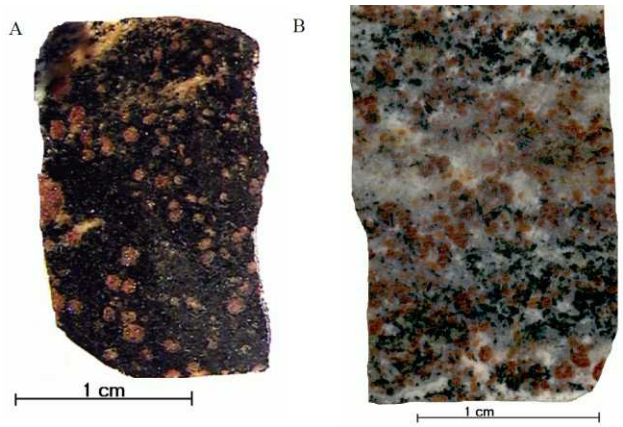

Fig. 6. Macrophotographs of metavolcanic amphibolites (A) and metasedymantary amphibolites (B).

samples 22aKK02 and 14KK03–17KK03, whereas Ca^{2+} contents was higher for samples 01KK00, 03KK02–23KK02 (except of 22aKK02) and 2dKK02, 30KK03 of amphibolite conditions (see Table 1). The garnets seem to originate from pyralspite group, with the domination of almandine, and from following transformation towards the ugrandite group with andradite and grossular as main components.

XRD POWDER PATTERN ANALYSIS AND SINGLE CRYSTAL DIFFRACTION

X-ray diffraction patterns for powdered samples of the garnets separated from amphibolites (08KK02, 15KK02, Table 3) and those from granulites (17KK03, 30KK03, Table 3) showed mainly the positions of spessartine (PDF2: 2-992, 10-354) lines with addition of almandine (PDF2: 02-1008). However the results of SEM-EDS analysis did not confirm such a high contents of manganese characteristic for the spessartine ($Mn_3Al_2Si_3O_{12}$). Similar line positions could be obtained for solid solution of almandine ($Fe_3Al_2Si_3O_{12}$) and andradite ($Ca_3Fe_2Si_3O_{12}$, PDF2:10-288) with the pyrope (PDF2: 02-1008) and grossular (PDF2: 33-260) additions. The diffraction patterns of the garnets from granulite samples (17KK03, 30KK03) are not in contradicton to the presence of pyrope phase indicated by SEM-EDS (Table 2). The garnets from granulite rocks (with high amount of pirope) are characteristic for the blastesy of of higher metamorphic conditions [7, 8]. The presence of grossular units among the garnets of both, amphibolite and granulite rocks, could have its origin in the advanced secondary processes in the rocks. The garnets have also small additives of

Fig. 7. Macrophotographs of metaintrusive granulites.

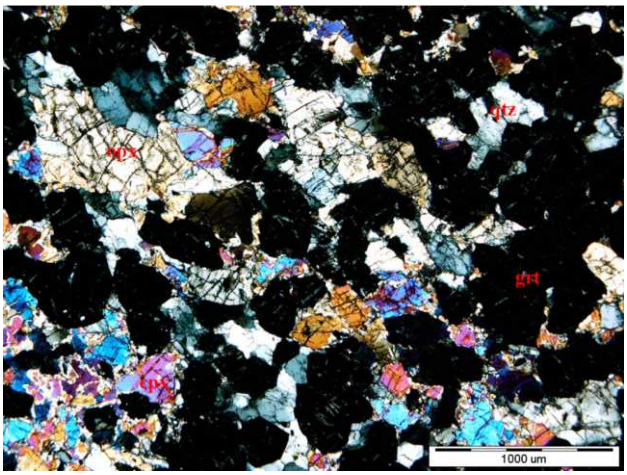

Fig. 8. Microphotographs of metaintrusive granulites in crossed-pollars thin-section. Legends is the same just like in the Fig. 4.

other mineral inclusions like common diopside, hornblende and quartz (Table 3). All studied garnet crystals, of typical composition X3Y2Z3O12, were cubic, space group No. 230, I a-3d (Z=8): X (24 c 222; 1/8, 0 1/4), Y(16 a -3; 0, 0, 0), Z(24 d -4; 3/8, 0, 1/4) with oxygen atoms in the general position. The shape of coordination polyhedra for X (dodecahedron), Y (octahedron) and Z (tetrahedron) are shown in Table 6.

IR PATTERN ANALYSIS

IR absorption bands for selected garnet powdered samples are given in Table 4 together with the standard spectra published earlier [9-13] and marked vibration types. B, C and D correspond to the ν3–type vibrations of the SiO_4 group (asymmetrical stretching vibrations of the $\tilde{Si}$-O bond). F and G bands correspond to ν2 + ν4

Table 3. XRD garnets analysis (2Θ for CuKα).

08KK02			15KK02			30KK03			17KK03			d	hkl	phase
2 Θ	d	I	2 Θ	d	I	2 Θ	d	I	2 Θ	d	I			
15,91	5,570	3				15.81	5.604	3				?	?	?
			20,81	4,269	3							4,257	100	Q 33-1161
									23,71	3,752	6	?	?	?
						25.58	3.482	3				?	?	?
						26.62	3.348	4	26,53	3,360	4	3,342	101	Q 33-1161
						27.95	3.192	6	27,92	3,195	13	2,991	-221	Di 11-654
									29,87	2,991	5	?	?	?
									30,35	2,975	7	?	?	?
30,71	2,911	3	30,71	2,911	36	30.74	2.909	81	30,82	2,901	35	2,893 2,91	400	Alm 33-568 Sp 10-354
									31,56	2,834	3	?	?	?
32,33	3,813	29										?	?	?
			33,04	2,711	3							2,720	151	Hbl 21-149
34,42	2,606	100	34,46	2,603	100	34.46	2.603	100	34,57	2,594	100	2,586 2,60	420	Alm 33-568 Sp 10-354
36,15	2,486	10	36,20	2,481	6	36.23	2.480	18	36,35	2,471	12	2,48	332	Sp 10-354
37,83	2,378	18	37,87	2,376	21	37.86	2.377	37	38,01	2,368	17	2,361 2,37	422	Alm 33-568 Sp 10-354
39,44	2,284	16	39,47	2,283	15	39.46	2.284	25	39,62	2,274	17	2,268 2,28	431	Alm 33-568 Sp 10-354
42,51	2,137	14	42,55	2,125	15	42.53	2.125	16	42,70	2,118	12	2,112 2,13	521	Alm 33-568 Sp 10-354
43,94	2,061	3	44,05	2,056	6	43.90	2.062	3	44,19	2,049	6	?	?	?
48,17	1,889	20	48,21	1,888	21	48.20	1.888	32	48,40	1,881	17	1,876 1,886	611	Alm 33-568 Sp 10-354
			49,49	1,842	3				49,76	1,832	4	?	?	?
50,38	1,811	3				50.16	1.819	8				1,817	112	Q 33-1161
									51,41	1,777	6	?	?	?
						53.15	1.723	3				?	?	?
54,58	1,681	9	54,63	1,680	7	54.60	1.681	11	54,83	1,674	8	1,669 1,681	444	Alm 33-568 Sp 10-354
57,01	1,615	30	57,06	1,614	28	57.05	1.614	23	57,28	1,608	23	1,604 1,614	640	Alm 33-568 Sp 10-354
						58.24	1.584	3	58,42	1,580	3	?	?	?
59,39	1,556	77	59,44	1,555	36	59.44	1.555	26	59,72	1,548	31	?	?	?
						60.23	1.537	3				?	?	?
						60.83	1.523	3				?	?	?
63,91	1,457	4	63,99	1,455	6				64,25	1,450	4	?	?	?
			68,64	1,367	3							?	?	?
72,57	1,303	3	72,69	1,301	8							?	?	?

Table 4. IR absorption bands for selected garnet samples (Ir model of garnets taken from Geiger, 1998; Görlich, 1998; Hofmeister et al.,1996; Langer, et. al., 1993; Moore, White and Long, 1971).

IR model of garnets					Samples									
Grossular	almandine	pyrope	andradite	spessartine	04KK02	05KK02	06KK02	08KK02	13KK02	15KK02	22aKK02	22eKK02	18KK03	30KK03
911**B**	963**B**	976**B**	929**B**	949**B**	954	953	954	955	955	955	959	952	960	953
860**C**	900**C**	906**C**	888**C**	885**C**	890	890	890	890	890	890	890	886	894	889
843**D**	877**D**	876**D**	810**D**	866**D**	869	869	870	869	869	869	870	867	869	857
619**E**	634**E**		670 **E**	661**E**	633	632	633	633	633	633	633	631	633	633
543**F**	566**F**	585**F**	591**F**	556**F**	561	561	562	562	562	562	562	560	567	562
506**G**	526**G**	538**G**	512**G**	525**G**										
473**H**	470**H**	476**H**	479**H**	471**H**	476	478	478	478	476	479	472	479	477	476
451**I**	448**I**	458**I**	439**I**	447**I**	456	455	456	456	456	456	460	455	457	454

Table 5. Mössbauer data of the studied garnets. Legend: IS – isomer shift versus room temperature alpha- Fe, QS – quadrupole splitting, Γ - full width at half maximum (FWHM), A – relative contribution to the total spectrum.

	doublet 1 Dodecahedral Fe(II)				doublet 2 Octahedral Fe(III)				contaminations additive 1				additive 2			
Sample	IS [mm/s]	QS [mm/s]	Γ [mm/s]	A [%]	IS [mm/s]	QS [mm/s]	Γ [mm/s]	A [%]	IS [mm/s]	QS [mm/s]	Γ [mm/s]	A [%]	IS [mm/s]	QS [mm/s]	Γ [mm/s]	A [%]
03KK02	1.28(1)	3.54(1)	0.19(1)	83.1(5)	0.36(1)	0.60(2)	0.29(2)	9.5(5)	1.06(1)	2.66(3)	0.19(2)	4.8(5)	0.39(1)	2.08(1)	0.10(1)	2.6(3)
05KK02	1.28(1)	3.56(1)	0.19(1)	90.5(3)	0.32(1)	0.50(2)	0.20 fix.	5.4(2)	1.02(2)	2.68(4)	0.19 fix.	2.4 (2)	0.43(2)	2.18(4)	0.20 fix.	2.1(2)
17KK02	1.28(1)	3.55(1)	0.16(1)	92.0(2)	0.34(1)	0.47(1)	0.20 fix.	8.0(1)	~	~	~	~	~	~	~	~
22aKK02	1.28(1)	3.55(1)	0.16(1)	88.9(3)	0.29(1)	0.52(1)	0.29(1)	11.1(3)	~	~	~	~	~	~	~	~
22eKK02	1.28(1)	3.55(1)	0.18(1)	88.9(3)	0.34(1)	0.44(1)	0.20 fix.	7..9(2)	0.98(2)	2.62(3)	0.20(3)	3.1(3)	~	~	~	~

Table 6. Crystal data and details of structure refinement for single crystals selected from given samples.

Sample	Unit cell parameters [Å]	D_x [gcm^{-3}]	Refined chemical composition: $X_3Y_2Z_3O_{12}$	x,y,z of O-atom position	R_1, wR2, S
03KK02	11.6379(5)	4.053	$(Ca_{1.41}Fe_{1.59})(Al_{1.93}Fe_{0.07})Si_3O_{12}$	0.0351(1), 0.0474(1), 0.6524(1)	0.0272 0.0614 1.075
22eKK02	11.6538(3)	3.913	$(Ca_{2.26}Fe_{0.74})(Al_{1.86}Fe_{0.14})Si_3O_{12}$	0.0352(1), 0.0472(1), 0.6524(1)	0.0204 0.0592 1.385
23KK02	11.5775(5)	3.975	$(Ca_{2.08}Fe_{0.92})(Al_2)Si_3O_{12}$	0.0343(1), 0.0483(1), 0.6528(1)	0.0223 0.0577 1.260
18KK03	11.5982(1)	3.836	$(Ca_3)(Al_2)Si_3O_{12}$	0.0344(1), 0.0481(1), 0.6526(1)	0.0292 0.0783 0.817

vibrations of the SiO_4 group (symmetrical bending ν2 and asymmetrical one ν4). H bands corresponds to octahedral YO_6 (mainly AlO_6) group.

The results confirm the presents of almandine–andradite solid state solution with the addition of grossular in the garnet samples from amphibolite rocks (04KK02 - 22eKK02 and 30KK03, except of 22aKK02) and the addition of pyrope in 18KK03 and 22aKK02. The presence of the pyrope units in 22aKK02, the sample from pyroxene-garnet blocks appearing among the ortoamphibolite rocks, has probably xenolitic origin. A different character of 30KK03 from the other granulite samples could be connected with the influence of prehnite–-albite–kalcite veins, which had caused the retrogresive amphibolitization granulites [14]. The detail analysis of IR spectra in the range 3000-3500cm^{-1} (lack of OH^- and H_3O^+ vibration bands) let us to exclude the presence of hydrogarnet units.

MÖSSBAUER ANALYSIS

The Mössbauer spectra of the studied samples recorded at room temperature have similar shape of one well resolved, almost symmetric doublet (Fig. 9). A small amounts of some additives are hardly visible at the spectrum as additional lines. The satisfactory fits could be obtained assuming two, three or four doublets depending on the sample. It can be seen from the results summarized in Table 5 that the Mössbauer parameters, isomer shift and quadrupole splitting, for doublet 1 are typical for high symmetry Fe(II) in high spin state, whereas doublet 2 parameters are characteristic for Fe(III) in high spin configuration.

The values are in agreement with the data given by Woodland and Ross [15]. The symmetry of iron

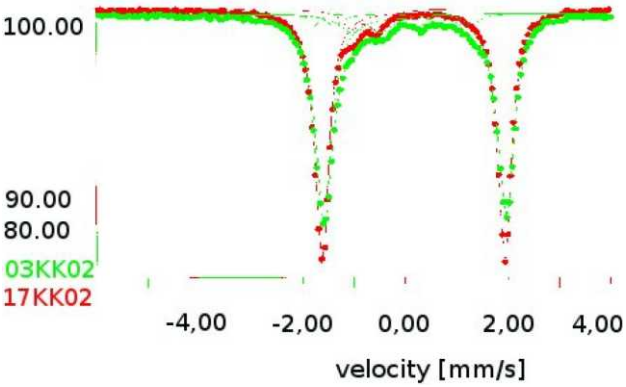

Fig. 9. Typical Mössbauer spectra of garnet samples.

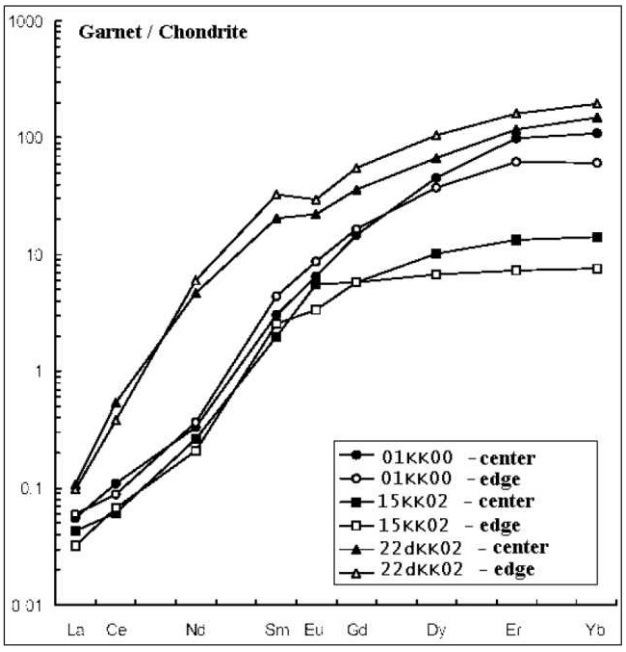

Fig. 10. REE distribution pattern in garnets.

positions was confirmed by single crystal X-ray diffraction. Fe^{2+} ions occupied the dodecahedral position, X, and Fe^{3+} were found in octahedral position, Y.

The remaining two phases present in the samples in smaller quantities (see Table 5) may be treated as impurities. The IS and QS values of the additive 1 doublet suggest octahedrally coordinated Fe(II) in high spin state. However the quadrupole splitting of the additive 2 doublet being too large for Fe(III) is difficult to assign.

REE DISTRIBUTION IN MINERALS

The chondrite-normalized REE distribution spectra in garnets exhibit a smooth rise towards heavy REE (HREE) with no Eu anomaly (Fig. 10) that is typical of high-calcium garnets [16]. The three garnets display slight zoning in HREE and Y. The content of these elements decreases in two of the three garnets towards the edge of the grain, but moves upward in the garnet from Sample 22d/02 (Fig. 10). These garnets demonstrate clear zoning expressed in diminishing HREE content from the center towards the edge of the grains at the overall low REE and enhanced titanium content, which it was similarly in the studied earlier samples from the Chaya-Nyurundukan Complex [17]. This zoning is not progressive that is typical of low-temperature low-calcium garnets crystallized under the conditions of raising temperature in the absence of a long-term superimposed high-temperature influence that could have smoothed the zoning. It is distinctive that the garnet displays no REE and Y correlation with a clearly defined progressive growth zoning in manganese. The concerned high-calcium garnets from the orthorocks of the Lapland Complex are also characterized by high titanium and low total REE (max. 100 g/t). The spread in HREE content (Fig. 10) does not correlate with the pyrop minal contribution and garnet producing temperature, as it was established for the low-calcium garnets from the felsic rocks, but most likely reflects the features of the parental rock compositions [16].

CONCLUSIONS

The studied garnets, from the rocks of Kandalaksha region, had been metamorphosed in high temperature and high pressure conditions (amphibolite and granulite facies). These rocks belong to two kinds of genetic types: the metamorphose extrusive–lavas and metasedimentary formation and the intrusive formation [1].

The first genetic type was a volcanic basalt–andesite formation [3], the second one, a gabbro–anorthosite intrusion [3]. The metamorphic transformation products of extrusive formations are plagioclase–garnet–quartz amphibolites whereas those of intrusive formations are pyroxene–-garnet–quartz granulites. The basement metamorphic produtcs of komplex is the garnet–quartz–pyroxene shists (white granulites) [3]. The amphibolites are composed of common hornblende, plagioclase (labradore), quartz and garnets with the additions of biotite, diopside, apatite, rutile, tytanite, ilmenite and zircone. In the granulites the main components are diopside, hyperstene, quartz and plagioclase (labradore, bytovnite) with the impurities of apatite, rutile and ilmenite.

The garnets from amphibolites were collected in Kandalaksha region near Zhieleznaya and Wolosyanaya mounts and the garnets from granulite samples were found from Siennaya Kurtiazhnaya and Sriedniy Myss mounts.

The minerals were studied by polarizing microscopy (PM), electron scanning microscopy (EDS), X-ray structure analysis of single crystals (CSA) and X-ray powder diffractometry (XRD), infrared (IR) and Mössbauer (M) spectrometry methods. The studied garnets from both rock formations have an idioblastic structure and they often form aggregates. These minerals make near 25-45% vol. of rocks. The proportion 9:1 of Fe(II): Fe(III) was found to be approximately the same in all garnets.

Calcium contents in the garnets from metamorphosed intrusive formation is probably connected with the high amount of this element in the metamorphic rocks. The appearance of diopside and plagioklase with 70% anorthite units justified the hypothesis. As it was confirmed by EDS, XRD, IR and CSA analyses, the almandine units predominate in these garnets.

Chemical composition and high contents of the almandine–andradite solid solution in the studied garnets from Kandalaksha region, confirm that the metamorphic rocks (plagioklase–garnet–quartz amphibolites and pyroxene–garnet–quartz granulites) were formed in the high metamorphic conditions: the amphibolites in hornblende–-plagioklase–garnet–quartz subfacies, whereas the

granulites in plagioclase–hyperstene–diopside–-garnet subfacies. The garnets seem to originate from pyralspite group, with the domination of almandine, and from following transformation towards the ugrandite group with andradite and grossular as main components. Small amount of pyrope units is characteristic for the facies of highest metamorphism in the area, while grossular units are typical for retrogressive metamorphism accompanied by hydrothermal processes connected with geochemical front interactions. The anomalies observed in chemical composition, especially concerning Ca^{2+} contents, confirm the existence of advanced retrogressive processes.

The features of REE distribution in the garnets from the mafic orthorocks in the southeastern part of the Lapland Granulite Complex reflect the fact that the diaphthoresis took place at amphibolite facies of metamorphism and cannot be recorded by conventional principles of temperature and pressure measurement. The decrease of metamorphism temperature and imbalance between garnets, biotites, amphiboles and pyroxenes are evidenced both by the individual REE distribution trends in the amphiboles and varying profiles of distribution coefficients in the field of light REE for the garnet-amphibole pairs. The zoning in HREE and some rare elements, as well as differences in their content in the high-calcium garnets, are affected rather by the composition of the surroundings rocks than by the parameters of metamorphism.

TRANSPARENCY DECLARATION

The authors declare no conflicts of interest.

ACKNOWLEDGEMENTS

Financial support was given from Geology, Geophysics and Environment Protection Faculty, University of Science and Technology (AGH), Kraków, under the grant 10.10.140.949.

We thank Prof. A. Piestrzyński (Department of Ore Deposits, AGH) for making the reflected light polarizing microscope available; Mr S. Olkiewicz and Mr A. Gaweł from Department of Mineralogy, Petrography and Geochemistry (AGH), for IR and XRD analyses, respectively; dr M. Michalik from Institute of Geological Sciences, Faculty of Biology and Earth Sciences, Jagiellonian University, for EDS analysis; Joint X-ray Diffraction Division, Faculty of Chemisty and Regional Laboratory Jagiellonian University, for making the Nonius KappaCCD diffractometer available; Department of Low Temperature Physics, Institute of Physics, Jagiellonian University, for making the apparatus for Mössbauer effect measurements available.

REFERENCES

1. Mitrofanov FP. (ed.). Geology of the Kola peninsula (Baltic Shield). 1995. Apatity: pp. 144.
2. Mitrofanov FP. (ed.).Geological map of the Kola region", scale 1:500000. 1996. Apatity.
3. Kozlov NE, Ivanov AA, Nyerovich LI. Laplandsky Granulitovyj Poyas, Piervichnaya P'riroda i Razvitie. 1990. Russian Academy of Science, Apatity Branch Press.
4. Huber M. Geological and Petrographic Characteristics of the Lapland Granulite Belt Near Kandalaksha at the White Sea, Kola Peninsula, Northern Russia. *Mineralia Slovaca* 2001; 2: 17-31.
5. Huber M, Bonarski JT. Investigation on the Texture of Lapland Granulite Belt Using X-Ray Diffraction Technique. Mineralogical Society of Poland – Special Papers 2003; 22: 73-77.
6. Holdaway MJ, Mukhopadhyay B, Dyar MD, Guidotti CV, Dutrow BL. Garnet-Biotite Geothermometry Revised: New Margules Parameters and a Natural Specimen Data Set from Maine. *Am Mineral* 1997; 82: 582-595.
7. Meagher EP. The Crystal Strustures of Pyrope and Grossularite at Elevated Temperatures. *Am Mineral* 1975; 60: 218-228.
8. Skublov SG, Huber M. Ossobyennosti geochimi REE v metamorficheskych mineralach S-E chas'ti Laplandskovo Granulitovovo Poyasa. *Viestnik SPBU* 2005; 7: 87-91.
9. Geiger ChA. A Powder Infrared Spectroscopic Investigations of Garnet Binaries. The System $Mg_3Al_2Si_3O_{12}$-$Fe_3Al_2Si_3O_{12}$-$Mn_3Al_2Si_3O_{12}$-$Ca_3Al_2Si_3O_{12}$. *Eur J Mineral* 1998; 10: 407-422.
10. Görlich E. Structural Chemistry of Silicates. Orthosilicates. 1998. Polish Academy of Science, Cracow Branch.
11. Hofmeister AM, Fagan TJ, Campbell KM, Schaal RB. Single-Crystal IR Spectroscopy of Pyrope-Almandine Garnets with Minor Amounts of Mn and Ca. *Am Mineral* 1996; 81: 418-428.
12. Langer K, Robarick E, Sobolev NV, Shatsky VS, Wang W. Single-Crystal Spectra of Garnets from Diamond Ferrous High-Pressure Metamorphic Rocks from Kazakhstan: Indications for OH-, H2O, and Fe/Ti Charge Transfer. *Eur J Mineral* 1993; 5: 1091-1100.
13. Moore RK, White WO, Long TV. Vibrational spectra of the common silicates: I. The garnets. *Am Mineral* 1971; 56: 54-71.

14. Huber M, Hałas S, Sikorska M. Evolution of prehnite-albite-calcite veins in Metamorphic rocks from the Lapland Granulite Belt (Kandalaksha region of Kola Peninsula. *Geologija* 2007; 57: 1-7.
15. Woodland AB, Ross IChR. A Crystallographic and Mössbauer Spectroscopy Study of $Fe_3^{2+}Al_2Si_3O_{12}$ – -$Fe_3^{2+}Fe_2^{3+}Al_2Si_3O_{12}$, (Almandine-Skiagite) and $Ca_3Fe_2^{3+}Al_2Si_3O_{12}$– $Fe_3^{2+}Fe_2^{3+}Al_2Si_3O_{12}$ (Andradite-Skiagite) Garnet Solid Solutions. *Phys Chem Minerals* 1994; 21: 117-132.
16. Drugova GM, Skublov SG, Vrievsky AB, Kozlov NE. Raspredelyenye redkozemelnych elementov w granatach Laplandskovo Granulitovovo Poyasa i copre'delnykh territoyi. *Geokhimia* 2001; 2: 232-237.
17. Skublov CG, Drugova GM. Redkozemyelnye elementy v zonalnykh metamorphicheskych mineralach, *Geokhimia* 2004; 3: 288-301.

Journal of Biology and Earth Sciences

EARTH SCIENCES ORIGINAL ARTICLE

Mass-spectrometric REE analysis in sulphide minerals

Irina R. Elizarova[1], Tamara B. Bayanova[2]

[1]I.V. Tananaev Institute of Chemistry and Technology of Rare Elements and Mineral Raw Materials of the Kola Science Centre, Russian Academy of Sciences, Apatity, Russia
[2]Geological Institute of the Kola Science Centre, Russian Academy of Sciences, Apatity, Russia

ABSTRACT

The standard samples of diorite, granite and anorthosite (National Centre for Petrographic and Geochemical Research (CRPG CNRS, Nancy, France) were analyzed to measure rare-earth element (REE) concentrations by the ICP MS method (quadrupole ELAN 9000 DRC-e) without preliminary dilution and concentration procedures. The certified values of REE concentrations measured on ELEMENT-2 mass-spectrometer by ICP MS method in Nancy are also well reproduced on ELAN 9000. The mass-spectrometer analytical environment and modes of operation were adjusted to detect REE in sulphide minerals by the example of the pyrite from the PGE Penikat layered intrusion (Finland) and chalcopyrite from the Talnakh deposit (Kazakhstan). The total REE content in the pyrite is ca. 3.5 ppm, that is enough to establish Sm-Nd age of pyrite. By the example of State Standard Sample 2463 (apatite, Russia) it is shown how to apply the mineral/chondrite spectra to evaluate the accuracy of the REE analytical results.

Key words: mass-spectrometry, ELAN 9000, rare earth elements, geological standards, sulphide minerals.

J Biol Earth Sci 2012; 2(1): E45-E49

Corresponding author:
Tamara B. Bayanova
Head of Laboratory for Geochronology and Isotope Geochemistry,
Geological Institute of the Kola Science Centre
of the Russian Academy of Sciences,
14, Fersman str., Apatity, Murmansk Region, 184209, Russia.
e-mail: bayanova@geoksc.apatity.ru

Original Submission: 20 April 2012; Revised Submission: 8 June 2012; Accepted: 9 June 2012

ISSN: 2084-3577
http://www.journals.tmkarpinski.com/index.php/jbes or http://jbes.strefa.pl
e-mail: jbes@interia.eu

INTRODUCTION

Sulphides are ore-forming minerals in PGE deposits and that may bear economic Pt-Pd mineralization. The investigations of the noble metal deposits located on the Kola Peninsula at certain stages involves geochronological research and analytical treatment of the accumulating data. The information on REE content and distribution in minerals is required to define the age of the ore-forming event and to study the behavior of light lanthanides in the course of sulphide magma generation.

The REE content in sulphides is often less than 0.1 ppm; the REE composition is not completely studied; and the information on REE analysis is scarce [1-4]. Palessky [5] in his review of the REE analytic methods used to examine geological samples notes that, as compared with X-ray fluorescence and neutron activation analyses, atomic absorption and atomic emission spectrometry is nowadays more widely adopted. These methods, however, do not enable to simultaneously reveal the whole range of elements in geological samples because of their low detection limits or constraints on the range of elements to identify. Thus, the content of such monoisotopic elements as Pr, Tb, Ho, and Tm cannot be measured by isotope dilution method. It is possible to analyze REE by ICP MS method on ELAN-9000 (Perkin Elmer) mass-spectrometers in the amount of up to 1 ppt (instrumental detection limit is 0.1 ppt). Timofeev [6] shows a possibility of analyzing microimpurities of rare and trace elements on ELAN mass-spectrometers without preliminary concentration. A simultaneous determination of the whole REE range without preliminary concentration is described in [7].

Rimskaya-Korsakova et al., [3] show the REE content in the chalcopyrite of the Talnakh deposit at a ppb level that is six to thirty times less than that in chondrite. The authors preliminarily separated REE from the matrix of the unsealed liquid samples, and concentrated REE to analyze on ICP MS, PlasmaQuad PQ2STE.

MATERIALS AND METHODS

There are no standard samples of sulphide minerals composition. In order to analyze REE in geological sulphide samples, first we have reproduces the certified REE concentrations in GSO 2463 (apatite) and international standard composition samples of the National Centre for Petrographic and Geochemical Research (CNRS), Nancy, France for granite (AC - E), diorite (DR - N), and anorthosite (AN - G). The analysis was made without preliminary separation and concentration on ELAN 9000 DRC-e GMS (Perkin Elmer, USA). Then we have analyzed the chalcopyrite of the Talnakh deposit (Kazakhstan) to compare with the data obtained by Rimskaya-Korsakova et al., [3]. The results of the comparison suggest the accuracy of the analysis. Afterwards, we have measured the REE content in the sulphides from the PGE Penikat deposit, Finland.

The analysis on ELAN 9000 DRC-e was based on the following parameters: plasma power of 1,300-1,350 W; sprayer gas flow (high-clean Ar) within 0.75-1.0 $lmin^{-1}$; ion lens voltage < 11 V; and level of doubly charged and oxide ions < 2.5%. A geological sample weighing up to 100 mg in the polystyrene hermetically sealed test tube mixed with distilled acids (HNO_3, HF, HCl 5 ml each) was exposed to water bath at a temperature of 50-60ºC until fully dissolved. No HCl was added in the course of opening of sulphide minerals. When opening the sample, we have registered an increased pressure of acid and nitrogen oxide vapour that suppressed the volatility of the components in the sample. The chilled sample was mixed with 0.1 ml H_2O_2, and the dissolved sample was diluted with 2% HNO_3. The level of total REE content in the blank sample was < 0.5 ppb (see the REE spectrum in Fig. 1, Curve 7). This blank sample qualifies the level of analytical accuracy and limit of element detection.

Since the samples have yielded high concentrations of those elements that may cause matrix effect and ion interference, the calibration curves were plotted with interfering agent added to the blank calibration solution. The multicomponent standard solutions by Perkin Elmer («Multi-element ICP-MS Calibration Std») were used. The sample itself was selected as an interfering agent. The amount of the interfering agent was chosen so that the macrocomponent concentration after mixing exceeded the REE concentration in the calibration solution by a factor of 100. The approximation linearity of the REE correction curves is ≥ 99.99%. Spectral superimposition was recognized by ELAN 9000 DRC-e MS software, and adjusted by the

introduction of correction equations (Table 1) into the analytic program defined with reference to natural abundance of REE isotopes. The blank sample solution free of the interfering agent was used to analyze the solution of the opened sample.

RESULTS AND DISCUSSION

The REE determination could have considerably been disturbed by Ba isotopes due to the superimposition of their monovalent oxide and hydroxide spectra on REE. The certified Ba concentration values in the geological standard samples were up to 391, 60 and 37 ppm in diorite, granite, and anothosite respectively. Such Ba concentrations have not disturbed the procedure of analysis. It is accountable for by the level of oxide ions concentration in plasma (adjustable parameter in optimizing mass-spectrometer operation) in the course of analysis. In addition, the sample has yielded high content of Si, Fe, Al, Mg, Ca, Na, K, Ti, and P ions that display higher affinity with oxygen than Ba. As well, Ba-bearing interfering agent that presents in the calibration solution permits to takes into account Ba oxide and hydroxide spectra superimposed on Sm and Eu.

The REE spectrum profile for the apatite state standard sample displays that the uncertified values for Gd, Er and Tm (Fig. 1, Curve 1, a) do not fit in with the smooth running of the curve, while those obtained in this research (Fig. 1, Curve 1, б) do. The uncertified values for Ho and Lu were well reproduced by our results and corresponded to the smooth REE distribution profile (La → Lu). It is possible to suggest that the uncertified values of Ho and Lu concentrations in state standards sample 2463 agree with the real values, while the uncertified values for Gd, Er and Tm stated in the certificate of the state standard samples are most probably exaggerated. The results of REE content test for the world-class geological standard samples conform satisfactorily to the certified values; the REE spectra are shown in Figure 1, Curves 2 – 4. Fitted and approved conditions of the sample opening and analysis on the on geological composition standard samples have confirmed the possibility to measure REE concentrations without preliminary mineral matrix separation and rare earth elements reconcentration. This has likewise enabled to analyze the sulphides of the Talnakh deposit (Kazakhstan) and Penikat PGE layered intrusions (Finland). As against to the results of REE analysis in the chalcopyrite of the Talnakh deposit [3], we have obtained higher concentrations of Ce, La, Nd and Pr. The results are shown in Table 1; the REE mineral/chondrite spectra are plotted (see Fig. 1, Curves 5 and 6 c, δ).

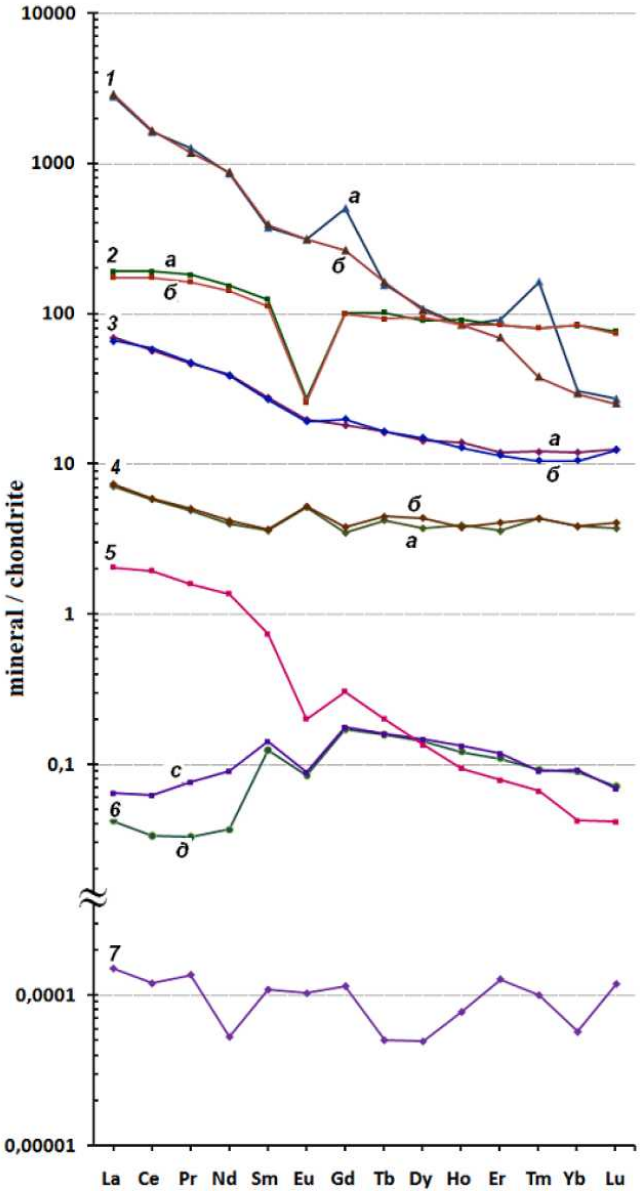

Fig. 1. REE ration in the chondrite and following samples:
1 - GSO 2463, apatite,
2 - AC-E, granite,
3 - DR - N, diorite,
4 - AN - G, anorthosite,
a – certified value, б – defined value
5 – pyrite from the gabbronorite of the PGE Penikat layered intrusion, Finland,
6 – chalcopyrite of the Talnakh deposit, Kazakhstan, c – obtained data, δ – present data [3];
7 – blank sample.

Table 1. REE analysis results for sulphide mineral.

Isotope	Penikat, Finland, pyrite		Talnakh, Kazakhstan, chalcopyrite		Overlapping of oxide masses allowed for by ELAN software	Intensity correction subtracted from definite intensity*
	Concentration, ppm	RSD,%, n=81	Concentration, ppm	RSD,%, n=81		
^{139}La	0.63±0.03	4.8	0.020±0.001	5.0		
^{140}Ce	1.557±0.007	0.4	0.050±0.003	6.0		
^{141}Pr	0.194±0.004	2.1	0.0092±0.0008	8.7		
^{142}Nd	0.82±0.03	3.7	0.054±0.003	5.6		0.125653·Int(^{140}Ce)
^{152}Sm	0.144±0.007	4.9	0.028±0.002	7.1	CeO, BaO	0.01278·Int (^{157}Gd)
^{151}Eu	0.0147±0.0005	3.4	0.0066±0.0006	9.1	BaO	
^{157}Gd	0.0794±0.0012	1.5	0.0460±0.0005	1.1	LaO, CeO, PrO	0.004016·Int(^{163}Dy)
^{159}Tb	0.010±0.001	10	0.0076±0.0007	9.2	NdO, PrO	
^{164}Dy	0.044±0.002	4.5	0.047±0.003	6.4	NdO, SmO	0.047902·Int(^{166}Er)
^{165}Ho	0.0068±0.0006	8.8	0.0095±0.0006	6.3	SmO	
^{166}Er	0.0165±0.0005	3.0	0.025±0.002	8.0	SmO, NdO	
^{167}Er					EuO, SmO	
^{169}Tm	0.0022±0.0002	9.1	0.0029±0.0003	10.3		
^{174}Yb	0.0089±0.0005	5.6	0.019±0.001	5.3	GdO, DyO	0.005865·Int (^{178}Hf)
^{175}Lu	0.0013±0.0001	7.7	0.0022±0.0002	9.1	GdO, TbO	
^{89}Y	0.150±0.006	4.0	0.34±0,03	8.8		
^{137}Ba	10.6±0.5	4.7				

*equation factors are reported by Timofeev (personal communication)

CONCLUSIONS

A possibility to analyze REE in sulphide minerals (Talnakh deposit, Kazakhstan, and PGE Penikat layered intrusion, Finland) on ELAN 9000 DRC-e (Perkin Elmer, USA) without preliminary separation of saline and oxide matrix, and REE reconcentration is demonstrated. The sample/chondrite distribution spectra are obtained.

The concentration of Sm and Nd in the sulphide minerals (Penikat, Finland) is enough to be detected by Sm-Nd isotope method for age measurements.

The sample/chondrite distribution spectra in GSO 2463 were used to clarify the values of Gd, Er and Tm concentrations.

TRANSPARENCY DECLARATION

The authors declare no conflicts of interest.

ACKNOWLEDGEMENTS

Many thanks to A. Dubinin (Russia) for chalcopyrite from Talnakh and J. Ludden (UK) for standards from Nancy.

The researches are supported by RFBR grants 08-05-00324, OFI-M 09-05-12028, 10-05-00038 and Interreg-Tacis K-0193 program.

REFERENCES

1. Zhao K-D, Jiang S-Y. Rare earth element and yttrium analyses of sulfides from the Dachang Sn-polymetallic ore field, Guangxi Province, China: Implication for ore genesis. Geochem J 2007; 41: 121.
2. Dubinin AV. Geochemistry of rare earth elements in the ocean. M: Nauka. 2006: pp. 360 /in Russian/.
3. Rimskaya-Korsakova MN, Dubinin AV, Ivanov VM. REE analysis in sulphide minerals by mass-spectrometric methods (IEC ICP MS – ion-exchange concentration inductively-coupled plasma mass-spectrometry). J Anal Chem 2003; 58: 975 /in Russian/.
4. Mils RA, Elderfield H. Rare earth element geochemistry of hydrothermal deposits from the active TAG mound, 26°N Mid-Atlantic Ridge. Geochim Cosmochim Acta 1995; 59: 3511.
5. Palessky SV. Inductively-coupled plasma mass-spectrometry: rare and trace elements analysis. Abstract of the candidate thesis in chemistry. Novosibirsk: Institute of Inorganic Chemistry. Siberian Department of RAS, 2008: pp. 20 /in Russian/.

6. Timofeev PV. ICP mass-spectrometry and evolution of the rare metal bearing mineral resources. Modern analytical procedures and instrumentation in geology and environmental protection. Tashkent, 1998: pp. 50 /in Russian/.
7. Elizarova IR, Bayanova TB, Mitrofanov FP, Kalinnikov V.T. Procedure of mass-spectrometric (ELAN 9000) REE analysis in reference geological samples // Proceedings of the 3rd All-Russian Conference with International contribution "Mass-spectrometry and applied problems", May 18-22, 2009, Moscow, NU-8 : 110 /in Russian/.

Contents